NOVEL ELECTROCHEMICAL AND FLUORESCENCE SENSORS FOR FOOD ADDITIVES AND NEUROTRANSMITTERS

Thesis submitted to

Cochin University of Science and Technology

in partial fulfilment of the requirements

for the award of the degree of

Doctor of Philosophy

in

Chemistry

by

Anuja E.V.

Department of Applied Chemistry

Cochin University of Science and Technology

Kochi – 22

August 2015

Novel Electrochemical and Fluorescence Sensors for Food Additives and Neurotransmitters

Ph.D. Thesis under the Faculty of Sciences

By

Anuja E.V.
Research Fellow
Department of Applied Chemistry
Cochin University of Science and Technology
Kochi, India 682022
Email: evanuja@gmail.com

Supervising Guide

Dr. K. Girish Kumar
Professor of Analytical Chemistry
Department of Applied Chemistry
Cochin University of Science and Technology
Kochi, India 682022
Email: giri@cusat.ac.in

Department of Applied Chemistry
Cochin University of Science and Technology
Kochi, India 682022

August 2015

DEPARTMENT OF APPLIED CHEMISTRY
COCHIN UNIVERSITY OF SCIENCE AND TECHNOLOGY
KOCHI - 682022, INDIA

Dr. K. Girish Kumar Tel: 0484 - 2575804
Professor of Analytical Chemistry E-mail: chem.@cusat.ac.in

Date: 06th August 2015

Certificate

Certified that the work entitled "**Novel Electrochemical and Fluorescence Sensors for Food Additives and Neurotransmitters**", submitted by Ms. Anuja E.V., in partial fulfilment of the requirements for the degree of Doctor of Philosophy in Chemistry to Cochin University of Science and Technology, is an authentic and bonafide record of the original research work carried out by her under my supervision at the Department of Applied Chemistry. Further, the results embodied in this thesis, in full or in part, have not been submitted previously for the award of any other degree. All the relevant corrections and modifications suggested by the audience during the pre-synopsis seminar and recommended by the Doctoral committee have been incorporated in the thesis.

K Girish Kumar
(Supervising Guide)

Declaration

I hereby declare that the work presented in this thesis entitled **"Novel Electrochemical and Fluorescence Sensors for Food Additives and Neurotransmitters"** is based on the original work carried out by me under the guidance of Dr. K. Girish Kumar, Professor of Analytical Chemistry, Department of Applied Chemistry, Cochin University of Science and Technology and has not been included in any other thesis submitted previously for the award of any degree.

Kochi-22 **Anuja E.V.**
06/08/2015

Dedicated to

My Parents…

Acknowledgement

This thesis has been kept on track and been seen through to completion with the support and encouragement of numerous people. It is a pleasant task to express my thanks to all those who contributed to the success of this study and made it an unforgettable experience for me.

First and foremost, I wish to express my deep and sincere gratitude to my guide, Prof. K. Girish Kumar, for his valuable guidance, patience and relentless optimism, which helped a lot in instilling confidence in me. I am deeply indebted to Girish sir for giving me the opportunity to work in the Sensor group. I sincerely thank him for continuously orienting me in the correct direction during my research and pertinently guiding me during the documentation of this thesis through his constant encouragement and advice. He has supported selflessly in my journey to scientific and personal development. His words have always inspired me and brought me to a higher level of thinking. He has been affectionate and ever ready to help me, even in the midst of his busy schedule. Without his guidance this thesis would have been a distant possibility. I have been extremely lucky to have Prof. K. Girish Kumar as my research guide.

I sincerely thank Dr. K. Sreekumar, my Doctoral committee member, for all his support and help. I wish to thank Dr. N. Manoj, Head, Department of Applied Chemistry, Cochin University of Science and Technology for providing me the research facilities in the department. I also extend my special thanks to all teaching and non-teaching staff of this department.

Dr. Anitha I., Associate Professor in Chemistry, Maharajas College, Ernakulam deserves a special mention here for her support and help.

It has been an exciting, fruitful and enjoyable experience for me to spend four and half years at the Analytical Chemistry lab. I am sure it will become one of the most

treasured memories of my life. No words can suffice to acknowledge the friendly and stimulating atmosphere created by my labmates. My sincere thanks to all my seniors, Dr. Renjini, Dr. Sobhana, Dr. Leena, Dr. Laina, Dr. Theresa and Divya chechi. They helped me at the initial stage of my research through their mentoring and caring. I expand my thanks to my lab colleagues Soumya chechi, Jesny chechi, Zafna chechi, Sreejith, Shanty chechi, Meera, Ambily chechi, Unni, Ammu, Shalini, Shruthi, Shinu and Sreelakshmy for creating a stimulating and fun filled environment. Once more, I thank all my labmates for making my days at the lab pleasant and productive. I take this opportunity to express my sincere thanks to Sheela Miss for her motherly affection to me. I also thank my friends from other labs for their help and wonderful friendship.

I gratefully recall the countless splendid memories of my stay at the Athulya hostel; which I had with Renjini chechi and Laina chechi. I also remember with affection the support and help from Jayalakshmy, my roommate.

I especially thank Jesny chechi for her encouragement and valuable suggestions. I admire her loving and helping nature. Because of her help and suggestions, in formatting the entire thesis, I could finish my thesis in good form. A special word of appreciation goes to Ammu for her willingness to proof read the entire pages of my thesis. Jesny chechi, Ammu and Shalini took efforts to correct grammatical mistakes and improve the language of the thesis. I would like to mention the technical expertise of Unni, which helped in the effective incorporation of schemes and figures in the thesis.

I would like to put in a word of gratitude to Council of Scientific and Industrial Research (CSIR), India for fellowship. I also extend my thanks to the Directorate of Extramural Research and Property Rights, DRDO, New Delhi and Kerala State Council for Science, Technology and Environment, Kerala for the financial assistance in the form of project.

I thank Sophisticated Test and Instrumentation Centre (STIC), CUSAT and Centre for Nanoscience and Nanotechnology (CNN) M.G. University for analysis.

I express my deep sense of gratitude to my family for their invaluable support and affection. I found no word to express my feelings towards my Amma and Achan for their unconditional love and caring though out my life. They were always with me patiently helping to achieve my dreams. My amazing sisters, Amrutha and Anjana are always a source of love and energy. They have also given me so many happy and beautiful memories throughout this journey. My sisters have been my best friends all my life and I thank them for their support. Words cannot express how grateful I am to my mother-in law, for all the love, sacrifice and caring that she has made on my behalf.

Words are insufficient to express my gratitude to my beloved husband, Rajesh for his endless love, all-out support and understanding. His motivation and encouragement helped me a lot to complete this journey. His careful editing and inspiring suggestions contributed enormously to the formation of this thesis. The blessing that was bestowed upon me during the last stages of my research work, our yet to be born baby, merits a special word of mention for being so considerate of me, not giving me any hassles, patiently staying within me during the tedious hours of thesis documentation. Completion of this thesis would not have been possible without the encouragement and understanding of my family. I am so lucky to have such a family.

I have felt God's love at all stages of my life and I immensely thank The God Almighty, for His continuous blessings, throughout my life.

Anuja

Preface

There is an enormous demand for chemical sensors in many areas and disciplines including chemistry, biology, clinical analysis, environmental science. Chemical sensing refers to the continuous monitoring of the presence of chemical species and is a rapidly developing field of science and technology. They are analytical devices which transform chemical information generating from a reaction of the analyte into an measurable signal. Due to their high selectivity, sensitivity, fast response and low cost, electrochemical and fluorescent sensors have attracted great interest among the researchers in various fields.

Development of four electrochemical sensors and three fluorescent sensors for food additives and neurotransmitters are presented in the thesis. Based on the excellent properties of multi walled carbon nanotube (MWCNT), poly (L-cysteine) and gold nanoparticles (AuNP) four voltammetric sensors were developed for various food additives like propyl gallate, allura red and sunset yellow. Nanosized fluorescent probes including gold nanoclusters (AuNCs) and CdS quantum dots (QDs) were used for the fluorescent sensing of butylated hydroxyanisole, dopamine and norepinephrine.

The thesis entitled “Novel Electrochemical and Fluorescence Sensors for Food Additives and Neurotransmitters” is divided into nine chapters. Brief outlines of the chapters are given below:

Chapter 1 outlines a concise introduction to different types of chemical sensors and discusses in detail about voltammetric and fluorescent sensors. A detailed review on the research work in the field of voltammetric and fluorescent sensors is also incorporated in this chapter.

Chapter 2 gives a brief sketch of the materials and methods used for the fabrication of various sensors. The instruments used for the studies are also

mentioned. Preparation of different kinds of buffer solutions are also included in this chapter.

Chapter 3 discusses the fabrication of a voltammetric sensor for propyl gallate (PG) using MWCNT modified glod electrode (MWCNT/GE). The experimental conditions such as supporting electrolyte, pH, amount of MWCNT-nafion suspension and scan rate were optimized. Fundamental kinetic parameters for the electrochemical oxidation of PG were established. A plausible two electron mechanism was suggested for the oxidation of PG which involves the formation of a quinone structure. Application studies of the developed sensor were carried out in commercially available vegetable oil samples.

Chapter 4 details the electrochemical oxidation of allura red (AR) on poly (L-cysteine) modified glassy carbon electrode (poly(L-cys)/GCE) and the sensing of AR using the polymer film modified electrode. The modified electrode was characterized by electrochemical impedance spectroscopy, cyclic voltammetry and scanning electron microscopy. Experimental conditions for sensor fabrication were optimized. The kinetic parameters of the electrochemical reaction such as heterogeneous rate constant, charge transfer coefficient, number of electrons, and diffusion coefficient were determined. The proposed method has been successfully applied for the determination of AR in soft drinks.

Chapter 5 describes the development of two electrochemical sensors for the quantification of sunset yellow (SY) based on MWCNT and MWCNT-AuNP nanocomposite film on GCE. The fast electron transfer ability of MWCNT and synergistic effect between MWCNT and AuNP accounts for the improved sensitivity of the modified electrodes. Various kinetic and thermodynamic parameters of the redox reaction such as standard heterogeneous rate constant, electron transfer coefficient, number of electrons exchanged, diffusion coefficient and free energy of activation (ΔG) were calculated. The response parameters and practical applications of the proposed sensor discussed in this chapter.

Chapter 6 presents the fluorescent sensing of butylatedhydroxy anisole (BHA) based on the protein template gold nanoclusters (AuNCs). FTIR spectroscopy, UV-Vis spectroscopy and high resolution transmission electron microscopy were used for the characterization of synthesized AuNCs. Based on the luminescence enhancement of AuNCs by BHA, a turn on fluorescence sensor was designed for the determination of BHA. The possible mechanism for the fluorescence enhancement of AuNCs by the addition of BHA was explained based on the aggregation of nanoclusters. The analytical application of the sensor was demonstrated by the successful determination of BHA in coconut oil samples.

Chapter 7 is on the development of CdS QDs based fluorescence sensor for dopamine (DA), a principal biomarker of Parkinson's disease. The fluorescence intensity of thioglycolic acid capped CdS QDs enhanced dramatically in the presence of DA. Based on this an efficient turn on sensor was developed for the quantification of DA. The addition of DA increases the passivation of surface traps of QDs and thereby increasing the fluorescence emission intensity. The developed fluorescence assay was employed for the selective and sensitive determination of DA in biological fluid (urine sample).

Chapter 8 describes the application of bovine serum albumin protected AuNCs as a fluorescent probe for the quantification of norepinephrine (NE), an important neurotransmitter. Upon addition of norepinephrine, the fluorescence emission intensity of gold nanoclusters increased remarkably, which is attributed to the restricted intramolecular rotation resulting from the aggregation of gold nanoclusters. The developed turn on sensor exhibits good analytical figures of merit and shows promising practical applications.

Chapter 9 gives the summary and important conclusions of the work presented in the thesis. An overview of the work is given in brief. Future prospects of the work are also presented.

Contents

List of Tables

List of Figures

List of Schemes

.....ꕥ.....

Chapter 1

INTRODUCTION

Contents

Sensors have become an indispensable part of our technology driven society and have found potential applications in pharmaceutical industry, clinical analysis, food quality control, environmental monitoring etc. The development of chemical sensors is currently one of the most active areas of research in analytical chemistry.

There are two types of sensors, chemical sensors and physical sensors. Chemical reactions involving the analyte give informations in chemical sensors while physical sensors are sensitive to physical responses like temperature, pressure, force etc.

Chemical sensors are analytical devices used for the qualitative and quantitative determination of a species, through a selective chemical reaction. Each chemical sensor consists of a sensing element and a transducer. The sensing element selectively recognizes the analyte and the transducer converts the chemical information to an amplified analytical signal which is proportional to the concentration of analyte.[1] Chemical sensors are catagerized, according to the type of transducer as[2]

(a) Electrochemical sensors: the electrochemical interaction taking place between the electrode and analyte is transformed into electric signal (potential or current). They are classified as potentiometric, voltammetric/amperometric and conductometric sensors.

(b) Optical sensors: changes in optical properties, as a result of chemical interaction are monitored mainly by photometry in optical sensors.

(c) Mass sensitive sensors: they record the change in mass on the surface of an oscillating piezoelectric crystal as a function of concentration of analyte.

(d) Heat sensitive sensors: also known as calorimetric sensors since they measure the heat of a chemical reaction involving the analyte. Heat of the reaction is monitored with the help of transducers like thermistor or a platinum thermometer.

1.1 Electrochemical sensors

Electrochemical sensors have become an active area of research due to their rapidly growing applications in clinical chemistry, food industry, and environmental monitoring. Here electrode is acting as a probe to measure electrochemical reaction that occurrs directly or indirectly at the surface of the electrode. This gives information about the electrode process.[3] In voltammetric sensors current resulting from the electrochemical reaction is registered as a function of applied potential.

1.1.1 Electrodes in voltammetry

Voltammetric measurements are carried out in a three electrode cell system involving the working electrode, reference electrode and auxiliary (counter) electrode immersed in an electrically conducting solution.

1.1.1.1 Working electrode

The working electode is the electrode on which the electrochemical reaction under study is taking place. Electrochemical inertness over a broad potential window, low residual current, high overvoltage towards hydrogen and oxygen evolution, low ohmic resistance and the possibility of simple surface regeneration are the important characteristics of a good working electrode.[4] Good stability is also a desirable property of the working electrode especially for long term in situ monitoring purposes. Commonly used working electrodes in voltammetry are glassy carbon, gold, platinum etc.

(a) Glassy carbon electrode

Due to its excellent electrical and mechanical properties, solvent resistance, wide potential window and reproducible performance glassy carbon electrode (GCE) has become very popular among electrochemists.[5] It is an isotropic and hard conductor having low porosity.[6] The glassy carbon material is prepared by a controlled heating program of a polymeric resin body in an inert atmosphere.[7] Electrochemical, chemical, heat and laser treatments are employed for the creation of active sites and improvement of analytical performance of GCE.

(b) Gold and platinum electrodes

Gold and platinum are the most widely used metallic solid electrodes.[8] Noble metals are ususlly preferred as electrode materials to avoid reaction

between the electrode and components of electrolyte.[9] Large anodic potential range and fast electron transfer kinetics are the advantages of these electrodes. However, low hydrogen over voltage restricts the cathodic potential window and limits their application. Self assembled monolayers can be easily formed on the surface of gold electrode which has many potential scientific and technological applications.[10]

1.1.1.2 Reference electrode

The potential of the working electrode is measured against the reference electrode. The necessary condition for a reference electrode is that its potential should not be changed by the electrolyte species, temperature and passage of current. Standard hydrogen electrode (SHE) is the most commonly used reference electrode. However, SHE is not often preferred in voltammerty because of the difficulty in construction and maintanace. Ag/AgCl and calomel electrodes are widely used in voltammetric techniques.

1.1.1.3 Auxiliary electrode

The role of counter/auxiliary electrode is to allow the passage of current through the cell without disturbing the potential of the reference electrode. Counter electrode serves as a source or sink for electrons.[11] Due to its inert character platinum wire is commonly used as counter electrode in electrochemical measurements.

1.1.2 Chemically modified electrodes (CMEs)

The progress and wide–spread use of CMEs has created a variety of new and potentially powerful avenues in the field of electroanalysis. Before 1970's, electrochemistry was confined with electrode materials like C, Pt,

Hg and Au. By the functional group transformation to SnO_2 and Pt-OH Murray and coworkers opened the field of CMEs.[12]

Direct electrochemical determinations at conventional electrodes generally face problems such as high overpotential, sluggish electrode kinetics, fouling of electrode surface, little selectivity and poor sensitivity.[13] Fouling of the electrode surface, due to the adsorption of analyte molecules or their reaction products, is the main drawback of bare electrodes, which greatly affect the stability of electrode response. These drawbacks could be minimized by changing the surface of electrode with suitable modifier. Through surface modification, we can exert more direct control over the chemical nature of an electrode surface. One of the most distinguishable features of CMEs is their capability to catalyze the electrode process via considerable decrease of overpotential in comparison with unmodified electrodes. These electrodes can significantly enhance the selectivity in the electroanalytical methods by facilitating selective interaction of the electron mediator with the target analyte.

All the important analytical parameters of the electrodes such as sensitivity, selectivity, reproducibility and even applicability are found to be enhanced by the careful use of modifiers. These remarkable properties of surface modified electrodes have been exploited in many different ways to yield amazing and exciting results.

Electrodes are usually chemically modified by the following approaches

1.1.2.1 Silanization

Due to the sensitivity of silane compounds to water, electrode modification with these reagents is possible. The electrode surface is pretreated with concentrated NaOH or atmospheric oxygen which produces

surface hydroxyl groups. This hydroxyl groups react with trialkoxy or trichloro silanes to form one to three bonds with the electrode surface.[14]

1.1.2.2 Sorption

Physical and chemical interaction properties are utilized in the formation of sorption-based CMEs. Easy modification of electrode and functional group attachment are the main advantages of this method. Sorption may be either physisorption or chemisorption.

(a) Physisorption

Many substances spontaneously adsorb on electrode surface from solution, generally because the environment is energetically more favorable than the solution. Pure organic or organometallic complexes can be physisorbed on porous carbon bases like graphite and ordinary pyrolytic graphite by simple coating with nonaqueous solution followed by droplet evaporation. Carbon nanotubes (CNT), a fast developing nano material adsorbed on the electrode surface in the same way by simple drop casting.[15]

(b) Chemisorption

Stability is always a serious problem of physisorbed systems even though they are useful for analytical applications. By a chemisorbed route, the stability problem can be solved. A good example is self-assembled monolayers (SAMs) of organosulphur compounds with long chain groups on gold electrode.

1.1.2.3 Covalent binding

Stronger attachment to the electrode surfaces can be accomplished by covalent linking of the desired component to surface groups present on the electrode surface to form a monolayer. Functionalization of the electrode

surface enables the formation of covalent bonds with molecules, through chemical reaction. Carbon surface is found to be efficient for the covalent modifications due to its alterable functionalities.[16] Monolayer coverage sometimes can restrict the amount of active species at the electrode surface is the limitation.

1.1.2.4 Polymer layer

Polymer based multilayer CMEs provide an attractive route to resolve the problem due to the monolayer coverage. Modification of electrode by polymeric films is a fascinating branch in electroanalytical chemistry.

Polymer film can be introduced on the electrode surface by the following methods

a) Dip casting- the electrode is dipped into a solution containing a dissolved polymer and allowing the solvent to evaporate.

b) Droplet evaporation- a droplet of polymer solution is applied to the electrode surface and the solvent is allowed to evaporate.

c) Spin coating- a droplet of a dilute solution of the polymer is applied to the surface of a rotating electrode. Excess solution is spun off the surface and the remaining thin polymer film is allowed to dry. Multiple layers are applied in the same way until the desired thickness is obtained.[17]

d) Electrochemical polymerization- a solution of monomer is oxidized or reduced to an activated form that polymerizes to form a polymer film directly on the electrode surface under the influence of applied potential.

e) Radiofrequency polymerization- vapors of the monomer are exposed to a radiofrequency plasma discharge. The high energetics of the radiofrequency discharge may result in chemical damage, thereby producing functionalities and structural modifications to the polymer.[17]

1.1.2.5 Electrodeposition

Adsorption is carried out under the influence of an applied potential and a uniform film is obtained. Electrodeposition of metal nanoparticles on the electrode has been found very beneficial in the field of electroanalysis. One of the most significant advantages of electrochemical deposition is the ability to control size and distribution of nanoparticles by varying potential, time or concentration of solution.[18]

1.1.2.6 Langmuir-Blodgett method

Langmuir-Blodgett assembly technique offers a versatile way to prepare modified electrodes. Attractive noncovalent interactions hold the film in a cohesive unit on the electrode surface. However the weak nature of these forces limits layer stability.

In the present work, carbon nanotube (CNT), conducting polymer and gold nanoparticle were used as modifiers for the fabrication of CMEs.

1.1.3 Carbon nanotubes

Recently, nanomaterials have received tremendous interest in different areas due to their versatile applications in the fields of physics, chemistry and materials science. The discovery of carbon nanotube (CNT) in 1991 by Lijima, is an important milestone in the world of scientific research which gave rise to a

new era in material science and nanotechnology. Currently, the study of CNT modified electrode is a forefront topic of research that offers enormous possibilities in the field of electorchemical analysis. The ease of its preparation and functionalization of CNTs makes them potential material for the fabrication of chemically modified electrodes. Due to the faster electron transfer rate over other carbon based materials, CNTs exhibit excellent electrocatalytic activity in the voltammetric response of various compounds.

The first ever application of CNTs in electrochemistry was carried out by Britto *et al*. Since then there has been numerous reports of fabrication of voltammetric sensors with CNTs.[19] Carbon nanotubes are molecular scale wires which are several nanometers in diameter and many microns in length with hexagonal honey comb lattices built from 'sp^2' carbon units. Owing to their special properties such as high electrical and thermal conductivity, good chemical stability, excellent mechanical strength, large specific surface area, excellent biocompatibility, flexible surface chemistry, ability to accelerate electronic transfer etc. CNTs behave as excellent materials for sensor fabrication.[20,21] Depending on the diameter and the degree of helicity, CNTs behave as either metals or semiconductors. CNTs are half-fullerene-like molecule with closed structures, having topological defects. The two regions of CNTs; the tube and the cap have different properties. Chemical and physical treatments cause the formation of edge-like defect sites and oxygen containing functional groups at both the caps and side walls resulting in a significant enrichment of the sensing application of CNTs. Among the two forms of CNTs (single walled and multi walled

CNTs), MWCNT has greater application because they can be prepared in bulk in the presence of a catalyst with high purity.[22]

The chief advantage of the incorporation of CNTs in electrochemical sensors is the significant reduction in overpotential and improvement of sensitivity. Compton's group proposed that the enhanced electrocatalytic activity of CNTs is due to the occurrence of edge-plane like sites located at the end and in the "defects" areas of the tubes.[19,21] Ab-initio calculations verified that the curvature of the tubes which creates changes in the energy bands close to the Fermi level is responsible for the enhanced electron transfer capacity of CNTs.[23] CNTs have huge length to diameter ratio which allows them to be used as molecular wires for facilitating electron transfer between analyte and electrode. Hence they are extensively used as the carrier platforms for fabricating electrochemical sensors.

The above mentioned outstanding properties of CNTs make them an exciting alternative for the construction of novel electrochemical sensors. High signal to noise ratio, reduction of overpotentials, high sensitivities, and resistance to surface fouling are the highlights of analytical sensing using CNTs based electrodes.

1.1.4 Conducting polymers

Extensive research on the 'conducting polymer' (discovered in 1963) was initiated by Mac Diarmid in 1976 for their possible applications in sensors, energy storage and actuators.[24,25] They have numerous analytical and technological applications on account of their conducting properties and unique chemical and biochemical properties. Their straight forward

preparation methods, unique properties and stability in air make conducting polymers an attractive material in electroanalysis.

Polymer-modified electrodes (PMEs) have received enormous interest in the electroanalytical field due to their advantages such as excellent selectivity, sensitivity and homogeneity in electrochemical deposition, strong adherence to electrode surface and chemical stability of the film.[26-28] The exciting properties such as high mechanical flexibility, electrical conductivity and ability to be electrochemically switched between electronically insulating and conducting states makes conducting polymers an important material for sensing devices. A thin film of conducting polymer, deposited onto the surface of a conventional electrode is able to improve the kinetics of electrode reaction.[29]

Conducting polymers (CPs) exhibit fascinating electrochemical and optical properties due to the presence of delocalized π electrons which can move around the whole system and become the charge carriers to make them conductive.[30] Electropolymerisation of a variety of monomers onto high-work function electronic conductors such as platinum, gold and carbon produce an ideal platform for the sensing of numerous chemical and biological analytes. The important feature of CPs used in amperometric and voltammetric sensors is their ability to behave as electron transfer mediators. Depending on the charge, size and chemical structure of the analyte (guest) as well as the conducting polymer (host) electroactive species may go into the polymer film, resulting the preconcentration of compounds before electrochemical oxidation or reduction.[31]

1.1.5 Gold nanoparticles

Nowadays, the incorporation of nanoparticles on to the sensor design has been attracting great interest because of the exciting new opportunities that they offer to the field of sensing. Because of their fascinating properties, nanoparticles have found broad range of applications in a variety of areas including clinical diagnostic, food safety and environmental protection. Metal nanoparticles are usually used for signal amplification in electrochemical sensors as its large surface area provides greater number of binding sites available for the detection of a particular analyte.[32] Gold nanoparticles (AuNPs) exhibit interesting physical, chemical and electronic properties such as size and shape dependent surface plasmon resonance, high surface energy and surface to volume ratio and tunable surface properties.[33,34] Due to their catalytic properties, AuNPs are extensively used in electrochemical sensors to enhance the performance of the analytical device.

The first ever preparation of colloidal gold was carried out by Faraday during 19th century.[35] Nowadays, the commonly used methods for the synthesis of gold nanoparticles are the Turkevich[36] (1951) and Frens[37] (1973) methods. Functionalized AuNPs simplifies the sensor design by improving the sensitivity and can function as both molecular receptor and signal transducer in a single sensing platform. AuNPs in electrochemical sensors takes the role of "electron antenne" which effectively tunnel electrons between electrode and the analyte and thus shows exceptional electrocatalytic activity towards various analytes.[38] Different methodologies such as the anchoring by electrostatic interaction, covalent linkage, electrochemical deposition etc. have been used for the tailoring of AuNPs on electrode surfaces.[39]

1.1.6 Mass transport processes

1.1.6.1 Diffusion

Diffusion occurs in solutions where there is an uneven concentration of reagents. Balancing the uneven distributions of concentration, maximizes the entropy which is the main driving force for the process.[40]

1.1.6.2 Convection

This is a process in which the species is transferred from one part of the solution to the other part by the mechanical motion of solution itself (as a result of pumping, flowing, vibrating, stirring etc.).

1.1.6.3 Migration

The movement of ions under the influence of electric field is called migration. By the application of potential to an electrode, a charged interface will be created. This can either attract or repel charged species near the interface by an electrostatic force.

1.1.7 Voltammetric techniques

Linear sweep voltammetery, square wave voltammetry, differential pulse voltammetry, cyclic voltammetry, electrochemical impedance spectroscopy and chronoamperometry were used for the development of sensors and extraction of kinetic parameters of electrode processes.

1.1.7.1 Linear sweep voltammetry

Linear sweep voltammetry (LSV) is one of the simplest voltammetric techniques, in which potential applied to the working electrode is swept linearly with time. The main difference between cyclic voltammetry (CV) and LSV is that in LSV, the potential is swept linearly only in one direction

while in CV potential is scanned in the reverse direction also. Hence LSV technique is mainly applied to study irreversible reactions.

1.1.7.2 Differential pulse voltammetry

Differential pulse voltammetry (DPV) is a popular technique for measuring trace amounts of inorganic and organic species. Fixed magnitude pulses (superimposed on a linear potential ramp) are applied to the working electrode. Current is measured twice (1) just before the application of pulse and (2) at the end of the pulse. The first current is instrumentally substracted from the second and the resulting current is registered in the output signal.[41]

1.1.7.3 Square wave voltammetry

Square wave voltammetry (SWV) is an excellent tool to study the mechanisms of electrode processes and kinetic parameters.[42] Square wave voltammetry can be used to perform an experiment much faster than normal and differential pulse techniques.

1.1.7.4 Cyclic viltammetry

Cyclic voltammetry (CV) has become an important and widely used electroanalytical technique for initial electrochemical studies of new systems and has proven very useful in providing information about fairly complicated electrode reactions.[43] CV has been applied to investigate multistep electrode processes and those involving coupled homogeneous reactions. It is also employed to study the presence of intermediates in redox reactions, electron transfer kinetics and reversibility of a reaction. Conventional CV is principally informative about the qualitative aspects of an electrode process since the response waveform provides poor information about quantitative parameters.[44]

CV is a kind of potentiodynamic technique in which the potential of the electrode is ramped linearly vs time.[45] In CV technique, a triangular potential sweep is applied to the working electrode whereby the initial potential rise to a final potential, and returns back to the starting potential. Starting from an initial potential $E_{i,}$ a staircase potential sweep is applied to the working electrode in CV. After reaching a switching potential E_f, the sweep is reversed and potential ramped to its initial value. The shape of cyclic voltammograms revealed the type of electrode reaction and about the additional phenomena coupled to the electrochemical reaction.[46]

In a cyclic voltammogram the current is plotted against the applied voltage of the working electrode. If there are reducible species in the system, as the potential is increased in the forward scan, the cathodic current increase over this time. Since the concentration of the reducible species is depleted after the reduction potential of the species is reached, the cathodic current will decrease. If the reaction is reversible, during the reversible scan the reduced species will start to be re-oxidized, giving rise to an anodic current having reverse polarity to before. In fact, CV is a simple extension of the linear sweep voltammetric technique. CV is a commonly used technique in electrochemical analysis for the evaluation of mechanism of charge transfer reactions and the measurement of kinetics of electrode reactions.

1.1.7.4.1 Reversible systems

When the electrode kinetics is much faster than the rate of diffusion, such systems are described as "reversible". The Nernst equation is the final boundary condition for a reversible system.

$$E_e = E_e^0 + \frac{RT}{nF} ln \frac{C_o}{C_R}$$

where E_e and E_e^0 are the equilibrium potential and standard potential. n is the number of electrons involved in the electrochemical reaction. R, T and F have their usual meaning. C_o and C_R represents the surface concentrations of the oxidized and reduced species. The peak current is given by Randles Sevcik equation

$$i_p = (2.69 \times 10^5) n^{3/2} A D^{1/2} C v^{1/2}$$

where A refers to the surface area of electrode (in cm^2), D refers to the diffusion coefficient (in cm^2s^{-1}), C refers to the concentration (in $molcm^{-3}$) and v refers to the scan rate (in Vs^{-1}). The separation of the peak potentials, ΔE_p ($E_{pa} - E_{pc}$), is the most important parameter in CV which can be used to calculate the reversibility of the electrode process. The peak potential separation for a reversible electron transfer reaction is expressed as

$$\Delta E_p = E_{pa} - E_{pc} = 2.218 \frac{RT}{nF}$$

The numerical value of ΔE_p at 298 K is approximately 59 mV. Another important parameter of reversible systems is the ratio of the peak currents, which is one. For reversible systems both the peak potential separation and the ratio of the peak currents are independent of scan rate. The formal potential which provides valuable thermodynamic information related to the electrode process, is calculated from the average of the cathodic and anodic peak potentials for a reversible system

$$E^0 = \frac{(E_{pa} + E_{pc})}{2}$$

This parameter is specific for the system studied, but independent of the concentration of the substance studied.

1.1.7.4.2 Irreversible systems

When the electrode kinetics are slower than the rate of diffusion the system is termed as "*irreversible".* The peak potential separation and the ratio of the peak currents are dependent of scan rate in irreversible systems. For totally irreversible systems the peak potential shifted with scan rate.

The equilibrium between the oxidized and reduced species is not maintained at the surface of electrode in the case of irreversible systems, hence the Nernstian boundary condition is substituted by kinetic boundary condition

$$\frac{i}{FA} = D\left[\frac{\partial C_0(x,t)}{\partial x}\right]_{x=0} = k_f(t)C_0(0,t)$$

where k_f is the rate constant of forward reaction.

The peak current for a irreversible system is expressed as

$$i_p = (2.99 \times 10^5)\alpha^{1/2}AC_0D^{1/2}v^{1/2}$$

where α is the charge transfer coefficient.

1.1.7.4.3 Quasi- reversible systems

Matsuda and Aybe introduced the new term '*quasi-reversible'* for reactions that show electron-transfer kinetic limitations. These systems are intermediate between reversible and irreversible systems. Both charge transfer and mass transfer controls the current in a quasi-reversible system.[47]

The boundary condition is given by

$$\boldsymbol{D_0\left(\frac{\partial C_0(x,t)}{\partial x}\right)_{x=0} = k^0 e^{-\alpha f[E(t)-E^0]}\left\{C_0(0,t) - C_R(0,t)e^{f[E(t)-E^0]}\right\}}$$

where $f = \frac{F}{RT}$ and $\psi(E)$ is a function of quasi reversible system. The peak current is given by the following equation

$$\boldsymbol{i = FAD^{1/2}C_0 f^{1/2} v^{1/2}\,\psi(E)}$$

1.1.7.4.4 Kinetics of electrode reaction

Consider the following reversible reaction

$$\boldsymbol{O + ne^- \rightleftharpoons R}$$

Butler-Volmer formulation of electrode kinetics can be applied to describe the kinetics of electrode reaction,[48] the anodic and cathodic rate constants are expressed by

$$\boldsymbol{k_a = k_0 exp[\alpha_a nF(E - E^{0\prime})/RT]}$$

$$\boldsymbol{k_b = k_0 exp[\alpha_c nF(E - E^{0\prime})/RT]}$$

where k_0 is the standard rate constant and $E^{0\prime}$ is the formal potential of the redox system. $\alpha_a$and α_c represents the cathodic and anodic charge transfer coefficients respectively.

The total current at the electrode surface under kinetic control is given by

$$\boldsymbol{I = I_a + I_c = nFA(k_a[R] - k_c[O])}$$

where I_a and I_c denotes the anodic and cathodic peak currents.

1.1.7.5 Electrochemical impedance spectroscopy

Electrochemical impedance spectroscopy (EIS) offers significant contributions in fields such as electrocatalysis, sensors, semiconductors, corrosion and dielectrics as well as in the rapidly growing fields of nanomaterials and nanotechnology, energy storage and conversion. EIS is a powerful and sensitive tool for examining charge transfer properties and mechanisms of electrochemical reactions occurring at the electrode/ electrolyte interphase.

In recent years, popularity of EIS methods has increased tremendously in the arena of electroanalytical chemistry because it can provide more accurate kinetic and mechanistic informations with less error. Since small amplitude excitation wave forms are used in EIS, only minimal perturbation occur in the electrochemical system thereby reducing errors caused by measurement technique. In the initial stages, EIS technique was generally used for the determination of double-layer capacitance and in ac polarography.[49,50] Now they are applied to study complex interfaces and for the characterization of electrode processes.

Both the terms impedance and resistance represents an opposition to the flow of current. In DC circuits only the resistor is responsible for the resistance, while in AC circuits capacitors and inductors, impede the flow of electrons. In such cases, the term impedance is used and it can be denoted by a complex number where the resistance is the real component and the combined capacitance and inductance is the imaginary component. In the electrochemical cells slow electrode kinetics, slow proceding chemical reactions, diffusion etc. impede the flow of electrons, and can be considered

similar to the resistors, inductors and capacitors that impede the electric current in AC circuits. In otherwords, Impedance is the opposition to the flow of electrical current in a complex system.[51]

EIS technique measures the variation of the impedance of the electrochemical cell with the frequency of a small amplitude AC perturbation. The time domain of the input and output signals are converted into a complex quantity which is a function of frequency.

EIS data for electrochemical reactions are most often presented in Nyquist and Bode plots of which Nyquist plots are more popular. Bode plots depicts the real or imaginary components of the impedance and phase angle as a function of frequency. Nyquist plot represents the imaginary impedance (indicative of the capacitative and inductive character of the cell) versus the real impedance of the cell. In a typical Nyquist plot, Z' represents the real part of measured impedance and Z" represent the imaginary part of the measured impedance. The real and imaginary components of the impedance data provide useful information about the kinetic and mass transport properties of the reaction. The Nyquist plot consists of a semicircular part at higher frequencies and a straight line at lower frequencies.

1.1.7.6 Chronoamperometry

Chronoamperometry is an important electroanalytical tool for the determination of diffusion coefficients and for studying kinetics and mechanisms of redox reactions. Chronoamperometry is also useful for determining the catalytic rate constant of electrochemical reactions. Another application of chronoamperometry is the estimation of electrode area, by the use of well defined redox couple (known D and C).

Chronoamperometry is an electroanalytical technique, which involves the application of a step potential and the measurement of current as a function of time using the same three electrode cell configuration as with voltammetry. The resulting current – time relationship is recorded which represents the change in concentration of electroactive species at the surface of electrode since the mass transport process during the reaction is governed by diffusion. The observed i-t response is a result of two components: one due to the charging the double layer and the other due to the faradaic current (due to electron transfer reaction between the electroactive species and electrode). As time progress, there is a continuing growth of diffusion layer coupled with the depletion of reactant and there is a decrease in the concentration gradient. Like other pulsed techniques, chronoamperometry generates high charging current, which decay exponentially with time.[52]

The variation of current as a function of $t^{-1/2}$ is described by Cottrel equation[53]

$$\boldsymbol{I = nFAD^{1/2}C\pi^{-1/2}t^{-1/2}}$$

where n is the number of electrons involved in reaction, A is the surface area of electrode, F is the Faraday's constant, D is the diffusion coefficient of electroactive species and C is the concentration of electroactive species.

Two types of chronoamperometric techniques are usually employed in electroanalytical field- the single potential step or the double potential step chronoamperometry. Measurements are carried out using planar electrodes, in unstirred condition and a potential sufficient to oxidize or reduce the electroctive species is applied. The potential of the working electrode is stepped from a value at which no electrochemical reaction occurs (E_1) to a

potential at which surface concentration of analyte is effectively zero (E_2). When potential goes from its initial value, the reaction occurs and current rapidly reaches its maximum value. In the end current decrease to zero value due to the increase of thickness of diffusion layer and depletion of electroactive species. Compared to other amperometric techniques, better signal to noise ratio is observed in chronoamperometry.[54]

1.1.8 Literature review of electrochemical sensors based on carbon nanotubes, conducting polymers and gold nanoparticles

The voltammetric behavior of butylated hydroxyanisole (BHA) has been studied by Rasheed *et al*. at MWCNT modified platinum electrode.[55] 0.1 M phosphate buffer solution of pH 4 was used as supporting electrolyte. Linear relation between the concentration of BHA and oxidation peak current was obtained in the range 1.00×10^{-6} to 1.00×10^{-7} M. The detection limit of the developed sensor was 9.49×10^{-8} M. The sensor was found to be tolerant against the high concentrations of common coexisting species. This method was successfully applied for the determination of BHA in commercially available vegetable oil and mayonnaise samples, providing a promising and effective method to monitor the large scale use of this synthetic phenolic antioxidant.

Electrochemical response of amaranth, an artificial colourant, was studied on a MWCNT film modified gold electrode in acetate buffer solution (pH 5) by Chandran *et al*.[56] On the MWCNT modified electrode, a well defined anodic peak was observed at 792 mV for the oxidation of amaranth. Experimental conditions for the sensor fabrication were optimized. Under optimum conditions, linear range and limit of detection of the

MWCNT modified gold electrode sensor was found to be from 1.00×10^{-5} to 1.00×10^{-6} M and 6.81×10^{-8} M respectively. Practical application of the proposed method was demonstrated by the determination of amaranth in soft drink samples and the recoveries were compared with spectrophotometric method.

Moheimanian and coworkers fabricated a novel voltammetric sensor for nitrite by the immobilization of hemoglobin and octylpyridinium chloride on MWCNT modified electrode.[57] The electrochemical behaviour of nitrite on modified electrode was studied by amperometry and CV. The linear concentration range was from 1.52×10^{-4} to 1.00×10^{-5} M, with a detection limit of 1.46×10^{-6} M. Influence of foreign compounds on the determination of nitrite was studied. The developed method showed low detection limit, fast response and excellent sensitivity.

Wu *et al*. reported a simple and sensitive electrochemical method for the determination of sudan I using a glassy carbon electrode (GCE) modified with a chitosan/carbon nanotube composite.[58] At the MWCNT/ chitosan-modified GCE, sudan I showed oxidation peak at 720 mV. Various experimental conditions such as pH, scan rate and chitosan: MWCNT mass ratio at the modified electrode were optimized. The detection limit of the developed sensor was found to be 3.00×10^{-8} M.

A sensitive electrochemical sensor for neotame, an artificial sweetner, was reported by Bathinapatla *et al*. based on nanoparticles modified electrode.[59] Copper nanoparticles decorated MWCNTs were used for the surface modification of GCE and an oxidation peak was observed at 1300 mV in pH 3 on the modified electrode. The modified electrode showed excellent

catalytic property towards the oxidation of neotame. Various techniques such as transmission electron microscopy (TEM), Fourier transform infrared specrosopy (FTIR), thermogravimetric analysis and CV were used to characterize the developed sensor. Practical application of the developed sensor in food samples were carried out and good results were obtained compared to capillary electrophoresis method with a confidence level of 96%.

A new voltammetric method for simultaneous determination of tert-butylhydroquinone (TBHQ) and BHA in biodiesel was developed by Caramit *et al*.[60] MWCNT modified screen printed electrode was employed for the simultaneous detection and quantification of TBHQ and BHA. The electrochemical measurements were carried out in Britton–Robinson buffer (0.04 M) containing 2.0% methanol and the cationic surfactant cetyltrimethylammonium bromide. The addition of surfactant increases the peak current and resolution of voltammetric response. The modified electrode showed a linear response in the concentration range of 1.00×10^{-5} M to 5.00×10^{-7} M for TBHQ and BHA with detection limits of 3.40×10^{-7} M and 1.76×10^{-7} M, respectively. The developed method was effectively applied for the determination of TBHQ and BHA in biodiesel samples with recoveries in the range 97 – 110 % and 91 - 101 %, respectively. Also the results are compared with high-performance liquid chromatography (HPLC) and satisfactory results were obtained.

Thomas *et al*. investigated the electrochemical response of TBHQ on MWCNT modified gold electrode (GE) using CV.[61] TBHQ exhibited redox behaviour on MWCNT/GE in 0.10 M phosphate buffer solution of pH 2.

The reversible oxidation of TBHQ occurred at a lower potential on the modified electrode compared to the bare GE. This lowering of oxidation potential of TBHQ proved the electrocatalytic effect of MWCNT. Based on this a sensitive voltammetric sensor was fabricated for TBHQ. The linear range and limit of detection of the sensor was 1.00×10^{-4} to 4.00×10^{-6} M and 3.24×10^{-8} M respectively. The proposed method was employed for the quantification of TBHQ in coconut oil samples and the results are compared with the standard method.

Caramit *et al*. successfully employed MWCNT coated GCE for the simultaneous determination of synthetic food colourants sunset yellow and tartrazine based on the unique properties of MWCNT film.[62] MWCNT dispersed in water by the addition of surfactant dihexadecyl hydrogen phosphate. The anodic peak currents of sunset yellow and tartrazine enhanced remarkably owing to the significant features of MWCNT such as large surface area, high sorption capacity and subtle electronic properties. The detection limits for sunset yellow and tartrazine were determined to be 2.21×10^{-8} M and 1.87×10^{-7} M respectively. The developed sensor was used to determine sunset yellow and tartrazine in soft drink samples.

A simple electrochemical sensor was developed by Zhang *et al*. for the monitoring of ponceau 4R and allura red using MWCNT film modified electrode as the sensing element.[63] Electrochemical behaviour of ponceau 4R and allura red was studied in phosphate buffer solution (pH 7). Oxidation signals of ponceau 4R and allura red increased remarkably on MWCNT film sensor due to its high surface area and large accumulation efficiency. The sensor parameters were optimized which includes accumulation potential and

time, amount of MWCNT and pH. Detection limit of 2.53×10^{-5} M for ponceau 4R and 5.06×10^{-5} M for allura red was obtained using the proposed sensor. The determination of ponceau 4R and allura red was successfully carried out using MWCNT sensor in various soft drinks.

The electrochemical oxidation of amaranth, a widely used food colour was investigated at MWCNT modified GCE by Wang *et al.*[64] Various operational conditions were optimized and the calibration graph was linear in the concentration range 0.82×10^{-6} M to 4.00×10^{-8} M with a limit of detection 3.56×10^{-8} M. Application studies were carried out in commercially available soft drink samples and the recoveries were compared with HPLC.

CNT modified GCE was employed for the electrochemical determination of phenolic antioxidants like hydroquinone, catechol, pyrogallol and its derivatives by Ziyatdinova *et al.*[65] Atomic force microscopic technique was used for the characterization of modified electrode surface. Surface roughness of the modified electrode increased by a factor of 20 fold and high degree of homogeneity obtained upon modification with nanotubes. Phosphate buffer solution of pH 7.4 was used as a supporting electrolyte in voltammetric studies.

Electroreduction of synthetic food colourants such as tartrazine, sunset yellow and allura red was investigated on polyallylamine modified tubular electrode by Silva *et al.*[66] Prevention of surface fouling and enhanced intensity of voltammetric signal were the advantages of polymer modified electrode. For the referred colourants a linear concentration range up to 2.00×10^{-4} M was found using the polyallylamine modified tubular electrode with a limit of detection of 1.80×10^{-6} M for tartrazine, 1.40×10^{-6} M

for allura red and 3.51×10^{-6} M for sunset yellow. The modified electrode was successfully used for the analysis of these colourants in different food samples and satisfactory results were obtained compared to HPLC.

Zhang and coworkers fabricated an electrochemical sensor for sunset yellow by polymerizing L-cysteine on the surface of GCE.[67] The chemically modified electrode was characterized by the techniques like CV and EIS. CV and chronoculometry was used to investigate the electrochemical behavior and kinetic parameters of sunset yellow. The sensor exhibited a working linear range $7.00 \times 10^{-7} – 8.00 \times 10^{-9}$ M. The minimum detectable concentration of sunset yellow using this method was found to be 4.00×10^{-9} M. The developed sensor has advantages such as extreme simplicity, high sensitivity, low cost, good stability and reproducibility.

Electrochemical behavior of vanillin was studied on a poly(valine) modified electrode using CV.[68] It was observed that in phosphate buffer solution (pH 7), the oxidation peak current is linearly proportional to concentration of vanillin over the range of 6.61×10^{-5} - 9.60×10^{-8} M, with a limit of detection of 1.00×10^{-8} M. This method is simple, highly sensitive and shows good reproducibility. The proposed method has been efficiently applied for the determination of vanillin in infant formula samples.

Poly(L-cysteine) film modified electrode was fabricated by electropolymerization technique and effectively used as a sensor for ascorbic acid by Zhengz *et al*.[69] The anodic peak potential of ascorbic acid shifted negatively along with an enhancement in peak current, on poly(L-cysteine) modified electrode compared to bare GCE. This proved the efficient electrocatalytic property of polymer film to the oxidation of ascorbic acid.

The anodic peak current of ascorbic acid varied linearly with its concentration over the range from 5.00×10^{-4} to 1.00×10^{-6} M. The limit of detection was calculated to be 4.00×10^{-7} M.

Ma *et al.* reported a sensitive electrochemical sensor for sudan II based on poly(aminosulfonic acid) modified GCE using CV.[70] Electrochemical polymerization technique was effectively employed for the construction of modified electrode. The polymer layer enhanced the voltammetric redox signal of sudan II through its electrocatalytic effect. The sensor exhibited two dynamic linear ranges 1.00×10^{-6} - 4.00×10^{-8} M and 1.21×10^{-5} - 1.00×10^{-6} M respectively. The detection limit of the proposed sensor was found to be 4.00×10^{-9} M.

Polydiphenylamine platinum composite modified GCE was prepared by electrochemical method and used for the successful determination of nitrite by Unnikrishnan *et al.*[71] EIS and scanning electron microscopy were used for characterization studies. Cyclic voltammogram of nitrite showed an anodic peak at 850 mV due to the irreversible oxidation of nitrite which 330 mV lower than that on bare GCE. The sensor exhibited a wide range of detection from 9.51×10^{-3} to 1.00×10^{-6} M. Several water samples were tested to check the application of the sensor and good recoveries were achieved.

Divya *et al.* studied the electrochemical behaviuor of BHA at a GCE modified with poly(L-cysteine).[72] BHA showed a pair of well defined redox peaks on the polymer modified electrode with E_{pa} = 69 mV and E_{pc} = 4 mV. Under optimal conditions, poly(L-cysteine) modified electrode exhibited a linear response in the range from 1.00×10^{-5} M to 1.00×10^{-6} M with

a correlation coefficient of 0.998. The detection limit was found to be 4.11×10^{-7} M. Kinetic parameters for the electrochemical redox process were evaluated and the average surface concentration of BHA on the modified electrode was calculated. The analytical application of the proposed method was evaluated by the effective quantification of BHA in coconut oil and seasame oil samples.

Jing studied the oxidation behaviour of nitrite on a GCE chemically modified with gold nanoparticles-polypyrrole nanocomposite.[73] CV, DPV and chronoamperometric techniques were used for the determination of diffusion coefficient, electron transfer coefficient and charge transfer rate constant. Reduction of the oxidation overpotential and enhancement in peak current indicated that gold nanoparticles-polypyrrole nanocomposite has excellent electrocatalytic activity for the oxidation of nitrite. The linear dependency of peak current vs concentration of nitrite was in the range 2.51×10^{-3} M to 8.00×10^{-7} M with a detection limit of 1.00×10^{-7} M. The practical utility of the nanocomposite sensor was established by the determination of nitrite in water samples. The developed sensor exhibited good sensitivity, reproducibility and excellent stability.

Electrocatalytic determination of nitrite was carried out on Fe_3O_4 nanoparticles/poly(L-cys) /MWCNTs/GCE in PBS (pH 5.5) by Qu *et al.*[74] Cyclic voltammetric studies were performed to investigate the electrochemical behaviour of nitrite on the sensor. The oxidation peak current of nitrite increased linearly with concentration in the range 3.32×10^{-3} to 7.57×10^{-6} M (R = 0.9998), under optimized conditions. The developed sensor has potential applications due to its good sensitivity, stability and repeatability.

Ghoreishi *et al*. proposed AuNPs modified carbon paste electrode as an effective sensor for the determination of sunset yellow and tartrazine, which has potential harmfulness to human health.[75] Two well resolved oxidation signals for sunset yellow and tartrazine was obtained at modified electrode using DPV and CV. AuNPs based carbon paste electrode has high selectivity and sensitivity, sub micromolar detection limit and excellent reproducibility. The developed sensor exhibited a detection limit of 3.00×10^{-8} and 2.00×10^{-9} M for sunset yellow and tartrazine respectively, which is lower than the previous reports.

Based on the electrocatalytic activity of AuNPs deposited on GCE, Thomas *et al.* developed an electrochemical sensor for sudan I in food samples.[76] Voltammetric response of sudan I was studied by CV and SWV. The nanoparticle modified electrode exhibited a pair of well-defined quasi-reversible redox peaks with a formal potential of 295 mV at a scan rate of 100 mV/s. The sensor exhibited two linear response ranges 1.00×10^{-3} – 4.00×10^{-5} M and 2.00×10^{-5} – 7.00×10^{-7} M. The kinetic parameters such as the number of electrons, the electron transfer coefficient and the standard rate constant were determined. Also the surface coverage of sudan I on the modified electrode was calculated. The proposed sensor has been successfully used to determine sudan I in ketchup and chilly sauce.

Zhang *et al*. applied AuNP/MWCNT composite film modified GCE for the voltammetric determination of vitamin B_6.[77] Surface morphology of the modified electrode was studied by SEM analysis. Vitamin B_6 exhibited an irreversible oxidation peak at 620 mV in 0.1 M phosphate buffer solution (pH 7). The oxidation peak current was linearly proportional to the

concentration of vitamin B_6 in the range $6.13 \times 10^{-4} – 9.46 \times 10^{-6}$ M with a detection limit of 3.32×10^{-6} M. Nano composte film modified electrode has good stability and reproducibility. The developed method has potential application in the field of pharmaceutical analysis.

Electrochemical behaviour of meclofenoxate hydrochloride was studied by Zhu *et al.* on a AuNP/CNT modified GCE.[78] Atomic force microscopy was used for the characterization of the modified electrode. The nanocomposite film exhibited good electrocatalytic ability towards the oxidation of meclofenoxate hydrochloride with high sensitivity and stability. The peak current showed a linear relationship with concentration in the range of 2.00×10^{-5} - 5.00×10^{-7} M, with the detection limit of 1.00×10^{-7} M. The electrochemical oxidation mechanism of meclofenoxate hydrochloride involves the transfer of two protons and two electrons. The developed sensor was employed to determine the meclofenoxate hydrochloride concentrations in capsule and tablet. The results were validated with HPLC.

Shahrokhian *et al*. fabricated a novel voltammeric sensor for cefotaxime based on GCE modified with AuNP/MWCNT film.[79] The modified electrode was prepared by the electrodeposition of AuNP on a MWCNT/GCE. Drop casting method was used for the incorporation of MWCNT film on GCE surface. EIS, CV and SEM were employed for the characterization studies of modified electrode. The influence of pH of electrolyte, electrodeposition condition, accumulation time and scan rate on the electrochemical response of cefotaxime was studied and the experimental conditions were optimized. The linear range and limit of detection of the sensor was $8.00 \times 10^{-5} – 4.00 \times 10^{-8}$ M and 4.00×10^{-9} M respectively. Satisfactory

results were obtained when the proposed method was applied for the determination of cefotaxime in pharmaceutical and clinical samples.

1.2 Optical sensors

An optical sensor measures the changes in optical properties, as a result of chemical interaction between recognition element and analyte by spectrophotometry. Colourimetric sensors and fluorescence sensors comes under the category of optical sensors.

Many materials especially nanoparticles undergo colour changes in response to stimuli (after exposure to some analytes), making them attractive candidates for use as sensor platform. Analyte induced aggregation of nanoparticles results a significant change in absorbance (colour) which can be employed for the sensing application.

Fluorescence involves the emission of photons, that occurs nanoseconds after the absorption phenomenon. Luminescent materials (fluorophores) act as recognition probe in fluorescence sensors. Interaction of analyte alters either the electronic structure or molecular structure of the fluorophores, which causes changes in the intensity or wavelength of light emission.[80] Many features like simplicity, versatility and excellent sensitivity make fluorescence one of the most powerful transduction mechanisms to report the chemical recognition event.

1.2.1 Jablonsky diagram or electronic transition diagram

When a molecule absorbs a photon, electrons are promoted from the singlet ground electronic level S_o to an excited state S_n. A molecule in the

excited state can return to the ground state by following two successive steps (Figure 1.1)[81]

1) Internal conversion - the phenomenon of nonradiative transition, from a higher excited state (S_n) to a lowest excited state (S_1) of a molecule by dissipating a part of its energy to the surrounding environment. This occurs when a vibrational state of an excited electronic state coupled to the vibrational state of a lower electronic state. This type of nonradiative transition is not observed in isolated molecules since this process involves the dissipation of energy from molecules to surroundings.

2) From the excited state S_1, the molecule can return to the ground state S_0 via different competitive processes

   - Radiative emission of a photon from S_1 to S_0 through fluorescence
   - Excited molecule can transfer some of their energy to the molecules which are located nearby through collisional quenching.
   - For each excited state S, there is an energetically unstable excited state T of lower energy. When electronic transitions takes place between spin states of different multiplicity the process is known as inter system crossing (ISC).

The de-excitation of the molecule from T_1 to S_0 occurs via a radiative process, known as phosphorescence. Processes like absorption and fluorescence do not involve the reorientation of spin; however ISC and

phosphorescence are accompanied by spin reorientation. Therefore fluorescence occurs much faster than phosphorescence. Absorption takes place within a time of 10^{-15} s while the fluorescence lifetime ranges from 10^{-9} to 10^{-12} s. Since the phosphorescence being a long transition, it can last from milliseconds to seconds, minutes or even hours.

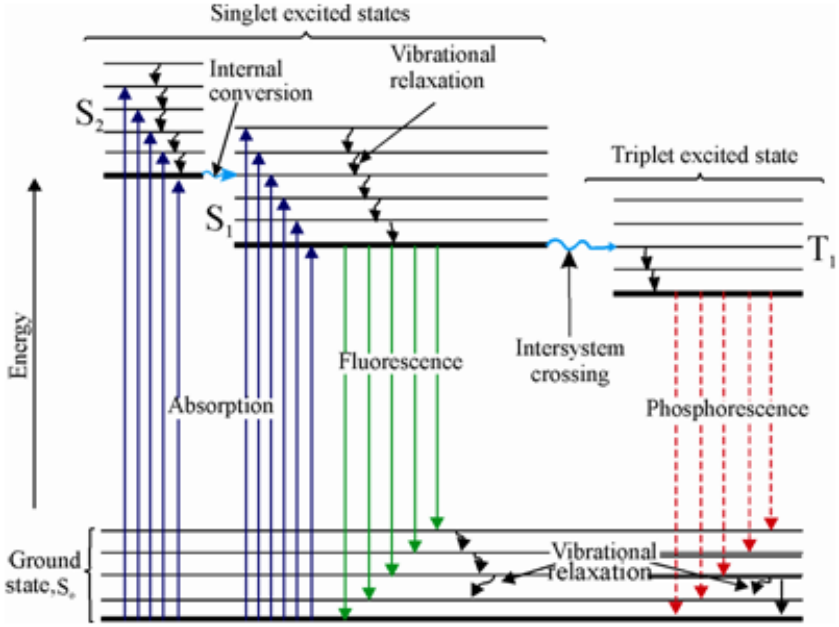

Figure 1.1: Jablonsky diagram showing fluorescence, phosphorescence, internal conversion, intersystem crossing and vibrational relaxation

1.2.2 Fluorescent probes or fluorophores

The sensing element in fluorescent sensor is a luminescent material which can re-emit radiation upon excitation and are called fluorescent probes or fluorophores. The intensity, life time and the position of emission wavelength are the important characteristic parameters of a fluorophore. Each fluorophore has its own intrinsic fluorescent properties which can be changed with the change in environment. Temperature variations influence

the local motions of fluorophore and its environment, thereby modifying the fluorescence features. Fluorescence intensity is dependent on the molar extinction coefficient, optical path length, concentration and quantum yield of fluorophore. The plot of fluorescence intensity as a function of wavelength is called a fluorescence spectrum. The fluorophore interacts with the target and translates the molecular recognition to fluorescence signal.[82]

1.2.3 Stokes shift

The energy absorbed (E_a) and emitted (E_{em}) by a fluorophore is expressed as[83]

$$\boldsymbol{E_a = \frac{hc}{\lambda_a}}$$

$$\boldsymbol{E_{em} = \frac{hc}{\lambda_{em}}}$$

where λ_a and λ_{em} are the absorption and emission wavewlengths. h is the planks constant and c is the velocity of light.
Since $E_a > E_{em}$, it is observed that $\lambda_{em} > \lambda_a$

Thus the wavelength of emission is red shifted compared to the absorption maximum. This phenomenon was first time observed by Sir George Stokes in 1852 and is known as stokes shift. The larger the stokes shift, the more useful the fluorophore in sensing application.

1.2.4 Life time

An important characteristic feature of a fluorophore is its fluorescence lifetime. When a fluorophore absorbs a photon and it is excited to higher

energy states, it remains in the excited state for a short time before it returns to the ground state. This time is known as fluorescence life time. Usually the life time ranges from nanoseconds to picoseconds and is denoted by τ.[84,85]

$$\frac{1}{\tau} = \sum k_i$$

where k_i is the rate of different decay processes.

1.2.5 Quantum Yield

When the molecules in the ground state absorb photons and move to excited state, different types of processes compete with each other to de-excite the molecules to the ground state. The quantum yield (ϕ) is the number of emitted photons relative to the number of absorbed photons.[86]

$$\phi = = \frac{\text{No.of quanta emitted}}{\text{No.of quanta absorbed}}$$

The quantum yield of a fluorescent molecule can be determined by comparing its fluorescence intensity with that of a reference compound whose ϕ value is known. The following equation is used for the calculation of ϕ

$$\frac{\phi_s}{\phi_R} = \frac{A_s I_R \eta_R^2}{A_R I_S \eta_S^2}$$

where ϕ_R is the quantum yield of reference. I_S and I_R are the integrated fluorescence intensities of sample and reference respectively. A_R and A_S are the absorbance of the reference and sample, η_S and η_R are the refractive indices of the solvents used. The quantum efficiency of most of the fluorophore is independent of the wavelength of exciting light.

1.2.6 Fluorescence sensors

Fluorescence sensing is a fascinating field of research due to its versatility and simplicity.

The recent progress in nanotechnology and nanomaterials has been incorporated into analytical chemistry for the design of highly sensitive fluorescent sensing probes. Eventhough no valuable structural information is gained from fluorescence measurements, this technique has become more popular because of its high sensitivity to the changes in the structural and environmental changes of fluorophores through any type of interaction with other molecules. Any phenomenon that results in a change of fluorescence intensity, lifetime or anisotropy can be used for sensing.

Interaction between analyte and fluorophore produces perturbation in the electronic structure of fluorescent probe leading to changes in their emission parameters. Analyte induced luminescence emission intensity change is the basic principle of fluorescence sensors. Mechanisms of such target binding are variable and include intra and intermolecular electron transfer and energy transfer processes. The fluorophore is mixed with the analyte solution and subjected to the corresponding excitation wavelength. The fluorescence intensity changes (enhancement or quenching) as a function of the concentration of the analyte.

During the early 1980's Tsien *et al*. first reported the fluorescence sensing of calcium. They synthesized 1,2-bis(o-aminophenoxy)ethane-N,N,N',N'-tetraacetic acid as a calcium ion chelate receptors and employed as a selective probe for calcium over magnesium.[87]

As the luminescence of fluorescent probes like nanoparticles, QDs etc. are very sensitive to their surface states; the fluorescence sensing is based on the principle that chemical or physical interactions occurring at the surface of probes change the efficiency of radiative electron-hole recombination process, either leading to fluorescence enhancement or quenching.[88] That is, there are two types of fluorescent sensors, one based on enhancement of fluorescence (turn on) and other based on quenching of fluorescence (turn off) (Scheme 1.1).

1.2.6.1 Turn off and turn on fluorescence sensors

In turn off sensors the fluorescence emission intensity of the fluorophore decreases upon analyte binding. In contrast, if the fluorescence intensity of the probe is enhanced due to the interaction with analyte, it is termed as turn on sensors. Molecular interactions with fluorophores resulting different processes like excited state reactions, energy transfer, molecular rearrangements, ground state complex formation, collisional quenching, aggregation etc.[89]

Most of the fluorescence sensors are based on the quenching of fluorescence signal. These are comparatively less sensitive than turn on sensors. Because it is quite easier to detect a bright signal in a dark background (turn-on) rather than diminishing of an already bright signal (turn-off). Hence the turn on sensors will offer high sensitivity together with low background signal.[90] Turn on sensors are preferable for more sensitive measurements since the chance of false positives are less in turn on sensors.

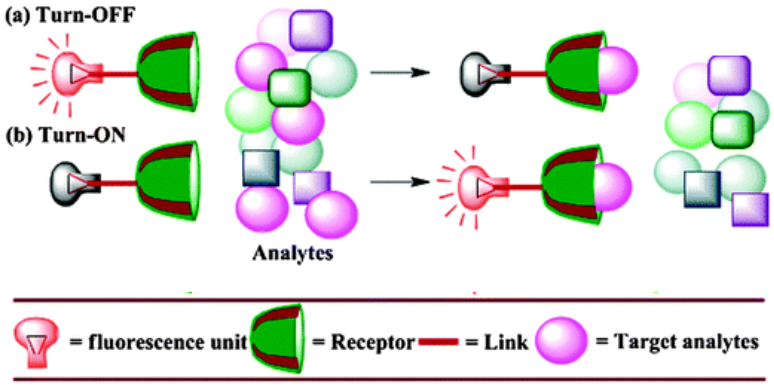

Scheme 1.1: Representation of turn off and turn on fluorescence sensors

In the present work gold nanoclusters (AuNCs) and quantum dots (QDs) were utilized as fluorescence probes for the development of sensors.

1.2.7 Gold nanoclusters

Recent developments in nanotechnology produced a new class of photo luminescent materials called noble metal nanoclusters possessing size below 2nm which is comparable to the Fermi wavelength of electrons (Figure 1.2).[91] They are composed of a few to about 100 atoms and have attracted significant interest among the researchers around the world since they bridge the missing link between the atomic and nanoparticle behaviour.

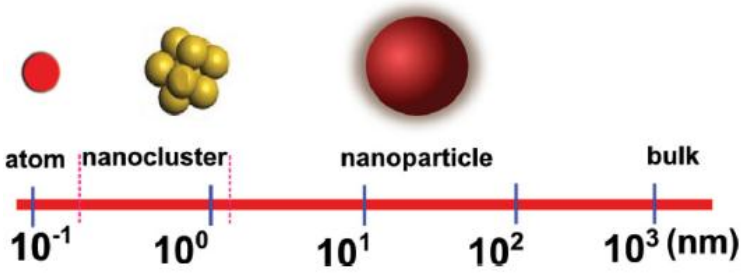

Figure 1.2: Hierarchy of materials from atoms to bulk

The striking properties of AuNCs such as long life time, biocompatibility, ease of conjugation, large stokes shift and size together with ligand dependent fluorescent properties are suitable for the development of sensitive and selective sensing systems.[92,93] Compared with traditional fluorescent probes such as semiconductor QDs, dyes, lanthanide doped nanoparticles and carbon nanodots AuNCs offer advantages like good water solubility, simple method of preparation, biocompatibility, low toxicity and ease of surface functionalization which gave them growing popularity in the analysis of biological and environmental samples.[94,95]

Electrons in the conduction band of nanoparticles can undergo collective oscillation which leads to the surface plasmon resonance (SPR) band in the visible region.[96] Such SPR band vanish in AuNCs, where the small size of AuNCs leads to significant quantization of conduction band. AuNCs exhibit molecular type properties such as large surface to volume ratio, facile surface modification ability and colour tunability due to the presence of discrete energy levels as a result of strong quantum confinement of free electrons.[91,97]

The synthesis strategies of AuNCs can be generally categorized in to two routes "Atoms to Clusters" and "Nanoparticles to Clusters" (Figure 1.3). In "Atoms to Clusters" approach the gold ions are first reduced to zero valent atoms by appropriate ligands like polymers, biomolecules, dendrimers etc. Then the nucleation of Au atoms takes place leading to the formation of AuNCs. Since AuNCs have a tendency for aggregation compared to nanoparticles, the synthesis of AuNPs is easier than AuNCs. So the other route is based on the conversion of "Nanoparticles to Clusters." This

technique involves etching surface atoms of AuNPs by excess ligands such as alkylated thiols and glutathione. The surface of nanoparticle undergoes ligand exchange and generates etchant-gold complex.[98]

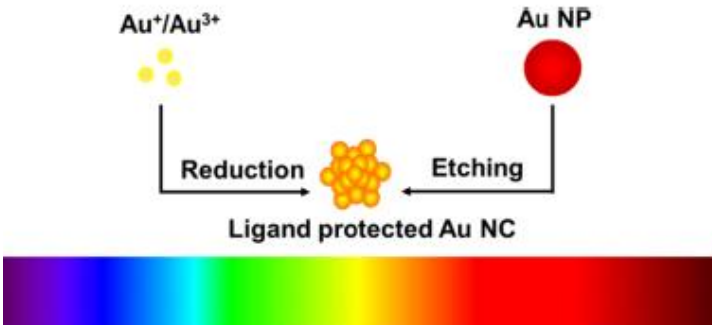

Figure 1.3: Synthesis strategies for fluorescent AuNCs

Even though the detailed mechanism of the origin of fluorescence of AuNCs is not completely understood yet, free electron theory is considered as a basic model to explain the fundamental optical properties of AuNCs.[99] According to this theory, the size dependent plasmonic optics of AuNCs depends on the number of free electrons. The free electrons on the surface of nanoparticles generate the polarization in an electric field.[100] However when the nanoparticles size come close to the Fermi wavelength and free electron number decreases to a critical value, the continuous band breaks up into discrete energy levels.[101] The fluorescence of AuNCs is attributed to the excitation of electrons into the '*sp'*-conduction band and subsequent radiative electron-hole recombination process (Figure 1.4).[102]

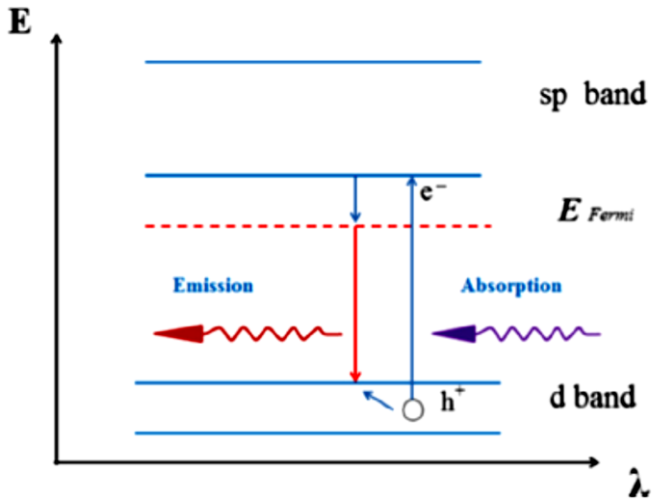

Figure 1.4: Energy diagram of fluorescence in AuNCs

The most important parameter that influences the luminescence of AuNCs is the value of energy level spacing (E_δ). An electron can undergo transition to excited state by absorbing an energy greater than E_δ. According to Spherical Jellium Model developed by Zheng *et al*. the value of E_δ and number of Au atoms (N) related to the Fermi energy (E_f) as follows[103]

$$E_\delta = {E_f}/{N^{1/3}}$$

As the size of the AuNCs increases, a red shift was observed in the fluorescence spectrum and when N is greater than 30, no emission peak was observed in the visible region. The numbers of atoms and the capping agents have a crucial role in the emission energy of AuNCs.

It is known that size and structure of the cluster, nature of surface ligand and environmental parameters (temperature, pH, ionic strength etc.) affects the optical properties of AuNCs. The fluorescence of AuNCs is enhanced through

the binding of ligands having strong electron donation ability. It was reported that ligands with electron rich groups (e.g. –COOH, -NH_2) or atoms (e.g. O, N) can significantly enhance the fluorescence of AuNCs.[104] Jin and coworkers proposed that surface ligands of AuNCs can greatly affect the luminescence of nanoclusters by charge transfer from ligand to Au core.[105] For example, ligands containing S atoms can enhance fluorescence behaviuor of AuNCs through charge transfer from S atom to the Au center (LMCT).[106]

Wen *et al*. suggested that there are two bands coupled in the luminescence spectrum of AuNCs. Band I arises from the icosohedral core of Au atoms while band II originates from the [-S-Au-S-Au-S-] semirings (Figure 1.5a).[107] Additionally the fluorescence emission spectrum of AuNCs consists of prompt fluorescence (ns timescale) and delayed fluorescence (μs timescale) as depicted in Figure 1.5b. Since the energy gap between the singlet and triplet states are very small in AuNCs, there is an efficient reverse ISC.[108]

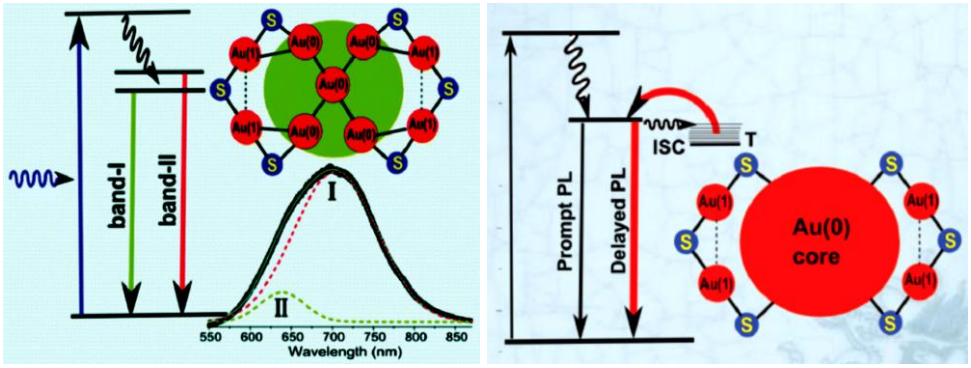

(a) (b)

Figure 1.5: (a) A schematic diagram showing the fluorescence of AuNCs originates from two transitions that are correlated to the structure. (b) Schematic representation of prompt and delayed fluorescence in AuNCs

Compared to QDs noble metal nanoclusters are more preferable for bioimaging and biolabelling applications because of their low toxicity and ultra-fine size. The heavy metal core of QDs is toxic, making them improper for in vivo clinical analysis which creates risks to human health.[109] Due to their remarkable properties AuNCs have found various analytical applications such as determination of metal ions, inorganic anions, biomolecules, proteins etc.

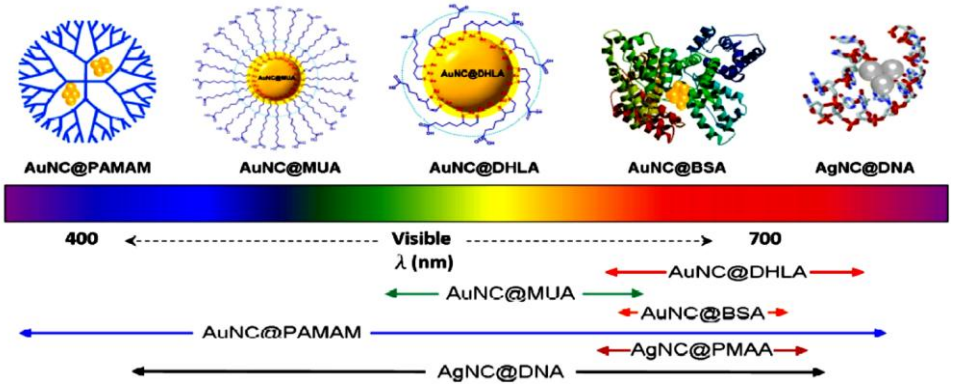

Figure 1.6: Effect of protecting agents on the fluorescence emission wavelength of AuNCs

Various substances like proteins, dendrimers, polymers and thiol containing organic compounds have been widely employed as protecting agent for the synthesis of AuNCs (Figure 1.6). Biomolecules like peptides and proteins have been established as excellent scaffolds to induce the nucleation and growth of AuNCs. Several proteins such as BSA,[110] lysozyme,[111] horseradish peroxidase (HRP),[112] transferrin-family proteins,[113] deoxyribonuclease I (DNase I),[114] and ribonuclease A (RNase A)[115] have been widely employed to prepare AuNCs with strong fluorescence emission. Among these, BSA protected AuNCs (AuNCs@BSA) are of particular interst because of its facile synthesis, biocompatibility and high photostability.[110] The tyrosine residues in BSA can reduce Au^{3+} ions while the cysteine and

histidine residues in BSA can coordinate with Au atoms, to form BSA templated AuNCs. The reducing strength of tyrosine residues can be increased by adjusting pH of the reaction medium to a value greater than 10.

1.2.8 Quantum dots (QDs)

Nanostructured materials have gained great attention during the last two decades because they can bridge the gap between the bulk and molecular levels and are found to have versatile applications in various fields such as electronics, sensing, optoelectronics and biology. They are catagerized as two dimensional (quantum wells), one dimensional (quantum wires) and zero dimensional (quantum dots). Although nanotechnology is a new branch of science, people have been exploiting nanomaterials for over a thousand years. The Romans and Greeks used PbS QDs as cosmetics to dye their hair more than 2000 years ago. In the early stages of 20th century CdSe and CdS QDs were mixed into silicate glasses to impart red and yellow colors.[116]

Colloidal quantum dots were discovered by Louis E. Brus in 1982 and the term "quantum dot" was introduced by Mark Reed. Brus in 1983, first characterized the QDs as semiconductor spheres in a colloidal suspension.[117]

Quantum dots are semiconductor nanocrystals, in which excitons confined in all three spatial dimensions and have a diameter typically ranges from 2 to 10 nm.[118] The core structure of QDs is normally made up of elements from groups II–VI (CdSe, CdS or CdTe) groups III–V (InP or InAs) or groups IV–VI (PbSe). Because of the similarities of quantized electronic states of QDs to atomic electronic states, they are also referred as "artificial atoms". QDs exhibited electronic properties which lie between that of bulk semiconductors and of discrete molecules. QDs possess unique

properties such as broad excitation spectra, narrow size-tunable emission spectra, high photochemical stability and negligible photobleaching due to quantum confinement effects.[119,120] As a result of their zero dimensions, QDs have sharper density of states than higher dimensional structures and exhibited superior optical properties.[121]

Valence band (filled with electrons) and the empty conduction band of QDs are separated by a band gap E_g. When photon having energy larger than the band gap fall on the surface of QDs, an electron is excited into the conduction band which left a hole of opposite charge in the valence band. These electron and hole together form an exciton by the columbic forces of attraction. This radiative combination of excited state electron in the conduction band and hole in the valence band is responsible for the origin of both linear and nonlinear optical properties of semiconductor nanocrystals.[122]

The electron in the conduction band and its hole in the valence band are separated by a distance known as the Bohr radius. QDs have a diameter which is in the same order as its exciton Bohr radius. If the radii of the QDS are on the order of the exciton Bohr radius, they are said to be in the 'weak confinement regime' and if the radii of the QDS are smaller than the exciton Bohr radius, they are said to be in the 'strong confinement regime'.[122]

In the zero dimensional QDs, the electron being more confined, its allowed energy states are more restricted and more size dependent. Size dependent quantum confinement effects observed in the nanocrystals when the radius of the semiconductor sphere is smaller than the bulk-exciton Bohr radius. Electronic and optical features of QDs are strongly dependent to the size and shape of the individual crystal. Henglein discovered that the

optical properties of colloidal QDs were dependent on their size, almost two decades ago.[123] As the size of the crystal is made smaller, the band gap energy increases and the colour of QDs shifts from red to blue (Figure 1.7a). That is their electric and optical properties are highly tunable. Life time of fluorescence is dependent on the size of the QDs. Electron-hole pairs in larger dots live longer since they have more closely spaced energy levels in which the electron-hole pair can be trapped resulting a longer life time.

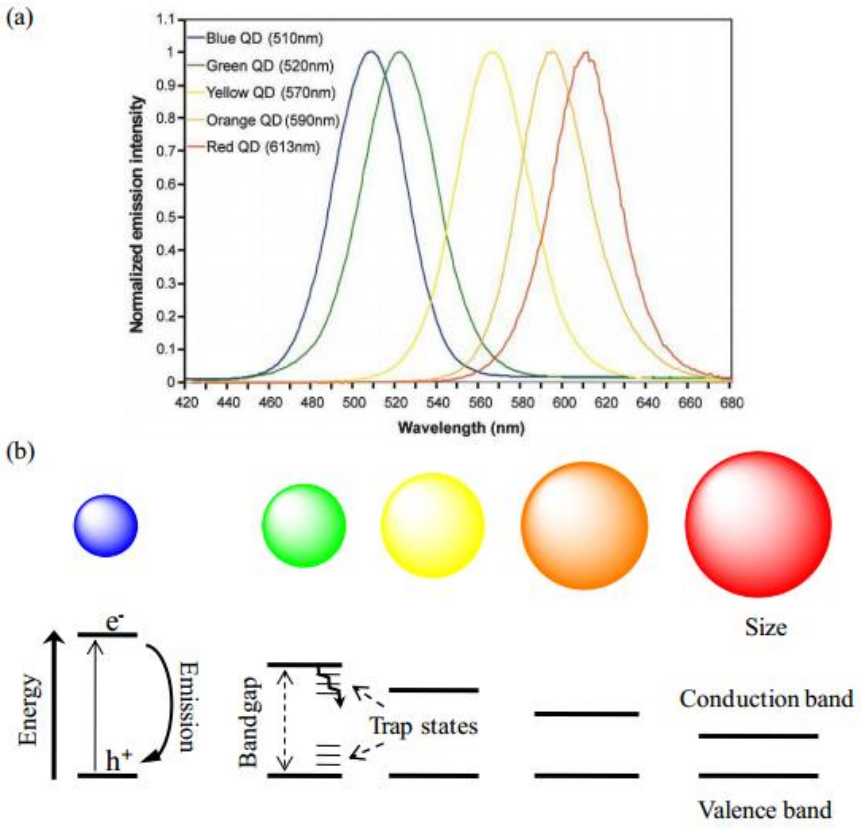

Figure 1.7: (a) Emission spectra of CdSe/ZnS QDs (excited at 350 nm) (b) Illustartion of size tunable emission of QDS and creation of exciton followed by radiative recombination or relaxation through trap states

Brus has developed a relationship between particle size and band gap energy of a semiconductor QDs expressed by the following equation

$$\boldsymbol{E_g(QD) = E_g(bulk) + (h^2/8R^2)\ (1/m_e + 1/m_h) - 1.8e^2/4\pi\epsilon_0\,\epsilon R}$$

where E_g is the band gap energy, R is the radius of quantum dot, m_e is the effective mass of electron, m_h is the effective mass of the hole and ϵ is the dielectric constant of the solid. The above equation is based on the effective mass model where special correlation effects are neglected.[124,125] Cyclic voltammetric studies are usually employed to determine the band gap energies of QDs.[126]

Luminescence in QDs originates from the radiative recombination of electron-hole pair. Small defects in the solid such as impurities, vacancies and adsorbates at the surface of QDs lead to the formation of 'surface defects' or 'trap states' into which photo-excited electron can fall or the photo-excited hole can 'float' (Figure 1.7b). Presence of surface defects increases the non radiative electron-hole recombination and decreases the efficiency of fluorescence. Since the energies of these surface states usually lie in the band gap of the QDs they can trap electrons, holes or excitons and behave as reducing and oxidizing agents.[127]

The surface coating of QDs with wider band gap semiconductor quantum shell decreases the trap state emission (eg. CdSe coated with ZnS as a core shell-nanocomposite) thus increases the photostability of the core and increases the quantum yield. Another way to increase the quantum yield and photostability of QDs is the passivation of surface of QDs by the introduction of capping ligands. Both organic and inorganic molecules are

used as capping agents during the synthesis of QDs.[88] Optical properties of QDs can be improved by doping which affects the band gap energies of QDs. The impurities or dopants perturb the band structures by creating local quantum states. The nature and amount of dopant also influences the optical properties of QDs. Numerous elements such as P, Na, Cr, Mn, Fe and Ag were doped in QDs for various applications.[128]

1.2.9 Literature review of fluorescence sensors based on gold nanoclusters and CdS quantum dots

The photoluminescence of AuNCs is a promising sensing tool for various analytes such as drugs, metal cations, anions, food additives and biomolecules. Protein templated AuNCs are of particular interest because of its facile synthesis, biocompatibility and high photostability.

Chen *et al*. successfully utilized protein templated AuNCs as efficient fluorescent probe for the determination of methotrixate, an antimetabolite used in the treatment of certain types of cancer.[129] BSA was selected as the capping agent which also act as reducing agent during the synthesis of AuNCs. The addition of methotrixate decreased the fluorescence intensity of AuNCs. The linear range and detection limit of the sensor was found to be 5.28×10^{-2} - 3.52×10^{-6} M and 1.98×10^{-9} M respectively. Application studies were performed in injections, serum and urine with satisfactory results.

Aswathy *et al.* fabricated Cu^{2+} modified BSA protected AuNCs for the fluorescence sensing of dopamine, an important neurotransmitter.[130] The turn on sensing mechanism and mode of interaction was studied using techniques such as fluorescence life time, IR spectroscopy and circular dichorism. The luminescence of AuNCs was found to be decreased upon addition of Cu^{2+} due

to its interaction with the surface of AuNCs. The fluorescence of AuNCs retrieved in the presence of dopamine, as Cu^{2+} ions which were removed from the surface of nanoclusters binds with dopamine. The assay showed a high selectivity over other catecholamines with a limit of detection of 1.00×10^{-8} M. The feasibility of the developed sensor was demonstrated in different real samples such as blood serum and urine samples.

Li et al. reported a turn on fluorescence sensing method for Ag (I) using BSA stabilized AuNCs.[131] Addition of Ag (I) to the AuNC@BSA solution, resulted in enhancement of fluorescence intensity, along with a blue shift in the emission wavelength. X-ray photoelectron spectroscopy, high resolution mass spectroscopy and MALDI –TOF mass spectrum measurements were used to characterize the nanoclusters. Gold core in AuNC@BSA reduces Ag^{+} to Ag^{0} and form a stable hybrid Au@AgNCs species which is responsible for enhanced fluorescence intensity and blue shift of wavelength of emission. The other metal ions do not enhance the fluorescence intensity under identical conditions indicating high selectivity of the developed sensor.

Fluorescent biosensing platform was developed by Chen *et al.* for the determination of cholesterol using BSA protected AuNCs.[132] The protein stabilized nanocluster probe was dissolved with cholesterol oxidase in a surfactant emusion system. Cholesterol oxidase selectively oxidizes cholesterol to cholest-4-en-3-one and produces stoichiometric amounts of H_2O_2 byproduct. This quenches the fluorescence signal of AuNCs significantly. Calibration plot between the fluorescence intensity and concentration of cholesterol was achieved in the range $0 – 3.00 \times 10^{-4}$ M, with a correlation coefficient of

0.986 and a limit of detection of 1.20×10^{-5} M. This sensing assay has relevant applications in clinical analysis.

Illegal feeding of clenbuterol (CLB) to domestic animals and its health risk to human beings lead an urgent requirement for the efficient detection of CLB, especially in edible meat. Fluorescent determination method using AuNCs@BSA was designed for the sensing of clenbuterol by *Cao et al.*[133] The linear response range and limit of detection of proposed assay was $3.00 \times 10^{-4} – 4.00 \times 10^{-9}$ M and 3.00×10^{-9} M respectively. The developed sensor was applied to determine clenbuterol in pork mince and satisfactory results were obtained when compared with HPLC method. Moreover the method was rapid, simple and cost effective.

Hemmateenejad *et al.* presented a simple and rapid method for the quantification of folic acid, based on the fluorescence quenching of protein modified AuNCs. The common protein, BSA was selected to protect AuNCs from aggregation. The fluorescence quenching intensity was fitted to Stern-Volmer equation in the linear concentration range 0.75×10^{-3} M - 0.27×10^{-6} M with a limit of detection 4.15×10^{-7} M. The fluorescence quenching was due to the crosslinking of folic acid with BSA, which induced intensity changes in the fluorescence of AuNCs. The practical utility of the sensor was demonstrated by the determination of folic acid content in pharmaceutical tablets and good results were obtained.[134]

BSA protected gold nanoclusters as fluorescent sensor for selective and sensitive determination of pyrophosphate was developed by Liu *et al*. in 2013. BSA capped AuNCs exhibited strong fluorescence emission in the visible region, which was quenched by the addition of Cu^{2+}. Cu^{2+} ions

undergo chelation with glycine residues in BSA, therby reducing the fluorescence intensity of AuNCs. Upon the addition of pyrophosphate the fluorescence intensity of AuNCs was restored, as Cu^{2+} formed chelated rings with pyrophosphate and thus removing Cu^{2+} from the surface of BSA. The sensor showed a wider linear range between 7.8×10^{-5} M and 1.63×10^{-7} M and detection limit of 8.32×10^{-8} M respectively. Morphology of AuNCs in the presence of Cu^{2+} and pyrophosphate was studied using high resolution transmission electron technique and mechanism of quenching was also discussed.[135]

Chen and coworkers successfully employed BSA stabilized AuNCs as a fluorescent probe for the sensitive determination of ciprofloxacin, the third generation member of quinoline antibiotics. [136] The fluorescence intensity of AuNCs at 635 nm was quenched in the presence of Cu^{2+}. Meanwhile the fluorescence intensity of Cu^{2+}-AuNC system was restored by the addition of ciprofloxacin. The enhancement in the fluorescence intensity of Cu^{2+}- AuNC system induced by ciprofloxacin was linear to concentration of ciprofloxacin in the range 1.51×10^{-7} M - 1.27×10^{-9} M. The limit of detection of the nanocluster based sensor was 9.05×10^{-10} M. Application studies were carried out in real samples such as human urine, ciprofloxacin tablets and human serum with satisfactory results.

A simple fluorescent sensing method was developed for the determination of sodium dodecyl sulphate using glutathione capped AuNCs by Zheng *et al.*[137] Glutathione acted as both reducing and stabilizing agent during the synthesis of AuNCs. The fluorescence of AuNCs enhanced dramatically upon the addition of poly(diallyldimethylammonium) chloride due to its

electrostatic interactions with nanoclusters. However, the fluorescence intensity decreased by the addition of sodium dodecyl sulphate due to its strong affinity to poly(diallyldimethylammonium)chloride. All experiments were conducted in 0.1 M tris-HCl buffer of pH 5. Under optimized experimental conditions, linear range between 5.25×10^{-5} M and 8.76×10^{-7} M was achieved with detection limit 8.76×10^{-8} M. Influence of other coexisting species on the fluorescence of AuNCs was studied and no significant interference was observed. Application studies were done in real water samples with satisfactory results.

Yang *et al.* incorporated DNA templated AuNCs for the development of fluorescence sensor for tetracycline. Plot of increase of fluorescence intensity against the concentration of tetracycline was linear in the range 5.00×10^{-6} M to 1.00×10^{-8} M with a correlation coefficient of 0.99. Detection limit of 4.00×10^{-9} M was found. Substances such as amino acids, glucose, vitamins and common metal ions did not interfere the performance of the sensor. Human urine and milk samples were used to study the practical application of the developed turn on sensor and satisfactory results were obtained. The developed sensor was simple, cost effective and exhibiting excellent sensitivity.[138]

A simple, selective and cost effective determination method was reported for Cu^{2+} by Xu *et al*. in 2014, using highly fluorescent lysine capped AuNCs.[139] The fluorescence of lysine stabilized AuNCs was found to be quenched remarkably by the addition of trace amount of Cu^{2+}. The observed quenching effect was due to the coordination of Cu^{2+} with the $–NH_2$ and –COOH groups of lysine. Developed fluorescent turn off sensor

displayed a linearity between the fluorescence intensity and concentration of Cu^{2+} from 7.00×10^{-6} M to 1.00×10^{-8} M with a limit of detection of 3.00×10^{-9} M. To validate the analytical application of the method, analysis of Cu^{2+} was carried out in tap water and river water samples. Application studies were conducted based on standard addition method.

Hu *et al.* used BSA protected AuNCs for the selective determination of Hg (II).[140] Determination is based on the fluorescence quenching of probe by Hg (II). Photo-induced electron transfer based quenching mechanism was proposed for the observed variation in fluorescence intensity. There exist a linear relationship between the decrease of fluorescence intensity and amount of Hg^{2+} over the range of 4.36×10^{-5} M – 4.00×10^{-7} M and the corresponding detection limit was found to be 8.00×10^{-8} M. The proposed method exhibited high selectivity for Hg^{2+} over other metal ions and anions. Real water samples were selected for application studies and satisfactory results were obtained.

Tao *et al.* reported a fluorimetric and colorimetric sensor for dopamine employing BSA protected AuNCs as sensing element.[141] Developed assay exhibited good selectivity and sensitivity for determination of dopamine. Due to the electrostatic attraction between dopamine and AuNCs@BSA, photo induced electron transfer process occurred and fluorescence of AuNCs decreased dramatically. The detection limit of the method was found to be 1.00×10^{-8} M. The system exhibited good selectivity for dopamine over other foreign species including ascorbic acid, uric acid, 3,4-dihydroxyphenylacetic acid, homovanillic acid, metal ions and amino acids. Application of sensor was

demonstrated in injection sample, human serum sample and PC12 cells. The developed method has a great potential for diagnostic purpose.

Tian *et al.* reported a novel microwave assisted method for the synthesis of water soluble BSA templated AuNCs and they applied AuNCs@BSA for the selective determination of glutathione.[142] The synthesized nanoclusters displayed a large stokes shift value of 140 nm. Linear concentration range between 1.61×10^{-5} M and 4.02×10^{-8} M was obtained under optimized experimental conditions. Detection limit of 7.00×10^{-9} M was obtained using the proposed sensor. The proposed turn on fluorescent sensor was used for the selective sensing of glutathione in human blood samples and living cells.

AuNCs@BSA based fluorescent sensor with a detection limit of 3.00×10^{-8} M for determination of histidine in biological samples was designed by He *et al.* in 2012.[143] In the presence of Ni^{2+}, due to static quenching, the fluorescence intensity of probe decreased which was restored upon the addition of histidine. The primary amine, carboxylic and imidazole side chains have tendency to bind with Ni^{2+}, thus removing Ni^{2+} from the surface of nanocluster resulting the activation of fluorescence. Other amino acids did not produce noticeable interference in the sensing of histidine. Application studies were carried out in human urine samples and good recoveries were obtained.

Cui and coworkers prepared AuNCs@BSA and characterization studies were carried out using FTIR and HRTEM techniques.[144] The photoluminescence intensity of AuNCs was increased greatly in the presence of cysteine, a sulphur containing amino acid. Based on this a turn on sensor was fabricated for

cysteine with a limit of detection of 1.20×10^{-6} M. The working linear range of the method was 8.00×10^{-4} M to 2.00×10^{-6} M. The cysteine molecules adsorbed on the core of AuNCs through S atoms reduced the surface defects and enhanced the fluorescence intensity. The developed sensor was applied to the analysis of cysteine content in human blood serum. The obtained results were compared with electrochemical biosensor.

Lysozyme capped AuNCs having average size of 1 nm were prepared in aqueous medium by Wei *et al.*[145] The synthesized AuNCs showed a strong fluorescence emission at 657 nm. Hg^{2+} quenches the fluorescence of AuNCs strongly and a linear relation was obtained between the fluorescence intensity and concentration of Hg^{2+} in the range 5.00×10^{-6} M – 1.00×10^{-8} M. Effect of other divalent metal ions on the fluorescence behavior of AuNCs was tested under identical conditions. The proposed sensor exhibited good selectivity for Hg^{2+} determination in presence of other metals.

Selective and sensitive sensor for Hg^{2+} was developed by Kawasaki *et al.* based on trypsin protected AuNCs. X-ray photon electron spectroscopy, circular dichorism and TEM were employed to characterize the nanoclusters. The prepared AuNCs exhibited high photochemical stability comparable to that of CdSe QDs. Based on the fluorescence quenching of trypsin template AuNCs a turn off sensor for Hg^{2+} was fabricated which exhibited a linear range 6.00×10^{-7} M - 5.00×10^{-8} M. The limit of detection was calculated to be 5.00×10^{-8} M. As Hg^{2+} have strong binding interaction with thiol sites in trypsin, it deposited on the surface of AuNCs resulting in the quenching of fluorescence.[146]

Near infrared luminescent AuNCs@BSA were synthesized through sonochemical method by *Liu et al*. and these nanoclusters were employed for the selective determination of nitrite.[147] The fluorescence of AuNCs was found to be selectively quenched in the presence of nitrite because of nitrite induced aggregation. The luminescence intensity decreased linearly upon increasing the amount of nitrite in the range 5.00×10^{-5} M to 2.00×10^{-8} M. The limit of detection as low as 1.00×10^{-9} M was obtained. The developed sensor displayed excellent analytical performances such as good selectivity, wide linear range, high sensitivity and applicability in neutral medium. The analytical application of the proposed method was demonstrated in real water samples.

A sensitive and simple method was developed by Wang *et al.* for the determination of melamine using thioglyclic acid capped CdS QDs.[148] The fluorescence intensity of CdS QDs increased greately in the presence of melamine. Based on this fluorescence enhancement, a turn on sensor was designed for the quantification of melamine. The fluorescence enhancement was due to the amine group induced passivation of surface states of QDs. A good linear relationship was obtained between the fluorescence intensity and concentration of melamine in the range 5.00×10^{-5} M to 2.00×10^{-9} M with a detection limit of 1.00×10^{-9} M. The sensor was successfully applied to the analysis of melamine in raw milk.

Tedsana *et al*. demonstrated cysteamine capped CdS QDs as a selective probe for the sensing of adenosine-5'-triphosphate (ATP) in aqueous solution.[149] It was observed that the photoluminescence of QDs was increased by the addition of ATP and the fluorescence enhancement was directly

proportional to the concentration of ATP. The proposed sensor was selective to ATP in the presence of other phosphate metabolites and anions. The linear working range was 8.0×10^{-5} M – 2.0×10^{-5} M. The limit of detection was 1.7×10^{-5} M. Good results were obtained when the method was employed for the monitoring of ATP in urine samples.

Determination of Pb^{2+} and Cr^{3+} were carried out by Abolhasani *et al.* using water soluble CdS QDs modified with thioglycolic acid.[150] Fluorescence intensity of the prepared QDs quenched effectively in the presence of Pb^{2+} and Cr^{3+} which was due to the aggregation of nanocrystals. The luminescence intensity of CdS QDs is proportional to the concentration of Pb^{2+} from 1.22×10^{-6} M to 9.75×10^{-9} M and for Cr^{3+} from 1.66×10^{-5} M to 1.25×10^{-7} M with a detection limit of 3.66×10^{-9} M (Pb^{2+}) and 5×10^{-8} M(Cr^{3+}). Other ions such as iron, calcium, sodium, potassium and magnesium have no influence on the fluorescence intensity of CdS QDs. The developed method has a lower limit of detection compared to other methods.

More recently Abolhasani *et al.* reported a simple and sensitive turn off sensor for Cu^{2+} and Ni^{2+} using water soluble thioglycolic acid stabilized CdS QDs. Transmission electron microscopy, absorption and fluorescence spectroscopy were used for the characterization of prepared QDs. The fluorescence intensity of synthesized QDs decreased dramatically by the addition of Cu^{2+} and Ni^{2+}. The decrease in fluorescence intensity of CdS QDs had a linear relationship with concentration of Cu^{2+} and Ni^{2+} in the range of 8.33×10^{-6} M - 2.07×10^{-6} M and 8.93×10^{-6} M to 3.57×10^{-8} M with detection limits of 5.17×10^{-9} M and 1.43×10^{-8} M, respectively. Other cations like iron, sodium, potassium, calcium and magnesium did not interfere

the determination of Cu^{2+} and Ni^{2+}. Application studies were conducted in real water samples.[151]

A novel sensor for sulfadiazine was reported by Liu *et al*. based on the fluorescence quenching of thioglycolic acid capped CdS QDs.[152] Microwave assisted synthesis was used for the preparation of QDs. Electrostatic interaction between sulfadiazine and the surface of QDs changes the luminescence intensity of QDs. Stern-Volmer equation was fitted in the linear range 2.34×10^{-3} and 1.21×10^{-5} M with a limit of detection 8.00×10^{-6} M. Application studies were carried out in sulfadiazine injections and satisfactory results were obtained.

A novel turn on fluorescent sensor was developed for cysteine by Wang *et al*. in 2011 using citrate capped CdS QDs as fluorescent probe.[153] The citrate capped CdS QDs exhibited an emission spectrum at 540 nm with a full width at half maximum of 130 nm. The fluorescence enhancement was due to the passivation of surface states of CdS QDs in the presence of cysteine. In the range 5.00×10^{-5} M to 1.00×10^{-8} M, a linear relationship between the fluorescence enhancement and concentration of cysteine was obtained. Langmuir binding isotherm equation was applied to find out the binding constant of cysteine on the surface of QDs. The detection limit of the sensor was found to be 5.43×10^{-9} M. No interference was observed from various cations, anions, amino acids and carbohydrates in the analysis of cysteine. The sensor was successfully employed for the determination of cysteine in human urine samples.

Chanu *et al*. reported a novel fluorescent sensor based on histidine stabilized CdS QDs for the determination of adenine and guanine.[154] Particle

size of the prepared colloidal QDs was calculated using equation developed by Brus *et al.* and was found to be 4.2 nm. Quantum yield of CdS QDs were found to be 1.5% by taking acridine yellow as a reference. The fluorescence intensity of QDs enhanced in the presence of adenine and quenched in the presence of guanine. The fluorescence quenching by guanine was due to its interaction with the surface of QDs. On the other hand, the interaction between QD stabilizer histidine and adenine was responsible for the fluorescence enhancement of CdS QDs.

Jiang and coworkers used glutathione capped aqueous CdS QDs as a fluorescent probe for the determination of BSA.[155] HRTEM was used to study the size of CdS QDs. A broad excitation spectrum in the range 200-480 nm was obtained for glutathione protected QDs. It was observed that the fluorescence intensity of QDs enhanced in the presence of BSA and this increment was proportional to the concentration of BSA in the range 1.0-10 mg/L.

Han *et al*. prepared BSA protected CdS QDs in aqueous media at room temperature and successfully applied for the determination of Cu^{2+}.[156] Other physiologically important cations like Zn^{2+} and K^{+} do not influence the fluorescence response of the system. The plausible sensing mechanism was discussed. A good linear relationship was observed between the concentration of Cu^{2+} and the fluorescence response in the range $0.00 – 8.00 \times 10^{-7}$ M. The developed sensor displayed a high sensitivity with a limit of detection 5.00×10^{-10} M. Since hair analysis attracted great importance in biological, medical, environmental and forensic sciences, application studies of the sensor were conducted in human hair and recoveries in the range 98 - 104 % was obtained.

Scope of the present investigation

There is a continuing demand for the fast and simple analytical methods for the determination of many clinically important biomarkers, food additives, environmental pollutants etc. In this respect, electrochemical and fluorescence sensors provide a promising means of analysis owing to their simplicity and reliability.

Quality control of food products is a hot area of research all over world. Most of the commercially available food items consist of a wide variety of different chemical additives. Electrochemical sensors, especially voltammetric sensors are widely used in food analysis due to its simplicity, reliability, fast analysis, relatively low instrument costs and suitability for in-situ determination etc. Integration of nanotechnology with electroanalytical chemistry will bring considerable progresses in the field of voltammetric sensors.

Clinical analysis, particularly the determination of biologically relevant compounds in physiological fluids, is a great challenge for researchers. Fluorescence sensing is a dominant analytical tool in medical diagnosis and bioimaging. The field of optical sensors is rapidly growing because of its advantages like simplicity, versatility and high sensitivity. Incorporation of nanomaterials in to the sensor design is expected to produce improvements in the analytical performance of the sensor.

With this point in view, an attempt has been made to develop viable and sustainable chemical sensors for food additives and neurotransmitters. Four electrochemical sensors and three fluorescence sensors were developed for analytes propyl gallate, allura red, sunset yellow, butylated hydroxyl

anisole, dopamine and nor epinephrine. Various experimental conditions for sensor fabrication were optimized. Analytical figures of merit for each sensor were determined and effect of foreign species on the analytical response of developed sensors was studied. Kinetic parameters and mechanism of electrochemical process were discussed in the case of voltammetric sensors. Based on the interaction between the probe and analyte, the fluorescence enhancement mechanism was studied. All the developed sensors were applied for the real sample analysis and the results were compared with existing method.

.....ൟ.....

Chapter 2

MATERIALS AND INSTRUMENTATION

Contents

This chapter gives a brief description of materials and methods used for the electrochemical and optical studies. The instruments employed for the characterization of sensing probes and analysis of food additives and neurotransmitters are included in this chapter. Also the preparation of various buffer solutions is explained.

2.1 Reagents

All the solvents and reagents used for the studies were of analytical grade. Water purified through a Millipore system (resistivity greater than 18 MΩcm) was used for the preparation of solutions. All the experiments were carried out at room temperature. MWCNT, nafion, sunset yellow and allura red were purchased from Sigma Aldrich. L-cysteine and chloroauric acid were purchased from SRL Chemicals. Dopamine, norepinephrine, cadmium chloride and sodium sulfide were purchased from s.d. fine Chemicals. Propyl gallate and butylated hydroxyanisole from Otto

chemicals was used for the analysis. Vegetable oil samples and soft drink samples for application studies were purchased from local super market.

2.2 Instruments

Electrochemical measurements were carried out using CH Instruments (USA) and BAS Epsilon electrochemical analyzer (USA) on IUPAC mode with anodic positive. A conventional three electrode cell system was employed. Nanomaterials and polymer film modified electrodes were used as working electrodes. Ag/AgCl electrode and platinum wire were used as the reference and auxiliary electrodes respectively. Various voltammetric techniques such as cyclic voltammetry, square wave voltammetry, differential pulse voltammetry, linear sweep voltammetry, electrochemical impedance spectroscopy and chronoamperometry were employed for various studies. Electrode cleaning was done with the help of Ultrasonicator (Oscar Ultrasonics Pvt. Ltd. Mumbai).

JAZ-EL-200-X spectroflurimeter was used for fluorescence measurements. Absorption studies were performed on a Spectro-UV-Visible double beam UVD-3500 instrument. Fourier transform infrared spectra were recorded on FTIR spectrometer (JASCO-4100 JAPAN) using KBr discs. Scanning electron microscopic images were obtained on a JEOL 6390LV. The morphology of the nanocrystals was investigated by TEM (JEM-2100HRTEM). pH measurements were carried out in a Metrohm pH meter.

2.3 Preparation of buffer solutions

2.3.1 Preparation of acetate buffer solutions (ABS)

By mixing sodium acetate trihydrate and acetic acid in different amounts, ABS of various pH values was prepared. The amounts of sodium acetate trihydrate and acetic acid used for the preparation are listed in Table 2.1.

2.3.2 Preparation of phosphate buffer solutions (PBS)

Monosodium dihydrogen phosphate and disodium hydrogen phosphate weighed in different amounts as listed in table, dissolved in water and diluted to 100 mL to prepare PBS of different pH values (Table 2.2).

2.3.3 Preparation of citrate buffer solutions (CBS)

CBS of different pH was prepared by mixing trisodium citrate and citric acid in varying amounts. The corresponding amounts of reagents are listed in Table 2.3.

2.4 Preparation of urine sample

Urine sample was prepared by mixing the chemicals listed in Table 2.4 in their corresponding weights.

Table 2.1: Preparation of 0.1 M acetate buffer solution

pH	CH_3COOH (in grams/100 mL)	$CH_3COONa.3H_2O$ (in grams/100 mL)
2	1.3799	0.0001
3	1.3790	0.0003
4	1.3780	0.0036
5	1.3615	0.0360
6	1.2143	0.3218
7	0.5836	1.5466
8	0.0940	2.4970
9	0.0100	2.6605
10	0.0010	2.6781

Table 2.2: Preparation of 0.1 M phosphate buffer solution

pH	NaH_2PO_4 (in grams/100 mL)	Na_2HPO_4 (in grams/100 mL)
2	0.5994	0.0024
3	0.5900	0.0237
4	0.5098	0.2054
5	0.2161	0.8711
6	0.0319	1.2885
7	0.0036	1.3534
8	0.0034	1.3602
9	.00038	1.3609
10	0.0000	1.3609

Table 2.3: Preparation of 0.1 M citrate buffer solution

pH	Citric acid (in grams/100 mL)	Sodium citrate (in grams/100 mL)
2	2.0544	0.0652
3	1.7963	0.4265
4	1.3115	1.1051
5	0.7819	1.8642
6	0.2650	2.5700
7	0.0375	2.8880
8	0.0039	2.9355
9	0.0004	2.9405

Table 2.4: Preparation of urine sample

No:	Compound	Quantity
1	$NH_4H_2PO_4$	0.7725 g
2	NaCl	1.2700 g
3	KCl	0.7150 g
4	$CaCO_3$	0.0780 g
5	$MgCl_2.6H_2O$	0.1045 g
6	HCl	2.1750 mL
7	H_2SO_4	0.1675 mL
8	Urea	4.6250 mg

Chapter **3**

MULTI WALLED CARBON NANOTUBE BASED VOLTAMMETRIC SENSOR FOR PROPYL GALLATE

Contents

Development of a voltammetric sensor for the determination of propyl gallate, a synthetic food antioxidant, is discussed in this chapter. Determination of propyl gallate was carried out using multiwalled carbon nanotube (MWCNT) modified gold electrode in a solution of 0.1 M acetate buffer solution (pH 7) as supporting electrolyte. Surface characterization of the modified electrode was carried out using scanning electron microscopy and electrochemical impedance spectroscopy. The developed sensor showed an excellent catalytic activity and stability for electrooxidation of propyl gallate. Effect of possible interfering ions, amount of MWCNT-nafion suspension, pH of the supporting electrolyte and scan rate were studied. Fundamental kinetic parameters such as charge transfer coefficient (α), heterogeneous rate constant (k_s), and diffusion coefficient (D) were determined by a detailed analysis of square wave voltammograms and chronoamperograms. Under optimized conditions, the nanotube film modified electrode exhibited a linear range of 1.00×10^{-4} - 1.00×10^{-5} M with a limit of detection of 6.31×10^{-7} M. The determination of propyl gallate in vegetable oils with the proposed sensor was in good agreement with the results obtained by spectrophotometric method.

3.1 Introduction

Man had been using additives and preservatives in food for several decades and its use has increased tremendously in the past 30 years.[157] Since prehistoric times natural preservatives have been used in foods without understanding the underlying chemistry. In ancient cultures sulfites were used to preserve wine whereas vinegar was used to preserve pickle. The introduction of more additives, both natural and artificial origin took place with the advent of processed foods in the second half of the 20th century. As of today it has been estimated that each person consumes on an average of 3.6 - 4.5 kg of food additives per year because 75% of the Western diet is made up of various processed foods.[158]

Food additives are substances added to food to preserve flavor or enhance its taste and appearance. They can be divided into several groups, such as anticaking agents, antioxidants, antifoaming agents, colourants, emulsifiers, flavor enhancers etc. The risks and benefits of food additives have been going through significant controversies over a while. Diseases such as cancer, digestive problems, neurological disorders, heart problems or obesity are linked with the excessive use of certain artificial food additives. Due to the increase in the usage of food additives, there has been a considerable scientific evidences linking food additive intolerance with various physical and mental disorders, particularly with childhood hyperactivity.[159] Though food additives may be linked with these diseases and health risks, they also preserve nutrient value which normally would not be retained in their natural levels.

To regulate the use of these additives, a unique number termed as "E numbers" is assigned to each additive by European Union. The Food and Drug Administration (FDA) and European food safety authority (EFSA) have set safety standards, for determining whether a substance is safe for its intended use.

Antioxidants (natural and synthetic) play a significant role in retarding or preventing the autooxidation reactions in food products. The development of antioxidants as intentional food additives began in 1920s and became a full-fledged industry in the 1940s. Prpoyl gallate (PG) [Figure 3.1] is a synthetic phenolic antioxidant commonly added to food and pharmaceutical products to improve their stability, especially to prevent rancidity in products containing lipids or fats.[160,161] PG suppresses the chain initiation or breaks the chain propagation steps taking place during the peroxidation of unsaturated fatty acids. Therefore it is commonly used as additive in a variety of products, particularly in food, in order to prevent the oxidative damage of fats and oils. These antioxidants appear as preservatives in food stuffs like edible oils, margarine, food concentrates and cookies.[162]

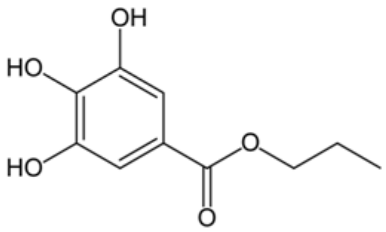

Figure 3.1: Structure of PG

Various studies have shown that antioxidants could enter human body through the intake of food, pharmaceutical etc. Recently people have also

found that excessive use of these artificial antioxidants may cause a loss of nourishment and even produce toxic substances that harm health. Therefore the use of additives is subject to regulations which defines the permitted compounds and their concentration limits.[163,164] Recent results have shown that the antimutagenic properties of some phenolic compounds such as gallates may be due to their inhibiting action on the cytochrome P-450 enzymes.[165-167] Therefore, the quantitative determination of PG is of immense importance, especially for food safety and quality control.

Since PG is suspected of being responsible for liver damage and carcinogenesis in laboratory animals, their harmful effects on health have been extensively discussed and studied. Therefore in several countries the use of these additives is subject to regulations, which define specific approved antioxidants, establish permitted levels, and include labeling requirements.[160,163]

Many methods for determining PG individually or simultaneously have been published, based on spectrophotomery,[168] HPLC with amperometric detection,[169] micellar electrokinetic capillary chromatography[163] and liquid chromatography.[170,171] But they are prone to many drawbacks, such as high cost, complicated and lengthy procedures, use of carcinogenic reagents and unsuitability for field use.

Electrochemical techniques are promising alternative to classical approaches due to their relatively low operational cost, good miniaturization possibility, and rapid and sensitive detection procedures, which are suitable for faster analysis.[164] Direct determination of electroactive compounds on unmodified electrode requires high overpotential. Also bare electrodes possess some disadvantages like low stability, easy deactivation or fouling

of the surface, poor sensitivity etc. These defects can be minimized by the application of chemically modified electrodes which attracted considerable interest over the past decades.

Carbon nanotubes (CNTs) possess various novel properties that make them useful material in various fields. Owing to their unique structural, mechanical and electronic properties, CNTs, especially multi walled carbon nanotubes (MWCNTs) have been recognized as attractive candidates for the design of electrochemical sensors.[172,173] The three dimensional spacial arrangement of nanotubes is favorable for the high loading of electroactve species to the electrode surface, thus increasing the sensitivity of the chemically modified electrodes. They can act as molecular wires, through which electrons can tunnel between electrode and analyte. Compton's group reported that the enhanced electrocatalytic activity of CNTs is due to the occurrence of edge-plane like sites located at the end and in the 'defects' areas of the tubes.[21,174]

An attempt has been made to develop a convenient and sensitive method for the determination of PG using MWCNT modified gold electrode (GE). Kinetic analysis of the electrochemical process was carried out by determining the parameters such as charge transfer coefficient, heterogeneous rate constant, diffusion coefficient and number of electrons involved in the oxidation reaction. Although there are reports of other sensors for PG, there is no report in the literature on a sensor based on MWCNT. Owing to the importance of MWCNT, a novel sensor has been developed. Further, the kinetic parameters of the electrode process have also been studied. A plausible mechanism for the electrooxidation of PG has also been proposed.

The developed method is applied for the determination of PG in commercial vegetable oils.

3.2 Experimental

3.2.1 Pre-treatment of GE

Pre- treatment of the working electrode is common in electrochemical measurements. This ensures reliable electrode performance. GE acquired from CH Instruments (USA), was used for sensor fabrication. Prior to modification, the electrode surface was mechanically polished with alumina slurries on flat pads, followed by rinsing with ultra-pure water and successive ultrasonication in ethanol and water for 3 min each. The electrode was then cleaned electrochemically by cycling the potential between 0 - 1500 mV in 0.5 M H_2SO_4, afterwards it was rinsed with water and allowed to dry.

3.2.2 Functionalization of MWCNT

The oxidation of CNTs by strong acids, shorten the nanotubes and introduce carboxylate and hydroxyl groups, mainly at the tube tips and the defect sites.[175] Due to the presence of –OH, and –COOH groups the CNTs becomes more dispersible in polar solvents.[176]

Acid treatment of MWCNT was carried out as described in literature.[177,178] MWCNT was refluxed in conc. HNO_3 for 48 hrs and the resulting suspension was diluted with water. The MWCNT was then filtered, washed with double distilled water and dried in air. As a result of this process, length of MWCNT got shortened and functional groups are introduced, which make them hydrophilic. The peaks at 1703 and 1558 cm^{-1} of the FTIR spectrum (Figure 3.2) demonstrated that carboxyl groups and carboxylate groups are present on the surface of acid treated MWCNT.

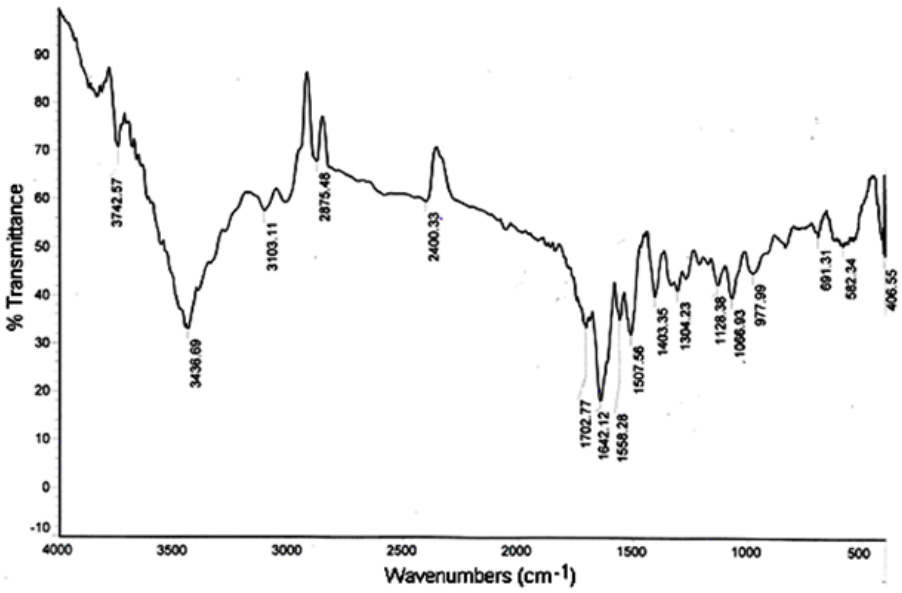

Figure 3.2: FTIR spectrum of acid treated MWCNT

3.2.3 Preparation of MWCNT modified gold electrode

The insolubility of MWCNTs in aqueous media is a main technical barrier, concerned with the development of CNTs based sensors.[179] To overcome this drawback, nafion, a sulphonated tetrafluoroethylene based polymer, discovered in 1960s by Walther Grot has been employed. The structure of nafion contains two regions: the hydrophobic polymer backbone and hydrophilic sulphonate groups outside the hydrophobic area. Due to this special amphiphilic structure, hydrophobic interactions exist between the hydrophobic backbone of nafion and the side wall of CNTs, and dispersing them in water by the hydrophilic groups.[180] Also nafion strengthen the mechanical connection of the CNTs with the electrode surface.[181]

5.0 mg of acid treated MWCNT was dispersed in a mixture of 2 mL water and 0.3 mL nafion (13% nafion – water solution) with the aid of

ultrasonicate agitation to form a 0.22% (w/v) black homogeneous suspension. 3 µL of the dark suspension was dropped on to the surface of cleaned GE.

3.2.4 Preparation of solution of PG

Stock solution of PG (1.00×10^{-2} M) was prepared in methanol. PG solutions of various concentrations were prepared by diluting the stock solution using acetate buffer solution (ABS).

3.2.5 Analytical procedure

10 mL acetate buffer solution (0.1 M, pH 7) containing appropriate amount of PG was transferred into an electrochemical cell, incorporating a three electrode system. The solution was then stirred for 60 s to reduce the variation between each measurement. Differential pulse voltammogram was recorded from -100 to 700 mV at a scan rate of 100 mVs^{-1}, with pulse amplitude of 50 mV, pulse period of 0.5 s, pulse width of 0.2 s and potential step of 4 mV. PG gave an oxidation signal at 196 mV on MWCNT modified GE. No reduction peak was observed for PG in the reverse sweep of CV indicating an irreversible electrochemical oxidation process. Since DPV gave more sensitive voltammograms than CV and SWV, DPV approach was selected for all the experiments.

3.2.6 Preparation vegetable oil sample

5.0 g of a vegetable oil sample was placed into an Erlenmeyer flask (with a screw cap) and 5.0 mL of pure methanol was added. After agitating in a laboratory shaker for 5min, the mixture was transferred to a 10 mL centrifuge tube, and centrifuged at 3000 rpm for 5 min. The extracts were transferred into a 25 mL flask after allowing to set for 2 min. The above

extraction procedure was repeated twice, all the extracts were collected and transferred into the 25 mL flask; and then the solution was diluted to the mark with methanol.[182] 1 mL aliquot of this sample solution was made up to 10 mL with buffer solution and analyzed for PG.

3.3 Results and discussion

3.3.1 Surface characterization

Evidences for the effective modification of electrode surface by MWCNT obtained from scanning electron microscopy (SEM) images, surface area calculations and electrochemical impedance spectroscopic studies.

3.3.1.1 Surface morphology studies

SEM was used to study the surface morphology of bare and modified electrode. SEM images of bare and MWCNT modified GEs are shown in Figure 3.3. From the SEM images it is clear that the surface character of GE has changed upon modification with MWCNT film and MWCNT distribute almost homogeneously at the electrode surface. MWCNT provides increased number of catalytic sites for the oxidation of PG. The particle diameter obtained from SEM images is of the order of 2-5 microns, which is due to the hydrophobic nature of CNTs. Spontaneous aggregation is caused by the hydrophobic nature, which increases the possibility of bundling and close packing on the electrode surface.[183]

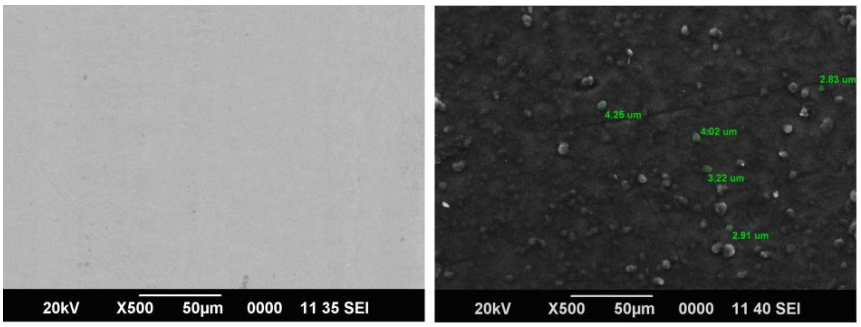

Figure 3.3: SEM images of (a) bare GE (b) MWCNT/GE

3.3.1.2 Surface area study

2 mM $K_3Fe(CN)_6$ was taken as a probe to measure the microscopic areas of the MWCNT modified and bare GE. Cyclic voltammograms were recorded in $K_3Fe(CN)_6$ solution using the bare and modified electrode at different scan rates (Figure 3.4). For a reversible system the relationship between the current and scan rate is given by the Randles-Sevcik equation[184]

$$\boldsymbol{i_p = 2.69 \times 10^5 A n^{3/2} D^{1/2} C v^{1/2}}$$

where i_p refers to the peak current, n is the number of electron transferred, A is the surface area of the electrode, D is the diffusion coefficient, C is the concentration of $K_3Fe(CN)_6$ and v refers to the scan rate. Here n = 1, D = 7.60 × 10^{-6} cm^2s^{-1}. Thus, from the slope of i_p vs $v^{1/2}$ relation (Figure 3.5), the effective surface area of the MWCNT modified GE was calculated to be 1.9932 cm^2 which is about two times greater than the bare GE (0.9842 cm^2). The increased surface area of the modified electrode could offer more number of binding sites for PG, resulting the greater sensitivity of MWCNT/ GE compared to unmodified electrode.

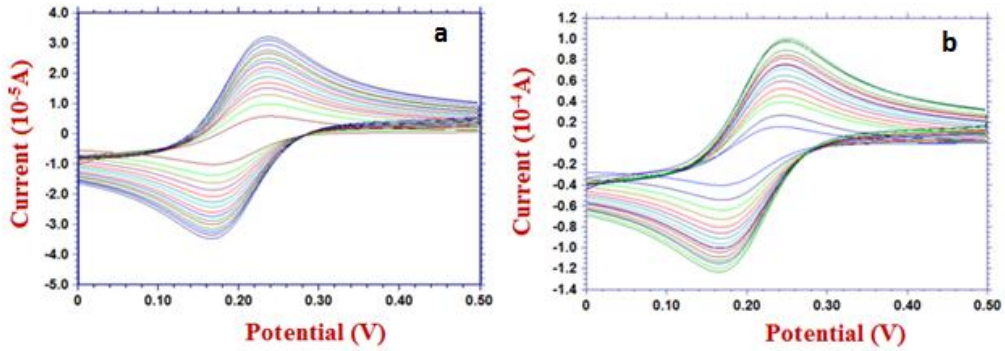

Figure 3.4: Surface area study of (a) bare GE and (b) MWCNT modified GE in $K_3Fe(CN)_6$ solution

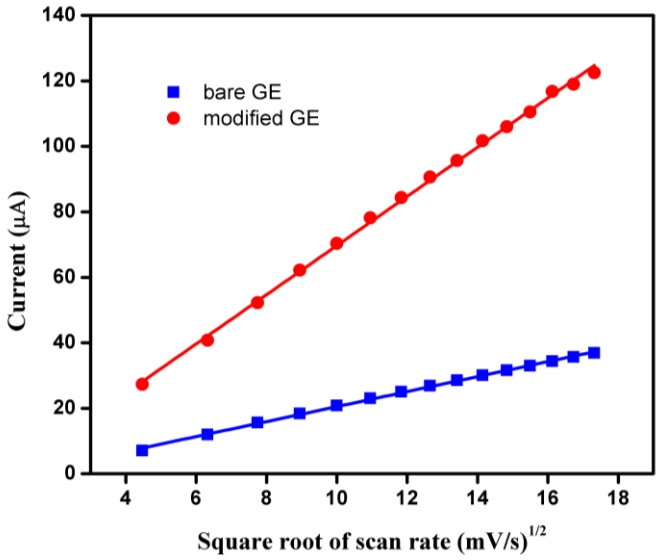

Figure 3.5: Plot of square root of scan rate vs peak current for bare GE and MWCNT modified GE

3.3.1.3 Electrochemical impedance analysis

Electrochemical impedance spectroscopy (EIS) is a sensitive technique for investigating the changes in conducting properties of an electrode surface. EIS measurements were conducted to study the charge transfer resistance of bare and modified electrode and the result is generally

expressed by Nyquist plot. The semicircle appeared in the Nyquist plot corresponds to the parallel combination of charge transfer resistance and double layer capacitance resulting from electrode impedance.[185] EIS studies were carried out at bare and MWCNT modified GE surfaces and the corresponding Nyquist plots are depicted in Figure 3.6. Both the modified and unmodified electrodes show semicircles with various diameters. The results show that the area of semicircle for bare GE is greater than MWCNT film modified GE, indicating that the charge transfer resistance decreased upon modification with MWCNT. In other words electron transfer rate increased between the electrode and PG which may be attributed to the topological defects present in MWCNT.

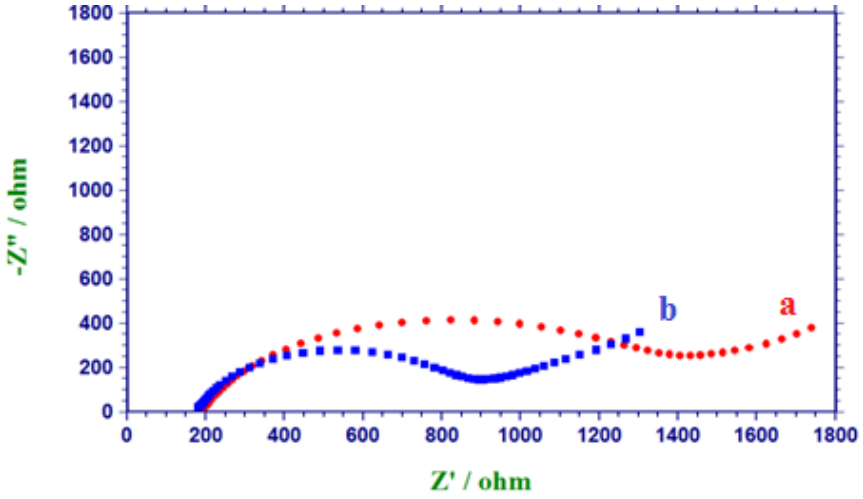

Figure 3.6: Nyquist plots for (a) bare GE and (b) MWCNT/GE

3.3.2 Electrochemical behaviour of PG on MWCNT/GE

The electrochemical behavior of PG was studied on bare GE and MWCNT film modified GE in 0.1 M ABS (pH 7). It was observed that, at

bare GE stable oxidation peak for PG was not obtained, may be due to surface fouling effect (probably due to the adsorption of reaction products at the surface). Under the same conditions, a well defined and sensitive irreversible oxidation peak appeared at 196 mV on MWCNT modified GE, which was 316 mV less than that obtained, on bare GE. Also the oxidation peak current of PG increased from 0.59 µA to 3.70 µA on the modified electrode. Figure 3.7 shows the DPV for the oxidation of 1.00×10^{-4} M PG in ABS (pH 7) at bare GE (curve a) and MWCNT/GE (curve b).The observed peak may be due to the oxidation of hydroxyl group present in PG. The significant enhancement in peak current and considerable negative shift in oxidation overpotential of PG on the modified electrode undoubtedly proved the electrocatalytic activity of MWCNT towards the oxidation of PG, suggesting that MWCNT/GE is an excellent sensor for determination of PG.

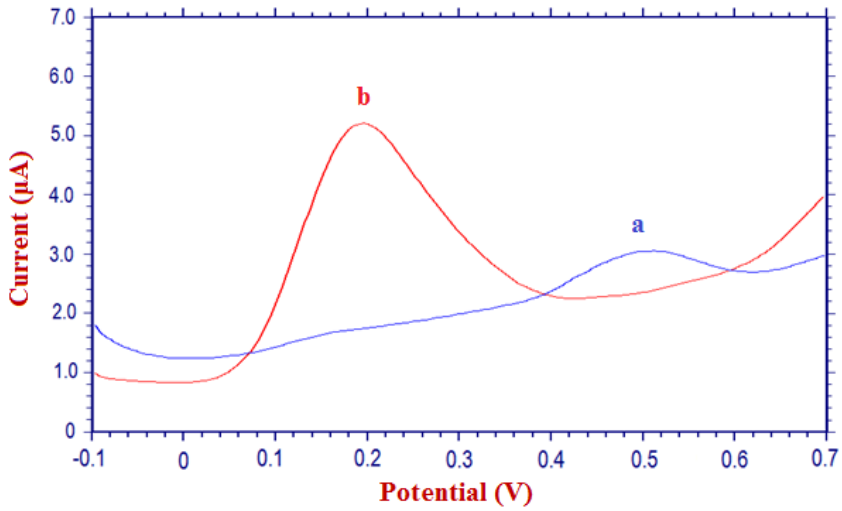

Figure 3.7: Differential pulse voltammograms of PG at (a) bare GE (b) MWCNT/GE

3.3.3 Optimization of experimental conditions

The conditions for sensor fabrication were optimized, which included effect of various supporting electrolytes, influence of the pH of the supporting electrolyte and the amount of MWCNT-nafion suspension.

3.3.3.1 Influence of supporting electrolyte and pH

Electrochemical behaviour of PG in various media such as 0.1 M solutions of phosphate buffer, acetate buffer, nitric acid, sulphuric acid, perchloric acid, NaCl and NaOH were studied by DPV and results are shown in Table 3.1. Lowest oxidation potential and highest peak current was obtained with acetate buffer solution and hence it was selected for further studies.

The effect of solution pH on the electrochemical response of PG was investigated in the pH range 2.0 to 8.0 in 0.1 M acetate buffer solution. The anodic peak potential showed a linear negative shift on increasing the pH of the solution (Figure 3.8). A slope of 0.0532 is obtained, which is approximately close to the theoretical value of 0.0576;[186] indicating that electron transfer is associated with an equal number of protons on the electrochemical oxidation of PG. It was found that minimum peak potential and maximum peak current appeared at pH 7.0. Therefore, pH 7.0 was chosen as the optimum pH.

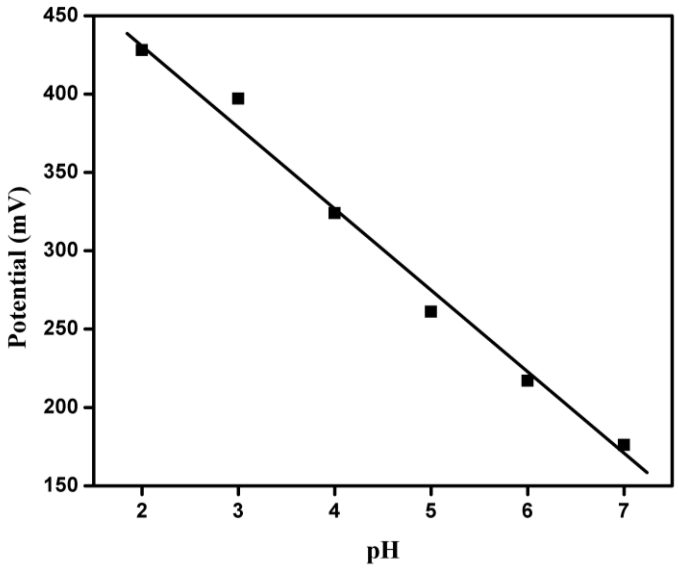

Figure 3.8: Effect of pH on the oxidation potential of PG

3.3.3.2 Effect of amount of MWCNT - nafion dispersion

The relationship between the amount of MWCNT- nafion suspension (1-6 µL) and the oxidation peak current (i_p) of PG was studied (Figure 3.9). As the amount of MWCNT- nafion suspension was increased from 1 to 3 µL, oxidation peak current increased gradually, and thereafter decreases. The maximum current was obtained when 3 µL of suspension was dropped on GE. This enhancement of current indicates that the specific surface area and number of catalytic sites increases with an increasing amount of MWCNT. Further increase in the amount of MWCNT-nafion suspension caused a decrease in the peak current. This may be due to the insulating property of nafion which blocks the electron transfer by lowering the charge transfer rate.[187] Hence the amount of MWCNT- nafion disperson was fixed as 3 µL.

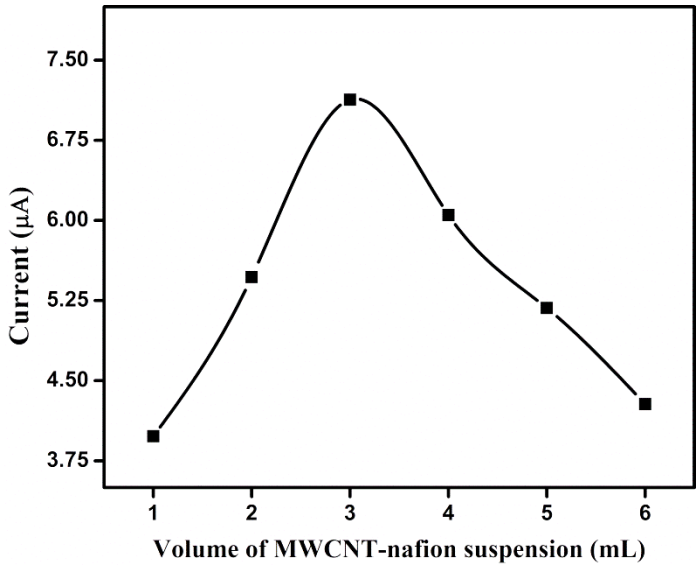

Figure 3.9: Effect of volume of MWCNT-nafion suspension

3.3.4 Effect of scan rate and characteristics of oxidation process

Linear sweep voltammograms of PG (1.00×10^{-4} M) was recorded at different scan rates between 10-100 mVs^{-1} (Figure 3.10a). Study of the oxidation process showed that the plot of the peak current versus square root of scan rate ($v^{1/2}$) is linear over the whole range of the scan rate studied (Figure 3.10b), which indicates that it is a typical diffusion-controlled process. Moreover, the peak potentials shift to more positive values as the scan rate increases, and also become slightly positive with the increase of concentration of the analyte. This behavior indicates the irreversible character of the oxidation process for PG.[182]

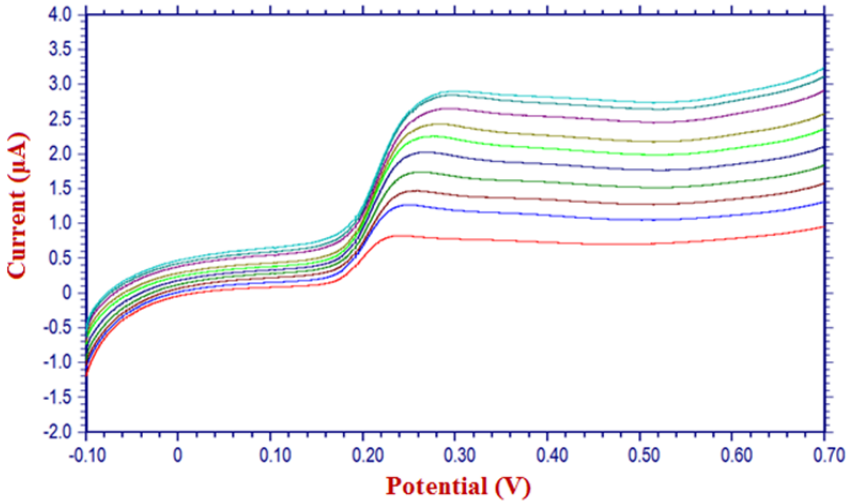

Figure 3.10a: Overlay of linear sweep voltammograms for oxidation of PG at various scan rates

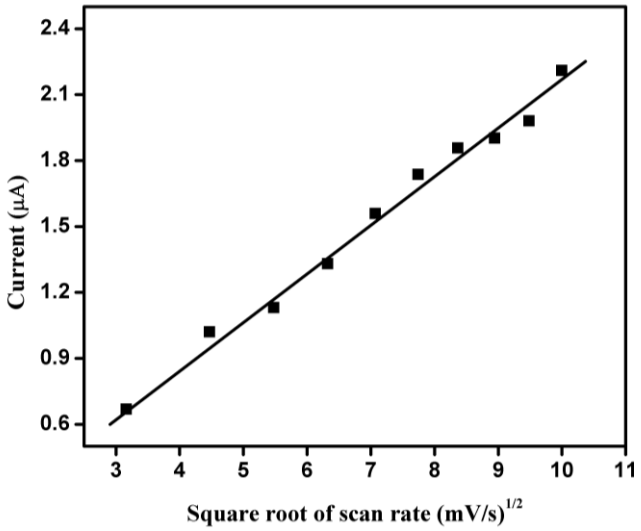

Figure 3.10b: Plot of square root of scan rate vs peak current

3.3.5 Calibration plot and limit of detection

The relationship between the anodic peak current and the concentration of PG was studied by DPV (Figure 3.11a). Under optimized experimental

conditions, the oxidation peak current increased linearly with concentration of PG in the range 1.00×10^{-4} - 1.00×10^{-5} M (Figure 3.11b). The corresponding regression equation can be expressed as $i_p = 68.32C + 0.443$ $(R^2 = 0.998)$.

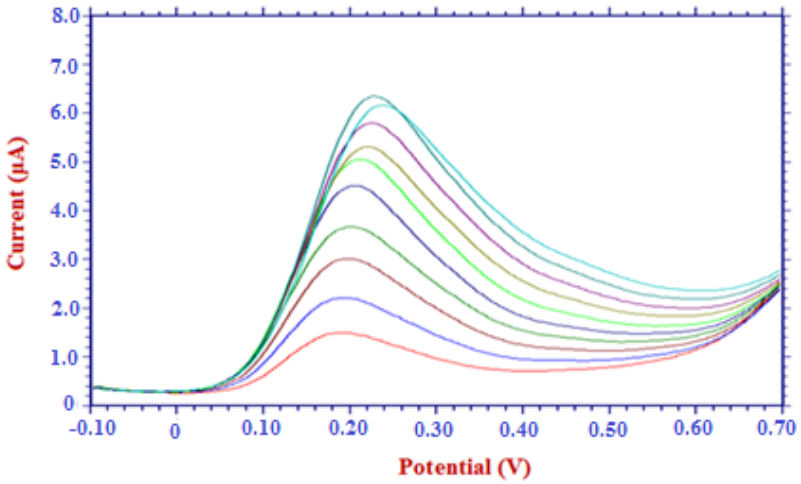

Figure 3.11a: Overlay of difference pulse voltamograms for oxidation of PG at various concentrations

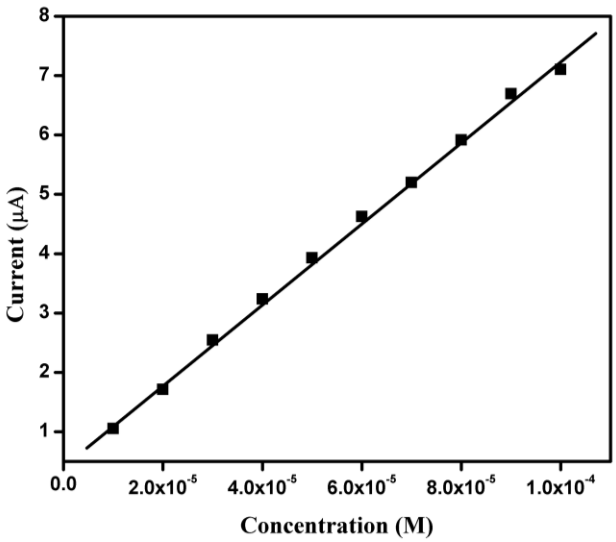

Figure 3.11b: Plot of various concentrations of PG vs peak current

The analytical performance of the MWCNT/GE was compared with other reported voltammetric sensors for PG and the results are summarized in Table 3.2. The limit of detection (LOD) obtained using the proposed MWCNT modified GE sensor is 6.31×10^{-7} M, which is much lower than that of the reported voltammetric works.

To estimate the reproducibility of the electrode, six electrodes were fabricated by same procedure and used to determine 1.00×10^{-4} M PG. The relative standard deviation (RSD) of the peak current was 2.96 %, implying good reproducibility.

3.3.6 Evaluation of kinetic parameters

3.3.6.1 Charge transfer coefficient

The charge transfer coefficient (α) is a significant parameter commonly employed in the kinetic investigation and mechamistic interpretation of electrode process. The term charge transfer coefficient was introduced in electrochemistry by Butler[188,189] and by Erdey-Gruz and Volmer;[190] and was defined as the fraction of the electrostatic potential energy affecting the oxidation/reduction rate in an electrode reaction.

The value of α for an irreversible electrode process can be estimated from Bard and Faulkner equation[191]

$$\boldsymbol{\alpha = \frac{47.7}{E_p - E_{p/2}}\ mV}$$

where $E_{p/2}$ denotes the potential where the current is at half the peak value E_p represents the peak potential. Using the above equation, the value of α was calculated to be 0.459.

3.3.6.2 Heterogeneous rate constant

The kinetic analysis of an electrochemical process involves two important steps: the validation of the proposed mechanism and extraction of kinetic parameters from the experimental data. The study of rates of electron transfer at the electrode/electrolyte interface gave information on the kinetics of the reaction at the electrode surface. In 1993, it was first pointed out by Alexander N. Frumkin that the kinetics of electrochemical reactions should strongly depend on the nature of electrode surface.

For an irreversible electrode process the relation between peak potential and the scan rate can be expressed by the Laviron equation[192]

$$E_{pa} = E^{0\prime} + \frac{RT}{\alpha nF}\left(ln\frac{RTk_s}{\alpha nF} - lnv\right)$$

where E_{pa} is the anodic peak potential, $E^{0\prime}$ is the formal potential. The variation of E_{pa} with lnv was shown in the Figure 3.12a. From the intercept of the plot the value of k_s was calculated. From the intercept of E_{pa} vs. scan rate plot (Figure 3.12b), by extrapolating to the vertical axis at $v = 0$, the value of $E^{0\prime}$ was obtained. The value of k_s for bare and modified electrodes was calculated to be 0.427 and 1.653 respectively. k_s is a very important parameter in electrode kinetics which is a measure of the 'kinetic facility' of the electrochemical process. In other words, systems with small values of k_s, have sluggish electron transfer. Here bare GE has a k_s value which is lower than MWCNT film modified GE indicating that the slow electron transfer is taking place at the bare electrode surface.

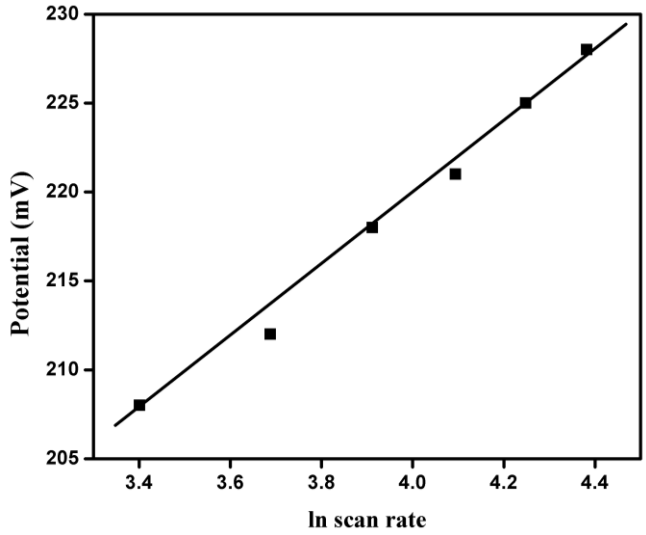

Figure 3.12a: Variation of E_{pa} with ln scan rate

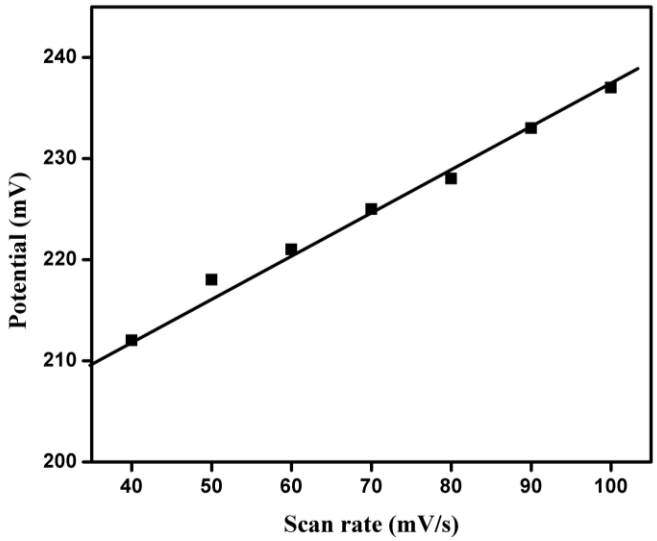

Figure 3.12b: Variation of E_{pa} vs scan rate

3.3.6.3 Chronoamperometric measurements: Determination of diffusion coefficient

The electrocatalytic oxidation of PG at MWCNT/GE was studied by chronoamperometry. Figure 3.13a depicts the chronoamperograms for

different concentrations of PG at MWCNT modified GE. A plot of I *vs* $t^{-1/2}$ for different concentrations of PG at the surface of MWCNT/GE gave straight lines (Figure 3.13b) with different slopes. The slopes of the resulting straight lines were then plotted vs the various concentrations of PG (Figure 3.13c) which was used to estimate the diffusion coefficient (D). For an electroactive material with a diffusion coefficient of D, the current for the electrochemical reaction (at a mass transport limited rate) is expressed by the Cottrell equation[193,194]

$$I = nFAD^{1/2}C\pi^{-1/2}t^{-1/2}$$

where C is the bulk concentration and D is the diffusion coefficient. Other symbols have their usual meaning. The mean value of the D for PG on MWCNT/GE was found to be 3.68×10^{-6} cm^2s^{-1}.

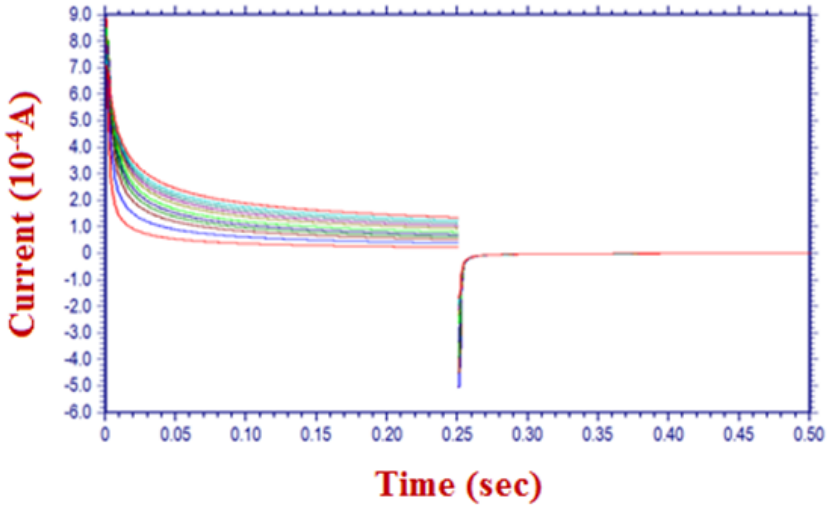

Figure 3.13a: Chronoamperometric response of PG in 0.1 M ABS (pH 7) for different concentration of PG (7.00×10^{-4} – 1.00×10^{-4} M)

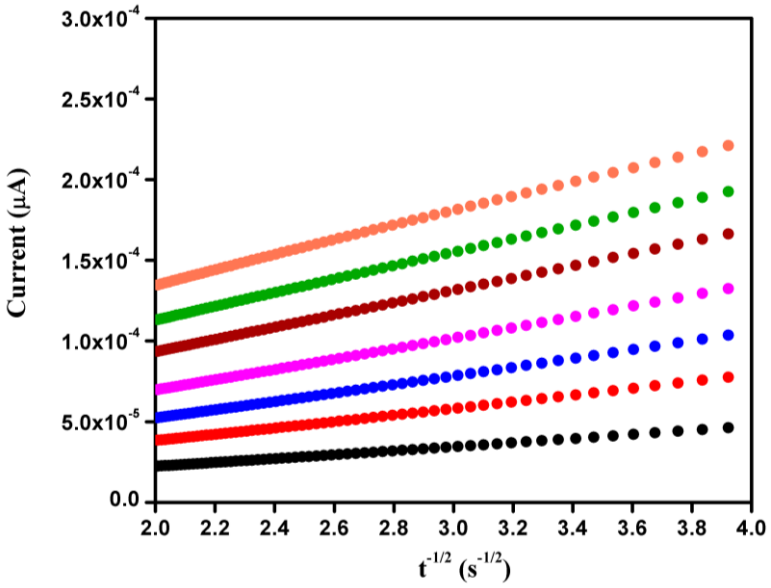

Figure 3.13b: Plot of I vs $t^{-1/2}$

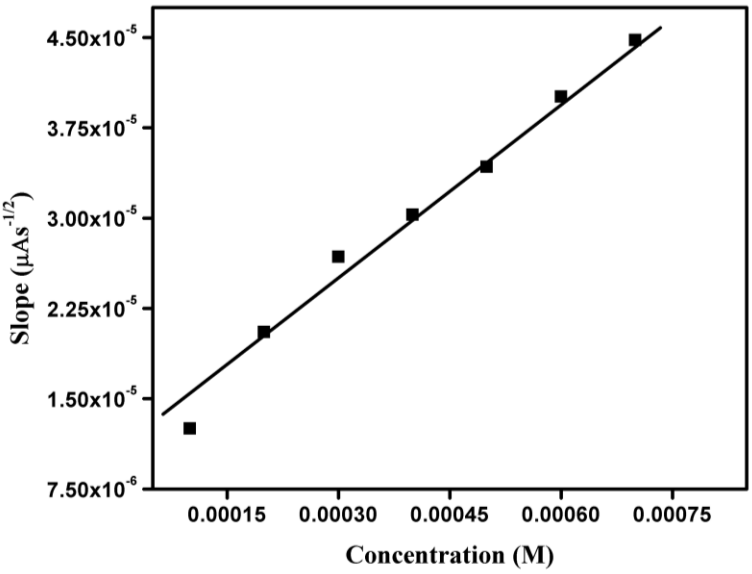

Figure 3.13c: Plot of the slope of the straight line against the concentration of PG

3.3.6.4 Determination of the number of electrons

The number of electrons involved in the reaction (n) can be calculated from the scan rate study using the Laviron's equation[185]

$$\frac{\Delta E_p}{lnv} = \frac{RT}{\alpha nF}$$

It was found that E varies linearly with the ln υ (Figure 3.12a). The slope of this plot (Tafel slope) is equal to, RT/αnF, where α = 0.459 and R, T, F have their usual meaning. For the irreversible oxidation of PG, value of n was calculated to be 1.9. It indicates that the oxidation of PG involves two electrons per molecule as other similar substituted phenols.[160]

3.3.6.5 Reaction mechanism

The observed anodic peak may be due to the oxidation of hydroxyl group present in PG. The mechanism is based on the well described route for the anodic oxidation of phenols, hydroquinones and derivatives.[195] The alkyl gallate radical formed in the first step is immediately converted into a quinone. The existence of alkyl gallate radical species, as proposed in the first de-electronation step reaction, has been previously proved by ESR measurements.[196] Futhermore, the resonance structures of the semiquinone radical have also been proposed for di-catechols[197] with strong oxidative character. The net reaction involves a $2e^-$, $2H^+$ transfer as explained in the Scheme 3.1.

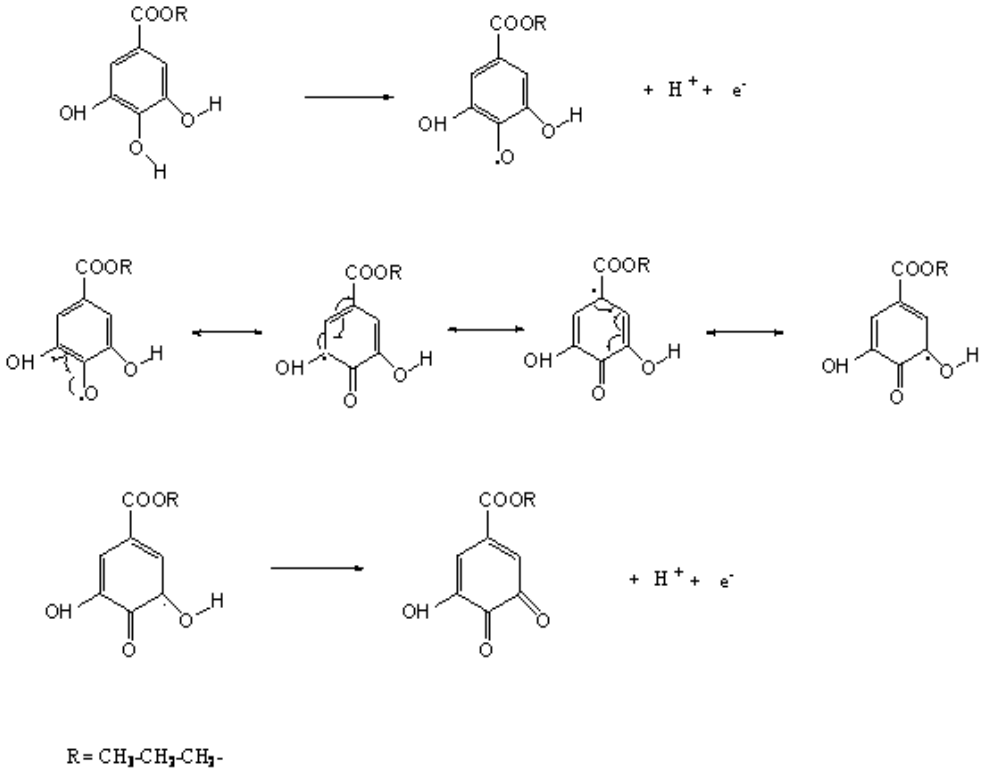

Scheme 3.1: Mechanism of electrooxidation of PG

3.3.7 Interference study

In order to evaluate the selectivity of the MWCNT/GE sensor towards the determination of PG, effect of common coexisting substances was tested (Table 3.3). It was found that even up to 100-fold excess of sodium sulfite, butylated hydroxyl anisole (BHA), butylated hydroxytoluene (BHT), citric acid, NaCl, CH_3COOH, and EDTA did not interfere with the performance of the sensor (signal change below 5 %). However ascorbic acid interferes severely when present even in 1:1 concentrations.

3.3.8 Application study

To assess the analytical applicability, the developed sensor was applied for the determination of PG in spiked vegetable oil samples. The obtained results are in good agreement with those of standard spectrophotometric method[198] (ferrous tartrate and ammonium acetate were used to impart colour to PG solutions and absorbance was measured at 540 nm) and results are listed in Table 3.4. Application study was conducted by spiking the sample with different concentrations of PG, ie at the lowest, average and maximum concentration value in the linear range. It can be seen that the proposed method display sufficient accuracy and precision for real sample analysis.

3.4 Conclusions

Electrochemical determination of PG was carried out using MWCNT modified GE. Compared to bare GE, on the modified electrode lower oxidation overpotential and enhanced peak current was obtained for PG due to the electrocatalytic ability of MWCNT film. Voltammetric studies indicated that the oxidation of PG at the MWCNT modified electrode surface take place through a two electron, irreversible pathway and controlled by diffusion. Optimizations of experimental parameters yield a detection limit much better than those reported in the literature. The increased sensitivity, lower limit of detection, good percentage recovery, ease of fabrication and regeneration of the electrode surface make this sensor a better alternative over the existing methods for the determination of PG. Furthermore it is very rapid, simple and cost effective method. The developed sensor can be successfully applied for the quantitative determination of PG in commercially available vegetable oils.

Table 3.1: Peak potential and peak current of PG (1.00×10^{-4} M) in different supporting electrolytes

Supporting electrolytes (0.1 M)	E_p (mV)	i_p (µA)
HNO_3	408	7.93
HCl	404	9.07
$HClO_4$	384	14.20
NaCl	364	8.41
NaOH	no peak	---------
ABS	180	13.80
PBS	320	6.74

Table 3.2: Comparison of different voltammetric sensors for PG

Electrode	Ep (mV)	Linear range (M)	LOD (M)	References
GCE	599	0.70×10^{-3} to 4.71×10^{-6}	2.54×10^{-6}	182
Pt/Ppy/NiPcTs	550	4.00×10^{-3} to 4.00×10^{-4}	7.23×10^{-6}	187
GCE	580	5.00×10^{-5} to 0.10×10^{-6}	9.90×10^{-5}	161
GE/MWCNT	180	1.00×10^{-4} to 1.00×10^{-5}	6.31×10^{-7}	Proposed Sensor

LOD- limit of detection
Pt/Ppy/NiPcTs - Pt/ polypyrrole electrode modified with tetrasulfonate nickel (II) phthalocyanine complex

Table 3.3: Effect of foreign species on the voltammetric signal of PG (1.00×10^{-4} M)

Foreign species	Concentration (M)	Signal change %
Sodium sulphite	1.00×10^{-2}	3.45
Citric acid	1.00×10^{-2}	2.39
Acetic acid	1.00×10^{-2}	1.89
EDTA	1.00×10^{-2}	4.09
NaCl	1.00×10^{-2}	2.78
BHA	1.00×10^{-2}	3.99
Ascorbic acid	1.00×10^{-4}	8.65

Table 3.4: Determination of PG in vegetable oil samples

Samples	Added (M)	Spectrophotometric method		Proposed method	
		Found (M ± RSD)	Recovery (%)*	Found (M ± RSD)	Recovery (%)*
Sample 1	2.00×10^{-5}	$2.01 \times 10^{-5} \pm 0.13$	100.5	$2.02 \times 10^{-5} \pm 0.19$	101.0
	5.00×10^{-5}	$4.96 \times 10^{-5} \pm 0.11$	99.2	$5.10 \times 10^{-5} \pm 0.26$	102.0
	9.00×10^{-5}	$9.08 \times 10^{-5} \pm 0.24$	100.9	$8.98 \times 10^{-5} \pm 0.11$	99.8
Sample 2	2.00×10^{-5}	$1.99 \times 10^{-5} \pm 0.09$	99.5	$2.05 \times 10^{-5} \pm 0.06$	102.5
	5.00×10^{-5}	$5.04 \times 10^{-5} \pm 0.13$	100.8	$5.07 \times 10^{-5} \pm 0.12$	101.4
	9.00×10^{-5}	$9.11 \times 10^{-5} \pm 0.18$	101.2	$8.97 \times 10^{-5} \pm 0.17$	99.7

* average of six replicates
RSD = relative standard deviation

Chapter 4

POLY(L-CYSTEINE) BASED VOLTAMMETRIC SENSOR FOR ALLURA RED

Contents

Fabrication of a voltammetric sensor by polymerizing L-cysteine (L-cys) on glassy carbon electrode for the determination of allura red (AR), a synthetic food colourant is explained in this chapter. The electropolymerized film of poly(L-cys) provides a stable matrix for the fabrication of a sensing interface. The electrochemical behavior of AR was investigated in 0.1 M citrate buffer solution (pH 6) by cyclic voltammetry, square wave voltammetry and chronoamperometry. Electrochemical impedance spectroscopy, cyclic voltammetry and scanning electron microscopy were used to characterize the modified electrode. The electrochemical reaction of AR at the modified electrode was a reversible process controlled by adsorption. Under optimum conditions, the poly(L-cys) modified electrode showed a linear response in the range from 3.00×10^{-6} *M to* 1.00×10^{-7} *M with a limit of detection of* 3.61×10^{-9} *M. The average surface concentration of AR on modified electrode was found to be* 1.94×10^{-10} $molcm^{-2}$*. The kinetic parameters of the electrochemical reaction such as heterogeneous rateconstant (*k_s*) charge transfer coefficient (*α*), number of electrons (n) and diffusion coefficient (D) were calculated to be 2.386* s^{-1}*, 0.496, 1 and* 1.39×10^{-5} cm^2s^{-1} *respectively. This method has been successfully applied for the determination of AR in soft drinks.*

4.1 Introduction

Colour is an important sensory attribute that influences a person's perception of quality of food. Addition of natural extracts to improve the colour and appearance of food and food products was practiced from ancient times in Egypt, China and India.[199] The use of synthetic food colourants started with the development of first artificial colour additive mauveine by Sir William Henry Perkin in 1856.The advent use of synthetic colorants in the late 1800s and early 1900s unfortunately prompted their misuse in popular foods. Because of the superior qualities of artificial colorants over natural extracts, the development of synthetic colorants became attractive to the food industry. A colourant or colour additive is any dye, pigment or substance which when added to a food, cosmetic or drug, is capable of imparting color by itself or through reactions with other substances. Artificial colours are frequently associated with adverse health effects when consumed excessively.[200]

Among the various food additives, synthetic colourants have been widely used to make food more attractive and to enhance the aesthetic appeal of foodstuffs to the consumer.[66,201] Synthetic azo dyes have found broad applications in food industry due to the in expensive production, wide spectrum of colours, high stability and low microbial contamination compared to natural colourants.[202,203] But some of these colourants and their metabolites create potential health risk to human beings such as allergies, migrains, eczema, anxiety, diarrhea and may provoke cancer, especially when they are consumed in excessive amounts.[204] Therefore, the use of synthetic dyes in foodstuff is strictly controlled by legislation throughout the world.

Allura red (AR), E 129 (Figure 4.1) is a water soluble synthetic azodye, which is usually added to syrups, drinks and sweets to give them fascinating red colour.[205] EU Scientific Committee for Food and Joint FAO/WHO Expert Committee on Food Additives have evaluated the harmful effects of AR and established an acceptable daily intake (ADI) of 0-7 mg/kg body weight/day.[206] Thus it is necessary to develop more sensitive, accurate and reliable analytical methods for the quantification of trace levels of colourants for the assurance of food safety and consumer health.

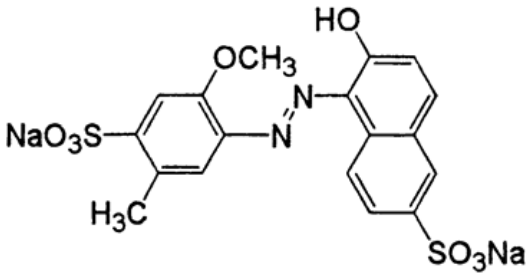

Figure 4.1: Structure of AR

Numerous methods have been reported for the determination of synthetic dyes in foodstuffs which include capillary electrophoresis,[207,208] thin layer chromatography,[209] spectrophotometry[210,211] and high performance liquid chromatography.[212] But these methods have shortcomings such as complex sample treatment, time consuming procedures and expensive instrumentation. Electrochemical methods are fast, convenient, low-cost, highly sensitive, easily adapted for in-situ determination and are environmentally friendly in comparison with other methods.[75,213]

Direct electrochemical determinations at conventional electrodes generally show problems such as high overpotential, sluggish electrode

kinetics, fouling of electrode surface, little selectivity and poor sensitivity.[214] These drawbacks could be minimized by changing the surface of electrode with suitable modifier. Chemically modified electrodes created new opportunities in the development of electrochemical sensors because of their ability to catalyze the electrode process via significant decrease of overpotential and enhancement of peak current with respect to conventional unmodified electrodes.[215] Polymer modified electrodes have received enormous importance in the electroanalytical field because of their selectivity, sensitivity, homogeneity in electrochemical deposition, strong adherence to electrode surface and good chemical stability of the film.[216,217] A thin layer of conducting polymer deposited on to the surface of conventional electrode is able to augment the kinetics of electrode process.[218]

Research on the application of amino acid polymers for the modification of electrodes has received immense attention in recent years.[219] L-Cysteine (2-amino-3-mercaptopropionic acid, L-cys), one of the sulfur containing amino acids, is a non-essential amino acid present in the human body. Due to the presence of functional groups such as sulfhydryl, amine and carboxyl, L-cys could effectively modify the glassy carbon electrode (GCE).[17]Amino acids modified electrodes have many merits such as good biocompatibility, ease of preparation and excellent stability.[220-222]

The excellent electrocatalytic properties of poly(L-cys) film is utilized in the present work to develop a sensitive and accurate method for the determination of AR. Electrochemical behavior of AR was examined at poly(L-cys) film coated GCE. Cyclic voltammetric technique was used to study various kinetic parameters of the redox reaction such as standard

heterogeneous rate constant (k_s), electron transfer coefficient (α) and number of electrons exchanged (n). Diffusion coefficient of AR on poly(L-cys)/GCE was determined using chronoamperometric measurements. The average surface coverage of AR on the polymer modified electrode was calculated to be 1.94×10^{-10} molcm^{-2}. Compared to GCE, the oxidation peak potential of AR shifts negatively and peak current increased drastically at the poly(L-cys)/GCE, indicating efficient catalytic ability and high sensitivity of the polymer film. The practical application of the polymer film modified electrode was verified by determining AR in soft drink samples and the proposed method has been validated using spectrophotometry.

4.2 Experimental

4.2.1 Pretreatment of GCE

Prior to the polymerization of L-cysteine on the surface of GCE, bare GCE was polished using 0.05 micronalumina slurry on a polishing pad, rinsed thoroughly with water and sonicated successively in methanol, 1:1 HNO_3 solution, acetone and double distilled water to remove any adsorbed alumina particles on the electrode surface.

4.2.2 Preparation of poly(L-cys)/GCE

The cleaned GCE was immersed in phosphate buffer (pH 7) containing 5.00×10^{-3} M L-cys, and the electro polymerization was carried out by cycling the potential between -800 mV and 2000mV at a scan rate of 100 mV/s (Figure 4.2).[223] Then the film was washed with ethanol and double distilled water to remove the remaining L-cys monomers and the resulting blue coloured poly(L-cys) film modified GCE was used to carry out the measurements.

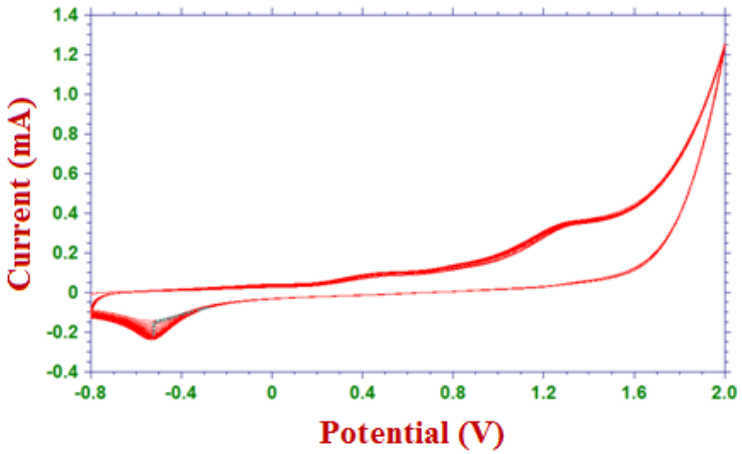

Figure 4.2: Electropolymerization of L-cys on GCE

L-cys contains amino and the carboxyl groups. In the anodic scan, amino group of L-cys is easily oxidized to its corresponding free radical by one electron transfer, and then the free radical reacts with carbon of the electrode surface forming a carbon-nitrogen covalent linkage. An oxidation peak was observed at 1300 mV in the first anodic scan, and a reduction peak was observed at -500mV in the reverse scan.[223,224] By varying the number of voltammetric scans, thickness of the poly(L-cys) film can be controlled.

4.2.3 Preparation of solution of AR

A stock solution (1.00×10^{-2} M) of AR was prepared by dissolving 0.496 g analyte in 10 mL water. Solutions of various concentrations of AR were prepared by diluting the stock solution using the supporting electrolyte.

4.2.4 Analytical procedure

0.1 M citrate buffer solution (pH 6) was used as the supporting electrolyte for all electrochemical measurements. A desired volume of AR solution was pipetted into an electrochemical cell containing 10 mL of

citrate buffer solution. Then square wave voltammograms were recorded from -500 mV to 600 mV at a scan rate of 100 mV/s with pulse amplitude of 25 mV, quiet time of 2 s, frequency of 15 Hz and increment of 4 mV. The peak corresponding to the oxidation of AR was measured at 52 mV. To regenerate the electrode surface, activation of poly(L-cys)/GCE was done by successive cyclic voltammetric sweeps from -500 mV to 600 mV in the buffer solution until the voltammograms remain unchangable.

4.2.5 Sample treatment

Two soft drink samples were purchased from local super market and used without any pre-treatment.[66] 1 mL of sample solution was added into 9.0 mL of 0.1 M citrate buffer solution (pH 6), for the determination of AR using a poly(L-cys)/GCE and then examined according to the analytical procedure

4.3 Results and discussion

4.3.1 Surface characterization

Scanning electron microscopic (SEM) images, surface area calculations and electrochemical impedance spectroscopy (EIS) gave evidences for the modification of GCE surface by polymer film of L-cys.

4.3.1.1 Surface morphology studies of poly(L-cys)/GCE

SEM analysis was carried out to study the surface morphology of the of GCE surface before and after modification. Figure 4.3a and 4.3b shows the changes in surface morphology obtained from SEM images for bare GCE and poly(L-cys)/GCE respectively. From SEM images it is clear that a homogenous film was formed on the surface of the GCE, after the electrochemical polymerization.

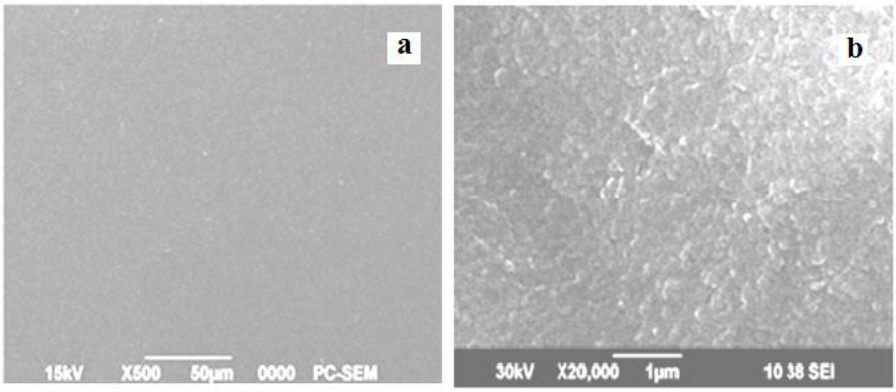

Figure 4.3: SEM images of (a) bare GCE (b) poly(L-cys)/GCE

4.3.1.2 Surface area study

Randles-Sevcik equation was applied for the determination of effective surface area of GCE before and after modification with polymer film.[184]

$$i_p = 2.69 \times 10^5 An^{3/2} D^{1/2} Cv^{1/2}$$

Cyclic voltammograms were recorded in 2 mM $K_3Fe(CN)_6$ in the potential range of 0-600 mV using bare GCE and polymer film modified GCE at different scan rates (Figure 4.4). From the slope of $i_p$vs $v^{1/2}$ plot (Figure 4.5), the effective surface areas of the bare GCE and poly(L-cys)/ GCE were calculated as 0.1643 cm^2 and 0.4791 cm^2 respectively, ie on modification there is a three fold increase in surface area. This enhancement in surface area of modified electrode compared to bare GCE, could give more catalytic sites, thereby increasing the sensitivity of determination of AR. This is a strong evidence for the effective and successful modification of GCE.

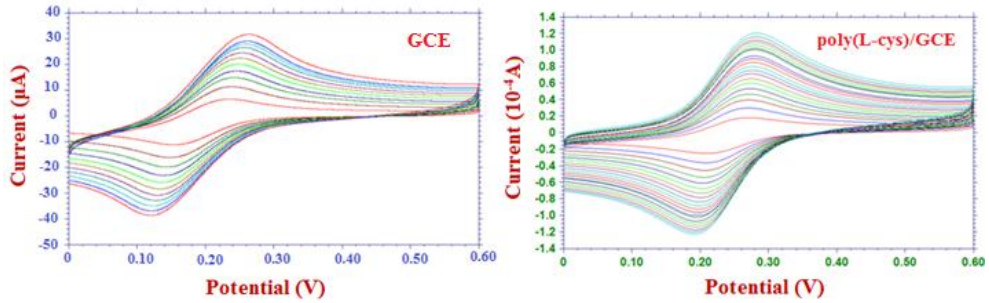

Figure 4.4: Surface area study of bare GCE and poly(L-cys)/GCE in $K_3Fe(CN)_6$ solution

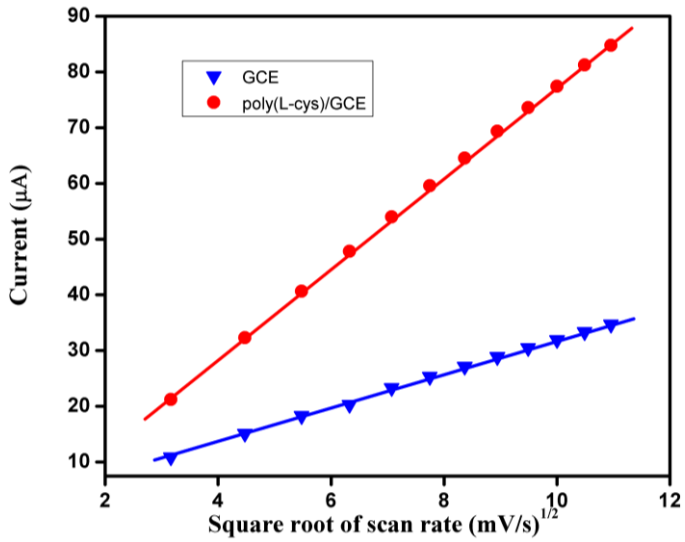

Figure 4.5: Plot of square root of scan rate vs current for bare GCE and poly (L-cys) modified GCE

4.3.1.3 Electrochemical impedance analysis

EIS is a powerful technique for convenient determination of kinetic parameters, mass transport and the charge transfer coefficient.[225] The impedance spectra consist of a semicircle portion and a linear portion. The semicircle part at higher frequency corresponds to the electron transfer limited process and the semicircle diameter equals electron transfer

resistance (R_{et}).[225] This resistance controls the electron transfer kinetics of redox probe at the electrode/electrolyte interface. The electrochemical impedance of AR was investigated on GCE and poly(L-cys)/GCE in citrate buffer (pH = 6) and corresponding Nyquist plots are shown in Figure 4.6. The diameter of the semicircle decreased after the modification of the polymer film, indicating that the modified electrode can effectively reduce the charge transfer resistance and increase the electronic exchange rate between the electrode surface and the electrolyte solution,[217] which can offer a high sensitivity for the determination of AR using poly(L-cys)/GCE.

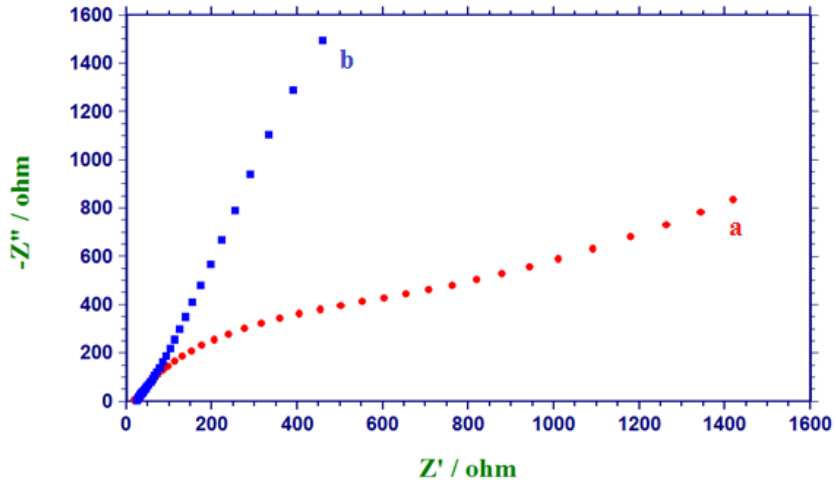

Figure 4.6: Nyquist plots for bare GCE (a) and (b) poly (L-cys)/GCE

4.3.2 Electrochemical behaviour of AR on the poly(L-cys) film modified electrode

The electrochemical response of AR on the poly(L-cys) modified GCE was examined using CV. Figure 4.7 shows the cyclic voltammograms of 1.00×10^{-5} M AR on the bare GCE (curve a) and poly(L-cys)/GCE (curve b) in 0.1M citrate buffer solution of pH 6. A pair of redox peaks

with anodic and cathodic peak potentials at 139 mV (i_{pa} = 5.04 µA) and 49 mV(i_{pc} = -7.37 µA) was observed at unmodified GCE. The peak to peak separation ($\Delta E_p = E_{pa} - E_{pc}$) was 90 mV, indicating a quasi-reversible electrochemical reaction, which may be due to the slow electron transfer kinetics on bare GCE. Under the same experimental conditions a couple of well defined reversible redox peaks (formal potential, $E^{0'}$ = 50 mV) were observed on the polymer film modified electrode with an anodic potential at 76 mV (i_{pa} = 34.47 µA) and cathodic potential at 24 mV (i_{pc} = -29.14 µA). Interestingly, upon modification along with the enhancement of peak currents, the peak potential separation (ΔE_p) was reduced to 52 mV from 90 mV, suggesting that the electron transfer process occurring at the electrode/electrolyte interface has accelerated significantly in the presence of polymer film. The chemical and physical stability and three dimensional structure of polymer film provide more reaction sites and effective potential for the electrode reaction.[226]

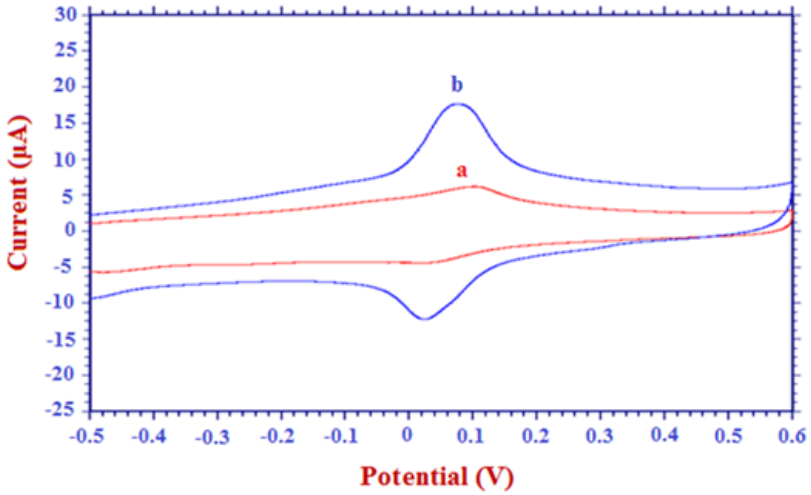

Figure 4.7: Cyclic voltammograms of AR at (a) bare GCE and (b) poly(L-cys)/GCE

Compared with GCE, poly(L-cys)/GCE remarkably increases the peak current and decreases the oxidation overpotential of AR. This can be attributed to the fast electron transfer ability and large surface area of polymer film modified electrode. To sum up, compared with the bare GCE, poly(L-cys) modified GCE enables a lower limit of detection ie, a higher sensitivity which is in great demand for the quantification of trace amounts of AR.

4.3.3 Optimization of experimental conditions

Effect of various factors such as supporting electrolyte, pH of the supporting electrolyte, accumulation time and the number of segments of electropolymerization of L-cys on the performance of the sensor have been studied and the suitable conditions were optimized.

4.3.3.1 Effect of supporting electrolyte and pH

The electrochemical response of AR at poly(L-cys) /GCE, was studied in various media such as 0.1 M solutions of phosphate buffer, acetate buffer, nitric acid, sulphuric acid, perchloric acid, NaCl and NaOH to study the influence of supporting electrolytes and results are shown in Table 4.1. Highest peak current was observed in citrate buffer solution (CBS) and hence it was selected as supporting electrolyte for further studies. (Eventhough high current was observed in perchloric acid, due to unstable response it was not selected for further studies).

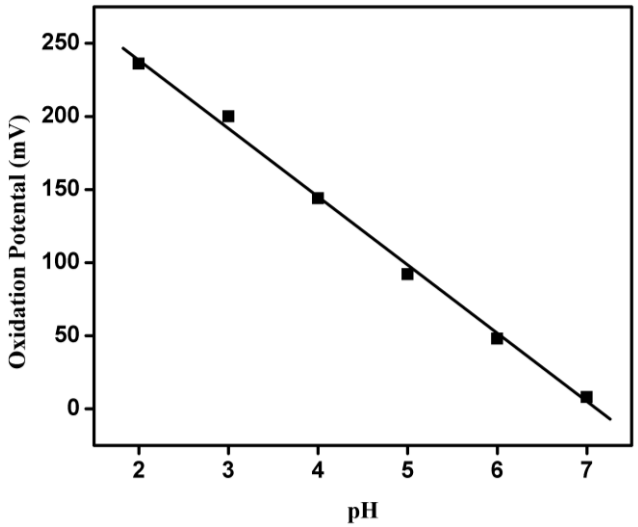

Figure 4.8a: Effect of pH on the oxidation potential of AR

Figure 4.8a shows the influence of pH on the oxidation peak potential of AR on poly(L-cys)/GCE. Both the oxidation and reduction peak potentials shifted negatively with increasing pH of the CBS, implying the participation of protons in the oxidation of AR. Based on the Nernst relation[227]

$$\frac{\mathbf{dE_p}}{\mathbf{dpH}} = \frac{\mathbf{2.303mRT}}{\boldsymbol{\alpha}\mathbf{nF}} = \frac{\mathbf{0.059m}}{\boldsymbol{\alpha}\mathbf{n}}$$

where n is the number of electrons and m is the number of protons involved in the reaction, α is the charge transfer coefficient. The value of m/n was calculated to be nearly 1, which was in accordance with previous report.[204] A linear relationship could be obtained between the peak potential and pH of the solution. pH dependence of E_{pa} is represented by the equation as $E_{pa}(V) = 0.0537\ pH - 333.24$ ($R^2 = 0.996$). The slope is close to the theoretical value -57.6 mV/pH, indicating that electrochemical oxidation reaction of AR involves an equal number of protons and electrons.[202,204]

The influence of pH (2 to 9) on the oxidation peak current of AR is shown in Figure 4.8b. On increasing pH from 2 to 6 the anodic peak current gradually increases, but on further increasing pH from 6 to 9 the anodic peak current gradually decreases. A maximum peak current was obtained at pH 6. Hence CBS of pH 6 was selected as the optimum pH for further studies.

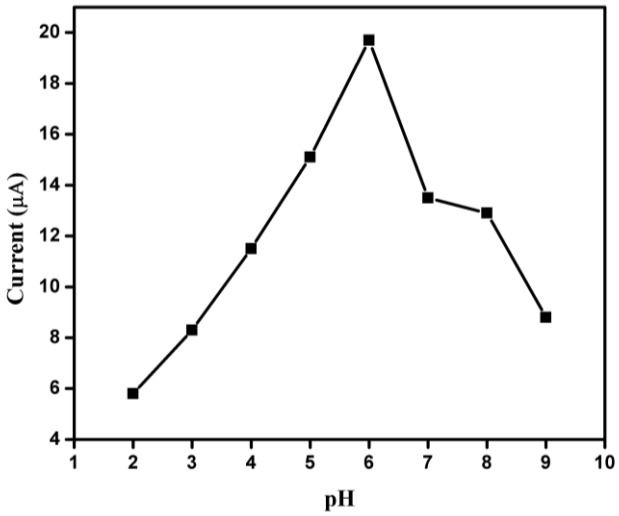

Figure 4.8b: Effect of pH on the oxidation current of AR

4.3.3.2 Effect of accumulation time

The influence of accumulation time on the anodic peak current of 1.00×10^{-6} M AR was investigated. The oxidation current of AR enhanced greatly with increasing the accumulation time in the first 4 min and then remained stable and the results are illustrated in the Figure 4.9. Taking into account both the sensitivity and the efficiency, an accumulation time of 4 min was selected in further studies.

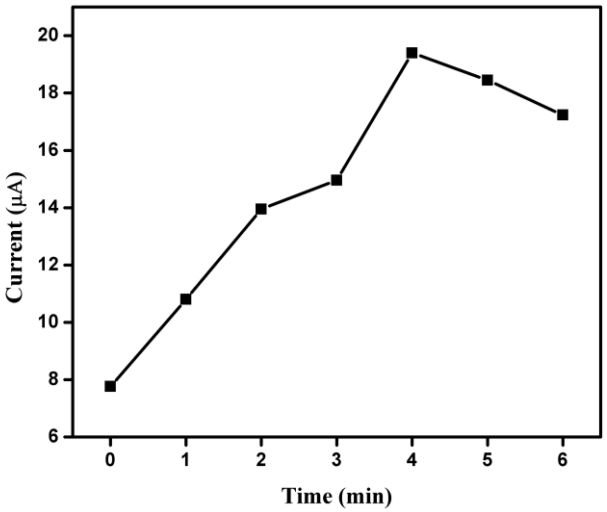

Figure 4.9: Effect of accumulation time

4.3.3.3 Effect of number of segments of electropolymerization

Relation between the peak current and number of segments of electropolymerization was studied from 10 to 50 segments and the results are shown in Figure 4.10.

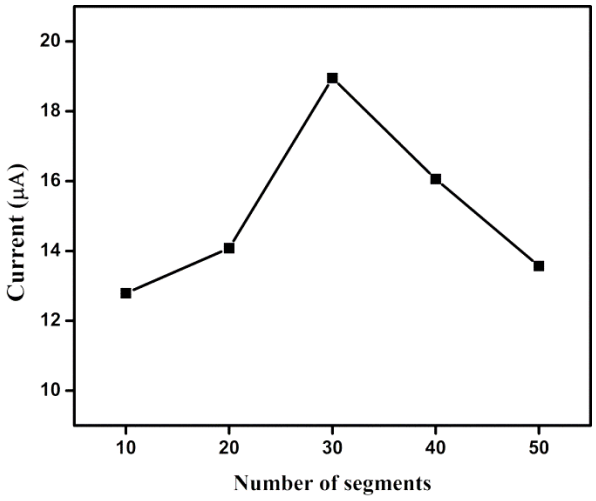

Figure 4.10: Effect of number of segments of electropolymerization

The peak current increased drastically with augment in number of segments from 10 to 30, and thereafter showed a gradual decrease. The maximum current was observed at 30 segments, hence polymerization by 30 segments was chosen for further experiments.

4.3.4 Effect of scan rate and characteristics of oxidation process

The influence of scan rate on the redox peak current of AR on poly(L-cys)/GCE was studied by CV and the results are shown in Figure 4.11a. Both the oxidation peak current and reduction peak current of AR increased linearly with the scan rate in the range of 40 - 400 mV/s (Figure 4.11b), suggesting that the electrochemical oxidation of AR is adsorption controlled. The linear regression equations could be expressed as follows;

$$i_{pa} = 0.0871v + 4.2115\ (R^2 = 0.991)\ \text{and}$$
$$i_{pc} = -0.0626 - 1.9254\ (R^2 = 0.991).$$

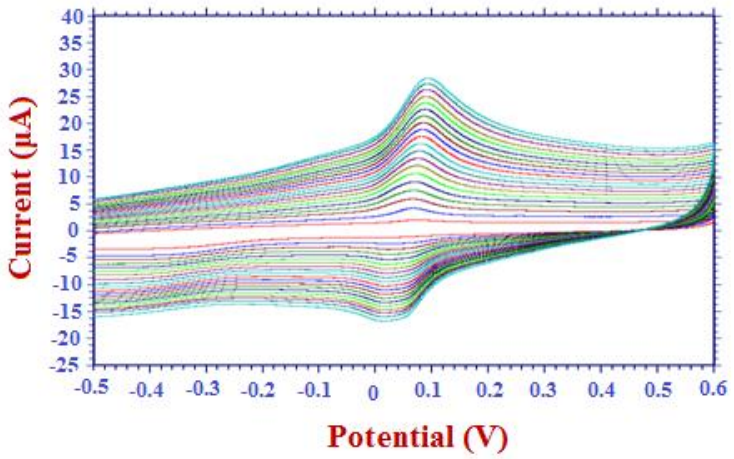

Figure 4.11a: Overlay of Cyclic voltammograms for oxidation of AR on poly (L-cys)/GCE at various scan rates

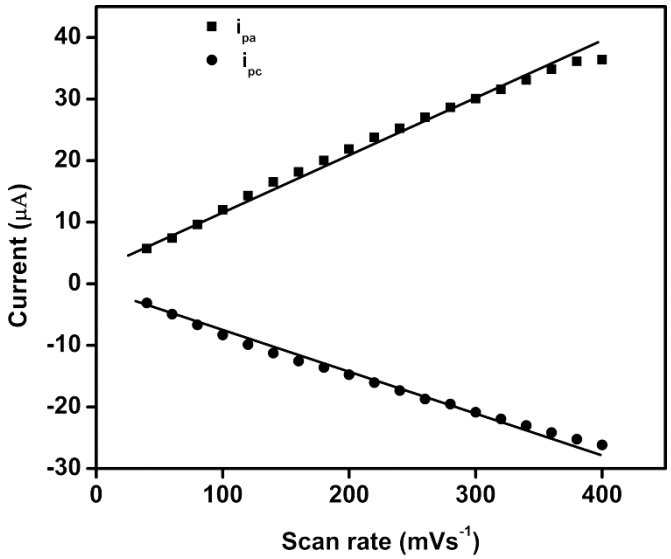

Figure 4.11b: Variation of anodic and cathodic currents of AR with scan rate

Also the trends of peak shift as a function of the scan rate (with the increase of scan rate, anodic peak potential shifted positively, while the cathodic peak potential shifted negatively, ie ΔE_p increases with scan rate) revealed that the reversibility of the electrode reaction decreased at higher scan rates.

In addition, plot of log $i_p$vs logυ yielded a straight line (Figure 4.11c) with slope of 0.867 for anodic peak and 0.873 for cathodic peak in the scan rate range 60-300 mVs^{-1} and the value of slope is close to the theoretical value of 1.00, which is expected for an ideal reaction condition for adsorption controlled electrode process.[228]

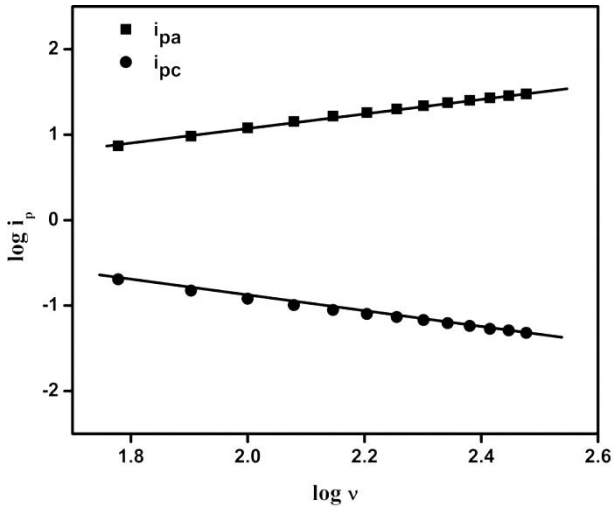

Figure 4.11c: Plot of log $i_p$vs log ν

4.3.5 Calibration plot and limit of detection

Since square wave voltammetry gave a much higher current sensitivity than CV, it was used for the quantification of AR on poly(L-cys)/GCE, under optimized experimental conditions. Figure 4.12a shows the square wave voltammograms of the different concentrations of AR at the polymer film modified GCE. The linear dependence of peak currents on the concentration of AR obtained was in the ranges $3.00 \times 10^{-6} - 1.00 \times 10^{-7}$ M (Figure 4.12b). The linear regression equation can be expressed as $i_p = 90.12C + 10.33$ ($R^2 = 0.997$). The limit of detection was found to be 3.61×10^{-9} M. The modified electrode showed a wider linear range and lower detection limit than bare GCE, which can be attributed to the introduction of the conducting layer of poly(L-cys) on the surface of GCE. The analytical performance of the developed sensor is further compared with some other reported determination methods of AR (Table 4.2). An examination of

Table 4.3 reveals that the proposed method is superior to other quantification methods for AR, especially with respect to limit of detection.

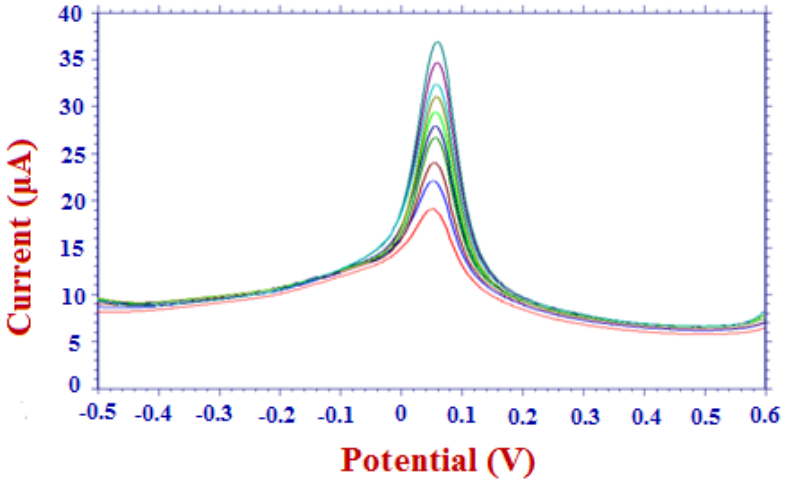

Figure 4.12a: Overlay of Square wave voltammograms for oxidation of AR at various concentrations

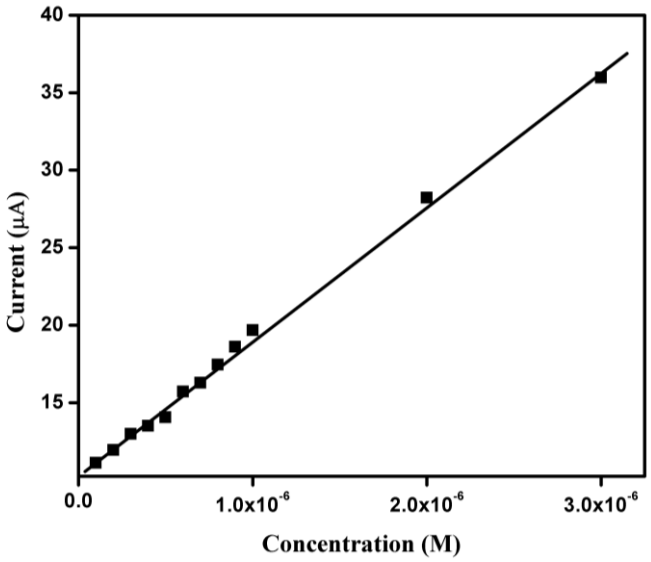

Figure 4.12b: Plot of peak current vs concentration of AR

The repeatability as well as the reproducibility of the modified electrode have been evaluated in CBS (pH 6) containing 5.00×10^{-7} M AR. It was found that the oxidation peak current of AR remained almost unchanged with a relative standard deviation (RSD) of 1.57 % for 8 repeated measurements. Reproducibility of the modified electrode was tested with six modified electrodes prepared by the same fabrication procedure and RSD was found to be 2.13%. These results illustrated that the proposed method could offer good repeatability and reproducibility for the determination of AR.

4.3.6 Evaluation of kinetic parameters

4.3.6.1 Charge transfer coefficient

Cyclic voltammetry has been recognized as the electrochemical method of choice for the evaluation of the kinetics of charge transfer redox reactions. In a reversible reaction, the symmetry between the forward and reverse electron transfer reactions can be expressed in terms of α, the charge transfer coefficient.[231] The following equations are used to find out anodic charge transfer coefficient (α_a) and cathodic charge transfer coefficient (α_c), where a and b are constants[232]

$$E_{pa} = a + \{2.303RT|(1-\alpha)nF\}log\upsilon$$

$$E_{pc} = b - \{2.303RT|\alpha nF\}log\upsilon$$

From the slope of the plot of the anodic and cathodic peak potentials with the logarithm of scan rate (Figure 4.13), the value of α was calculated as 0.496 (α_a = 0.531, α_c = 0.461) for poly(L-cys)/GCE. The linear regression equations of the E_{pa} and E_{pc} vs the logarithm of the scan rates are expressed as $E_{pa} = 0.1113log\upsilon - 138.31$ and $E_{pc} = -0.1282log\upsilon + 342.97$, in the

scan rate range 360-600 mV/s. Similar studies were carried on bare GCE and the value of α was calculated as 0.513. For bare GCE the values of α_a and α_c were found to be 0.437 and 0.589 respectively.

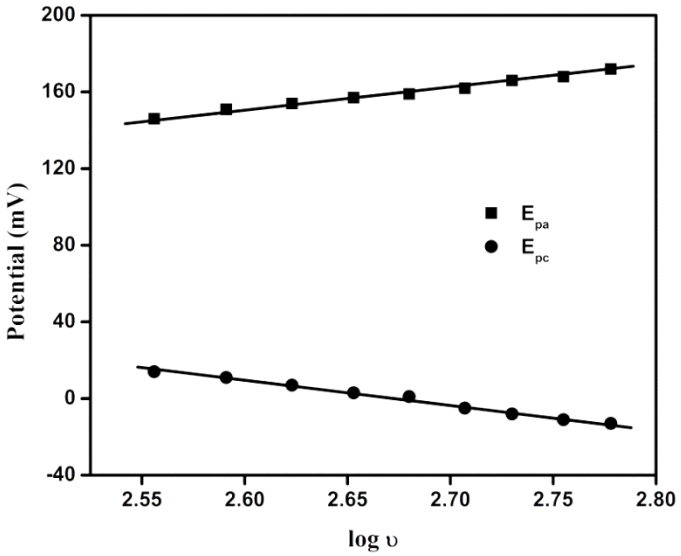

Figure 4.13: Variation of E_{pa} and E_{pc} with log scan rate

4.3.6.2 Heterogeneous rate constant

For reversible systems, Nernstian equilibrium is always maintained at the electrode surface, since the electron transfer rates are significantly greater than the mass transport rate.[233] k_s, the heterogeneous rate constant is the most significant parameter to explain electron transfer rate between an electrode surface and the redox system, hence the value of $k_s$was evaluated using the following equation. Laviron model which is based on the amount of peak separation between the forward and reverse scans in a cyclic voltammogram was applied for the calculation of k_s[234,235]

$$\boldsymbol{logk_s = \alpha log(1-\alpha) + (1-\alpha) log\alpha - log\frac{RT}{nFv} - \frac{\alpha(1-\alpha)nF\Delta E_p}{2.3RT}}$$

the rate constant k_s for poly(L-cys)/GCE was calculated to be 2.386 s^{-1} (by taking charge transfer coefficient α = 0.496, v =100 mV/s, ΔE_p = 52 and n = 1). k_s value for poly(L-cys) modified electrode is higher than those obtained for bare GCE (1.553 s^{-1}), shows that the feasibility of the reaction increased on the modified electrode. From these results it is clear that poly(L-cys) layer can greatly enhance electron transfer rate between the electrode and AR. In addition to this, presence of conducting layer of poly(L-cys), increases the effective surface area of GCE and leads to an increase in the surface concentration of AR, resulting in a high value of k_s .

Consider the electron transfer reaction occurring at the electrode surface at a fixed potential (chemically reversible system)[236,237]

$$\boldsymbol{Ox + ne^{-} \rightleftharpoons Red}$$

The forward and reverse rate constants, k_f and k_b are given by the equations

$$\boldsymbol{k_f = k_s exp}\left[\frac{-\alpha nF\left(E-E^{0\prime}\right)}{RT}\right]$$

$$\boldsymbol{k_b = k_s exp}\left[\frac{(1-\alpha)nF\left(E-E^{0\prime}\right)}{RT}\right]$$

From the above equations the values of k_f and k_b for the redox couple ofAR were calculated to be 1.393 s^{-1}, 1.378 s^{-1} respectively at 100 mVs^{-1} on poly(L-cys)/GCE.

4.3.6.3 Chronoamperometric studies: Determination of diffusion coefficient

The catalytic oxidation of AR at the surface of conducting film modified GCE was also studied by chronoamperometry and diffusion coefficient of AR for a poly(L-cys)/GCE was determined. For an electroactive

compound with a diffusion coefficient of D, the current of the electrochemical reaction (at a mass transport limited condition) is expressed by the Cottrell equation[193,194]

$$I = nFAD^{1/2}C\pi^{-1/2}t^{-1/2}$$

where D is the diffusion coefficient and C is the bulk concentration. The value of D can be calculated from the slope of I vs $t^{-1/2}$ plots (Cottrell plots). Chronoamperometric measurements were carried out in various concentrations of AR (1.00×10^{-4} to 1.00×10^{-5} M) on poly (L-cys)/GCE (Figure 4.14a) and the Figure 4.14b shows the corresponding I vs $t^{-1/2}$ plots. The slopes of the resulting straight lines were then plotted against the concentration of AR (Figure 4.14c). From the resulting slope and Cottrell equation the mean value of the D was calculated to be 1.39×10^{-5} cm^2s^{-1}.

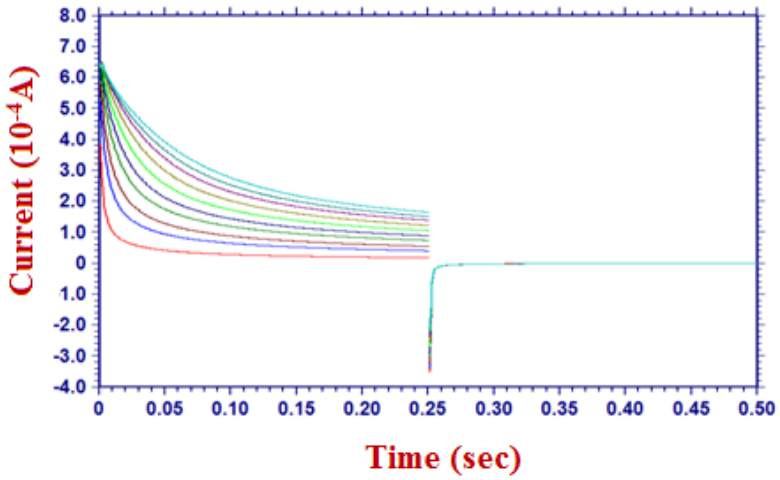

Figure 4.14a: Chronoamperometric response of AR in 0.1 M CBS for different concentrations (1.00×10^{-4} – 1.00×10^{-5} M)

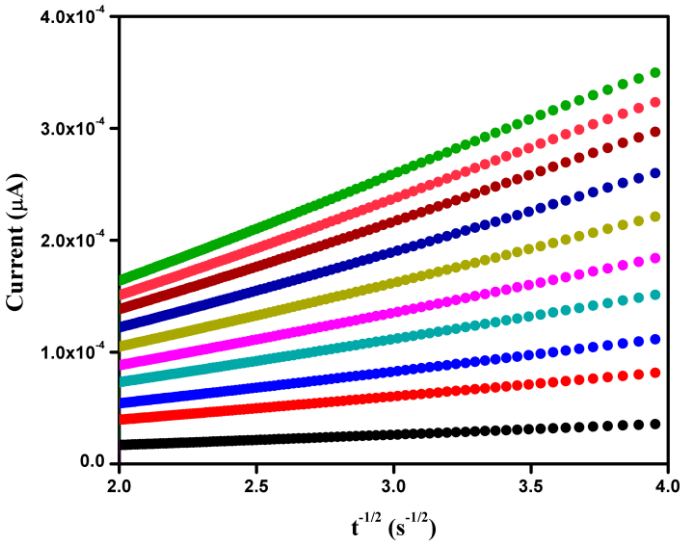

Figure 4.14b: Plot of I vs $t^{-1/2}$

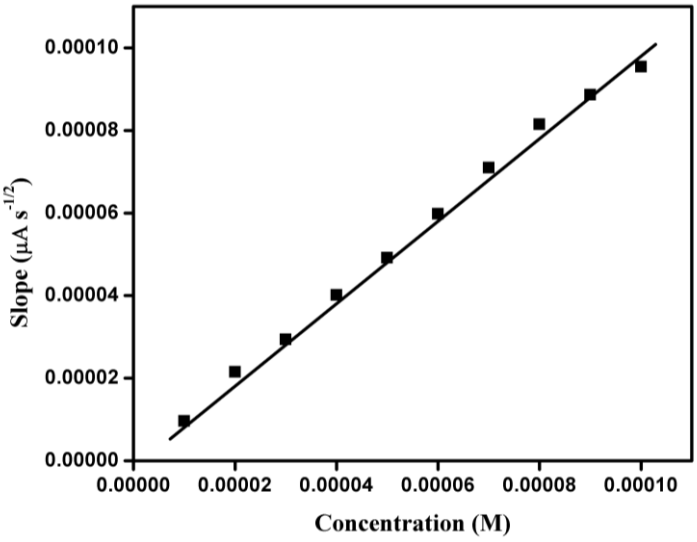

Figure 4.14c: Plot of the slope of the straight line against the concentration of AR

4.3.6.4 Average surface concentration of AR on poly(L-cys)/GCE

The relationship between the amount of AR adsorbed on the surface of poly(L-cys)/GCE (Γ) and the peak current (i_p) can be expressed as[238]

$$i_p = \frac{n^2F^2A\Gamma v}{4RT}$$

where A is the effective surface area of poly(L-cys)/GCE; n is the number of electrons; v is the scan rate; R, T and F have their usual meaning. Based on the slope of peak current versus scan rate plot, the value of Γ was calculated to be 1.94×10^{-10} molcm^{-2}.

4.3.6.5 Number of electrons

The redox potential of AR shifted positively with scan rate and the relationship is expressed with the following equation[239]

$$E_p = E^{0\prime} + \frac{RT}{\alpha nF}\left[0.780 + \ln\frac{D^{1/2}}{k_s} + \ln\left(\frac{\alpha nFv}{RT}\right)\right]^{1/2}$$

$$= K + \frac{RT}{2\alpha nF}\ln v$$

where $E^{0\prime}$ is the formal potential, and other symbols have their usual meaning. The value of n can be calculated from the slope of E_p vs ln v plot (Figure 15) and it was found that the oxidation of AR involves one electron.

The number of electrons (n) involved in the electrochemical oxidation of AR can also be calculated using the equation[202]

$$\Delta E = \frac{59}{n}$$

The potential difference of 52 mV was observed between the redox peaks ($\Delta E = E_{pa} - E_{pc}$) of AR on poly(L-cys)/GCE at a scan rate of 100 mV/s. Using the above equation the number of electrons involved in the oxidation of AR was calculated to be 1.

4.3.6.6 Reaction mechanism

pH study gives significant information about the electrochemical reaction of AR on poly(L-cys)/GCE. As pH increases the oxidation potential of AR shifted positively, indicating that protons are involved in the reaction. From slope of the plot E_{pa} against pH (53.7 mV/pH), it was clear that equal number of protons and electrons are taking part in the process. It was calculated that number of electrons involved in the oxidation of AR was one. Naphthols are known to undergo electrochemical oxidation to naphthyloxy radical by a one electron transfer process (Scheme 4.1).[240] Based on this the observed oxidation peak may be due to the oxidation of hydroxyl group present in AR, by a one proton, one electron reaction.[66]

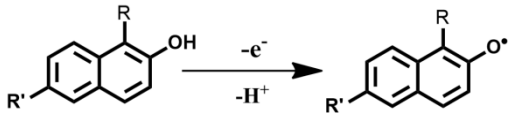

Scheme 4.1: Electro oxidation of naphthols to naphthyloxy radical

This radical may further undergo non electrochemical reactions, resulting in the formation of a quinone.

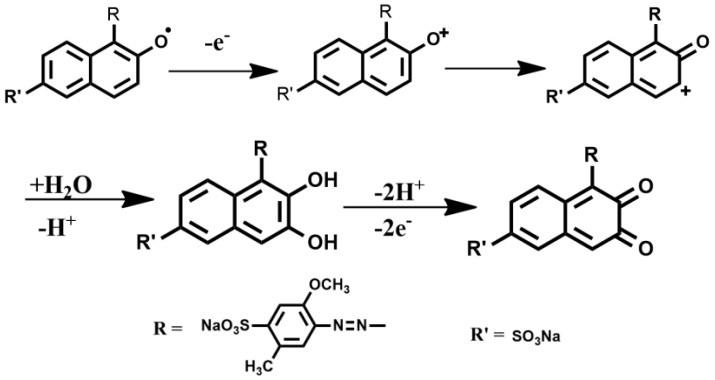

Scheme 4.2: Mechanism for the formation of quinone

4.3.7 Interference study

To evaluate the selectivity of the proposed sensor, the influence of various species on the oxidation peak current of AR was studied. The voltammetric signal was recorded for 1.00×10^{-6} M AR in the presence of various concentrations (1:1 fold, 1:10 fold and 1:100 fold) of foreign species such as quinoline yellow, sodium sulphite, amaranth, citric acid, tartrazine, aspartame, fructose and ascorbic acid (Table 4.3). The results demonstrated that even up to 100 fold excess concentration of quinoline yellow, sodium sulphite, citric acid, tartrazine, aspartame and fructose had no influence on the electrochemical signal of AR. However ascorbic acid interferes the determination even when present in 1:1 concentration of AR. A signal change greater than 5 % was observed when amaranth was present 50 fold in excess of AR. This suggested that poly(L-cys)/GCE had good selectivity for the determination of AR.

4.3.8 Application study

In order to further verify the performance and feasibility of the developed sensor, it was used for the analysis of AR in soft drink samples. The percentages of recovery values were calculated by comparing the concentrations obtained from the samples with actually added concentrations. The results are listed in Table 4.4. The results indicate that there are no matrix interferences in the analysis of the samples. The recoveries were obtained in the range from 98.5 to103.5 %, which revealed that the developed sensor has good accuracy and could be effectively used for the determination of AR in real samples. The obtained results are in good agreement with that of the spectrophotometric method.[241]

4.4 Conclusions

The electrochemical behavior of AR has been studied on a GCE modified with electropolymerized film of L-cys in 0.1 M CBS (pH 7). A reversible redox process was observed for AR with a formal potential of 50 mV on the poly(L-cys) modified electrode. The conducting layer of poly(L-cys) showed excellent electrocatalytic activity for the oxidation of AR. In addition, the modified electrode exhibited satisfactory stability, sensitivity and reproducibility, and could be applied to the determination of AR in soft drink samples. The results were comparable with that of spectrophotometric method.

Table 4.1: Peak potential and peak current of AR (1.00×10^{-5} M) in different supporting electrolytes

Supporting electrolytes (0.1 M)	E_{pa} (mV)	i_p (µA)
KNO_3	56	14.96
$HClO_4$	308	24.08
NaOH	472	6.32
CBS	52	18.78
ABS	140	5.74
PBS	40	8.71

Table 4.2: Comparison with other methods for the determination of AR

Method	E_p (mV)	Linear range (M)	LOD (M)	References
Voltammetry (MWCNT/GCE)	680	1.07×10^{-7} - 1.21×10^{-8}	5.04×10^{-8}	205
Voltammetry (polyallylamine/GCE)	550	1.50×10^{-4} - 1.00×10^{-5}	1.40×10^{-6}	66
Differential pulse polarography	-596	9.06×10^{-6} - 4.03×10^{-9}	8.66×10^{-8}	229
Adsorptive stripping voltammerty	-620	……	7.60×10^{-10}	230
HPLC-MS/MS	……	2.00×10^{-7} - 4.03×10^{-9}	2.90×10^{-8}	206
poly L-cys)/GCE	-52 mV	3.00×10^{-6} - 1.00×10^{-7}	3.61×10^{-9}	Proposed Sensor

Table 4.3: Effect of foreign species on the voltammetric signal of AR (1.00×10^{-6} M)

Foreign species	Concentration (M)	Signal change %
Quinoline yellow	1.00×10^{-4}	3.56
Sodium sulphite	1.00×10^{-4}	2.24
Citric acid	1.00×10^{-4}	4.89
Tartrazine	1.00×10^{-4}	4.68
Aspartame	1.00×10^{-4}	4.74
Fructose	1.00×10^{-4}	3.72
Amaranth	5.00×10^{-5}	4.04
Ascorbic acid	1.00×10^{-6}	8.65

Table 4.4: Determination of AR in soft drink samples

Samples	Added (M)	Spectrophotometric method		Proposed method	
		Found (M ± RSD)	Recovery (%)*	Found (M ± RSD)	Recovery (%)*
Sample 1	2.00×10^{-7}	$2.02 \times 10^{-7} \pm 0.19$	101.0	$1.98 \times 10^{-7} \pm 0.07$	99.0
	5.00×10^{-7}	$5.11 \times 10^{-7} \pm 0.26$	102.2	$5.06 \times 10^{-7} \pm 0.13$	101.2
	9.00×10^{-7}	$8.98 \times 10^{-7} \pm 0.11$	99.8	$8.89 \times 10^{-7} \pm 0.06$	98.8
Sample 2	2.00×10^{-7}	$2.05 \times 10^{-7} \pm 0.06$	102.5	$2.03 \times 10^{-7} \pm 0.14$	101.5
	5.00×10^{-7}	$5.07 \times 10^{-7} \pm 0.12$	101.4	$5.09 \times 10^{-7} \pm 0.07$	101.8
	9.00×10^{-7}	$8.97 \times 10^{-7} \pm 0.17$	99.7	$8.93 \times 10^{-7} \pm 0.04$	99.2

*average of five replicates

RSD: relative standard deviation

.....ꕥ.....

Chapter 5

MULTIWALLED CARBON NANOTUBE AND GOLD NANOPARTICLE BASED VOLTAMMETRIC SENSORS FOR SUNSET YELLOW

Contents

Two electrochemical sensors were developed for the determination of synthetic food colourant, sunset yellow (SY), based on the electrocatalytic properties of gold nanoparticles (AuNPs) and multiwalled carbon nanotubes (MWCNTs). The electrochemical oxidation of SY was studied on AuNP modified glassy carbon electrode (GCE). On further modification of AuNP/GCE with MWCNT, the nanocomposite film modified sensor exhibited excellent electron transfer ability towards the oxidation of SY with high sensitivity and stability. Various kinetic and thermodynamic parameters of the redox reaction such as standard heterogeneous rate constant ($k_s = 7.944 \times 10^{-1}\ s^{-1}$), electron transfer coefficient ($\alpha = 0.487$), number of electrons ($n = 1$) exchanged, diffusion coefficient and free energy difference between forward and reverse reactions (125 J) were calculated. Average surface concentration of SY on modified electrodes was found out. Under optimum conditions, the nanocomposite film modified electrode showed a linear response in the concentration range from 1.00×10^{-5} to 1.00×10^{-6} M, with a limit of detection 4.03×10^{-8} M. Analytical application of the developed sensor for quantitative determination of SY in commercially available soft drink samples was investigated.

5.1 Introduction

Synthetic colourants are usually added to foodstuffs and soft drinks to make them more attractive[202,203] and the use of these dyes in food industry, is strictly controlled by different national legislations.[210] If colourants are consumed above the acceptable daily level, it may result in allergic reactions, migraine, eczema, anxiety, diarrhoea and even cancer.[75,242] Sunset yellow (SY), E 110 (Figure 5.1) is one of the most commonly used synthetic dye which is added to many food products. The maximum permissible level of SY in food stuffs should not be more than 100 μgmL^{-1} either individually or in combination with other dyes.[75] Consequently, accurate and reliable methods for the determination of SY are essential for ensuring the quality and safety of food products.

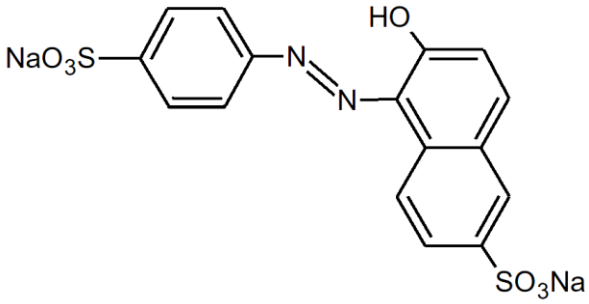

Figure 5.1: Structure of SY

Several analytical methods based on spectrophotomery,[243,244] high performance liquid chromatography,[245,246] thin layer chromatography,[247] capillary electrophoresis[248] and column chromatography[249] for the determination of SY individually or in combination with other dyes have been reported. But they are prone to many drawbacks, such as expensiveness, cumbersome procedures and not suitable for field use. Electrochemical

methods are also used for the determination of SY and their advantages include high sensitivity, simplicity and low cost and suitability for in-situ determination over conventional classic methods.[14,75,204,242]

Integration of nanotechnology with electrochemistry is expected to bring about significant progress in the field of electrochemical sensors.[250] Carbon nanotubes (CNTs), especially multiwalled carbon nanotubes (MWCNTs) have wide range of applications in electrochemistry due to their small dimensions, high surface area, excellent electrical conductivity, unique structures, significant mechanical strength and good chemical stability,[251] therefore regarded as a potential material to modify the surface of conventional electrodes. Recently, composite materials based on CNTs with metal nanoparticles have gained growing interest among researchers across the globe.[252,253] Gold nanoparticles (AuNPs) are one of the most stable metal nanoparticles that provide advantages such as narrow size distribution, large surface to volume ratio, efficient surface modification, enhancement of electron transfer kinetics and desirable biocompatibility.[254]

Establishing thermodynamic parameters for electron transfer reactions involving redox process is essential for a complete description of these reactions. The analyte response can be affected by the thermodynamic and kinetic parameters of adsorption, the rate of mass transport and electrochemical behaviour of the adsorbed species. The free energy and the rate of adsorption, depend on the electrode potential, the electrode material and to some extent, on the choice of the concentration and type of supporting electrolytes. The measurement of formal potential for a redox couple provides knowledge of thermodynamic driving force for the electron transfer reaction.[255]

Coupling the advantages of two nanostructured materials (AuNPs and MWCNTs) a convenient and sensitive method for the determination of SY has been developed. A layer by layer procedure was used to modify GCE with AuNP and MWCNT,[256] and the nanocomposite film modified electrode greatly enhanced the electron transfer rate and electrocatalytic ability compared to bare glassy carbon electrode (GCE). Various kinetic and thermodynamic parameters of the redox reaction such as standard heterogeneous rate constant (k_s), electron transfer coefficient (α), number of electrons exchanged (n) and free energy of activation (ΔG) were calculated using cyclic voltammetric studies. Chronoamperometric measurements were employed to determine the diffusion coefficient of SY on the MWCNT/AuNP/GCE. The average surface concentration of SY on AuNP/GCE and MWCNT/AuNP/GCE were calculated and found to be 9.12×10^{-10} molcm^{-2} and 4.14×10^{-10} molcm^{-2} respectively. The practical utility of the developed sensor was verified by determining SY in soft drink samples and satisfactory results were obtained when compared with standard spectrophotometric method.[241]

5.2 Experimental

5.2.1 Pretreatment of GCE

Prior to modification, the GCE was polished with 0.05 micron alumina slurry on a polishing pad, rinsed thoroughly with water and sonicated successively in methanol, 1:1 HNO_3 solution, acetone and double distilled water.

5.2.2 Fabrication of AuNP/GCE

Electrodeposition technique was applied for the preparation of AuNP modified GCE. Electrodeposition of AuNP film on the surface of cleaned

GCE was carried out by potential cycling between 0 to 1300 mV at a scan rate of 100 mV/s for a total of 40 cycles in 0.05 M H_2SO_4 solution containing 1 mM $HAuCl_4$ (Figure 5.2).[257] The modified electrode (AuNP/GCE) was then washed with double distilled water and dried in air.

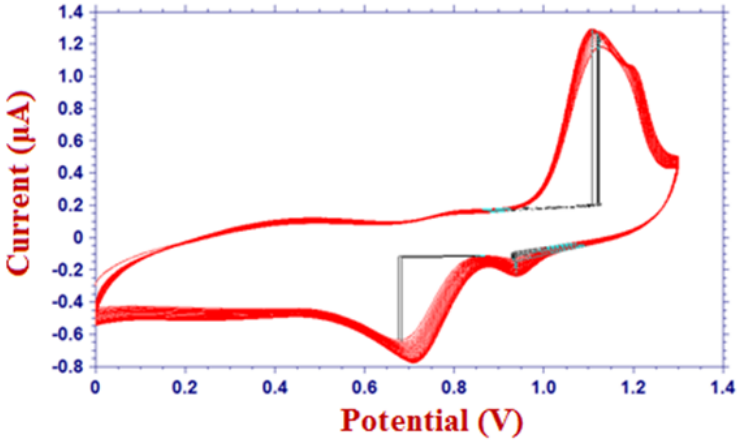

Figure 5.2: Electrodeposition of AuNP on GCE

5.2.3 Fabrication of MWCNT/AuNP/GCE

The major problem on the promising applications of CNTs in electrochemical sensors is their insolubility in aqueous media, which hinder the capacity of forming uniform and stable films.[258] To overcome this deficiency MWCNT was first acid treated to functionalize surface with –COOH groups and dispersed in nafion-water mixture. Drop casting method was used for the preparation of CNT modified electrode.

Acid treatment of MWCNT was carried out as described in literature.[177,178] MWCNT was refluxed in conc. HNO_3 for 48 hrs and the resulting suspension was diluted with water. The MWCNT was then

filtered, washed with double distilled water and dried in air. As a result of this process, length of MWCNT got shortened and functional groups are introduced, which make them hydrophilic.

5.0 mg of acid-treated MWCNT was dispersed in 13 % (v/v) nafion-water solution (2 mL water + 0.3 mL nafion) with the aid of ultrasonicate agitation to give a 0.22 % (w/v) black homogenous suspension. Finally, the MWCNT/AuNP/GCE was fabricated by dropping 4.0 µL MWCNT-nafion suspension on AuNP deposited GCE and allowed to dry.

5.2.4 Preparation of solution of SY

Stock solution of SY (1.00×10^{-2} M) was prepared by dissolving 0.452 g of analyte in water (10 mL). Solutions of SY at various concentrations were prepared by diluting the stock solution using phosphate buffer solution (PBS).

5.2.5 Analytical procedure

0.1 M PBS (pH 8) was used as the supporting electrolyte for the analysis of SY. The analytical procedure mainly consists of two steps: accumulation step and determination step. Firstly, SY was accumulated at the surface of modified electrodes. Then, square wave voltammograms (SWVs) were recorded from -630 mV to 100 mV with following parameters; increment of 4 mV, amplitude of 25 mV, frequency of 15 Hz, quiet time of 2 s and an oxidation peak current at -80 mV was measured for SY on MWCNT/AuNP/GCE. For electrode regeneration several cyclic sacns were carried out from -700 to 200 mV in the buffer solution until a stable voltammogram was obtained.

5.2.6 Sample treatment

Two soft drink samples were purchased from local super market and used without any pre-treatment. 1 mL sample solution was added into 9.0 mL of 0.1 M PBS (pH 8), for the determination of SY using a MWCNT/AuNP/GCE and then examined according to the analytical procedure.[66]

5.3 Results and discussion

5.3.1 Surface characterization

Evidences for the effective modification of electrode surface by MWCNT and AuNP was obtained from techniques such as scanning electron microscopy (SEM) and electrochemical impedance spectroscopy (EIS). Surface area calculations using cyclic voltammetric technique also gave clear evidence for the modification of electrode surface.

5.3.1.1 Surface morphology studies

SEM is a very powerful tool which gave information about the surface topography of the electrodes. Surface morphology studies using SEM gave evidence for the modification of GCE surface. Figure 5.3a, 5.3b and 5.3c shows the changes in morphology obtained from SEM images for bare GCE, AuNP/GCE and MWCNT/AuNP/GCE respectively. A homogeneous distribution of AuNPs was observed on the surface of AuNP/GCE.

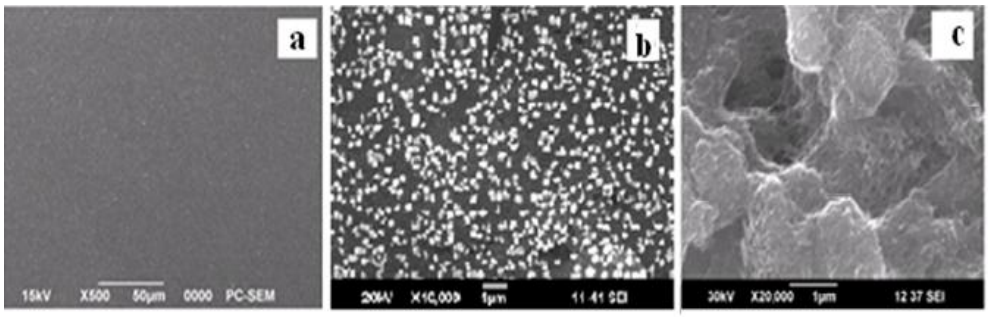

Figure 5.3: SEM images of bare (a) GCE, (b) AuNP/GCE and (c) MWCNT/AuNP/GCE

5.3.1.2 Surface area study

Surface areas of bare and modified electrodes were calculated using Randles-Sevcik equation.[184] 2 mM $K_3Fe(CN)_6$ was taken as a probe to measure the microscopic areas of electrodes and cyclic voltammograms were recorded at different scan rates (Figure 5.4). For a reversible system, the anodic peak current i_p is linear to $v^{1/2}$as follows

$$i_p = 2.69 \times 10^5 An^{3/2} D^{1/2} Cv^{1/2}$$

where n is the number of electron transferred, D is the diffusion coefficient, i_p is the peak current, A is the surface area of the electrode, C is the concentration of $K_3Fe(CN)_6$ and ν is the scan rate. Here n = 1, D = 7.60 × 10^{-6} cm^2s^{-1}. Thus, from the slope of i_p vs $v^{1/2}$ plot (Figure 5.5), the effective surface areas of the bare GCE, AuNP/GCE and MWCNT/AuNP/GCE were calculated to be 0.1643 cm^2, 0.2783 cm^2, 0.3773 cm^2 respectively. This enhancement of surface area of modified electrodes compared to bare GCE, could give more sensitive response to the electroactive species.

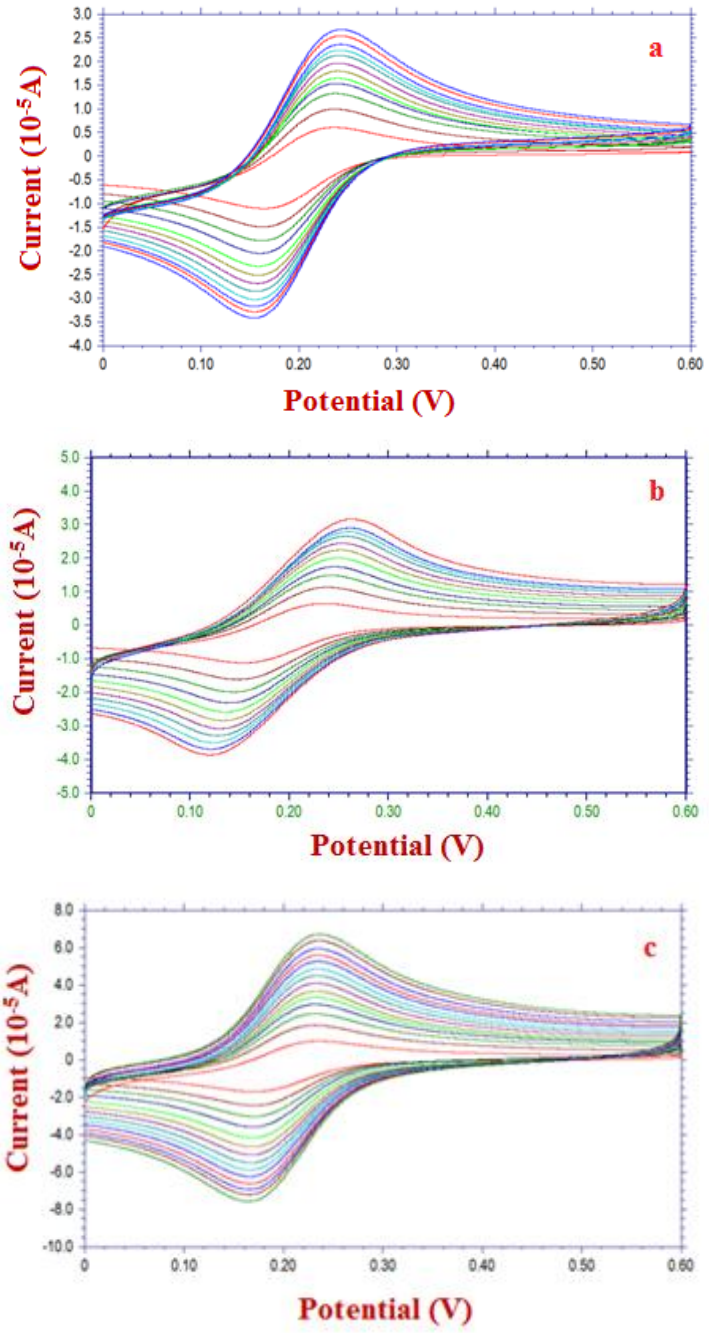

Figure 5.4: Cyclic voltammograms of (a) bare GCE, (b) AuNP/GCE and (c) MWCNT/AuNP/GCE in $K_3Fe(CN)_6$ at different scan rates

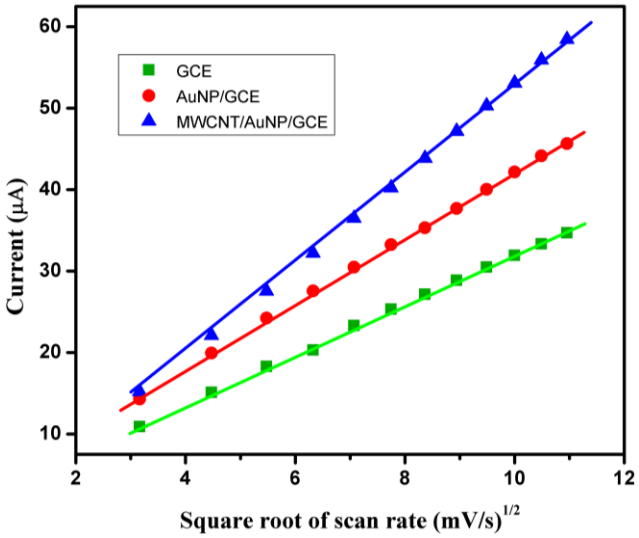

Figure 5.5: Plot of peak current vs square root of scan rate for bare GCE, AuNP/GCE and MWCNT/AuNP/GCE

5.3.1.3 Electrochemical impedance analysis

EIS is an effective technique to study the interface properties of modified electrode. Impedance data usually expressed in the form of Nyquist plots (imaginary part Z'' of the total impedance is plotted against the real part Z'), which consist of a low semicircle at higher frequencies and a linear portion at lower frequencies. The higher frequency semicircle corresponds to the heterogeneous electron transfer kinetics between the electrode and analyte species, whereas lower frequency linear part represents the diffusive transport of the solution phase electroactive species to the electrode surface. Moreover the real axis intercept at high frequency is equal to the sum of tunneling and solution resistance.[233]

Figure 5.6 showed the Nyquist plots for bare GCE (a), AuNP/GCE (b) and MWCNT/AuNP/GCE (c) in 1.00 × 10^{-2} M $Fe(CN)_6^{-3/-4}$ solution.

Nyquist plot displayed a semicircle type response for bare GCE due to the hindrance to electron transfer and semicircle radius was obviously smaller for AuNP/GCE indicating the reduction of charge transfer resistance. Impedance spectra of MWCNT/AuNP/GCE exhibited a straight line which suggested very fast electron transfer for the redox reaction. These results confirmed that nanocomposite film effectively decrease the charge transfer resistance and increase electronic exchange rate, which resulted in a high sensitivity for SY on MWCNT/AuNP/GCE.

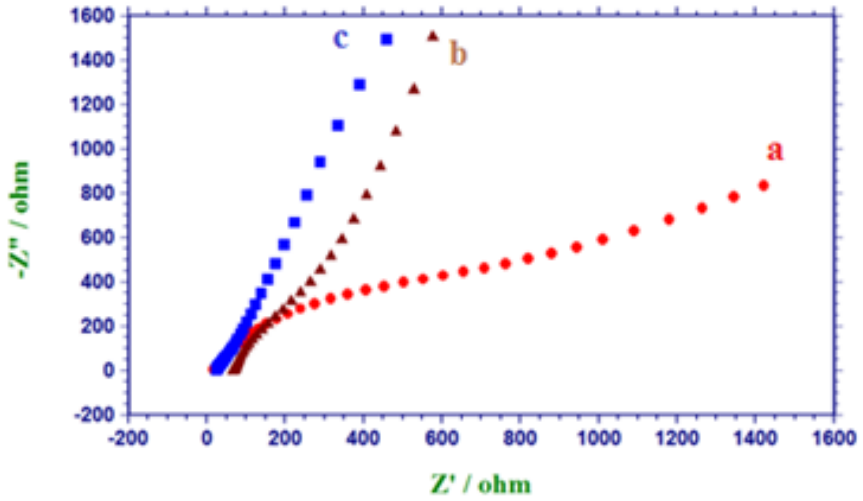

Figure 5.6: Nyquist plots for (a) bare GCE, (b) AuNP/GCE and (c)MWCNT/AuNP/GCE

5.3.2 Electrochemical behaviour of SY on bare and modified electrodes

Electrochemical response of SY (1.00×10^{-4} M) was studied at bare GCE (a), AuNP/GCE (b) and MWCNT/AuNP/GCE (c) using CV, in 0.1 M PBS at a scan rate of 100 mVs^{-1} and the results are compared in Figure 5.7. Bare GCE showed an irreversible oxidation peak at 156 mV (i_{pa} = 1.34 µA) in the first cycle of CV, but the electrochemical activity of SY was poor at

the unmodified electrode. In the subsequent cycles, the oxidation peak current was decreased. This may be attributed to the adsorption of oxidative products at the electrode surface. Under identical experimental conditions, a well defined reversible oxidation peak with lower potential (E_{pa} = -79 mV, E_{pc} = -141 mV) and enhanced current (i_{pa} = 15.59 µA, i_{pc} = -7.54 µA) was obtained on AuNP/GCE, indicating the catalytic role of AuNPs towards the oxidation of SY. The formal potential, $E^{0'}$ was found to be -110 mV. Compared to bare GCE, the AuNP/GCE has larger surface area, more active sites and higher conductivity, which help to enhance the electrocatalytic properties of the modified electrode. The potential difference between the redox peaks ($\Delta E_p = E_{pa} - E_{pc}$) of SY on AuNP modified GCE is 62 mV. The number of electrons (n) involved in the electrochemical oxidation of SY can be calculated using the equation, $\Delta E = \frac{59}{n}$. Therefore, the oxidation of SY involves one electron transfer mechanism.[66]

Further modification of AuNP/GCE with MWCNT resulted in a tremendous increase in both anodic and cathodic peak currents, which may be due to the electronic structure and topological defects present in MWCNT surface.[251] A pair of well defined quasi-reversible cyclic voltammetric peaks were observed with the formal potential ($E^{0'}$ = -108 mV) on MWCNT /AuNP/GCE in 0.1 M PBS at a scan rate of 100 mV/s. The anodic and cathodic peaks were observed at -59 mV (34.40 µA) and -157 mV (30.30 µA) respectively. ΔE_p (98 mV) increases with increasing scan rate, a positive shift in E_{pa} and negative shift in E_{pc} were observed, indicating the slower electrode kinetics at higher scan rates. The ratio of i_{pa} and i_{pc} was 1.09. (On MWCNT/GCE, SY showed a reversible cyclic voltammertic peak with

E_{pa} = -33 mV (i_{pa} = 3.49 µA) and E_{pc} = -85 mV (i_{pc} = 4.39 µA), which was not a much better result compared to AuNP/GCE.)

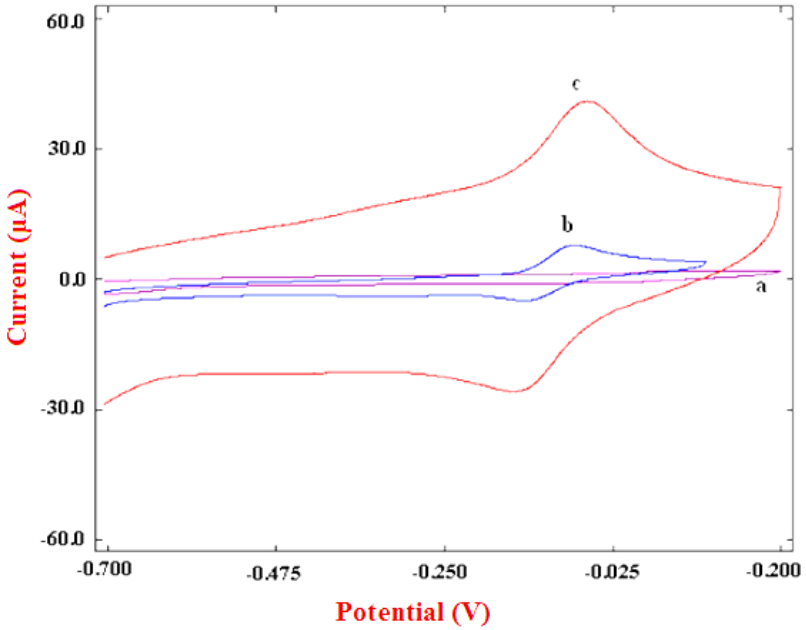

Figure 5.7: Cyclic voltammograms of SY at (a) bare GCE, (b) AuNP/GCE and (c) MWCNT/AuNP/GCE

Although the MWCNT/AuNP/GCE has higher E_{pc} value compared to AuNP/GCE, it exhibited very high current signal, which may be due to higher material porosity providing more effective surface area and active sites, which amplifies the signal and thereby enhance the sensitivity of the electrode. Compared to bare GCE, oxidation peak current of SY significantly enhanced by a factor of 11.63 and 25.62 at the surface of AuNP/GCE and MWCNT/AuNP/GCE respectively. From Figure 5.7, it is clear that MWCNT/AuNP modified GCE has enhanced catalytic activity and excellent surface enhancement effects towards the electrooxidation of SY than

AuNP/GCE, which may be attributed to the synergic properties of MWCNTs and AuNPs. The MWCNT/AuNP nanocomposite film may act as a conducting layer to accelerate the electron transfer between the analyte and the electrode.

5.3.3 Optimization of experimental conditions

The experimental conditions for the quantification of SY were optimized such as supporting electrolyte, pH of the supporting electrolyte, accumulation time, number of cycles for the electrodeposition of AuNP and the amount of MWCNT-nafion suspension.

5.3.3.1 Influence of supporting electrolyte and pH

Electrochemical behaviour of SY in various media such as 0.1 M solutions of PBS, acetate buffer, nitric acid, sulphuric acid, citrate buffer, NaCl and NaOH were studied by SWV (Table 5.1). Highest peak current was obtained with PBS and hence it was selected for further studies.

Voltammetric response of SY in 0.1 M PBS with different pH values (2 to 10) was studied. The anodic peak current of SY gradually increased on increasing the pH (2 to 8) and reached the maximum value in pH 8 both on AuNP/GCE (Figure 5.8) and MWCNT/AuNP/GCE (Figure 5.9a). On further increase of the pH value to 10, the peak current decreased significantly and disappeared after pH 10. By comparing the peak currents, it was found that pH 8 was the best pH for sensitive determination of SY. Therefore, PBS at a pH value of 8.0 was chosen as the supporting electrolyte for subsequent studies.

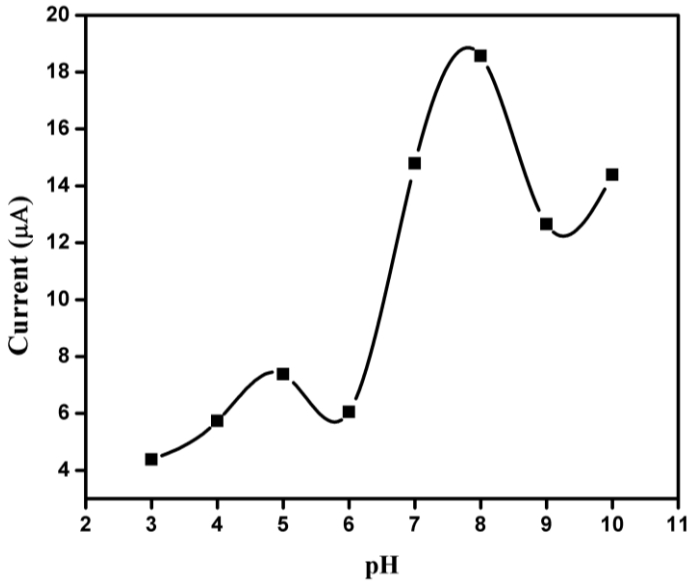

Figure 5.8: Effect of pH on the oxidation current of SY at AuNP/GCE

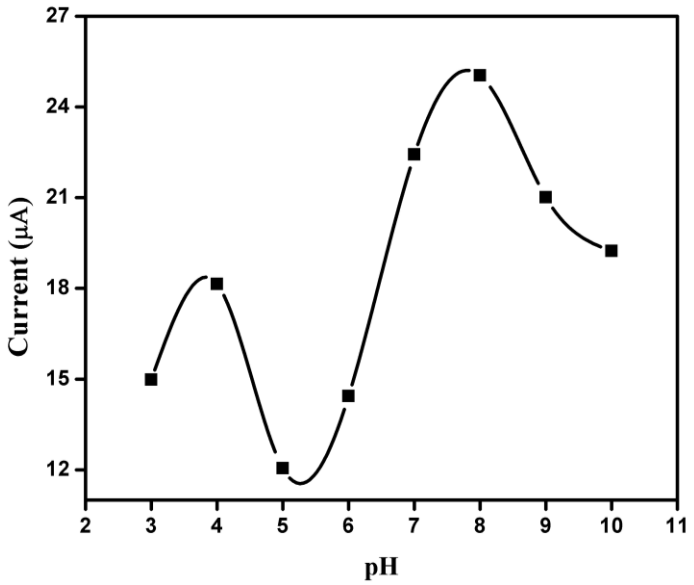

Figure 5.9a: Effect of pH on the oxidation current of SY at MWCNT/ AuNP/GCE

The anodic peak potential showed a negative shift on increasing the pH of the solution (Figure 5.9b) on MWCNT/AuNP/GCE. The linear regression equation can be expressed as $E_{pa}(V) = 0.0497\ pH - 453.92$ ($R^2 = 0.997$). A slope of 0.0504 is approximately close to the theoretical value of 0.0576; indicating that electron transfer is accompanied by an equal number of protons on the electrochemical oxidation of SY.[66,75]

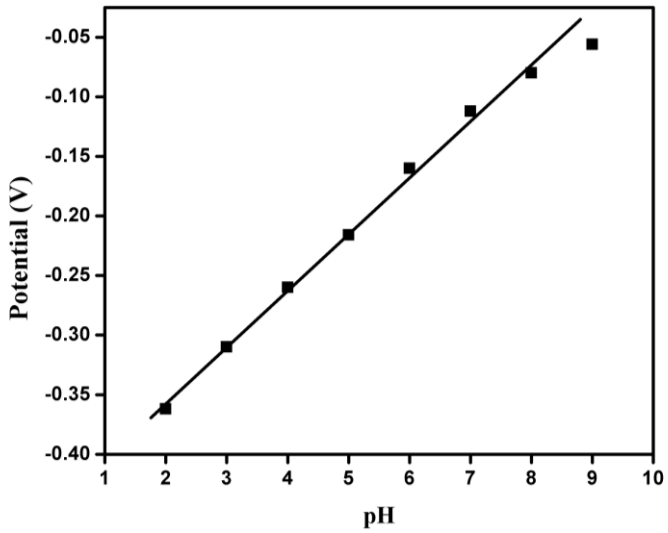

Figure 5.9b: Effect of pH on the oxidation potential of SY at MWCNT/AUNP/GCE

5.3.3.2 Effect of accumulation time

Accumulation can improve the amount of SY adsorbed on the electrode surface, thus increase the sensitivity of determination. Figure 5.10a and 5.10b depicts the influence of accumulation time on the oxidation peak current of SY in the range 0-6 min at AuNP/GCE (1.00×10^{-4} M) and MWCNT/AuNP/GCE (1.00×10^{-5} M) in 0.1 M PBS. It was observed that without accumulation (0 s) the oxidation peak current was very low, indicating that accumulation is an effective way for the enhancement of sensitivity.

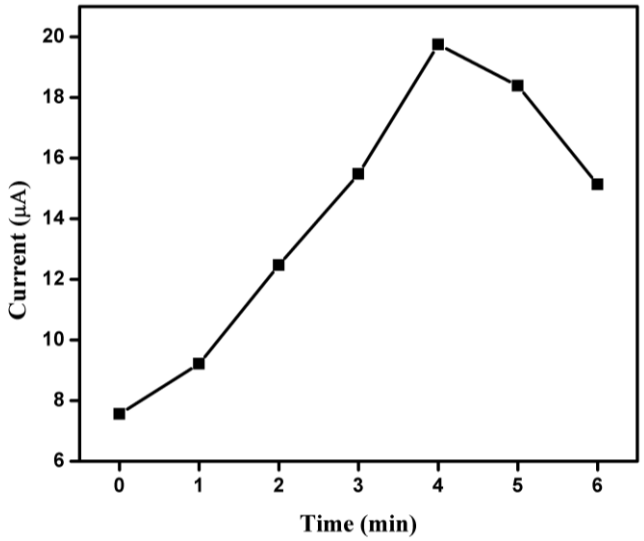

Figure 5.10a: Effect of accumulation time on the oxidation current of SY at AuNP/GCE

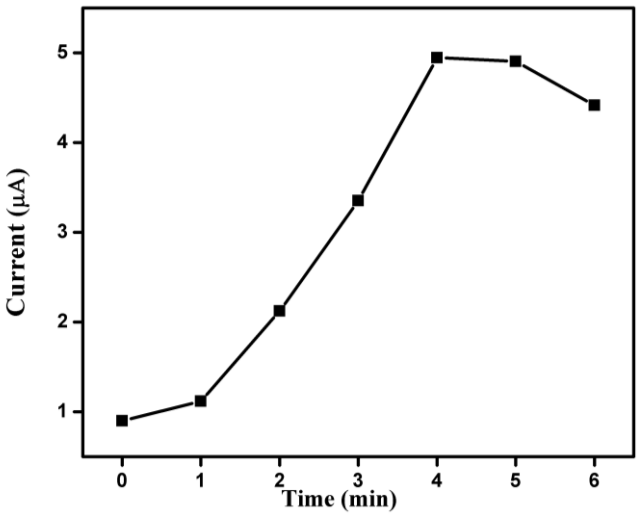

Figure 5.10b: Effect of accumulation time on the oxidation current of SY at MWCNT/AuNP/GCE

On increasing the accumulation time from 0 to 4 min, peak current progressively increased. However, the oxidation current changed only slightly on further increase of accumulation time from 4 to 6 min, indicating

accumulation has no further effect on the oxidation of SY on the electrode surface. Considering both sensitivity and working efficiency, an accumulation time of 4 min was employed for the determination of SY.

5.3.3.3 Effect of number of scan cycles for the electrodeposition of AuNPs

The influence of scan cycles of the electrodeposition of AuNPs on the peak current of SY was studied (Figure 5.11). The amount and the size of the deposited AuNPs can be controlled by changing the number of scan cycles in the electrodeposition process. The oxidation peak current increases with an increase of scan cycles and highest current was observed at a scan of 40 cycles. After 40 cycles of scan, anodic current decreased gradually, may be due to the slow electron transfer with increase in film thickness. Also the stability of the AuNP/GCE electrode was not good when the scan cycles were greater than 40. Hence 40 cycles were selected as the optimum number of scan cycles in the electrodeposition of AuNPs.

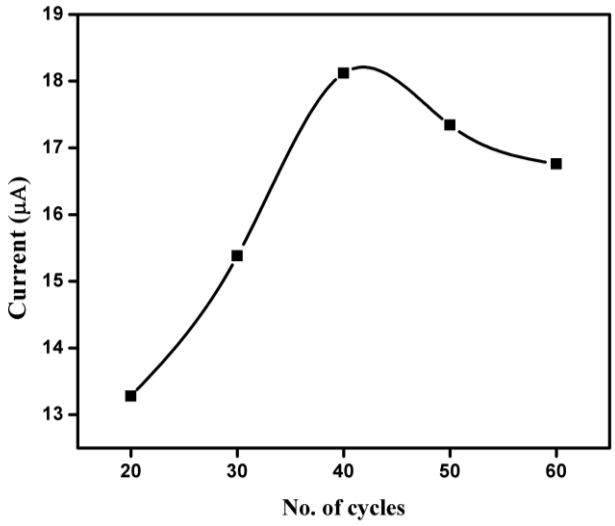

Figure 5.11: Effect of number of cycles of electrodeposition

SEM images of AuNP/GCE prepared at different cycles (20, 40 and 60) of electrodeposition are shown in Figure 5.12. From SEM analysis it was observed that AuNPs are formed on the surface of GCE homogeneously. However, the size of the particles increased as the number of cycles of electrodeposition increased. When the scan cycle was above 40, current was decreased, as a result of agglomeration of large sized AuNPs which is clear from SEM images.

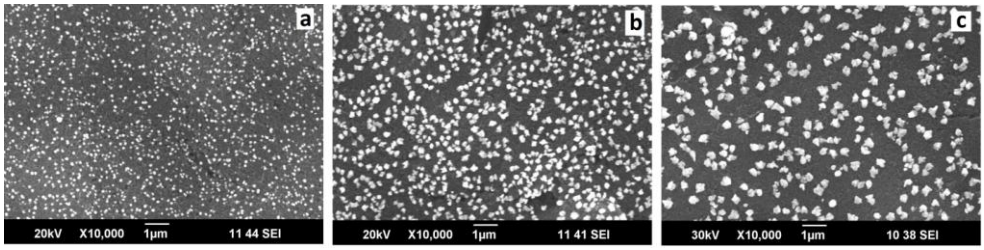

Figure 5.12: SEM images of AuNP/GCE at cycles 20 (a), 40 (b) and 60 (c) of electrodeposition

5.3.3.4 Effect of amount of MWCNT - nafion dispersion

In the case of film modified electrodes, thickness of the modified film is an important parameter which can affect the electrochemical response of the analyte species. Influence of volume of MWCNT-nafion suspension on the anodic peak current of SY was studied by dropping different volumes (from 1 to 7 µL) of a fixed concentration of MWCNT-nafion suspension (5.0 mg MWCNT in a mixture of 2 mL water and 300 µL nafion) on the AuNP/GCE and the results are shown in Figure 5.13. As the amount of MWCNT-nafion suspension was increased up to 4 µL, the oxidation peak current increased significantly. This enhancement of the current indicates that, the specific surface area and the number of catalytic sites increased with an increase in volume of MWCNT-nafion dispersion. When the

amount of MWCNT-nafion dispersion was more than 4 µL, the peak current decreased which may be because nafion acts as an insulator. This along with excess of MWCNT may hamper electron transfer.[259] Hence the amount of MWCNT- nafion dispersion was fixed as 4 µL, for further studies.

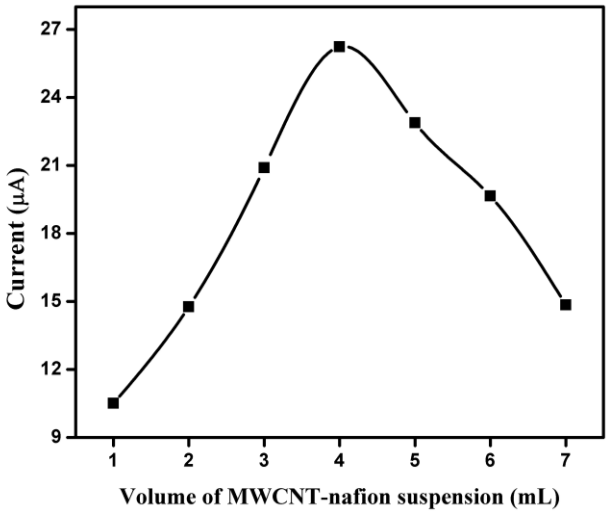

Figure 5.13: Effect of volume of MWCNT-nafion suspension

5.3.4 Effect of scan rate and characteristics of oxidation process

Variation of oxidation peak current of 1.00×10^{-5} M SY with scan rate was studied using CV on MWCNT/AuNP/GCE and AuNP/GCE (Figure 5.14a and 5.15a). The anodic peak current of SY varied linearly with the scan rate from 40 to 220 mVs^{-1} (Figure 5.15b) with a linear regression equation $i_{pa} = 0.2419v + 4.2115$ ($R^2 = 0.996$), indicating a typical adsorption controlled process. The plot of log i_{pa} vs log v (Figure 5.15c) yielded a straight line with slope of 1.12 in the scan rate range 100-220 mVs^{-1} and the value of slope is close to the theoretical value of 1.00, which is expected for an ideal reaction condition for adsorption controlled electrode process.[228]

Similar adsorption controlled oxidation was observed for SY on AuNP/GCE also (Figure 5.14b).

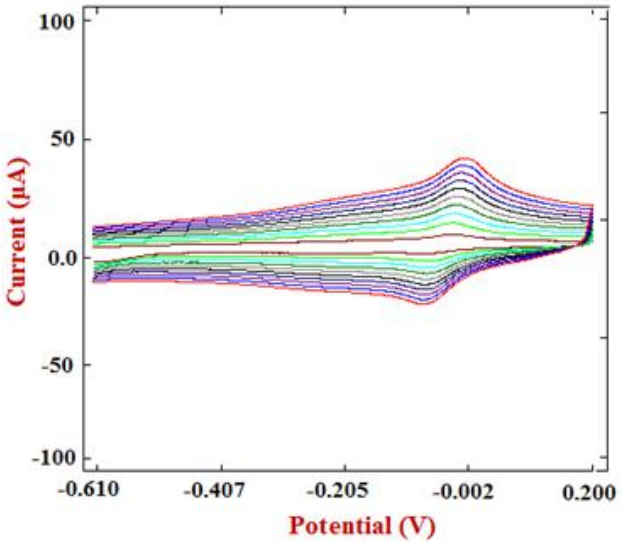

Figure 5.14a: Overlay of cyclic voltammograms of SY on AuNP/GCE at different scan rates

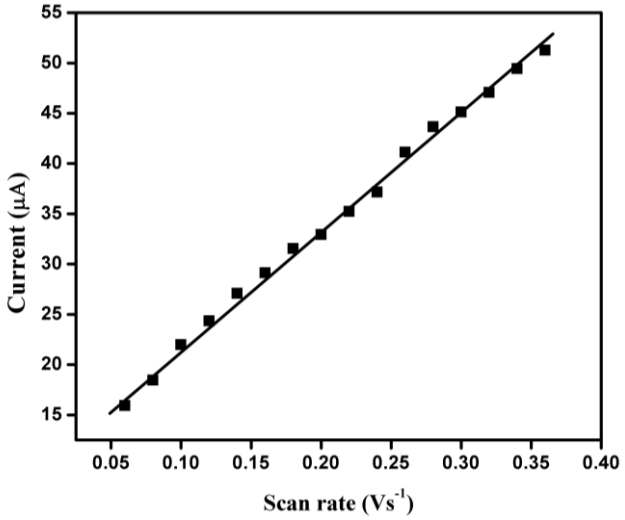

Figure 5.14b: Variation of anodic current of SY with scan rate on AuNP/GCE

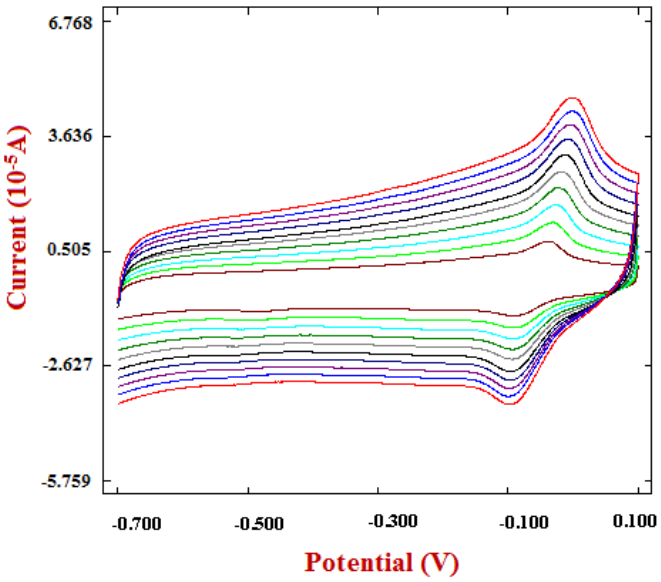

Figure 5.15a: Overlay of cyclic voltammograms of SY on MWNT/ AuNP/GCE at different scan rates

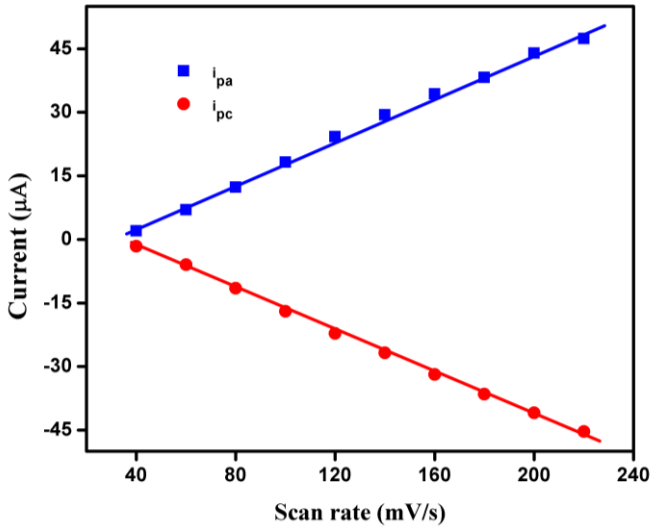

Figure 5.15b: Variation of anodic and cathodic currents of SY with scan rate on MWCNT/AuNP/GCE

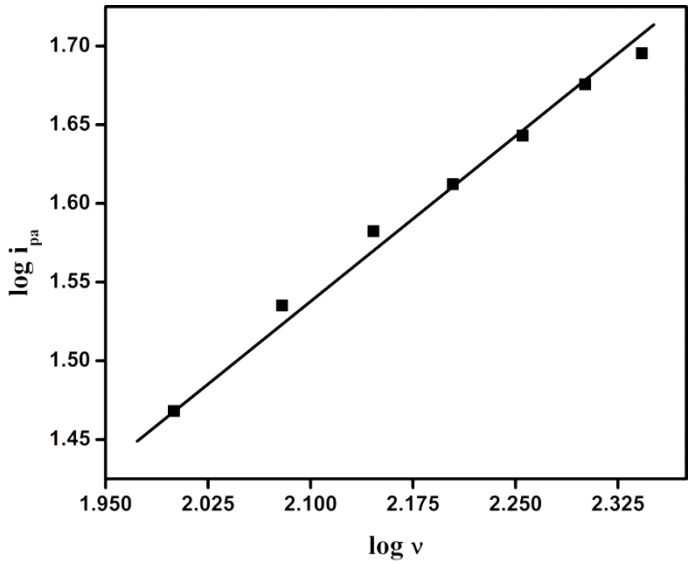

Figure 5.15c: Plot of log i_{pa} vs log ν

5.3.5 Calibration plot and limit of detection

Under optimized experimental conditions, linear range and limit of detection of SY were investigated using SWV in 0.1 M PBS (pH 8). Compared to CV and differential pulse voltammetry (DPV), SWV gave higher current for the oxidation of SY, so SWV was selected for concentration studies. The oxidation peak current of SY was found to be linear to its concentration (Figure 5.16a and 5.16b) in the range $1.00 \times 10^{-4} - 1.00 \times 10^{-5}$ M on AuNP/GCE with the following linear regression equation $i_p = 115.28c + 6.2355$ ($R^2 = 0.997$). The limit of detection (LOD) was calculated to be 7.06×10^{-7} M.

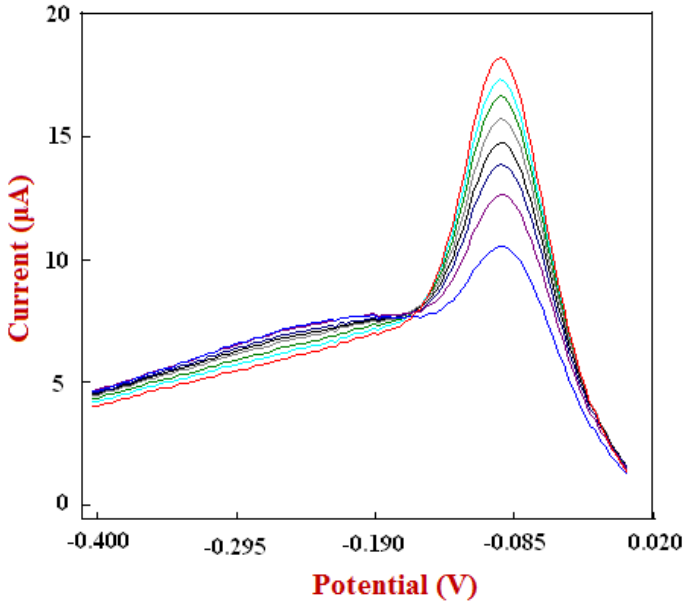

Figure 5.16a: Overlay of square wave voltammograms for oxidation of SY at various concentrations on AuNP/GCE

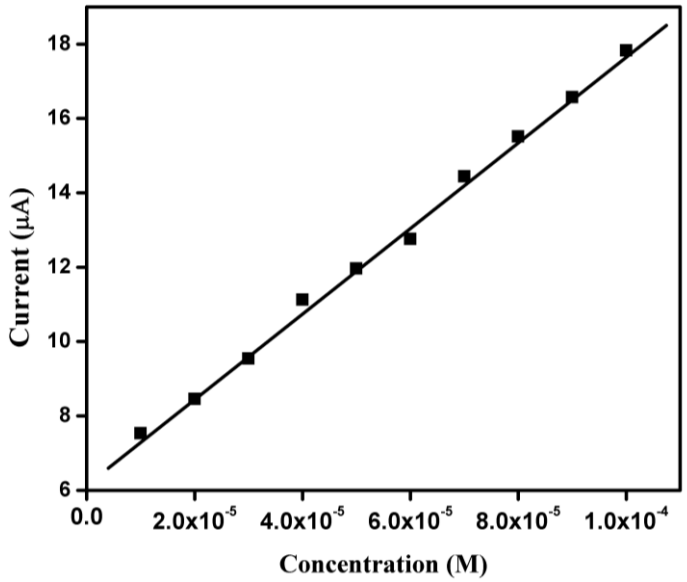

Figure 5.16b: Plot of anodic peak current vs concentration of SY at AuNP/GCE

MWCNT/AuNP/GCE sensor showed a linear dependence between the peak current and concentration of SY in the range 1.00×10^{-5} to 1.00×10^{-6} M (Figure 5.17a and 5.17b) with a limit of detection 4.03×10^{-8} M. The linear regression equation obtained was $i_p = 201.76c + 3.3546$ ($R^2 = 0.997$). The analytical figures of merit of the sensor are compared with other reported voltammetric sensors for SY (Table 5.2). The oxidation potential obtained using the proposed sensors (AuNP/GCE and MWCNT/AuNP/GCE) is much lower than that of the reported voltammetric works.

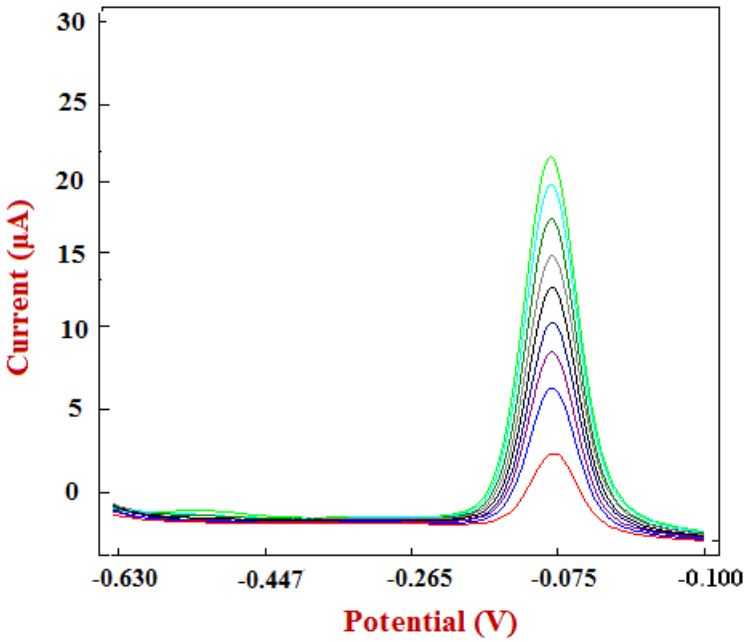

Figure 5.17a: Overlay of square wave voltammograms for oxidation of SY at various concentrations on MWCNT/AuNP/GCE

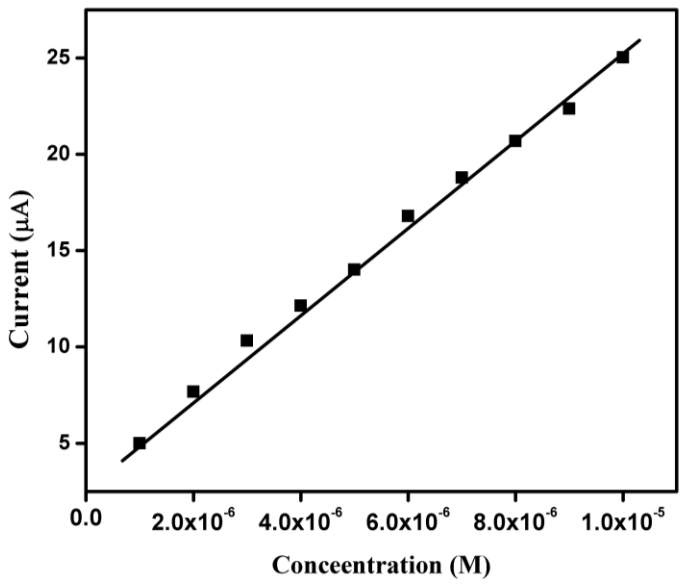

Figure 5.17b: Plot of anodic peak current vs concentration at MWCNT/AuNP/GCE

Electrochemical response of SY (8.00×10^{-6} M) was determined with six modified electrodes (MWCNT/AuNP/GCE) prepared by the same fabrication procedure. The relative standard deviation (RSD) of the peak currents was calculated to be 4.14 %. The high reproducibility indicates that the developed sensor is stable. To study the repeatability of the modified electrode, the electrochemical experiments were repeatedly performed 8 times with the same MWCNT/AuNP/GCE in a solution containing 3.00×10^{-6} M SY. RSD based on these replicates was 1.27 %. These results indicate that the proposed sensor has a good repeatability and reproducibility.

5.3.6 Evaluation of kinetic parameters

5.3.6.1 Charge transfer coefficient

Cathodic and anodic peak currents in a quasi-reversible system are a function of mass transport and charge transfer coefficients (α), where α describe the preference of the charge transfer to either oxidation or reduction reactions. Charge transfer coefficients for oxidation (α_a) and reduction (α_c) may be different, but their sum should be equal to one.[258]

α, the charge transfer coefficient, (indicator of the symmetry between the forward and reverse electron transfer steps) for the electron transfer between the MWCNT/AuNP/GCE and the surface confined redox couple of SY can be evaluated by CV, using the variation of the anodic and cathodic peak potentials with the logarithm of scan rate (Figure 5.18). In the scan rates ranging from 160-260 mVs^{-1}, the linear regression equations of the E_{pa} and E_{pc} vs the logarithm of the scan rates are expressed as $E_{pa} = 0.1564 log\upsilon + 333.51$ and $E_{pc} = 0.1682 log\upsilon - 148.97$. The following equations can be used to determine α_a and α_c, where a and b are constants.[232]

$$\boldsymbol{E_{pa} = a + \{2.303RT|(1-\alpha)nF\}log\upsilon}$$

$$\boldsymbol{E_{pc} = b - \{2.303RT|\alpha nF\}log\upsilon}$$

Based on the above equations the value of electron transfer coefficients α_a and α_c are calculated to be 0.62 and 0.35 respectively. Deviation from the ideal value of 0.5 is indicative of an asymmetrical relationship between the oxidized and reduced forms of a compound.

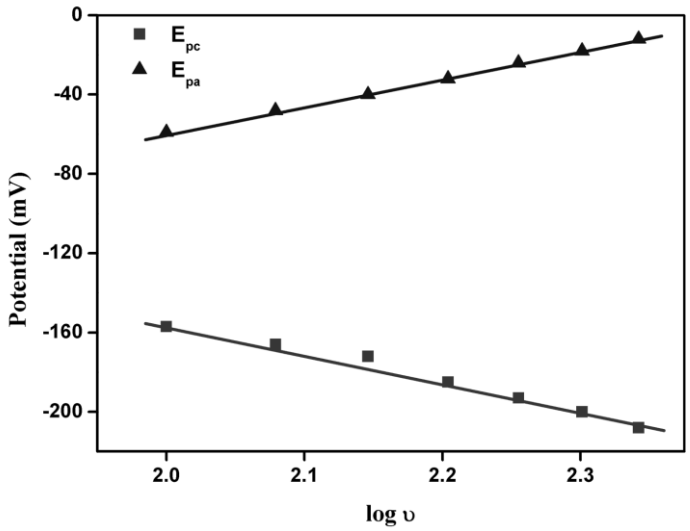

Figure 5.18: Variation of E_{pa} and E_{pc} with ln scan rate

5.3.6.2 Heterogeneous rate constant

The oxidation and reduction at the electrode surface is fast enough to maintain dynamic equilibrium between the redox couple in reversible electron transfer kinetics. The maximum current occurs when the reactant concentration at the electrode surface is dominated by mass diffusion.[260] But in the case of quasi-reversible reactions, the electrode surface is not able to maintain the equilibrium between the redox species, at the applied potential of the electrode.

k_s measures the intrinsic ability of an oxidized species to exchange electrons with the electrode in order to convert to its reduced form, and *vice versa*.[261] k_s is the most important factor to describe the electron transfer rate. When $n\Delta E_p \leq 200$ mV, the heterogeneous rate constant k_s, which refers to the rate of electron transfer between the analyte in solution and the electrode, could be estimated from the following Laviron equation[234,235]

$$\boldsymbol{logk_s = \alpha log(1-\alpha) + (1-\alpha) log\alpha - log\frac{RT}{nFv} - \frac{\alpha(1-\alpha)nF\Delta E_p}{2.3RT}}$$

where α is the charge transfer coefficient (0.49), ΔE_p is the potential difference (98 mV), n is the number of electrons (1). The value of k_s for AuNP/GCE, MWCNT/AuNP/GCE and GCE was calculated to be 1.567 s^{-1}, 7.499 × 10^{-1} s^{-1}, 3.546 × 10^{-1} s^{-1} respectively at 100 mVs^{-1}. Small values for k_s indicate slow kinetics and longer time requirement for equilibrium. For an irreversible electrode reaction (bare GCE), the following equation is used to calculate k_s.[192]

$$\boldsymbol{E_p = E^{0\prime} + \frac{RT}{\alpha nF}\left(ln\frac{RTk_s}{\alpha nF} - lnv\right)}$$

where $E^{0'}$ is the formal potential and the other symbols have their usual meanings. The value of $E^{0'}$ was obtained from the intercept of the E_p vs v plot, by the extrapolation to the vertical axis at v = 0.

Consider the electron transfer reaction occurring at the electrode surface at a fixed potential (chemically reversible system) [236,237]

$$\boldsymbol{Ox + ne^- \rightleftharpoons Red}$$

The forward and reverse rate constants (k_f and k_b) are

$$\boldsymbol{k_f = k_s exp\left[\frac{-\alpha nF(E-E^{0\prime})}{RT}\right]}$$

$$\boldsymbol{k_b = k_s exp\left[\frac{(1-\alpha)nF(E-E^{0\prime})}{RT}\right]}$$

From the above equations and the values of k_f and k_b for the redox couple of SY were calculated to be 1.4667 s^{-1}, 1.543 s^{-1} respectively at

100 mVs^{-1} on MWCNT/AuNP/GCE. The forward and backward rate constants can also be expressed in terms of free energy as follows [236]

$$k_f = Ae^{\frac{-\Delta G_f}{RT}}$$

$$k_b = Ae^{\frac{-\Delta G_b}{RT}}$$

From the equations (8) and (9) it was found that $\frac{\Delta G_f}{\Delta G_b} = -0.222$, ie. $\Delta G_f >> \Delta G_b$. In other words, free energy for reduction is higher than the free energy for oxidation.

In the non equilibrium condition, the free energy of forward and backward reactions can be expressed as [236,237]

$$\Delta G'_f = \Delta G_0 + \alpha nF(E - E^{0\prime})$$

$$\Delta G'_b = \Delta G_0 - (1-\alpha)nF(E - E^{0\prime})$$

It can be deduced from equations, that $\Delta G_f - \Delta G_b$ correspond to a numerical value of 125 units. This confirms that reduction of the oxidised product of SY needs higher free energy compared to the oxidation of SY. Due to this thermodynamic barrier, reduction may be less preferred on MWCNT/AuNP/GCE surface; hence reduction peak appeared at higher potential compared to AuNP/GCE.

5.3.6.3 Chronoamperometric measurements: Determination of diffusion coefficient

For the determination of diffusion coefficient (D), the catalytic oxidation of SY on the surface of MWCNT film modified GCE was also studied by chronoamperometry. Cottrel equation was used to find out the diffusion coefficient of SY. The Cottrel equation is expressed as[193,194]

$$I = nFAD^{1/2}C\pi^{-1/2}t^{-1/2}$$

Figure 5.19a shows the chronoamperograms and the corresponding current-time$^{-1/2}$ plots (Figure 5.19b) for different concentrations (1.30×10^{-4} to 3.00×10^{-5} M) of SY. The slope of the Cottrel plots was used to estimate the value of D (Figure 5.19c) and it was found to be 5.29×10^{-6} cm^2s^{-1}.

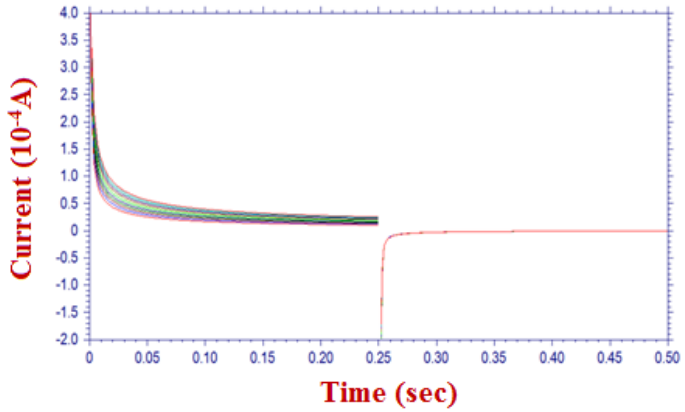

Figure 5.19a: Chronoamperometric response of SY at different concentrations (1.30×10^{-4} to 3.00×10^{-5} M)

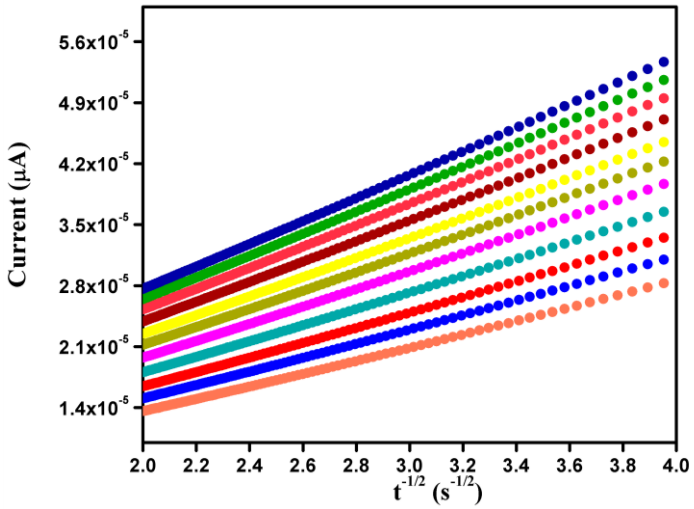

Figure 5.19b: Plot of I vs $t^{-1/2}$

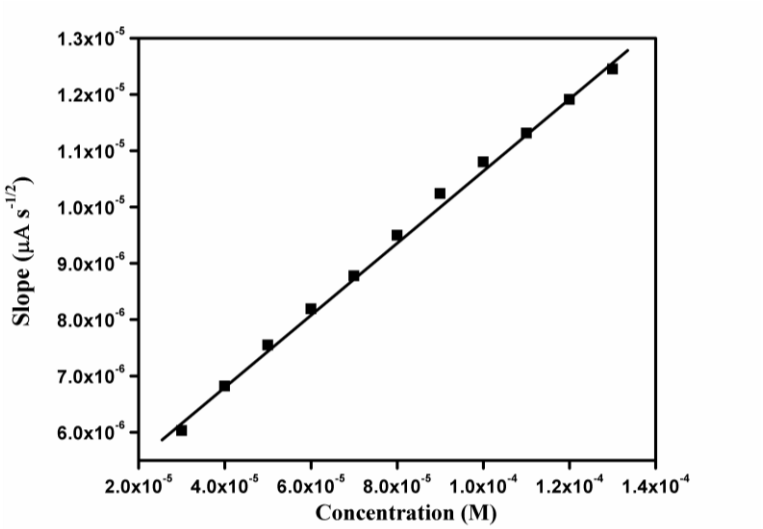

Figure 5.19c: Plot of the slope of the straight line against the concentration of SY

5.3.6.4 Average surface concentration of SY on modified electrodes

The average surface concentration of SY on the modified electrodes were estimated using the equation[238]

$$i_p = \frac{n^2F^2A\Gamma v}{4RT}$$

where A is the effective surface area electrode, Γ is the surface coverage (molcm^{-2}), and the other symbols have their usual meanings. From the slope of peak current vs scan rate (Figure 5.15b), the value of Γ was calculated to be 9.12×10^{-10} molcm^{-2} for MWCNT/AuNP/GCE which is higher than the obtained Γ value of AuNP/GCE (4.14×10^{-10} molcm^{-2}). The larger surface area of the MWCNT/AuNP nanocomposite film may be helpful for more efficient entrapment of SY in the composite film, thereby providing more active sites to take part in the electron transfer process.

5.3.6.5 Determination of the number of electrons and reaction mechanism

The potential difference between the redox peaks ($\Delta E_p = E_{pa} - E_{pc}$) of SY on AuNP modified GCE was found to be 62 mV at a scan rate of 100 mVs^{-1}. The number of electrons (n) involved in the electrochemical oxidation of SY can be determined using the equation, $\Delta E = \frac{59}{n}$ which suggest that the oxidation of SY involves one electron transfer mechanism.[204]

The number of electrons involved in the quasi-reversible oxidation of SY was calculated using the Laviron equation [259]

$$i_p = \frac{nFQv}{4RT}$$

where i_p represents the anodic or cathodic peak current, Q is the amount of charge integrated from the area of cyclic voltammetric peak, T is the temperature in Kelvin (298 K), R is the gas constant (8.314 $Jmol^{-1}K^{-1}$), F is the Faraday constant (96500 $Cmol^{-1}$) and n is the number of electrons transferred. From the slope of i_p vs v, n was calculated to be 0.96 (≈ 1) which was in accordance with the previous reports. Therefore it again confirmed to be a single electron transfer reaction. Naphthols are known to undergo electrochemical oxidation to naphthyloxy radical by a one electron transfer process (Scheme 4.1).[240] Based on this the observed oxidation peak may be due to the oxidation of hydroxyl group present in SY, by a one proton, one electron reaction.[204,241]

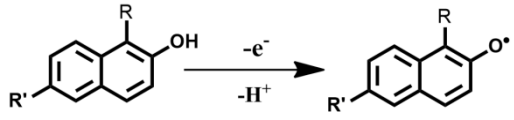

Scheme 5.1: Electro oxidation of naphthols to naphthyloxy radical

This radical may further undergo non electrochemical reactions, resulting in the formation of a quinone.

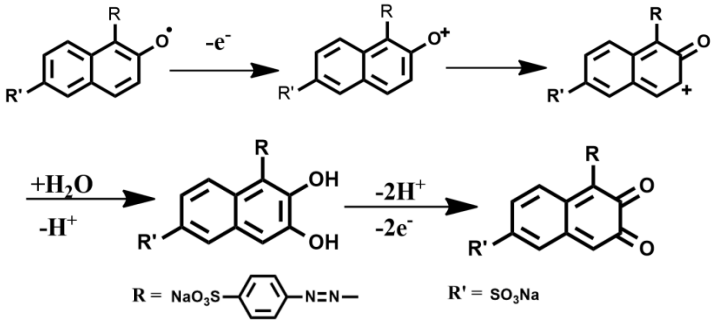

Scheme 5.2: Mechanism for the formation of quinone

5.3.7 Interference study

The influence of various foreign species on the electrochemical response of SY on the modified electrodes was examined (Table 5.3). The voltammetric signal was recorded for 1.00×10^{-5} M SY in the presence of various concentrations (1:1 fold, 1:10 fold and 1:100 fold) of foreign species such as quinoline yellow, sodium sulphite, amaranth, citric acid, tartrazine, aspartame, fructose and ascorbic acid. It was found that up to 100-fold excess concentration of amaranth, fructose, quinoline yellow, aspartame and tartrazine did not interfere the response of the developed sensors, under optimized experimental conditions (signal change below 5%). However, ascorbic acid interferes severely. A signal change greater than 5 % was obtained on AuNP/GCE when 50 fold excess of sodium sulfite was present along with SY. These results suggested that proposed sensors had good selectivity for the determination of SY.

5.3.8 Application study

To demonstrate the application of the developed sensors for food analysis, the proposed method was used for the determination of SY in commercially available soft drinks. Each spiked sample solution was subjected to five parallel determinations and experimental results are given in Table 5.4 (AuNP/GCE) and Table 5.5 (MWCNT/AuNP/GCE). The results obtained by spectrophotometric method[241] and the proposed sensors were in good agreement, revealing that this method is satisfactory. Good recoveries were obtained, suggesting that the developed sensors display sufficient accuracy and precision for real sample analysis.

5.4 Conclusions

Merging the unique properties of AuNPs such as high effective surface area and efficient electron tunnelling together with intrinsic properties of carbon nanotubes, two sensors were fabricated for the sensitive determination of SY. A pair of quasi-reversible redox peak for SY with one electron-transfer reaction mechanism was obtained on the nanocomposite film modified electrode. The value of α, k_s and D at the MWCNT/AuNP modified electrode was estimated. The proposed sensor has high sensitivity, antifouling nature, good reproducibility and lower oxidation potential. The developed sensors have been successfully applied for the analysis of SY in real samples.

Table 5.1: Peak potential and peak current for SY (1.00×10^{-5} M) on AuNP/GCE and MWCNT/AuNP/GCE in different supporting electrolytes

Supporting Electrolytes (0.1 M)	AuNP/GCE		MWCNT/AuNP/GCE	
	E_{pa} (mV)	i_p (µA)	E_{pa} (mV)	i_p (µA)
ABS	180	0.19	172	10.31
KNO_3	220	0.43	214	15.42
PBS	-96	18.44	-80	25.21
NaCl	316	0.25	264	18.26
NaOH	164	0.95	184	11.24
H_2SO_4	276	11.53	304	24.37

Table 5.2: Comparison with other electrochemical sensors for the determination of SY

Electrode	E_p (mV)	Linear range (M)	LOD (M)	References
BDD	-150	4.76×10^{-6} - 2.00×10^{-8}	13.1×10^{-9}	242
HMDE	-600	1.99×10^{-7} - 1.10×10^{-8}	1.11×10^{-8}	210
Polyallyline/GCE		1.50×10^{-4} - 1.00×10^{-5}	3.5×10^{-6}	75
BiFE	-530	9.72×10^{-9} - 7.73×10^{-9}	0.72×10^{-9}	243
AuNP/GCE	-96	1.00×10^{-4} - 1.00×10^{-5}	7.06×10^{-7}	Proposed sensor
MWCNT/AuNP/GCE	-80	1.00×10^{-5} - 1.00×10^{-6}	4.03×10^{-8}	Proposed sensor

BDD – boron dopped diamond electrode, HMDE- hanging mercury drop electrode, BiFE- bismuth film electrode

Table 5.3: Effect of foreign species on the voltammetric signal of SY on AuNP/GCE (3.00×10^{-5} M SY) and MWCNT/AuNP/GCE (5.00×10^{-6} M SY)

Foreign species	AuNP/GCE		MWCNT/AuNP/GCE	
	Concentration	Signal change %	Concentration	Signal change %
Tartrazine	3.00×10^{-3} M	2.41	5.00×10^{-4} M	4.86
Aspartame	3.00×10^{-3} M	4.82	5.00×10^{-4} M	3.80
Sodium sulphite	1.50×10^{-3} M	4.21	5.00×10^{-4} M	2.87
Citric acid	3.00×10^{-3} M	2.58	5.00×10^{-4} M	2.26
Amaranth	3.00×10^{-3} M	4.63	5.00×10^{-4} M	3.14
Fructose	3.00×10^{-3} M	1.66	5.00×10^{-4} M	3.52
Quinoline Yellow	3.00×10^{-3} M	2.74	5.00×10^{-4} M	3.31
Ascorbic acid	3.00×10^{-5} M	5.44	5.00×10^{-6} M	15.47

Table 5.4: Determination of SY in soft drink samples using AuNP/GCE

Samples	Proposed method		Recovery (%)*
	Added (M)	Found (M ± RSD)	
Sample 1	3.00×10^{-6}	$3.11 \times 10^{-6} \pm 0.37$	103.7
	5.00×10^{-6}	$5.06 \times 10^{-6} \pm 0.22$	101.2
	9.00×10^{-6}	$9.22 \times 10^{-6} \pm 0.31$	102.4
Sample 2	3.00×10^{-6}	$3.04 \times 10^{-6} \pm 0.17$	101.3
	5.00×10^{-6}	$4.93 \times 10^{-6} \pm 0.26$	98.6
	9.00×10^{-6}	$9.24 \times 10^{-6} \pm 0.11$	102.7

*average of five replicate measurements

Table 5.5: Determination of SY in soft drink samples using MWCNT/ AuNP/ GCE

Samples	Added (M)	Spectrophotometric method		Proposed method	
		Found (M ± RSD)	Recovery (%)*	Found (M ± RSD)	Recovery (%)*
Sample 1	3.00×10^{-6}	$3.01 \times 10^{-6} \pm 0.12$	100.3	$3.02 \times 10^{-6} \pm 0.07$	100.7
	5.00×10^{-6}	$5.13 \times 10^{-6} \pm 0.13$	102.7	$5.10 \times 10^{-6} \pm 0.14$	102.0
	8.00×10^{-6}	$8.14 \times 10^{-6} \pm 0.22$	101.8	$8.05 \times 10^{-6} \pm 0.15$	100.6
Sample 2	3.00×10^{-6}	$3.03 \times 10^{-6} \pm 0.07$	101.0	$3.05 \times 10^{-6} \pm 0.12$	101.7
	5.00×10^{-6}	$5.09 \times 10^{-6} \pm 0.11$	101.8	$5.07 \times 10^{-6} \pm 0.23$	101.4
	8.00×10^{-6}	$8.23 \times 10^{-6} \pm 0.19$	102.9	$8.09 \times 10^{-6} \pm 0.15$	101.1

*average of five replicate measurements

Chapter 6

GOLD NANOCLUSTER BASED FLUORESCECE SENSOR FOR BUTYLATED HYDROXYANISOLE

Contents

A facile one pot strategy was employed for the synthesis of protein templated fluorescent gold nanoclusters (AuNCs). Bovine serum albumin (BSA) added during the synthesis, reduces Au^{3+} ions and stabilizes the AuNCs. FTIR spectroscopy, UV-Vis spectroscopy and high resolution transmission electron microscopy (HRTEM) were used for the characterization of AuNCs. BSA stabilized AuNCs displayed a strong fluorescence emission at 653 nm, which was enhanced significantly on addition of butylated hydroxyanisole (BHA). The emission spectrum of AuNCs was slightly red shifted from the original spectrum in the presence of BHA. Based on the luminescence enhancement of AuNCs by BHA, a turn on fluorescence sensor was developed for the determination of BHA. The enhancement of fluorescence intensity of AuNCs was linear over the concentration of BHA from 4.76×10^{-8} to 4.98×10^{-9} M and from 4.31×10^{-6} to 4.98×10^{-7} M. The proposed method has high stability and sensitivity with limit of detection as low as 8.99×10^{-10} M. The analytical application of the proposed sensor was demonstrated by the successful quantification of BHA in coconut oil samples.

6.1 Introduction

Butylated hydroxyanisole (BHA) E 320, (Figure. 6.1) is one of the most widely used antioxidant in food industry. This synthetic phenolic antioxidant is commonly used to prevent the oxidative rancidity of food, cosmetics, pharmaceuticals and other commercial products.[262] BHA is added to food products to increase their stability, especially to retard the chain propagation of free radicals and thereby preventing rancidity in products containing fats or lipids.[263] The conjugated aromatic ring of BHA is able to stabilize free radicals and acting as free radical scavengers which prevent further radical reactions.[264] Because of its high thermal stability it is widely used in baked and fried food, to provide them extended shelf life.[265]

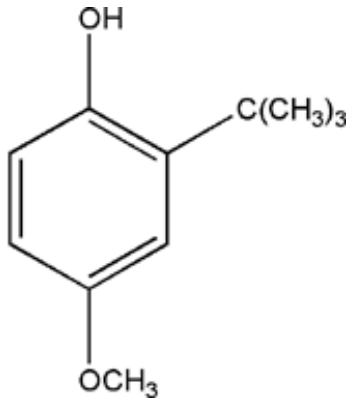

Figure 6.1: Structure of BHA

According to the Joint FAO/WHO Expert Committee on Food Additives (JECFA), the acceptable daily intake (ADI) of BHA is 0-0.5 mg/kg of bw.[266] Excess intake of BHA can cause asthma and hives, as well as developmental disorders in children. Studies have shown that BHA can

block cell respiration by inhibiting the activity of NADH-CoQ reductase, succinate-CoQ oxidoreductase and complex cytochrome c-ubiquinol reductase.[267] Due to these harmful effects on human health, use of this artificial antioxidant is subject to regulations which define the permitted concentration limits.[268] Hence the determination of BHA is of great significance in the quality control of various food products.

The reported analytical methods for the determination of BHA includes spectophotometry,[269] micellar electrokinetic capillary chromatography,[270] gas chromatography,[271] HPLC coupled with different detection systems,[272] voltammery[264,265] etc. Although the above mentioned methods are appropriate to the analysis of BHA, most of them require time-consuming preliminary steps such as extraction and clean-up. Fluorescence techniques coupled with nanosized luminescent probe offer alternative methods to those discussed above due to its high sensitivity and selectivity.

Fluorescent gold nanoclusters (AuNCs) offer exciting new ways for bioimaging,[273] biosensing[274] and photonics[275] due to their remarkable optical and electrical properties.[276-279] AuNCs exhibit discrete electronic states and interesting optical properties due to their small size and quantum confinement effect.[280,281] These nanoclusters are of significant attention because they provide the missing link between the atomic and nanoparticles bahaviour.[282]

In recent times, synthesis of many protein based AuNCs has been reported.[283-285] Bovine serum albumin (BSA), the most ubiquitous plasma protein widely used in biological studies was selected in the preparation of AuNCs.[286] AuNCs prepared in the presence of BSA is highly water soluble

and stable against aggregation.[284] The high stability of BSA protected AuNCs (AuNCs@BSA) would greatly facilitate their application in vivo and in vitro bioimaging.[284] Furthermore, when compared with semiconductor quantum dots (QDs) AuNCs@BSA are more biocompatible, nontoxic and more readily bioconjugated.[285]

This chapter discusses the fabrication of fluorescent sensor for the analysis of BHA based on the luminescence enhancement effect of AuNCs induced by BHA. AuNCs@BSA were employed as the selective fluorescent probe for the quantification of BHA. The sensor exhibited two linear ranges, one from 4.76×10^{-8} M to 4.98×10^{-9} M and the other from 4.31×10^{-6} M to 4.98×10^{-7} M and the limit of detection was found to be 8.99×10^{-10} M. The observed fluorescence enhancement of AuNCs in the presence of BHA was due to the aggregation and the resulting restricted rotation of AuNCs. The proposed method was used for the determination of BHA in commercially available vegetable oil samples.

6.2 Experimental

6.2.1 Synthesis of BSA stabilized AuNCs

BSA protected AuNCs were synthesized by the method described by Chen *et al.*[284] with minor modification. All glassware used in the experiments were cleaned in a bath of freshly prepared aquaregia, and rinsed thoroughly in water prior to use. In a typical experiment, 10 $mgmL^{-1}$ stock solution of $HAuCl_4.4H_2O$ was prepared by dissolving 1.0 g $HAuCl_4.4H_2O$ in 100 mL double distilled water. Then aqueous $HAuCl_4$ solution (4.1 mL) was added to BSA solution (10 mL, 50 $mgmL^{-1}$) under vigorous stirring. Two minutes later, NaOH solution (1.0 mL, 1.0 M) was added, and the reaction mixture

was incubated for 12 h at 37^0C. The resulting solution was deep brown in colour which exhibited strong red fluorescence under UV light.

It is known that amino acids specially tryptophan and tyrosine have the ability to reduce metal ions to their metallic form and stabilize resulting nanoparticles.[287-289] BSA has a single polypeptide chain comprising of 583 amino acid residues, and act both as a protecting ligand and reducing agent during the synthesis of AuNCs.[290] Recent studies have shown that peptides containing tyrosine residues can reduce Au(III) ions in alkaline medium through their phenolic groups.[291] In BSA solution, the AuNCs might have been stabilized by Au-S bonding with protein (via 35 Cys residues in BSA), and the steric protection offered by the bulkiness of the protein. The encapsulation of AuNCs in BSA molecules has no effect on the structure of BSA scaffolds which is evident from FTIR studies.[292] Clusters composed of 25 gold atoms were formed and it has been reported that AuNCs with 25 atoms have a stable structure and corresponded to the size of most common magic cluster.[293-295]

6.2.2 Preparation of solution of BHA

Stock solution of BHA (1.00×10^{-2} M) was prepared in methanol by dissolving 0.180 g of analyte. Standard solutions of BHA were prepared by serial dilution of the stock solution with methanol.

6.2.3 Analytical procedure

AuNCs@BSA solution was mixed with phosphate buffer solution of pH 7 in the volume ratio 1:6. Appropriate volumes of BHA solution were added to 2 mL of the above solution and the corresponding fluorescence

emission spectra were recorded. The luminescence intensity of AuNCs@BSA in the absence and presence of BHA was assigned as I_0 and I respectively.

6.2.4 Preparation of vegetable oil sample

Vegetable oil treatment was carried out according to the procedure described in section 3.2.6 in chapter 3.

6.3 Results and discussion

6.3.1 Characterization of AuNCs

The synthesized BSA protected AuNCs were characterized by UV-Vis spectroscopy, fluorescence spectroscopy, FTIR spectroscopy and transmission electron microscopy. The UV-Vis absorption spectrum of AuNCs displayed a broad absorption band at around 500 nm (Figure 6.2). The aqueous solution of the AuNCs was deep brown in color under visible light and exhibited bright-red fluorescence under UV irradiation (Figure 6.3). The fluorescence spectrum showed an emission signal at 653 nm (Figure 6.4). The observed fluorescence emission of AuNCs at 653 nm was attributed to electronic transitions and radiative electron hole recombination process between excited 'sp' bands and low lying 'd' bands of AuNCs.[296] The Stokes shift of AuNCs@BSA was 153 nm, which was favorable to prevent self-quenching of fluorescence and the measurement errors caused by light scattering.[297]

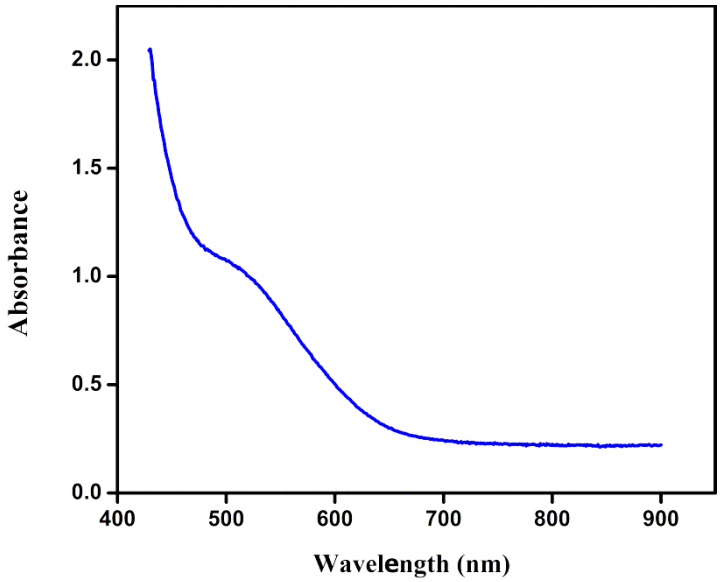

Figure 6.2: Absorption spectrum of BSA stabilized AuNCs

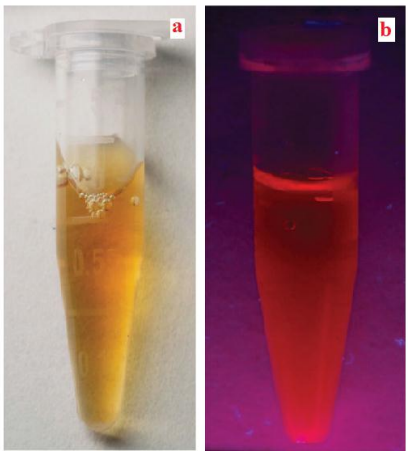

Figure 6.3: Photographs of AuNCs under (a) visible light and (b) UV light

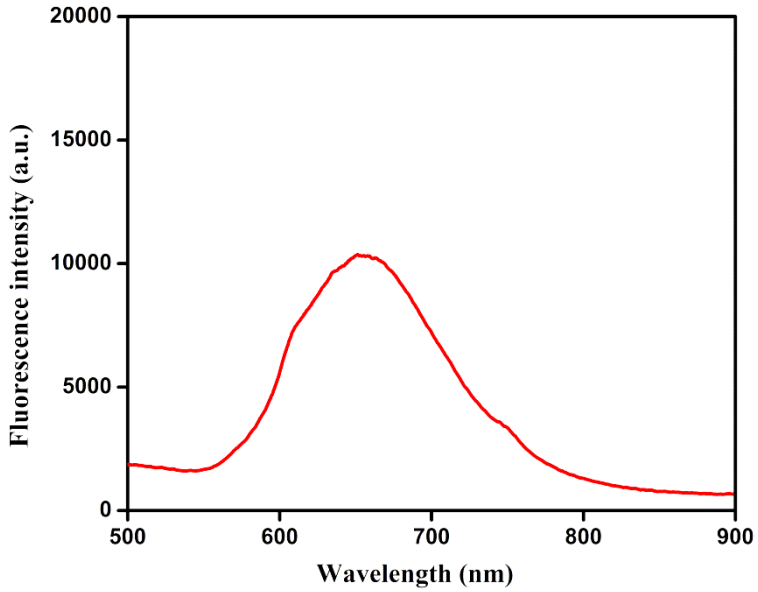

Figure 6.4: Fluorescence emission spectrum of BSA stabilized AuNCs

FTIR spectra of free BSA and AuNCs@BSA are compared in Figure 6.5. Only slight change in intensity was observed for the vibrational bands of BSA upon the formation of AuNCs. The characteristic band of amide at 1640 cm^{-1} was due to the C=O stretching vibrations and out of phase C-N stretching vibrations. This amide I band provides information about the secondary structure of protein. A small band observed at 1450 cm^{-1}, is attributed to the C-N stretching vibration with the N-H bending mode (amide II band). No significant changes were observed in the amide I and amide II bands, implying that the AuNCs embedded in the BSA (Figure 6.6) would not change the secondary structure of BSA. TEM analysis was used to study the surface morphology of the prepared AuNCs. Figure 6.7 shows the TEM image of BSA capped AuNCs.

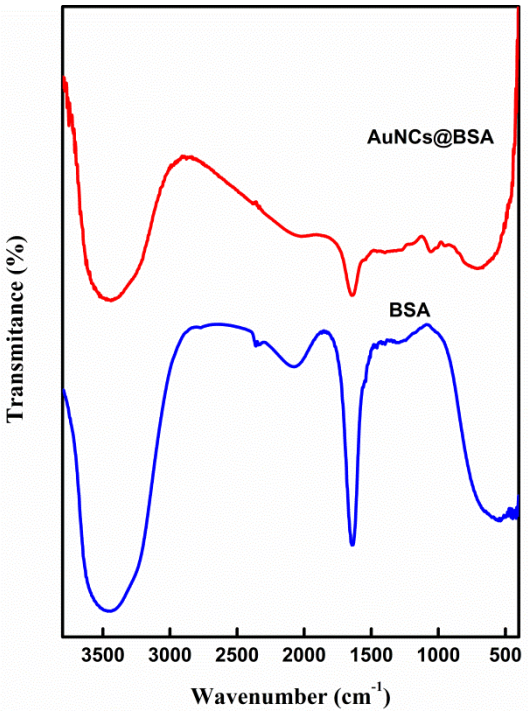

Figure 6.5: FTIR spectra of free BSA and BSA stabilized AuNCs

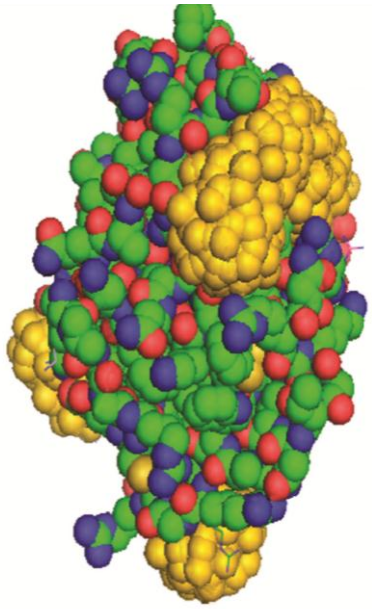

Figure 6.6: Structure of AuNCs embedded in BSA

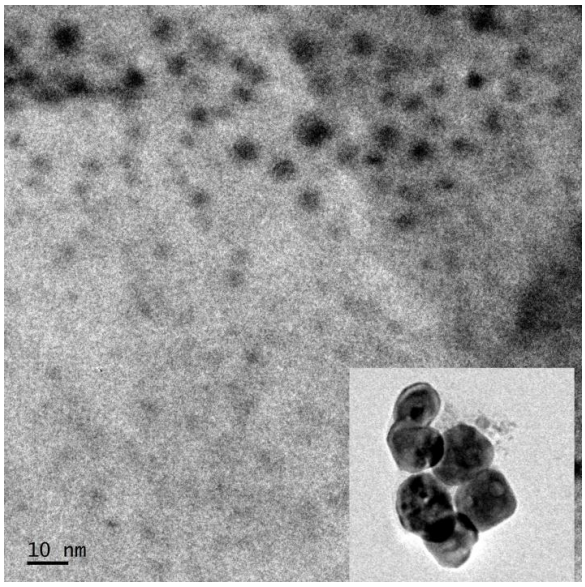

Figure 6.7: TEM image of BSA stabilized AuNCs

6.3.2 Fluorescence enhancement of AuNCs by BHA

The fluorescence spectrum of AuNCs@BSA showed a signal at 653 nm with a full width at half maximum (FWHM) of 116 nm when excited at 400 nm. However, the fluorescence intensity of AuNCs increased drastically in the presence of BHA (Figure 6.8). The fluorescence intensity increased with the successive addition of BHA. Along with the increment in intensity, there was a red shift of 11 nm in the emission maximum of AuNCs. The difference in the emission wavelength of AuNCs in the presence and absence of BHA suggests a change in the surface states of AuNCs@BSA due to the interaction with BHA molecules.[298] Based on this phenomenon, a novel turn on sensor was designed for the determination of BHA.

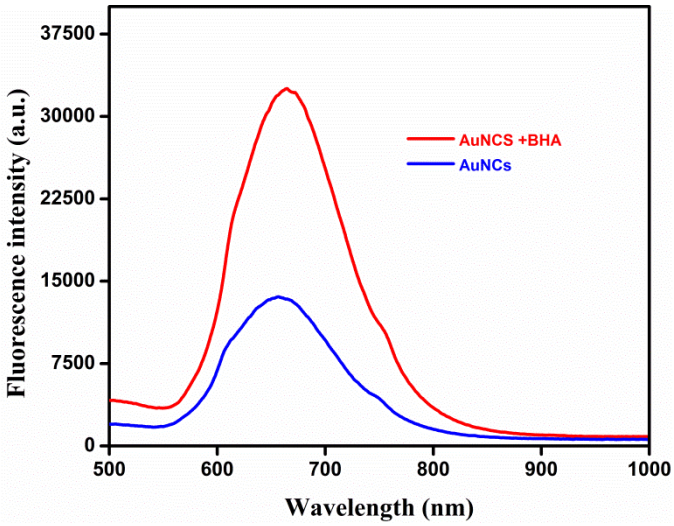

Figure 6.8: Fluorescence spectra of AuNCs in the absence and presence of BHA

The UV-Vis absorption spectrum of AuNCs before and after the addition of BHA was recorded (Figure 6.9). The absorption maximum in UV-Vis spectrum of AuNCs@BSA disappeared on addition of BHA, which also indicated the changes in the surface states of AuNCs, may due to aggregation.

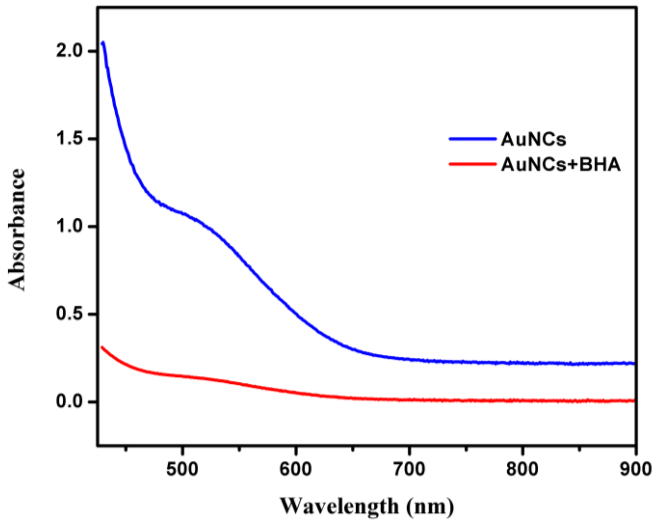

Figure 6.9: Absorption spectra of AuNCs in the absence and presence of BHA

6.3.3 Effect of buffer solutions

The influence of various buffer solutions on the fluorescence enhancement of AuNCs by BHA was studied. Citrate buffer, acetate buffer and phosphate buffer were selected for studies and maximum fluorescence enhancement was obtained in phosphate buffer solution (PBS). Therefore further experiments were conducted in PBS.

The effect of the volume of PBS on the BHA induced fluorescence enhancement of AuNCs was also examined. Relative fluorescence intensity of AuNCs in the presence of BHA was studied at different volume ratios of nanocluster and buffer solution. Maximum value of relative fluorescence intensity, I/I_o was obtained when the volume ratio of AuNCs and PBS is 1:6 (Figure 6.10).

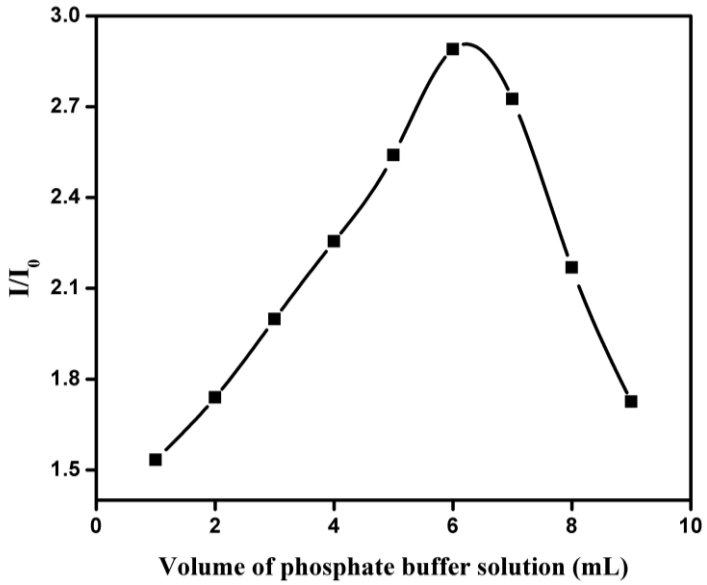

Figure 6.10: Effect of volume of PBS on the fluorescence enhancement of AuNCs by BHA

6.3.4 Effect of pH

Effect of pH on the fluorescence intensity of AuNCs was studied with PBS of pH values 2 to 9, before and after the addition of BHA (Figure 6.11a). The maximum relative fluorescence intensity was observed in pH 7 (Figure 6.11b), hence it was chosen for further studies.

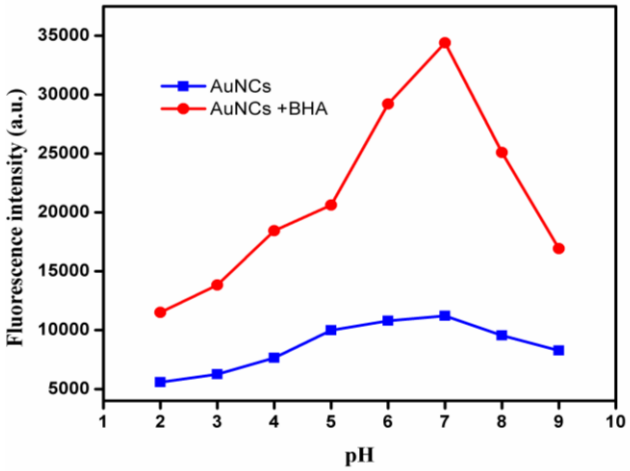

Figure 6.11a: Effect of pH of PBS on the fluorescence intensity of AuNCs and AuNCs in the presence of BHA

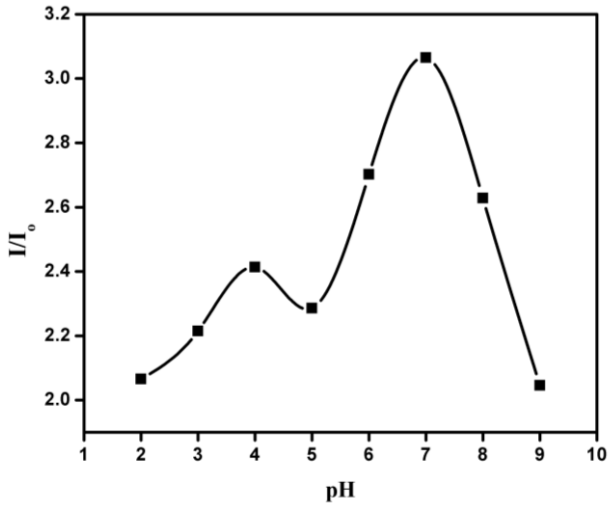

Figure 6.11b: Effect of pH of PBS on the fluorescence enhancement of AuNCs by BHA

6.3.5 Effect of time

The influence of incubation time on the fluorescence enhancement of AuNCs by BHA was investigated. Fluorescence intensity of AuNCs@BSA in the presence of BHA was recorded every 30 sec for 30 min immediately after mixing. From the results it was clear that the reaction between AuNCs and BHA was quick and the luminescence intensity reached a stable value within one min after mixing. Thereafter is no change in the fluorescence intensity of AuNCs and remains stable up to 30 min. The photoluminescence intensity vs time plots for various concentrations of BHA are depicted in Figure 6.12.

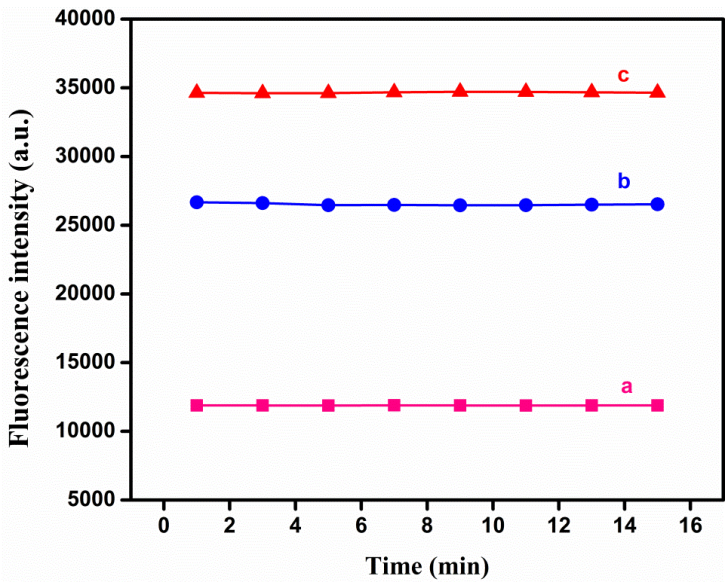

Figure 6.12: Effect of time on the fluorescence intensity of (a) AuNCs (b) AuNCs + 2.91 × 10^{-8} M BHA (c) AuNCs + 4.76 × 10^{-8} M BHA

6.3.6 Quantum yield

The determination of quantum yield of AuNCs is based on comparing the variation of the integrated fluorescence intensity with absorbance to the standard rodamine 6G solution.[299] The quantum yield of AuNCs is given by

$$\phi_{AuNCs} = \phi_{Rh} \frac{I_{AuNCs}}{I_{Rh}} \frac{A_{Rh}}{A_{AuNCs}} \frac{\eta_{AuNCs}^2}{\eta_{Rh}^2}$$

where ϕ_{Rh} is the quantum yield of standard rhodhamine 6G. I_{AuNCs} and I_{Rh} are the integrated fluorescence intensities of AuNCs and Rh 6G respectively. A_{Rh} and A_{AuNCs} are the absorbance of the reference and AuNCs, η is the refractive index of the solvent used. The integral fluorescence intensity of different concentrations of rhodhamine 6G and AuNCs was determined and then plotted vs absorbance (Figure 6.13). The slopes of the resulting straight lines were used to calculate the quantum yield. The quantum yield of BSA stabilized AuNCs was found to be 5.18 % which is in aggrement with reported values.[300,301]

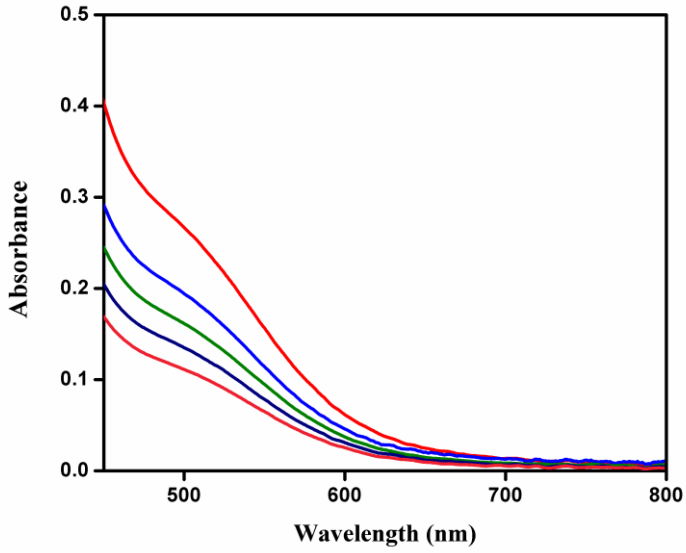

Figure 6.13a: Absorption spectra of AuNCs at different concentrations

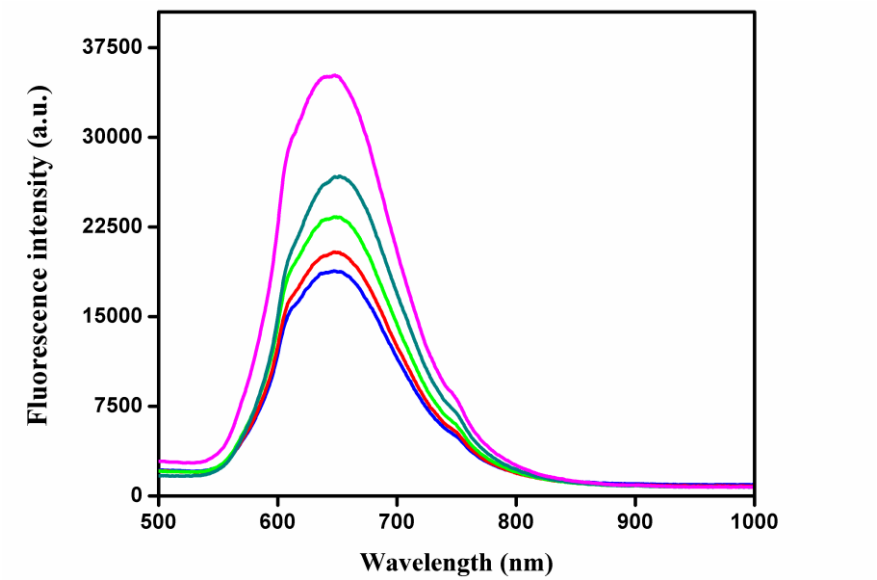

Figure 6.13b: Fluorescence spectra of AuNCs at different concentrations

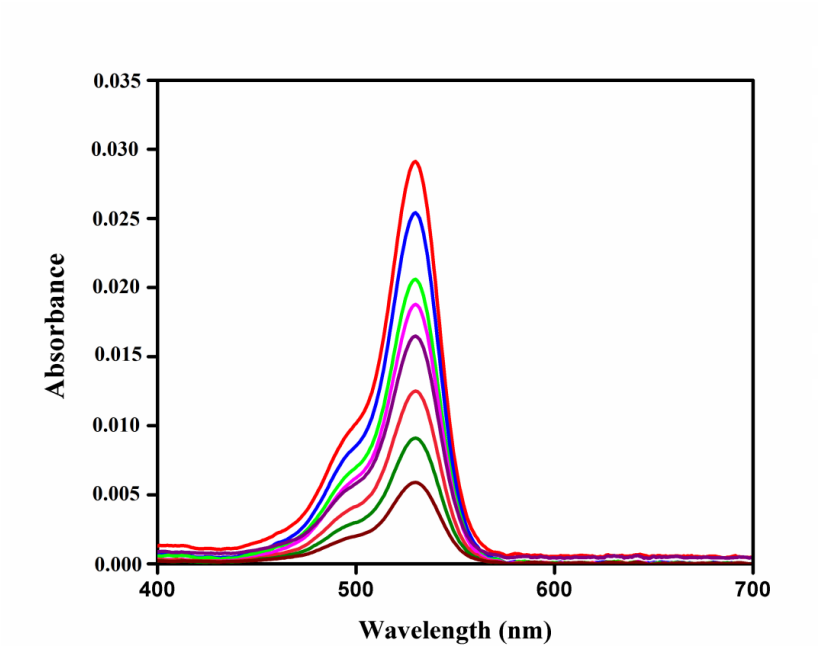

Figure 6.13c: Absorption spectra of Rhodamine 6G at different concentrations

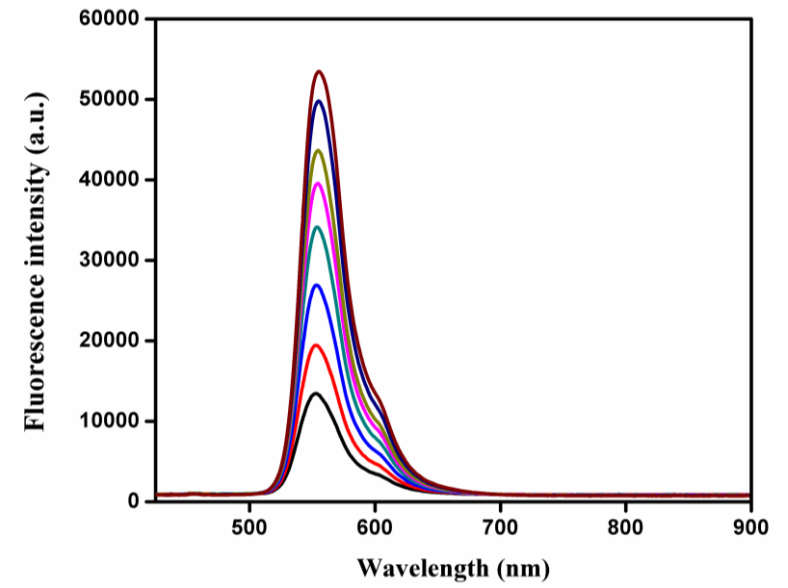

Figure 6.13d: Fluorescence spectra of Rhodamine 6G at different concentrations

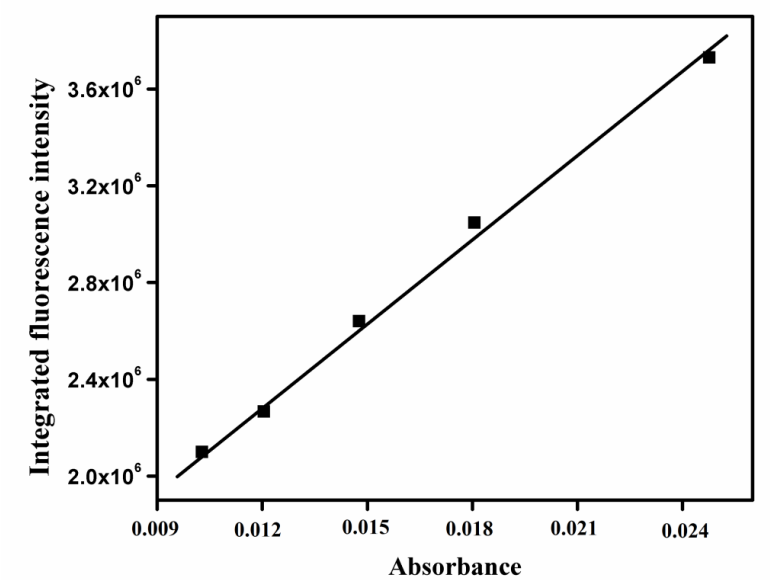

Figure 6.13e: Variation of integrated fluorescence intensity with absorbance for AuNCs

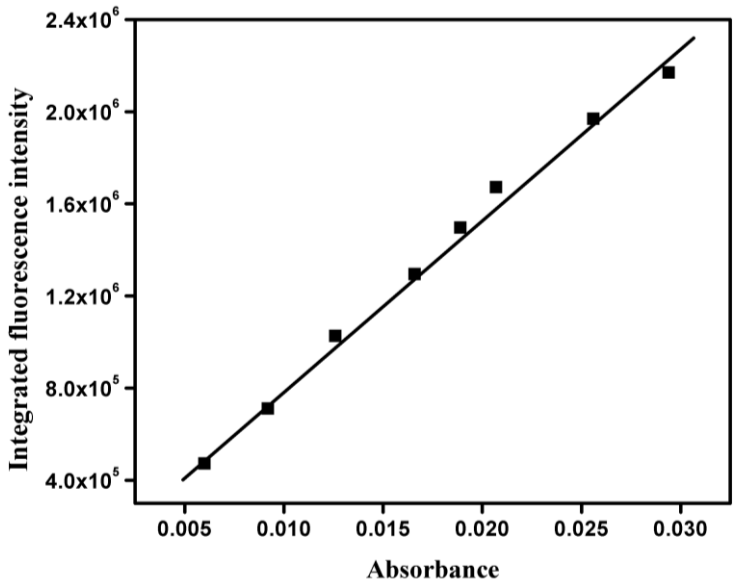

Figure 6.13f: Variation of integrated fluorescence intensity with absorbance for Rhodamine 6G

6.3.7 Concentration study

It was observed that the fluorescence intensity of AuNCs@BSA increased gradually by the successive addition of BHA solution (Figure 6.14a). A linear relationship between the relative fluorescence enhancement intensity, I/I_0 and the concentration of BHA was obtained in the ranges 4.76×10^{-8} - 4.98×10^{-9} M and 4.31×10^{-6} - 4.98×10^{-7} M (Figure 6.14b and 6.14c). The corresponding regression equations can be expressed as $\frac{I}{I_0} = 28.18\ C\ (\mu M) + 1.477, R^2 = 0.995$ and $\frac{I}{I_0} = 0.357\ C\ (\mu M) + 3.047, R^2 = 0.998$ respectively. The limit of detection of the proposed sensor was calculated to be 8.99×10^{-10} M.

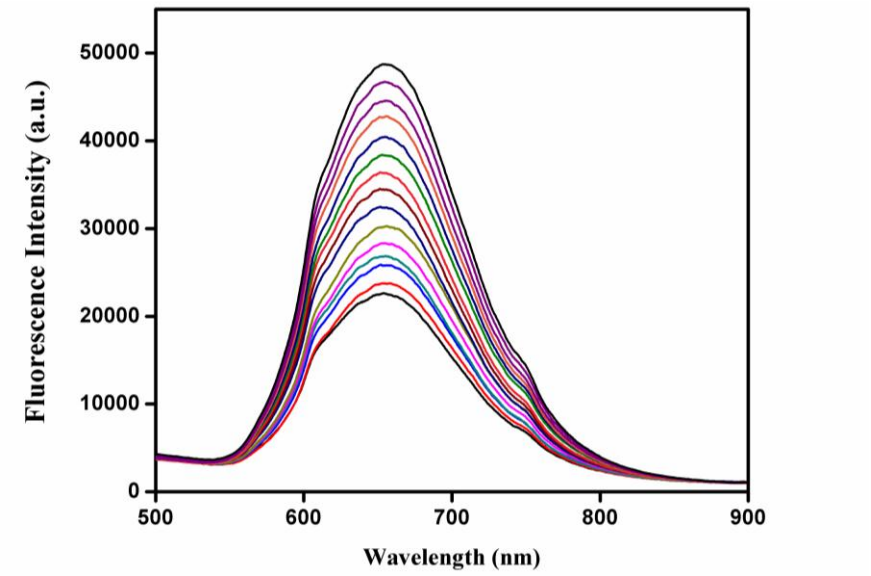

Figure 6.14a: Fluorescence spectra of AuNCs in the presence of various concentrations of BHA

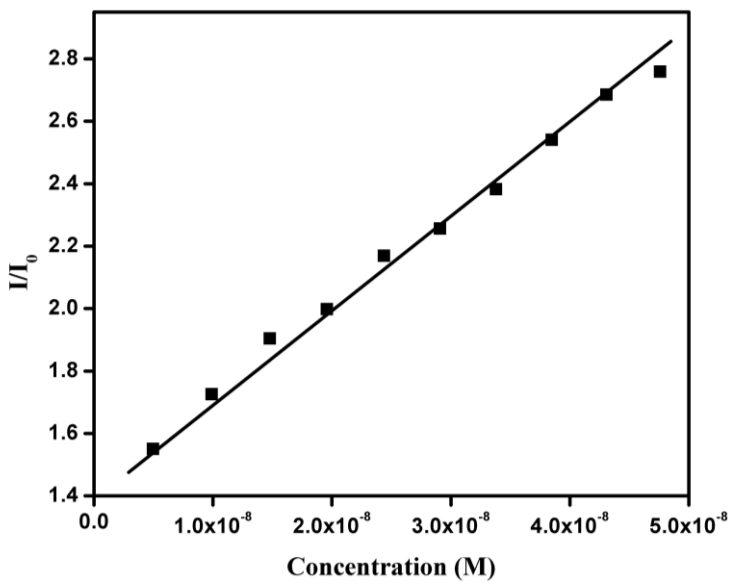

Figure 6.14b: Calibration curve for BHA in the range 4.76×10^{-8} - 4.98×10^{-9} M

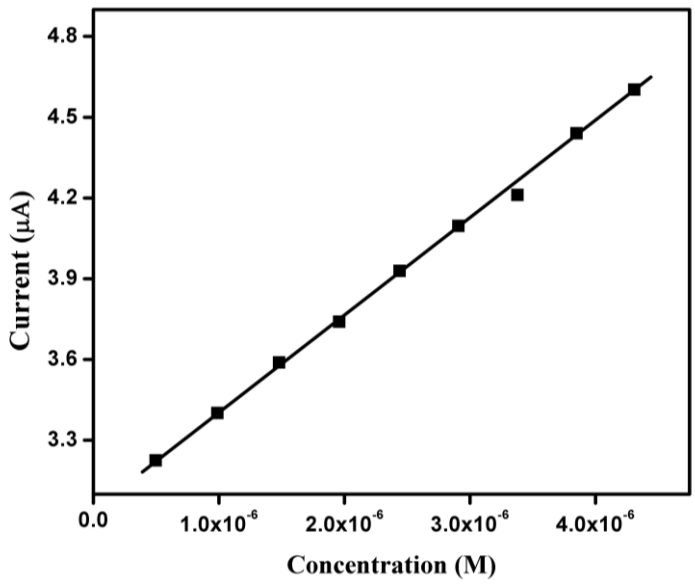

Figure 6.14c: Calibration curve for BHA in the range $4.31 \times 10^{-6} – 4.98 \times 10^{-7}$ M

The measurement of six repetitive fluorescence intensity (AuNCs + 4.98×10^{-7} M BHA) gave a RSD of 1.5 %, suggesting the good reproducibility of the proposed method. The analytical performance of the developed fluorescence sensor is compared with other reported methods for determination of BHA (Table 6.1). The proposed method showed a very low detection limit, which is superior to other methods.

6.3.8 Mechanism

The fluorescence emission signal of AuNCs at 653 nm originated due to the radiative electron-hole recombination process between the excited 'sp' electrons and low lying 'd' band electrons.[302] An enhancement in the fluorescence intensity along with a red shift in emission wavelength of AuNCs@BSA was observed by the addition of BHA. It was reported

that the electron rich atoms (O, N etc.) or functional groups can increase the fluorescence intensity of nanoclusters through surface interactions.[303] Electron rich functional groups present in the structure of BHA enhances the luminescene intensity of AuNCs by changing surface states.

The change in the fluorescence signal of AuNCs may be attributed to the interaction of BHA either with the surface BSA molecules or with the core AuNCs. This results the aggregation of AuNCs. UV-Vis spectra of AuNCs in the presence and absence of BHA was recorded and it was observed that the absorption maximum of AuNCs almost vanished in the presence of BHA (Figure 6.9). This significant change in absorption spectra may be due to the aggregation or surface state changes of AuNCs as a result of the interaction with BHA. TEM image of AuNCs after the addition of BHA is shown in Figure 6.15, which gave clear evidence for the aggregation of AuNCs. Also the FTIR spectra of AuNCs before and after the addition of BHA are compared in Figure 6.16. From Figure 6.16, it is clear that in the presence of BHA, there is a shift and broadening in the –OH stretching vibration frequency accompanied by an increase in intensity, which indicates improved H bonding in the presence of BHA, resulting in the aggregation of AuNCs.

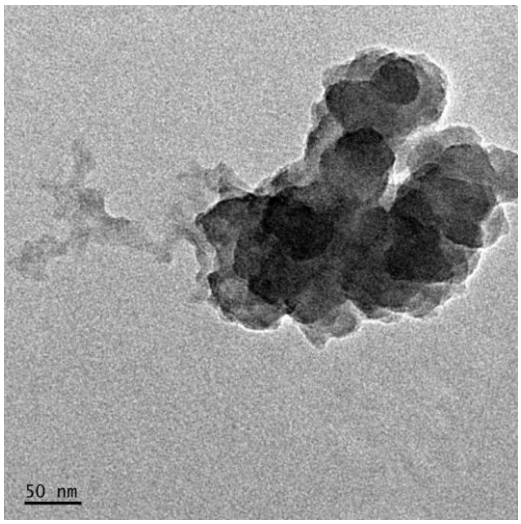

Figure 6.15: TEM image of AuNCs after the addition of BHA

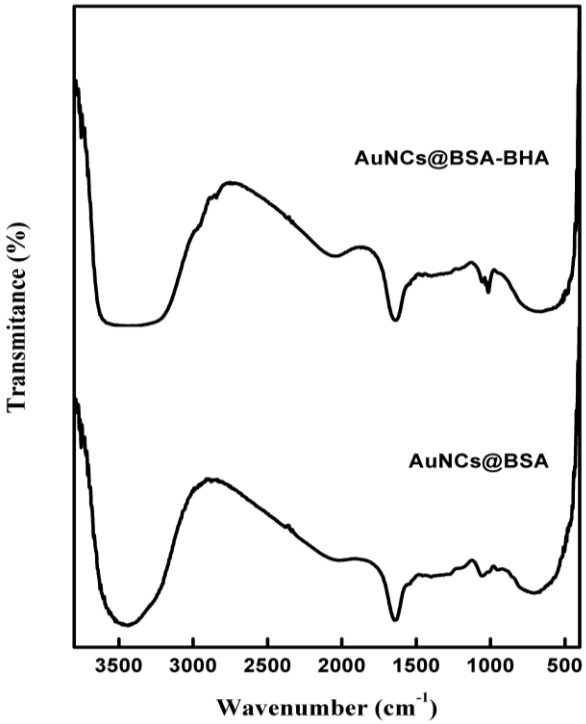

Figure 6.16: FTIR spectra of AuNCs before and after the addition of BHA

Aggregated AuNCs have low rotational and vibrational speed because of their large diameter. Additionally the Brownian motion is weakened and this decreases the collision probability between the AuNCs thereby increasing the external energy transfer rate.[304] As a result of the physical constraint in the aggregates, intramolecular rotations are restricted and new radiative decay channels are opened. This increases the rate of electron-hole recombination process, thereby increasing the fluorescence intensity.

6.3.9 Selectivity

The selectivity of the method was evaluated in the presence of possible co-existing species such as sodium sulphite, citric acid, NaCl, acetic acid, EDTA, propyl gallate and butylated hydroxytoluene. The change in fluorescence signal of AuNCs on the addition of above mentioned compounds is compared in Figure 6.17a. It is clear from Figure 6.17a that only BHA can enhance the luminescence intensity of AuNCs considerably,

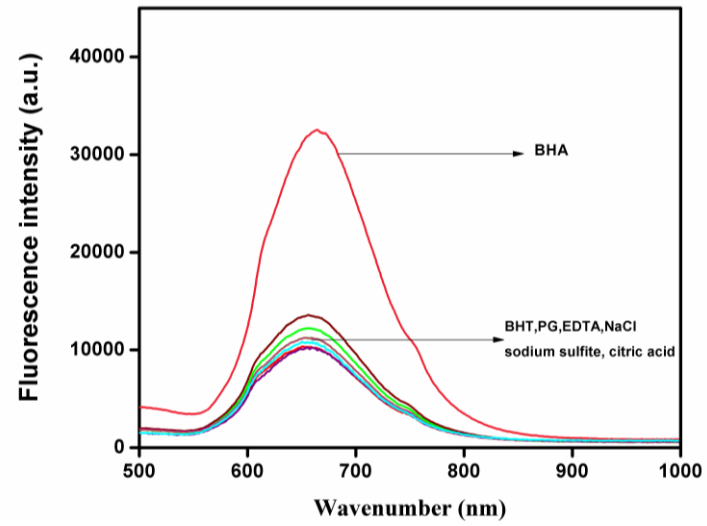

Figure 6.17a: Selectivity of the sensor: Fluorescence emission changes of AuNCs in the presence of other substances

other foreign species have no influence on the fluoresce intensity of AuNCs except propyl gallate. A slight decrease in the luminescence intensity of AuNCs was observed in the presence of propyl gallate. The results suggested that the nanocluster based fluorescent probe showed good selectivity for BHA over other species.

Furthermore the interference study was carried out by mixing BHA with various concentrations (1:1, 1:10 and 1:100) of the above mentioned substances. The corresponding fluorescence intensity was measured using the proposed sensor (Figure 6.17b).

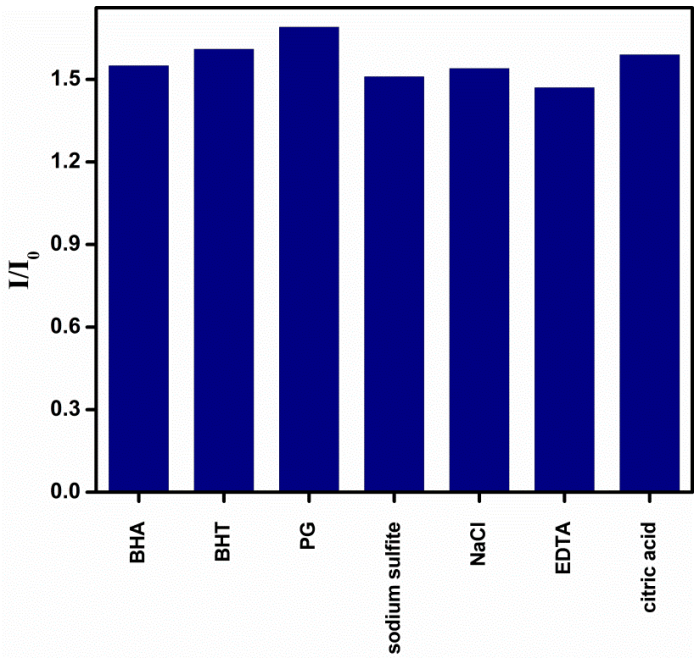

Figure 6.17b: Fluorescence behaviour of AuNCs in the presence of 4.98×10^{-9} M BHA with the coexistence of other substances at 100 fold excess concentrations

Most of the above mentioned species except propyl gallate displayed a negligible interference (signal change below 5%, Table 6.2) on BHA sensing

using AuNCs even when present up to 100 fold excess (Figure 6.17b). Propyl gallate when present in greater than 40 fold excess concentration of BHA, signal change greater than 5 % was observed and interfere the determination. The analytical results confirmed that BHA could be determined in the presence of other species.

6.3.10 Application study

The analytical applicability of the developed sensor was tested in spiked vegetable oil samples. For this purpose, known quantities of BHA were added into the oil samples, and analyzed. The recoveries in the range from 97 to 103 % were obtained, illustrating the validity of the developed method. The analytical results are listed in Table 6.3. The results were compared with those obtained from the liquid chromatography with UV detector[304] and good results were obtained.

6.4 Conclusions

A novel fluorescent sensor for the artificial antioxidant, BHA was developed successfully using protein stabilized AuNCs. In the presence of BHA, the luminescence intensity of AuNCs enhanced linearly as a function of concentration of BHA. Experimental parameters influencing the enhancement phenomenon was studied. The proposed method exhibited good selectivity and sensitivity towards the quantification of BHA. The working concentration ranges were found to be 4.31×10^{-6} - 4.98×10^{-7} M and 4.76×10^{-8}- 4.98×10^{-9} M. The limit of detection of the turn on fluorescence sensor was found to be 8.99×10^{-10} M. Also the developed sensor was applied for the monitoring of BHA in commercially available vegetable oil samples.

Table 6.1: Comparison with other determination methods for BHA

Method	Linear range (M)	LOD (M)	Reference
Micellar electrokinetic capillary chromatography	5.00×10^{-4} - 5.00×10^{-6}	5.00×10^{-6}	270
Gas chromatography	8.32×10^{-4} - 2.77×10^{-5}	1.11×10^{-5}	271
HPLC	5.54×10^{-5} - 1.11×10^{-6}	6.10×10^{-7}	272
Voltammetry (Pt/MWCNT)	1.00×10^{-6} - 1.00×10^{-7}	9.50×10^{-8}	265
Voltammetry Poly(L-cys)/GCE	1.00×10^{-5} - 1.00×10^{-6}	4.10×10^{-7}	264
Fluorescence	4.76×10^{-8} - 4.98×10^{-9}	8.99×10^{-10}	Proposed method

L-cys: L-cysteine, Pt: platinum electrode, MWCNT: multiwalled carbon nanotube

Table 6.2: Effect of foreign species on the determination of BHA (4.98×10^{-9} M)

Foreign Species	Concentration (M)	Signal change %
Sodium sulphite	4.98×10^{-7}	1.95
Citric acid	4.98×10^{-7}	3.25
BHT	4.98×10^{-7}	4.54
NaCl	4.98×10^{-7}	0.62
EDTA	4.98×10^{-7}	4.54
Propyl gallate	1.99×10^{-7}	4.73

BHT: butylated hydroxytoluene

Table 6.3: Application study

	Proposed method				LC-UV method			
	Added (M)	Found (M)*	RSD	Recovery (%)	Added (M)	Found (M)*	RSD	Recovery (%)
Sample 1	4.98×10^{-9}	5.11×10^{-9}	0.04	102.6	2.00×10^{-7}	2.03×10^{-7}	0.33	101.5
	3.33×10^{-8}	3.31×10^{-8}	0.07	99.4	5.00×10^{-7}	5.08×10^{-7}	0.17	101.6
	2.33×10^{-8}	2.29×10^{-8}	0.06	98.3	9.00×10^{-7}	9.20×10^{-7}	0.24	102.2
Sample 2	4.98×10^{-9}	5.08×10^{-9}	0.05	102.0	2.00×10^{-7}	2.06×10^{-7}	0.28	103.0
	3.33×10^{-8}	3.36×10^{-8}	0.03	100.9	5.00×10^{-7}	5.10×10^{-7}	0.13	102.0
	2.33×10^{-8}	2.27×10^{-8}	0.15	97.4	9.00×10^{-7}	9.11×10^{-7}	0.31	101.2

*average of five replicates
RSD: relative standard deviation

Chapter 7

CADMIUM SULPHIDE QUANTUM DOTS BASED FLUORESCENCE SENSOR FOR DOPAMINE

Contents

This chapter explains the selective determination of dopamine (DA), using thioglycolic acid (TGA) capped CdS quantum dots (QDs). The fluorescence emission spectrum of TGA functionalized CdS QDs which was at about 527 nm showed an enormous increase in emission intensity in the presence of DA. The addition of DA increases the passivation of surface traps of QDs and thereby increasing the fluorescence emission intensity. The linear range and detection limit of the developed turn on sensor was 3.94 × 10^{-7} M to 4.67 × 10^{-8} M and 2.55 × 10^{-9} M respectively. The influence of some biologically important compounds that are structurally similar to DA on the fluorescence emission intensity of the CdS fluorescent probe was studied to evaluate the selectivity of the sensor. The developed turn on sensor exhibits good analytical figures of merit, excellent selectivity and shows promising practical applications.

7.1 Introduction

Neurotransmitters are the endogenous chemicals that communicate information throughout our brain and body. They transmit signals between nerve cells, called "neurons." Until the early 20th century, the transmission of signals from one neuron to another was believed to be electrical. But in 1921, it was confirmed by German pharmacologist Otto Loewi that neurons communicate by releasing certain chemicals called neurotransmitters.[305] Neurotransmitters play a vital role in controlling everyday life and functions. They can also influence sleep, weight, mood, concentration, and can cause adverse symptoms when they are out of balance.

Dopamine (DA) [Figure 7.1] is an important neurotransmitter, which plays a key role in the functioning of the cardiovascular, hormonal, renal and central nervous system of mammals.[307,308] Abnormal levels of DA in the brain may result in serious neurological disorders such as Parkinson's disease, Schizophrenia, Alzheimer's disease, Huntington's disease etc.[309-311] Monitoring of DA in urine is very significant since the concentration of DA in urine reflects the activity of sympathoadrienal system. Hence DA is considered as a biomarker for these diseases, whereby monitoring of DA becomes significant in clinical analysis. Biomarkers, which are molecular signatures of diseases have dominant role in the medical diagnosis.

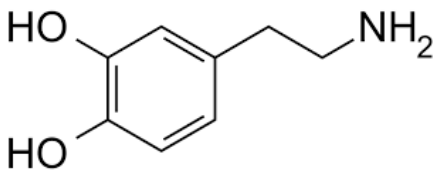

Figure 7.1: Structure of DA

Various traditional analytical methods have been reported for the quantification of DA, which include spectrophotometry,[312] liquid chromatography combined with mass spectrometry (LC-MS),[313] HPLC,[314] fluorometry,[315] flow injection analysis[316,317] and electrochemical techniques.[318] However, these methods have some limitations. Although LC-MS method have very low limit of detection, the determination needs pretreatment of sample, expensive instruments and lengthy analysis time.[319] Because of the electroactive nature of DA, the determination of DA has been usually carried out by electrochemical methods, but the main problem is the overlapping of voltammetric signals of DA with that of the coexisting species such as ascorbic acid and uric acid (oxidation potentials close to that of DA).[320] Owing to its rapid response and high sensitivity fluorescence technique is preferred over the various methods.

Quantum dots (QDs), the semiconductor nanocrystals have emerged as attractive fluorescent materials in the fields such as of sensing,[321] photocatalysis,[322] imaging[323] and biological labeling[324] due to their size dependent optical properties. They belong to a class of material lying in the transition regime between molecules and bulk materials.[325]

Due to quantum confinement effect, QDs show unique optical properties such as high photo bleaching threshold, size dependent luminescence spectra, good chemical stability, broad absorption and narrow emission wavelengths, which make them potential materials for the design of novel sensitive sensors.[326] The onset of absorption and the position of fluorescent bands are shifted to shorter wavelengths in these materials due to size quantization effect.[327,328] Surface states play a crucial role in the luminescence properties

of QDs since the interaction between certain analytes and the surface of QDs can affect the efficiency of electron-hole recombination process.[329]

Fluorescent sensors have emerged as a dynamic technique for quantitative analysis of biomarkers in clinical diagnosis. In the present work, water soluble CdS QDs were prepared using TGA as capping agent by a simple procedure. FTIR, HRTEM and UV-Vis spectroscopy were used for characterization studies. Luminescence measurements indicated that TGA functionalized CdS QDs (TGA-CdS QDs) exhibited broad emission peak at 527 nm. The fluorescence of CdS QDs was enhanced by the addition of trace amount of DA, and the fluorescence intensity of CdS QDs increased with increasing concentrations of DA. Based on this, a novel fluorescent sensor was developed for the quantification of DA, which was sensitive and reliable. The newly developed sensing method, can serve as a potential diagnostic tool for the biomarker DA.

7.2 Experimental

7.2.1 Synthesis of TGA capped CdS QDs

CdS QDs protected by TGA were synthesized following the procedure described by Wang *et al.*[326,330] 1.3 mL of TGA solution (0.15 M) and 80 mL of $CdCl_2$ solution (0.001 M) were mixed in a round bottom flask. Then 3 mL (0.1 M) NaOH was added into the above solution to make the pH value of the solution about 8.0. Nitrogen was purged through the solution for 20 min, followed by the addition of 20 mL (0.002 M) of Na_2S and the mixture was allowed to react for 20 min at room temperature under nitrogen atmosphere.

7.2.2 Preparation of solution of DA

A stock solution (1.00×10^{-2} M) of DA was prepared in water. Solutions of various concentrations of DA were prepared by diluting the stock solution using the Milli Q water.

7.2.3 Analytical procedure

Working solution of TGA-CdS QDs was prepared by diluting the stock solution of TGA capped CdS QDs with 0.1 M acetate buffer solution (pH 7). The spectrofluorimetric measurements were carried out as follows: - an aliquot of the prepared QDs were transferred into a 1 cm × 1 cm quartz cell and different amounts of DA stock solutions were added to the cell. I_0 and I, the fluorescence intensities of TGA capped CdS QDs in the absence and presence of DA was measured.

7.3 Results and discussion

7.3.1 Characterization of TGA capped CdS QDs

Optical properties of synthesized water dispersible QDs were characterized by UV-Vis spectrometry and fluorescence spectroscopy. Figure 7.2a and 7.2b shows the absorption and fluorescence emission spectra of TGA functionalized CdS QDs respectively. TGA-CdS QDs exhibited long emission wavelengths and a large separation between the excitation and emission wavelengths. Figure 7.3 showed the photographs of CdS QDs under visible light and UV light. The UV-Vis absorption spectrum of colloidal CdS QDs showed weak broad absorption in the UV range. The maximum absorbance was obtained at about 344 nm. The onset of absorption is considerably blue shifted relative to the bulk CdS (515 nm) indicating a significant quantum confinement effect of synthesized CdS QDs.[331]

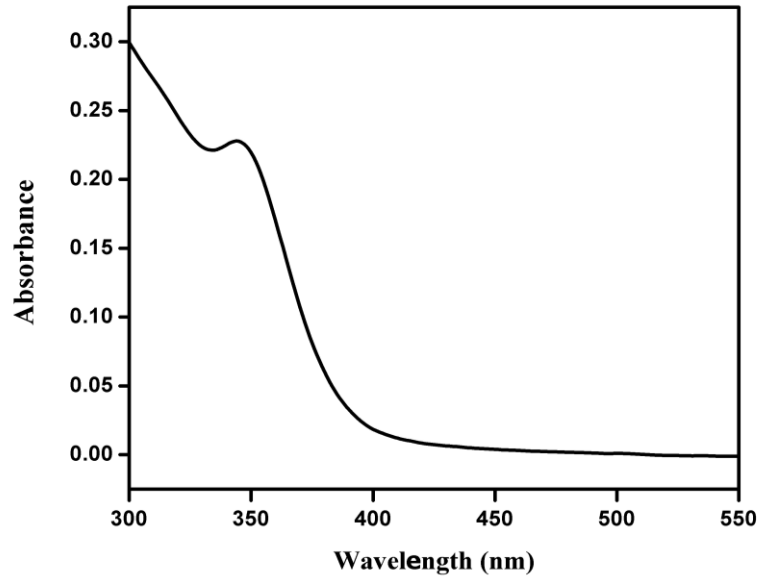

Figure 7.2a: Absorption spectrum of TGA capped CdS QDs

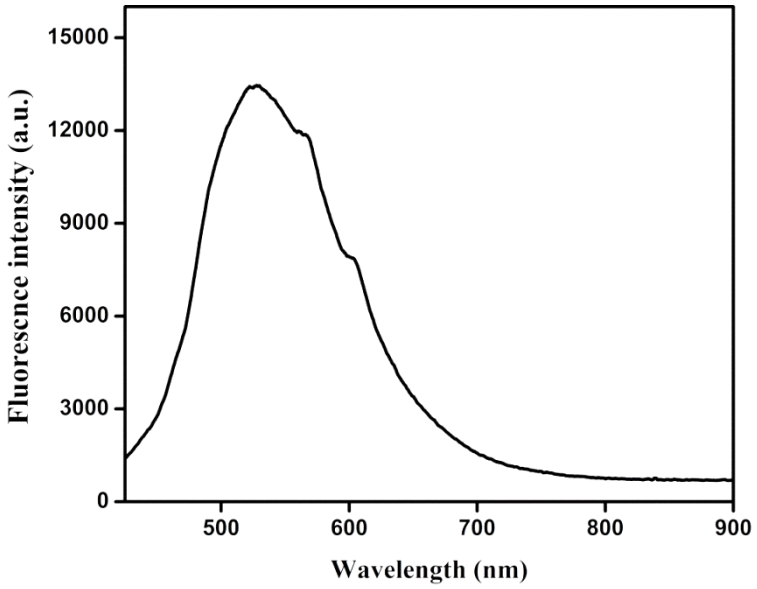

Figure 7.2b: Fluorescence spectrum of TGA capped CdS QDs

Figure 7:3 Photographs of TGA capped CdS QDs under visible light and UV light

When excited at 400 nm, CdS QDs exhibited a broad emission band centered at 527 nm, which was attributed to trap state emission arising from surface trap states of CdS nanocrystallites.[332]

The morphology of the TGA protected CdS QDs was studied by HRTEM. TEM image of CdS QDs showed spherical particles (Figure 7.4) and particle size of the CdS QDs was calculated using the following equation reported by Peng *et al.*[333]

$$\mathbf{D} = (-\mathbf{6.6521} \times \mathbf{10^{-8}})\boldsymbol{\lambda}^{\mathbf{3}} + (\mathbf{1.9557} \times \mathbf{10^{-4}})\boldsymbol{\lambda}^{\mathbf{2}} - (\mathbf{9.2352} \times \mathbf{10^{-2}})\boldsymbol{\lambda} + (\mathbf{13.29})$$

The average particle size was calculated to be 1.96 nm. The synthesized colloidal CdS QDs were found to be stable for about 4 months, when stored at 4^0C.

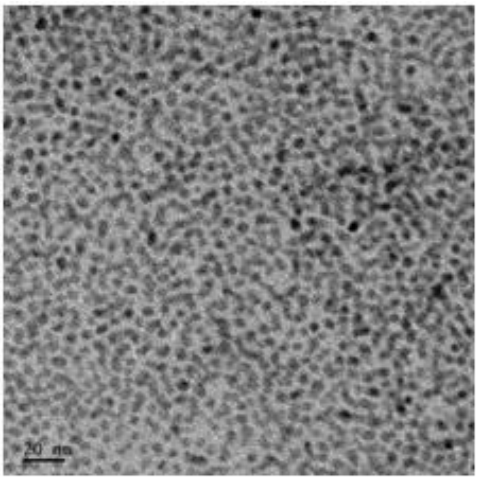

Figure 7.4: TEM image of TGA capped CdS QDs

If extinction coefficient of nanocrystals is known, the concentration of nanocrystals could be obtained by recording the absorption spectrum of the sample. According to Beer-Lambert's Law

$$\boldsymbol{A = \varepsilon c l}$$

ε is the extinction coefficient, c is the molar concentration of nanocrystals, l is the path length in cm. For CdS nanocrystals, $\boldsymbol{\varepsilon = 21536(D)^{2.3}}$ [333]. Hence the concentration of CdS QDs was calculated to be 0.0034 M.

Figure 7.5 depicts the FTIR spectra of free TGA and TGA stabilized CdS QDs. IR spectra of both TGA protected CdS QDs and free TGA showed absorption peaks for carboxyl and carbonyl groups. While the peak for S-H (2550-2670 cm^{-1}) vibration was absent in IR spectrum of TGA-CdS QDs as a result of covalent bonding between thiols and Cd atom on the QDs surface.[334]

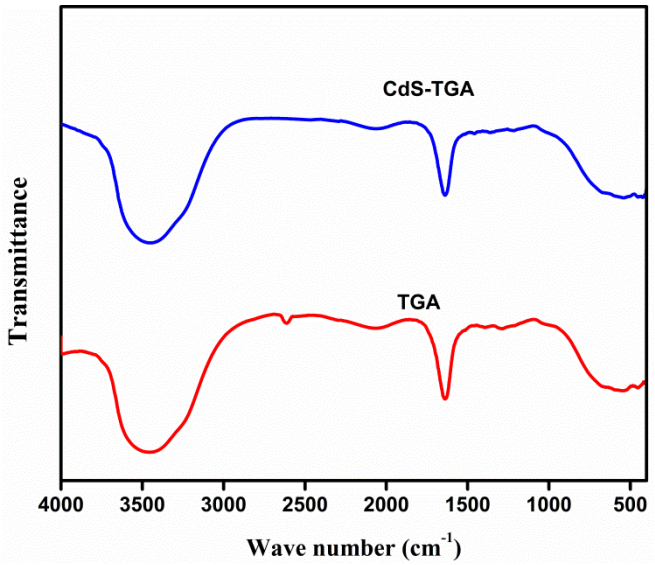

Figure 7.5: FTIR spectra of free TGA and TGA capped CdS QDs

7.3.2 Fluorescence enhancement of TGA functionalized CdS QDs by DA

Luminescence spectroscopy is a well known sensitive technique to study the changes of the surface chemistry of semiconducting nanoparticles. With an excitation at 400 nm, TGA-CdS QDs displayed an emission maximum around 527 nm with a full width at half maximum (FWHM) of 120.65 nm. The broad emission indicated the presence of large number of surface defects.[320] The fluorescence intensity of CdS QDs increased dramatically by the addition of trace amount of DA (Figure 7.6). A red shift in the fluorescence emission wavelength was also observed.

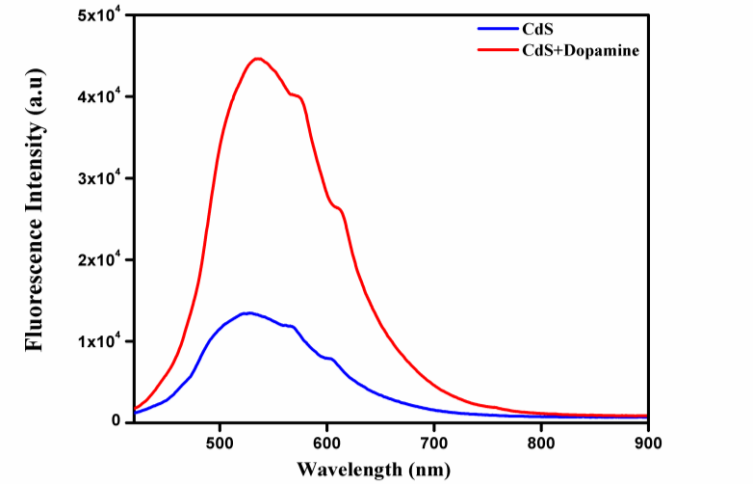

Figure 7.6: Fluorescence spectra of CdS QDs in the absence and presence of DA

The UV-Vis absorption spectra of CdS QDs were taken in the absence and presence of DA (Figure 7.7a) and it was observed that there was a blue shift in the absorption maxima along with a decrease in absorbance which indicated the changes in the surface states of CdS QDs. Also the absorbance of QDs gradually decreased with increasing the concentration of DA (Figure 7.7b).

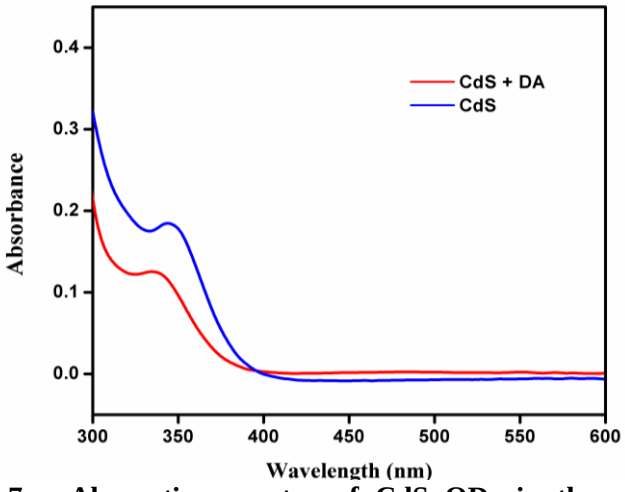

Figure 7.7a: Absorption spectra of CdS QDs in the absence and presence of DA

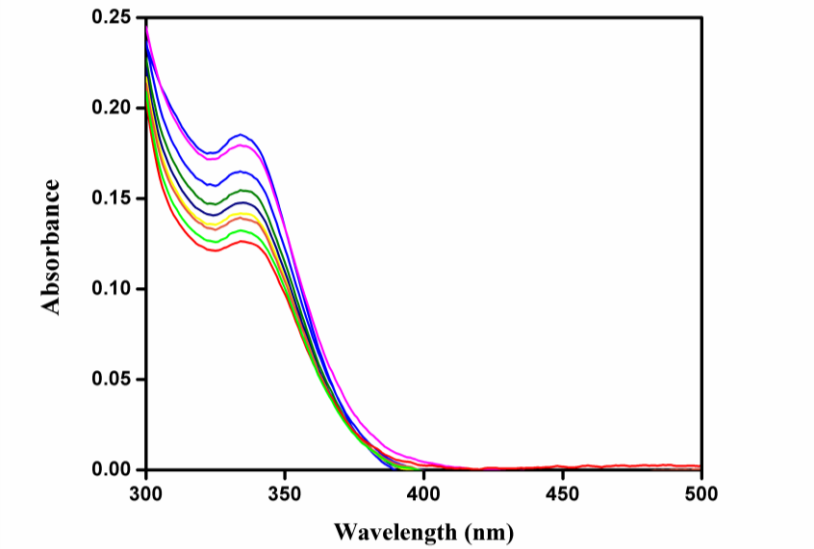

Figure 7.7b: Absorption spectra of CdS QDs in the presence of different concentrations of DA

7.3.3 Effect of buffer Solutions

The fluorescence enhancement of CdS-TGA by DA was analyzed in different kinds of buffer solutions, such as phosphate buffer, citrate buffer and acetate buffer solution (ABS). Maximum fluorescence enhancement was observed in ABS, suggesting that acetate buffer solution was preferable for the interaction between DA and TGA stabilized CdS QDs. Therefore, ABS was selected for further studies.

In addition, the effect of the volume of ABS on the DA induced fluorescence enhancement of CdS QDs was also examined (Figure 7.8). Maximum relative fluorescence intensity was obtained when the ratio of CdS QDs and ABS is 1:5 and this ratio was followed in all experiments.

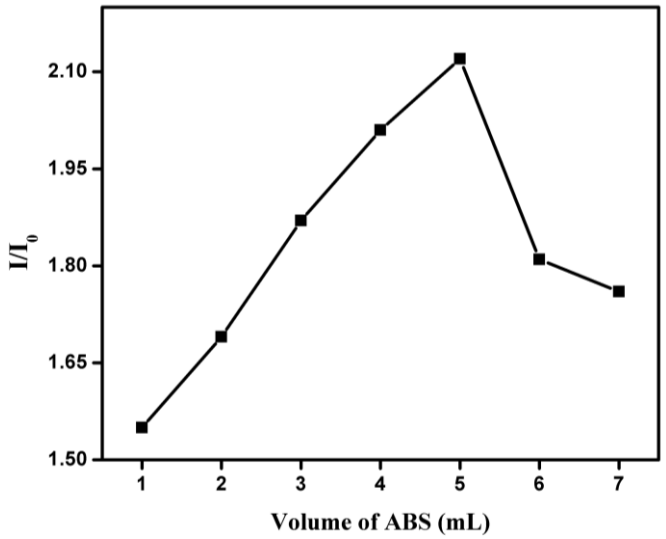

Figure 7.8: Effect of volume of ABS on the fluorescence enhancement of CdS QDs by DA

7.3.4 Effect of pH

It is well known that QDs are sensitive to pH changes. The fluorescence intensity of CdS QDs was studied by diluting it with 0.1 M ABS of different pH values (Figure 7.9a). The studies revealed that the emission wavelength of TGA functionalized CdS QDs did not show any pH dependence. However, the emission intensity changed noticeably. DA-TGA CdS system showed maximum enhancement in relative fluorescence intensity at pH 7 (Figure 9b). Hence pH 7 was chosen as the optimum pH for the effective determination of DA.

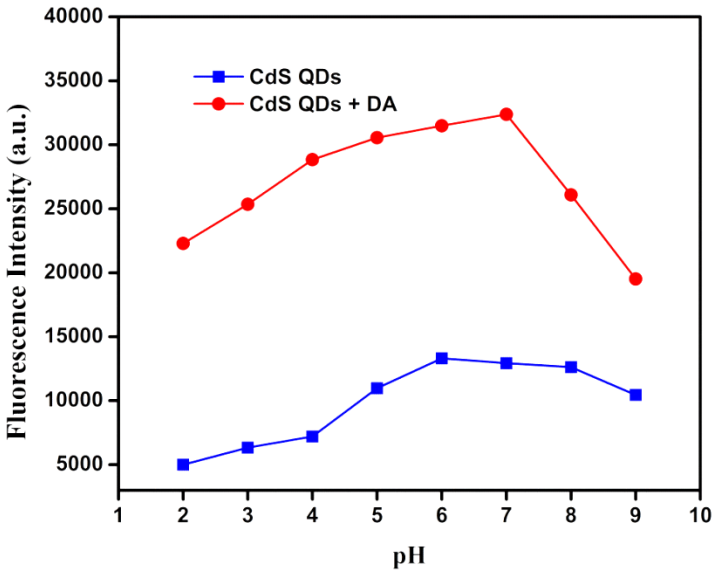

Figure 7.9a: Effect of pH of ABS on the fluorescence intensity of CdS QDs and CdS QDs in the presence of DA

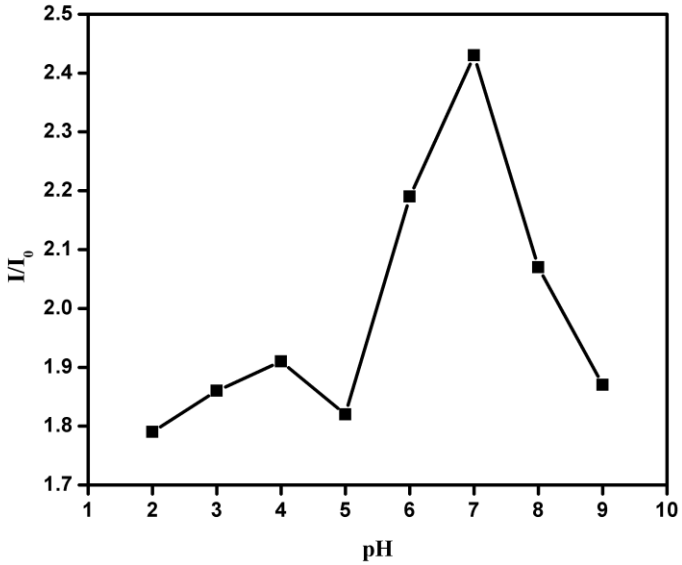

Figure 7.9b: Effect of pH of ABS on the fluorescence enhancement of CdS QDs by DA

7.3.5 Effect of time

The effect of incubation time on the fluorescence intensity of CdS-DA system was tested. The influence of time was studied by measuring the emission intensities every 30 sec for 1 hr immediately after mixing. The results indicated that the reaction between CdS QDs and DA occurred rapidly at room temperature and fluorescence intensity reached maximum value immediately after mixing. Also the fluorescence intensity remains almost constant up to 1 hr. Figure 7.10 shows the photoluminescence intensity-time plots for various concentrations of DA.

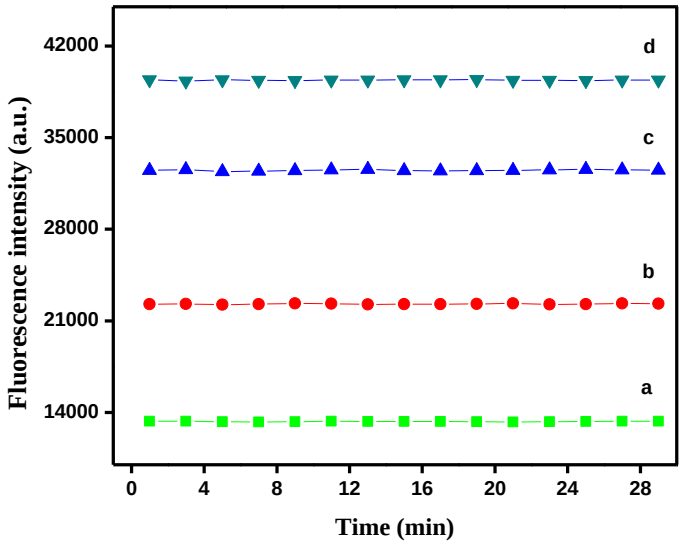

Figure 7.10: Effect of time on the fluorescence intensity of a) CdS QDs b) CdS QDs + 9.09 × 10^{-8}M DA c) CdS QDs + 2.59 × 10^{-7} M DA d) CdS QDs + 3.33 × 10^{-7} M DA

7.3.6 Quantum yield

Quantum yield of the synthesized TGA protected CdS QDs was determined using rhodhamine 6G as an emission standard. The following equation is used for the calculation of quantum yield [299]

$$\phi_{CdS} = \phi_{Rh} \frac{I_{CdS}}{I_{Rh}} \frac{A_{Rh}}{A_{CdS}} \frac{\eta_{CdS}^2}{\eta_{Rh}^2}$$

where ϕ_{Rh} is the quantum yield of reference rhodhamine 6G. I_{CdS} and I_{Rh} are the integrated fluorescence intensities of CdS and Rh 6G respectively. A_{Rh} and A_{CdS} are the absorbance of the reference and CdS, η_{CdS} and η_{Rh} are the refractive indices of the solvents used. The integral fluorescence intensities of different concentrations of rhodhamine 6G and CdS QDs were measured and then plotted vs absorbance (Figure 7.11). The slopes of the resulting straight lines were used to calculate the quantum yield. Quantum yield for TGA capped CdS QDs was calculated to be 0.16.

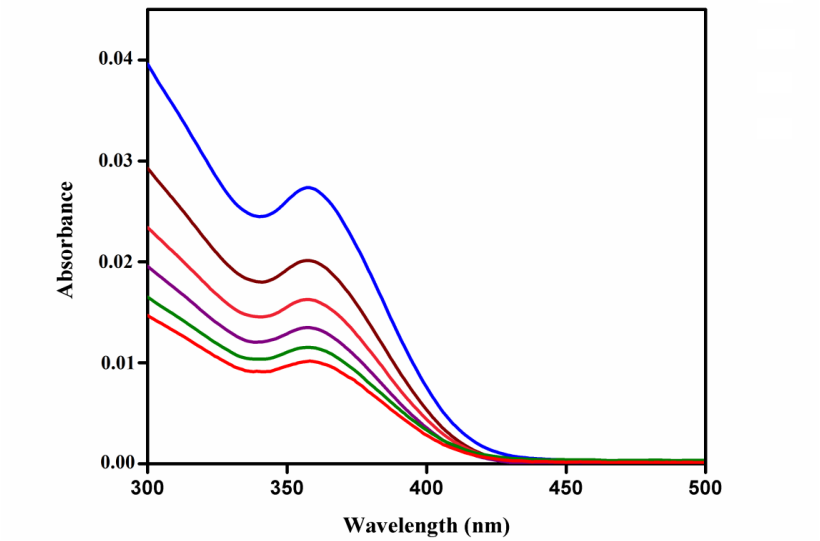

Figure 7.11a: Absorption spectra of CdS QDs at different concentrations of DA

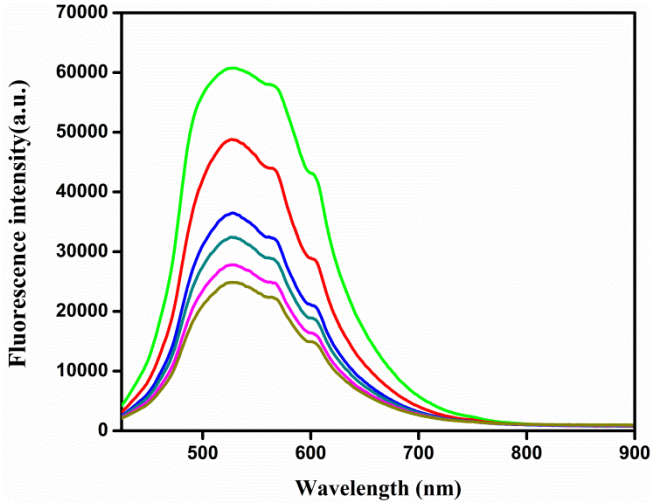

Figure 7.11b: Fluorescence spectra of CdS QDs at different concentrations

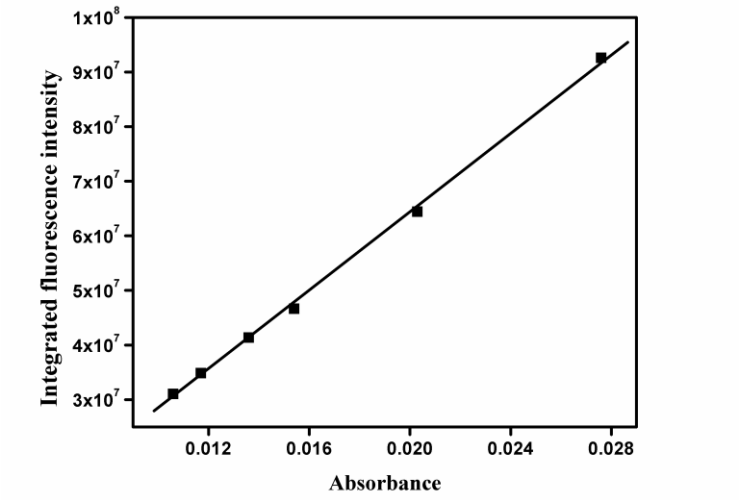

Figure 7.11c: Variation of integrated fluorescence intensity with absorbance for CdS QDs

7.3.7 Concentration study

Langmuir-binding isotherm was applied to explain the binding of DA molecules to the surface of QDs. It was assumed that the surface of QDs contains a finite number of binding sites and these sites could adsorb one

molecule from the solution. The fraction of occupied sites is denoted by θ and 1- θ represents the fraction of available binding sites. The rate of binding is proportional to the concentration of adsorbing molecule and 1- θ. The rate of binding of molecule to the surface of QDs is given by the following equation

$$\boldsymbol{R_b = K_b C(1-\theta)}$$

The rate of desorption is expressed as

$$\boldsymbol{R_d = K_d \theta}$$

At equilibrium condition the rate of adsorption is equal to the rate of desorption

$$\boldsymbol{K_b C(1-\theta) = K_d \theta}$$

By taking θ as a function of the ratio, the equilibrium binding constant,

$$\boldsymbol{B = K_b / K_d}$$

$$\boldsymbol{\theta = \frac{(BC)}{(1+BC)}}$$

The value of θ is related to the ratio of the fluorescence intensity obtained at a given concentration *I* and the I_{max}

$$\boldsymbol{\theta = \frac{I}{I_{max}}}$$

The above expression can be expressed in terms of concentration as

$$\boldsymbol{\frac{I}{I_{max}} = \frac{(BC)}{(1+BC)}}$$

The equation can be rewritten in the following form

$$\frac{C}{I} = \left(\frac{1}{BI_{max}}\right) + \left(\frac{1}{BI_{max}}\right) C$$

It was observed that the fluorescence emission intensity of QDs increased with increasing concentration of DA, as depicted in Figure 7.12a. The relationship between the fluorescence intensity of CdS QDs and the concentration of DA can be described by Langmuir-binding isotherm equation[336,337] as shown in Figure 7.12b. The linear range was from 3.94×10^{-7} M to 4.67×10^{-8} M the data fitting gave the correlation coefficient of 0.998 and the equilibrium binding constant of 5.8. The remarkable Langmuir fit suggested that there is a possibility that more than one DA molecules bind to the surface of individual QDs. A detection limit of 2.55×10^{-9} M was obtained.

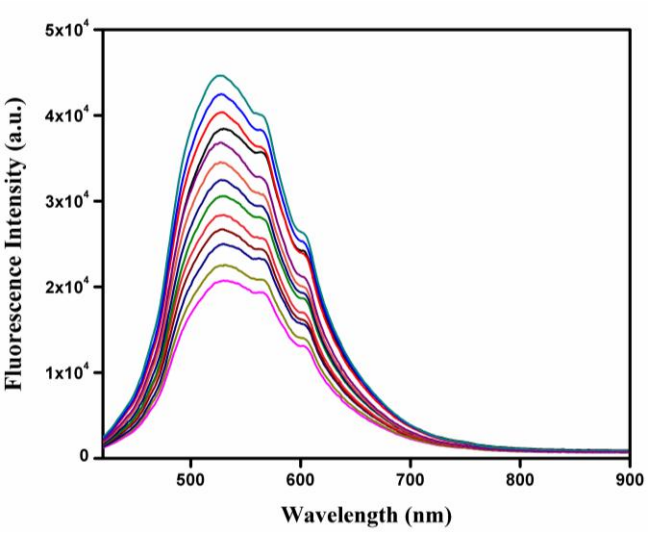

Figure 7.12a: Fluorescence spectra of CdS QDs in the presence of various concentrations of DA

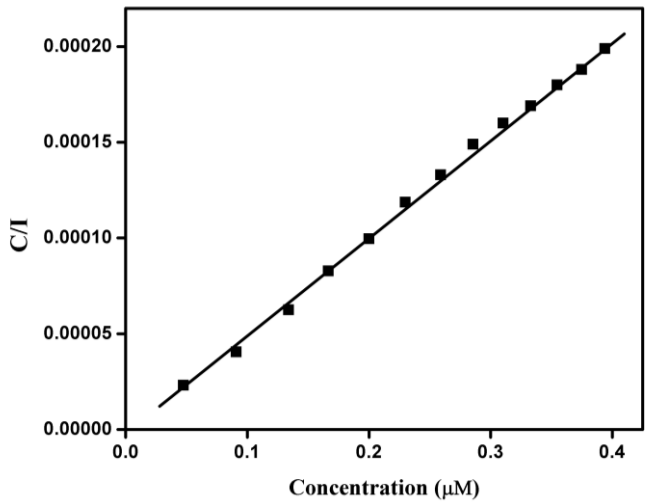

Figure 7.12b: Langmuir binding isotherm relationship between the fluorescence enhancement and concentration of DA

The standard deviation for ten replicate measurements of CdS QDs containing 3.94 × 10^{-7} M DA was 2.6 %, indicating that the method has good repeatability. A comparison of the analytical performance of the developed sensor with the other reported fluorescent sensors is listed in Table1. The developed sensing probe exhibited low limit of detection, which is superior to other sensors.

ΔG, the free energy for binding of DA to the surface of CdS QDs was calculated. The following equation was used for the calculation of free energy of binding [342]

$$\Delta G = -RT \ln B$$

where R is the gas constant, T is the experimental temperature, and B is the binding constant at the temperature T. The free energy of binding was found to be -3.99 KJ/mol, indicating the binding of DA to the surface of CdS QDs is a spontaneous and feasible reaction.

7.3.8 Mechanism

Physical and chemical interactions between QDs and certain small molecules can bring about changes in the surface property and efficiency of electron-hole recombination process in QDs which changes their photoluminescent intensity.[343] There are reports that compounds containing amino group could enhance the fluorescence intensity of QDs.[328,344] Wang *et al*. developed a turn on fluorescent sensor for melamine based on the interaction of $-NH_2$ group with the surface of CdS QDs.[326] Citrate capped CdS QDs were used as the sensing probe for the ultra-sensitive determination of cysteine. According to Wang *et al*. this observed fluorescence enhancement of CdS QDs was due to the surface passivation of QDs by amino group of cysteine.[345]

It was reported that amine functional group could bind to the surface of CdS QDs through the N-Cd bond thereby eliminating the surface defects which acts as electron traps. This result in the enhancement of fluorescence intensity of CdS QDs.[326] The fluorescence spectrum of TGA capped CdS QDs red shifted (527 to 537 nm) in the presence of DA (Figure 7.6), suggesting that DA bound to lower energy sites of CdS QDs (Scheme 7.1).[346]

Surface trap states reduce the photoluminescence efficiency of QDs. The addition of DA to CdS QDs decrease the surface defects due to the adsorption of DA on the surface of QDs. The removal of trap states from the surface by DA molecules increase the emission intensity of QDs.[320] Due to the removal of local trap states, more radiative centers are created on the surface and nonradiative electron/hole recombinations on the surface of

QDs are blocked thereby increasing the intensity of fluorescence emission.[347] In other words surface passivation occurs at the surface of QDs, since $–NH_2$ group of DA can provide electron to bind with the defect sites.[326]

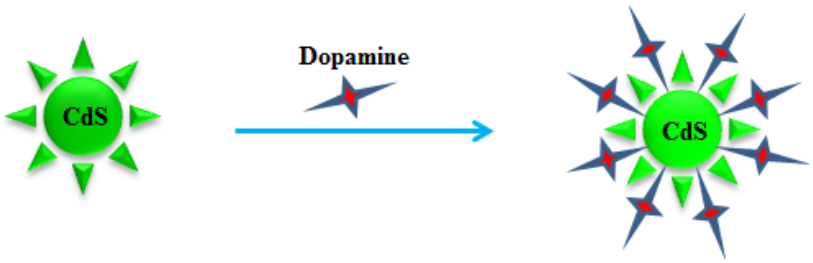

Scheme 7.1: Sensing of DA using TGAcapped CdS QDs

UV-Vis spectroscopy is a reliable method to study the structural changes undergone by fluorophore and to understand about the mechanism of interaction of the probe with DA. Absorption spectra of CdS QDs were taken before and after the addition of DA (Figure 7.7a). It is clear from UV-Vis spectra that the absorbance of QDs at 344 nm was decreased and the absorption maximum shows a slight blue shift which means that the environment changed due to the interaction with DA. CdS QDs exhibited a decrease in absorbance with increase in concentration of DA (Figure 7.7b). Due to the decreased self-absorption of QDs in the presence of DA, radiative electron-hole recombination rate is increased.

The structure of DA is suitable for effective attachment of its $–NH_2$ group to the surface of CdS QDs even in the presence of TGA capping ligand. The other $–NH_2$ containing compounds fail to attach to the QD surface probably due to the structural hinderence. This results in the selective recognition of DA by CdS QDs.

7.3.9 Selectivity

Selectivity is one of the most significant analytical parameter to evaluate the performance of a new fluorescent probe. A highly selective response to the target analyte over other potentially competing species is a necessary condition for a sensor. To evaluate the selectivity of the system, the fluorescence intensity of the CdS-TGA was measured in the presence of compounds such as dopamine, epinephrine, nor epinephrine, 3,4-dihyroxy phenylalanine (L-DOPA), creatinine, ascorbic acid and uric acid. As shown in Figure 7.13a, only DA induced a prominent fluorescence enhancement, whereas weak fluorescence variations were observed for other materials. The high selectivity of CdS QDs for dopamine over other catecholamines can be explained on the basis of the steric effect. In the case of epinephrine and norepinephrine, which are substituted ethanolamines binding to the surface of QDs is much weaker.[348]

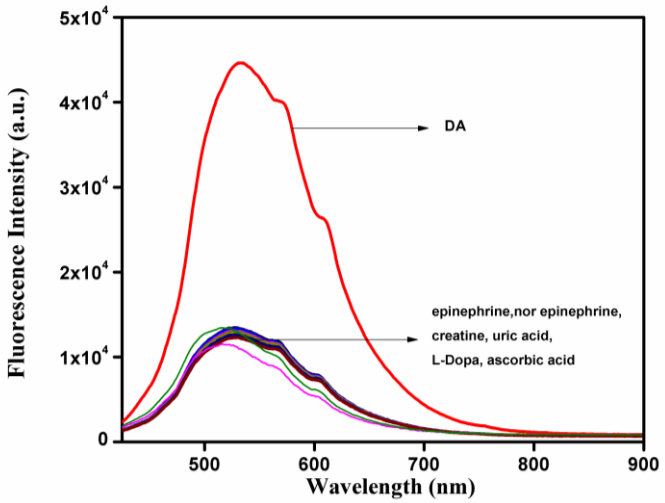

Figure 7.13a: Selectivity of the sensor: Fluorescence emission changes in TGA-CdS QDs presence of various biological compounds

Additionally, the fluorescence intensity was recorded in the presence of DA (4.67×10^{-7} M) and various concentrations (1:1, 1:10 and 1:100) of the above mentioned substances. None of the coexisting substances interfered the sensing of DA by QDs when present in 10 fold excess concentrations. Most of the above mentioned species except creatinine showed a negligible interference (signal change below 5%) on DA sensing by CdS QDs (Table 2) even present up to 100 fold excess (Figure 7.13b). The probe was tolerant up to 50 fold excess concentration of creatinine, but when present above this concentration, creatinine interfered the analysis producing a signal change greater than 5%. All these results indicates that TGA functionalized CdS QDs have good selectivity for the determination of DA.

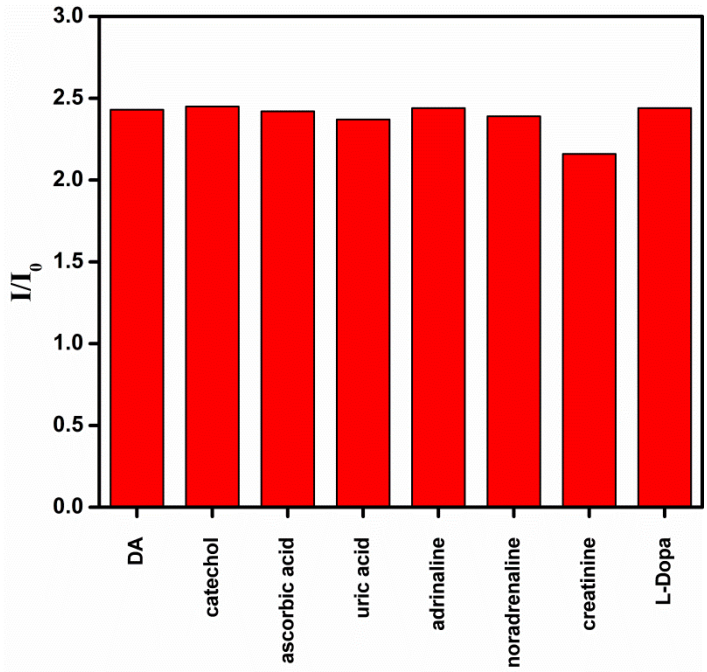

Figure 13b: Fluorescence behaviour of CdS QDs in the presence of 3.94×10^{-7} M DA with the coexistence of other substances at 100 folds excess concentrations

7.3.9 Application study

The applicability of the quantum dot based fluorescent sensor for the analysis of real samples was studied by the determination of DA in spiked urine sample. The results are shown in Table 3. The fluorescence signal of DA obtained from the spiked urine was comparable with that of the standard solution of DA with same concentration. The recoveries were obtained in the range of 98 – 101 %. Based on five replicate measurements, RSD for the DA determination in the examined urine samples was found to be 3.6 %. The recoveries were compared with HPLC method and satisfactory results were obtained.[349] The results suggested that the developed sensor could be effectively used for the monitoring of DA in urine samples. Since it had been reported that the DA level in urine reflects the activity of the sympathoadrenal system, the detection of DA in urine is very important for the diagnosis of pheochromocytoma and related diseases.[350]

7.4 Conclusions

A simple fluorescent sensor for the biomarker DA was developed based on the strong fluorescence increment of TGA capped CdS QDs induced by DA. The enhancement in the fluorescence of TGA protected CdS QDs in the presence of DA is due to the passivation of surface states of QDs by the amine group of DA. The proposed sensor showed linear range and limit of detection 3.94×10^{-7} - 4.67×10^{-8} M and 2.55×10^{-9} M respectively. TGA capped CdS QDs showed good selectivity for DA, over other structurally similar biologically important compounds. The developed fluorescence assay was employed for the selective and sensitive determination of DA in biological fluid (urine sample).

Table 7.1: Comparison with other fluorescence sensors for DA

Fluorescence probe	Linear range (M)	LOD (M)	Reference
AuNC@ BSA	1.00×10^{-5} - 1.00×10^{-6}	1.00×10^{-9}	338
Hg imprinted silica nanospheres	2.50×10^{-4} - 5.00×10^{-7}	1.70×10^{-9}	319
TGA –CdTe QDs	1.00×10^{-1} - 0.30×10^{-3}	6.00×10^{-3}	339
Carbon dots	0.50×10^{-3} - 0.10×10^{-3}	3.30×10^{-5}	340
Polydopamine nanoparticles	2.00×10^{-5} - 0.10×10^{-6}	4.00×10^{-8}	341
Adenosine capped CdSe/ZnS QDs	1.00×10^{-4} - 2.00×10^{-5}	2.93×10^{-8}	323
TGA-CdS QDs	3.94×10^{-7} - 46.7×10^{-8}	2.55×10^{-9}	Proposed method

Table 7.2: Effect of foreign species on the determination of DA (4.67×10^{-7} M)

Foreign Species	Concentration (M)	Signal change %
L-DOPA	4.67×10^{-5}	0.41
Catechol	4.67×10^{-5}	0.82
Ascorbic acid	4.67×10^{-5}	0.41
Uric acid	4.67×10^{-5}	2.47
Epinephrine	4.67×10^{-5}	0.62
Creatinine	2.23×10^{-5}	2.88
Nor epinephrine	4.67×10^{-5}	1.65

Table 7.3: Determination of DA in urine sample

Added (M)	Proposed method			HPLC method		
	Found (M)*	RSD	Recovery %	Found (M)*	RSD	Recovery %
9.09×10^{-8}	9.19×10^{-8}	0.06	101.2	9.12×10^{-8}	0.05	100.3
2.59×10^{-7}	2.61×10^{-7}	0.04	100.8	2.56×10^{-7}	0.07	98.8
2.10×10^{-7}	2.07×10^{-7}	0.07	98.6	2.16×10^{-7}	0.11	102.9

*average of five replicate measurements

…..ஜ۞ஜ…..

Chapter 8

GOLD NANOCLUSTER BASED FLUORESCENCE SENSOR FOR NOREPINEPHRINE

Contents

This chapter describes the application of protein stabilized gold nanoclusters (AuNCs) as the fluorescent probe for the determination of norepinephrine (NE). The aqueous solution of the bovine serum albumin protected AuNCs was deep brown in color under visible light and exhibited bright-red fluorescence under UV irradiation. Upon addition of NE, the fluorescence emission intensity of AuNCs increased remarkably, which can be attributed to the restricted intramolecular rotation resulting from the aggregation of AuNCs. Under optimum conditions, the relative fluorescence intensity, I/I_0 showed a linear relationship with the concentration of NE in the range 4.76×10^{-7} M to 4.98×10^{-8} M, and the limit of detection was found to be 8.55×10^{-9} M. The proposed method was applied for the determination of NE in urine sample and the results were compared with HPLC method.

8.1 Introduction

Norepinephrine (NE) otherwise known as noradrinaline (Figure 8.1), is one of the most important catecholamine neurotransmitter in the mammalian central nervous system, whose structure is closely related to dopamine. It is the major chemical messenger of the sympathetic nervous system. Many automatic functions of the body, such as heart rate and blood pressure are controlled by the sympathetic nervous system. NE is an endogenous hormone secreted by the adrenal medulla, and relinquished as a neurotransmitter from nerve endings in the sympathetic nervous system and some areas of the cerebral cortex.[351]

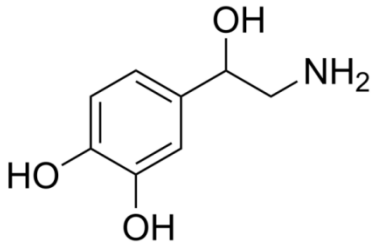

Figure 8.1: Structure of NE

NE has crucial role in muscle and tissue control. It decreases peripheral circulation, stimulates arteriole contraction and activates lipolysis in adipose tissue.[352] The low level of NE is related with mental depression, DNA breakage in cardiac myoblast cells, heart failure, and diabetes. Recent studies revealed that abnormal level of NE enhances adhesion of human immune deficiency virus-1 (HIV-1)-infected leukocytes to cardiac microvascular endothelial cells and also accelerates HIV replication via proteinkinase.[353,354] NE is one of the stimulants that have been prohibited in 2005 by World Anti-Doping Agency.[355] Hence the development of a sensitive and convenient method for quantitative determination of NE in biological fluids is of great significance

in clinical medicine, since it provides useful information on physiological functions and the diagnosis of some diseases.

Various analytical methods such as spectrophotometry,[355] capillary electrophoresis,[356] gas chromatography,[357] ion chromatography,[358] high-performance liquid chromatography (HPLC)[359] and voltammetric methods[360] have been employed for the determination of NE. Nevertheless, most of these techniques have several inconveniences. Since NE being an electroactive compound, the commonly used method for its determination is voltammetric techniques. But the main problem related to voltammetric method is the interference from the associated compounds such as uric acid and ascorbic acid, which usually results in overlapping of signals due to their very similar oxidation peak potentials.[361,362] The requirement of sample treatment with ion pair reagents makes GC-MS method tedious and time consuming. HPLC based methods have several draw backs since they normally require a previous extraction and purification of the sample.[363,364] Fluorescence has proved to be a more powerful optical technique for the detection of low concentration of analytes, owing to its simplicity and excellent selectivity.[365]

Recent advances in nanotechnology have given rise to a new class of fluorescent materials namelymetal nanoclusters (NCs), which consist of several to hundred atoms and exhibit molecule like properties. As the density of states is insufficient to merge the valence and conduction bands, NCs show molecule like transitions.[366,367] These materials emerged as a hot area of research since they provide the missing link between atomic and nanoparticle behaviour in metals.[368] They exhibit remarkable properties including the discrete electronic states and size-dependent fluorescence.[369]

Among the various metal NCs, AuNCs have attracted significant attention in sensing and imaging applications due to their biocompatibility and strong fluorescence.[370] Fluorescent AuNCs possesses special features such as strong photoluminescence, good photostability, high emission rates, large stokes shift and size-dependent tunable fluorescence.[371,372] Compared to other fluorophores such as semiconductor nanoparticles, carbon nanodots and dye doped nanoparticles, AuNCs have many advantages like simplicity in preparation, good water solubility, biocompatibility and low toxicity.[373]

The surface modification of AuNCs endows a number of new applications for them like targeting, imaging and therapeutic effects. The stabilizing or capping ligand has a profound role on the photoluminescence of AuNCs.[374,375] In recent years, many proteins such as bovine serum albumin (BSA), human serum albumin (HSA), lyzozyme, trypsin, pepsin and insulin have been used as protecting agents for the preparation of fluorescent AuNCs, since they contain active sites for metal ion accumulation and reduction.[145,146,376-378]

AuNCs based fluorescence sensor has been designed for monitoring of NE in body fluids, since it can be used as a powerful indicator for an early warning sign of certain diseases. Fluorescent AuNCs were synthesized using BSA as reducing and capping agent[110] and employed as a novel platform for simple and sensitive determination of NE. The fluorescence intensity of AuNCs increased with increasing concentration of NE and the limit of detection was found to be 8.55×10^{-9} M. The mechanism of fluorescence enhancement of AuNCs by the addition of NE is discussed. Application study of the developed sensor has been carried out in urine sample and results are validated with HPLC method.

8.2 Experimental

8.2.1 Synthesis of BSA stabilized AuNCs

Highly fluorescent BSA protected AuNCs were synthesized by the method[284] explained in section in 6.2.1 in chapter 6.

8.2.2 Sample preparation

A stock solution of NE (1.00×10^{-2} M) was prepared by dissolving 0.169 g NE in 10 mL water and desired concentrations were prepared by the serial dilution of stock solution using water.

8.2.3 Analytical procedure

AuNCs@BSA solution was mixed with phosphate buffer solution of pH 7 in the volume ratio 1:4. Appropriate amount of NE solution was added to 2 mL of the above solution, and the fluorescence emission spectrum was recorded. The luminescence intensity of AuNCs@BSA before and after the addition of NE was assigned as I_0 and I respectively.

8.3 Results and discussion

8.3.1 Characterization of AuNCs

The synthesized BSA protected AuNCs were characterized by UV-Vis spectroscopy, fluorescence spectroscopy, FTIR spectroscopy and TEM as explained in chapter 6.

8.3.2 Fluorescence enhancement of AuNCs by NE

Upon excitation at 400 nm, the photoluminescence spectrum of AuNCs@BSA showed an emission maximum at 653 nm. The fluorescence

intensity of AuNCs were strongly enhanced upon the addition of NE (Figure 8.2), and the enhancement of fluorescence intensity at 653 nm was proportional to the concentration of NE. Emission spectra of AuNCs@BSA displayed a slightly red shifted emission peak at 666 nm instead of 653 nm in the presence of NE. The observed red shift in the fluorescence emission wavelength of AuNCs is about 13 nm, which indicate the changes in the surface states of AuNCs@BSA arising from the interaction of NE molecules. Based on the fluorescence enhancement of AuNCs by NE, a novel turn on sensor was developed for the quantification of this neurotransmitter.

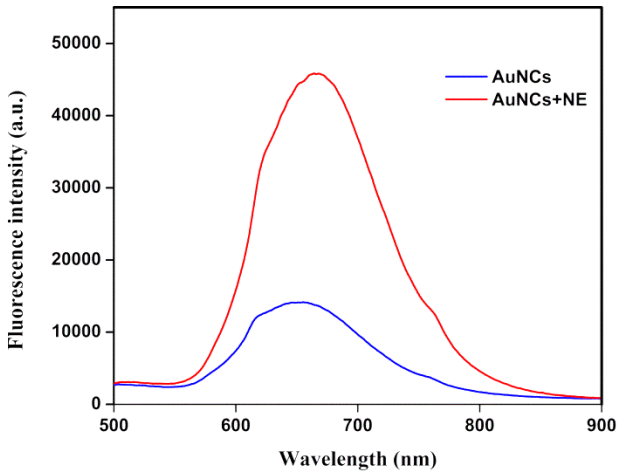

Figure 8.2: Fluorescence spectra of AuNCs before and after the addition of NE

8.3.3 Effect of buffer solutions

NE induced fluorescence enhancement of AuNCs was studied in various types of buffer solutions, such as phosphate buffer, acetate buffer and citrate buffer solutions. Maximum relative fluorescence intensity, I/I_0 for NE-AuNCs system was observed in phosphate buffer solution, indicating that phosphate buffer solution was preferable for the interaction between NE

and BSA stabilized AuNCs. Hence, phosphate buffer solution (PBS) was chosen for the subsequent studies.

In addition, the influence of the volume of buffer solution on the fluorescence intensity of NE-AuNC system was also examined. Five different volume ratios were studied and the maximum I/I_o valuewas obtained when the ratio of AuNCs and PBS was 1:4 (Figure 8.3).

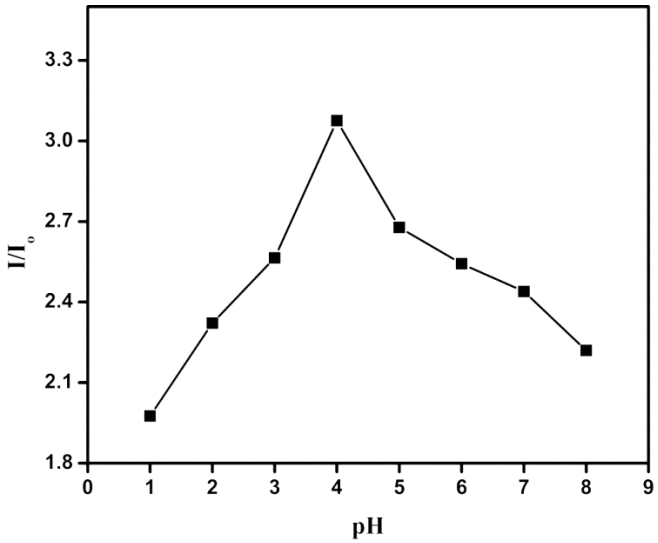

Figure 8.3: Effect of volume of PBS on the fluorescence enhancement of AuNCs by NE

8.3.4 Effect of pH

pH value of the system played a crucial role in the sensing of NE by AuNCs. In order to study the effect of pH on the relative fluorescence intensity of NE-AuNCs system, PBS with different pH values (2 to 9) wereemployed (Figure 8.4a). Maximum I/I_0 value was obtained at pH 7 (Figure 8.4b) and it was selected as optimal pH for further studies.

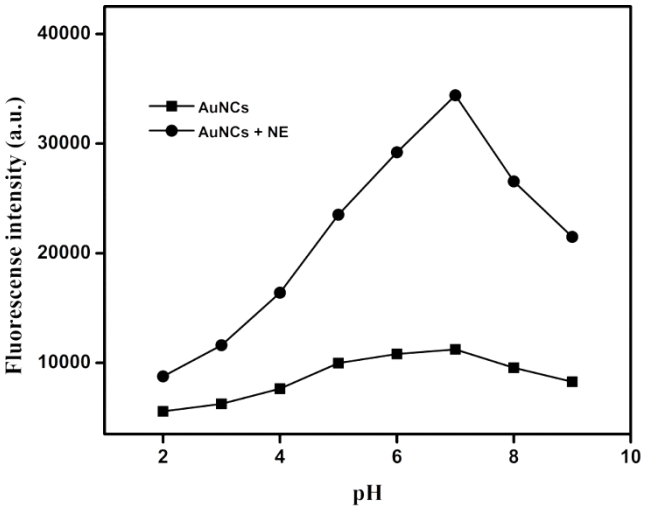

Figure 8.4a: Effect of pH of PBS on the fluorescence intensity of AuNCs and AuNCs in the presence of NE

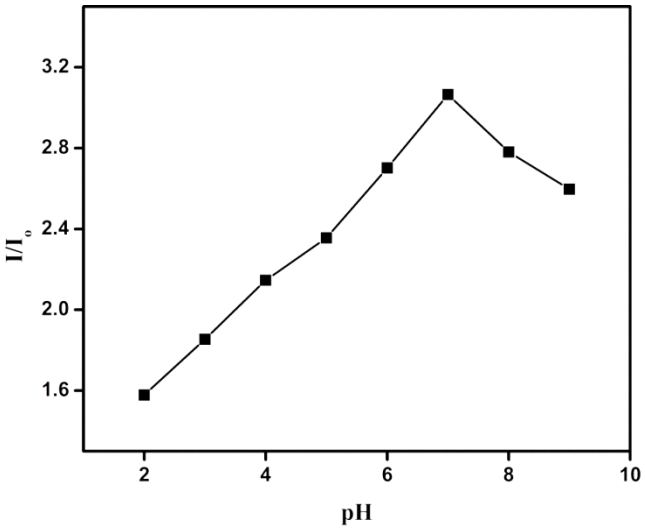

Figure 8.4b: Effect of pH of PBS on the fluorescence enhancement of AuNCs by NE

8.3.5 Effect of Time

To investigate the kinetic stability of the developed assay, fluorescence intensity of AuNCs before and after the addition of different concentrations

of NE was recorded at different time intervals (Figure 8.5). It was observed that the interaction between NE and AuNCs was rapid and fluorescence intensity reached maximum immediately after mixing. The emission intensity remains almost constant at least for about 35 min indicating the high stability of the assay.

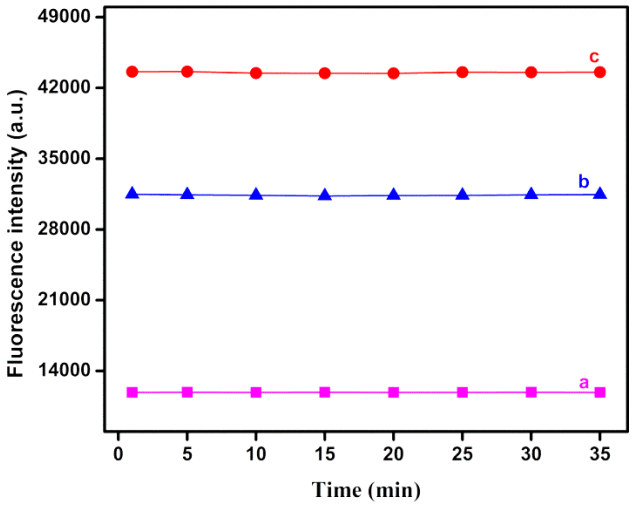

Figure 8.5: Effect of time on the fluorescence intensity of (a) AuNCs (b) AuNCs + 1.48 × 10^{-7} M NE (c) AuNCs + 4.31 × 10^{-7} M NE

8.3.6 Concentration study

The luminescence intensity of AuNCs increased gradually with increasing concentrations of NE (Figure 8.6a). The relative fluorescence intensity, I/I_0 was plotted as a function of concentration of NE (Figure 8.6b). A good linear relationship between I/I_0 and concentration of NE was obtained over the range of 4.76 × 10^{-7}M to 4.98 × 10^{-8} M, with a detection limit of 8.55× 10^{-9}M. The concentration dependence of relative fluorescence intensity follows the equation $^{I}/_{I_0} = 2.539C(\mu M) + 1.854,\ R^2 = 0.977.$

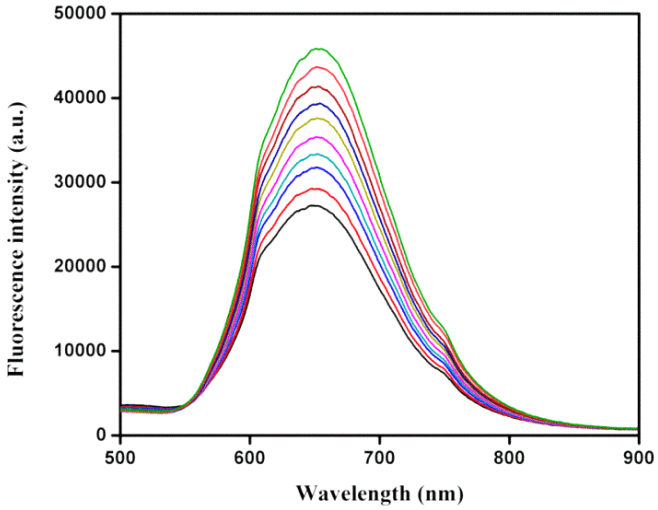

Figure 8.6a: Fluorescence spectra of AuNCs in the presence of various concentrations of NE

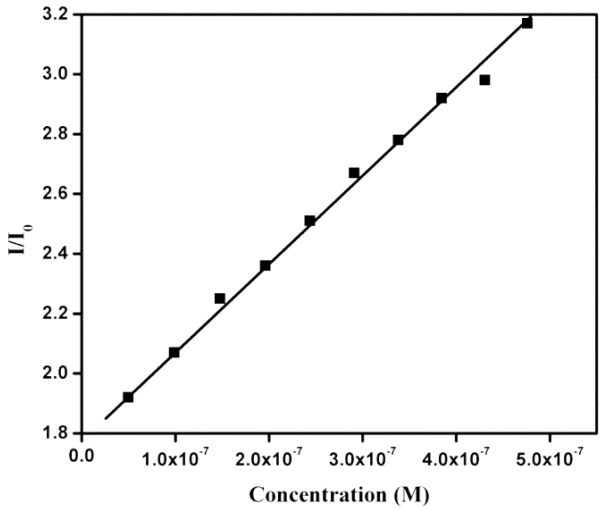

Figure 8.6b: Calibration curve for NE in the concentration range 4.76×10^{-7} - 4.97×10^{-8} M

A comparison between other determination methods of NE and proposed method is shown in Table 8.1. As listed in table, the proposed assay is found to be superior in terms of lower limit of detection to that of the other quantification methods for NE. To study the precision of the developed

method, a series of 6 repetitive measurements were taken, and a RSD of 2.7 % was obtained, suggesting the good repeatability of the proposed method.

8.3.7 Mechanism

The luminescence observed in the AuNCs is attributed to the excitation of electrons into the *sp*-conduction band and subsequent radiative electron-hole recombination process.[102] Gold colloids are a highly dispersed multiphase system with a distinct interfacial region which has an affinity to adsorb other substances to decrease the interfacial energy.[379]

To study the interaction between NE and AuNCs@BSA UV-Vis absorption spectra and fluorescence spectra of nanoclusters were recorded before and after the addition of NE. Upon the addition of NE, the absorbance of AuNCs@BSA was decreased significantly (Figure 8.7) suggesting the surface state changes of AuNCs@BSA. Fluorescence spectra of AuNCs@BSA displayed a slightly red shifted emission peak at 666 nm instead of 653 nm in the presence of NE. The red shift and the enhancement of intensity of fluorescence emission peak of AuNCs by NE may be due to the interaction of NE either to the capping molecule (BSA) or the AuNCs core which led to the aggregation of AuNCs. The electron rich amine groups of NE have a strong charge transfer interaction with the aromatic nucleus of BSA on the surface of AuNCs.[380] Also it was reported that electron-rich atoms (O, N) or functional groups can effectively enhance fluorescence via surface interactions.[381] NE contains electron rich $–NH_2$ and -OH groups which can interact with AuNCs, thereby enhancing of luminescence intensity of BSA protected AuNCs.

Such type of interactions decrease the interparticle distance between nanoclusters and causes aggregation. From TEM analysis it was confirmed that aggregation occurred for nanoclusters after the addition of NE (Figure 8.8).

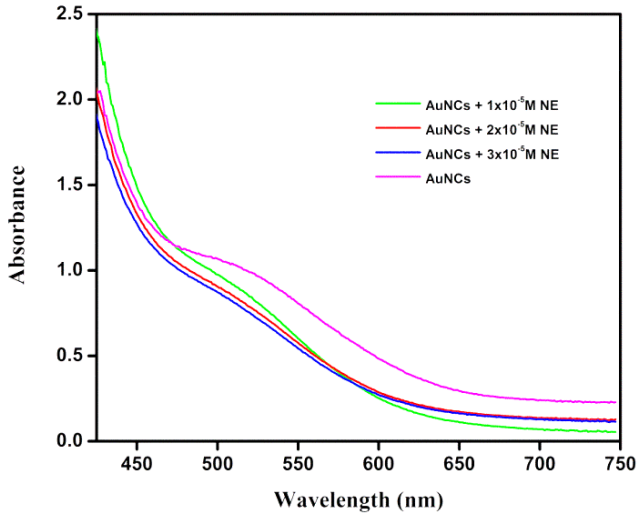

Figure 8.7: UV-Vis absorption spectra of AuNCs in the presence of different concentrations of NE

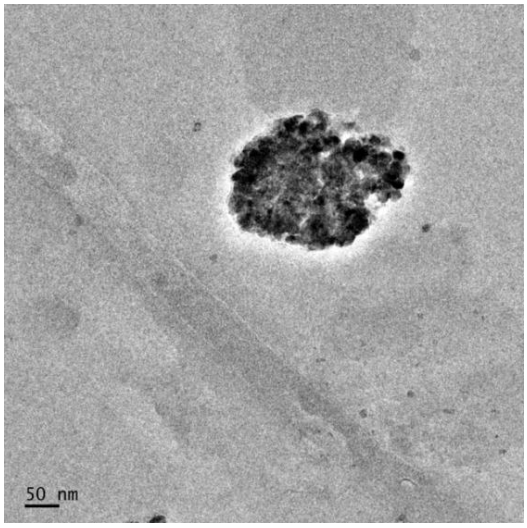

Figure 8.8: TEM image of AuNCs after the addition of NE

Aggregation induced emission enhancement (AIEE) have attracted more attention since 2001 when Tang's group first reported that the luminescence of silose molecules was stronger in the aggregate state than that in the non-aggregated form.[382-384] Restriction of intramolecular rotation and the prohibition of non radiative deactivation are the major causes of AIE effect.[385]

Due to the large diameter of the AuNCs-NE aggregates, their vibration and rotation speed may decrease. The Brownian motion and collision probability also may be weakened which result in an increase of external energy transfer rate.[386] When large diameter AuNCs-NE aggregates are formed, self-absorption decreased considerably, due to the increasing degree of conjugation [387] (Figure 8.7). Because of the physical constraint in the aggregates, intramolecular rotations are restricted and new radiative decay channels are opened, that is electron-hole recombination increases.[388] The above reasons might have led to the enhancement of fluorescence intensity of AuNCs.

FTIR spectra of AuNCs and AuNCs in the presence of NE are shown in Figure 8.9. From Figure 8.9 it is clear that in the presence of NE, there is a shift in the –OH stretching vibration frequency accompanied by an increase in intensity, which indicates improved H bonding in the presence of NE, resulting in the aggregation of AuNCs.

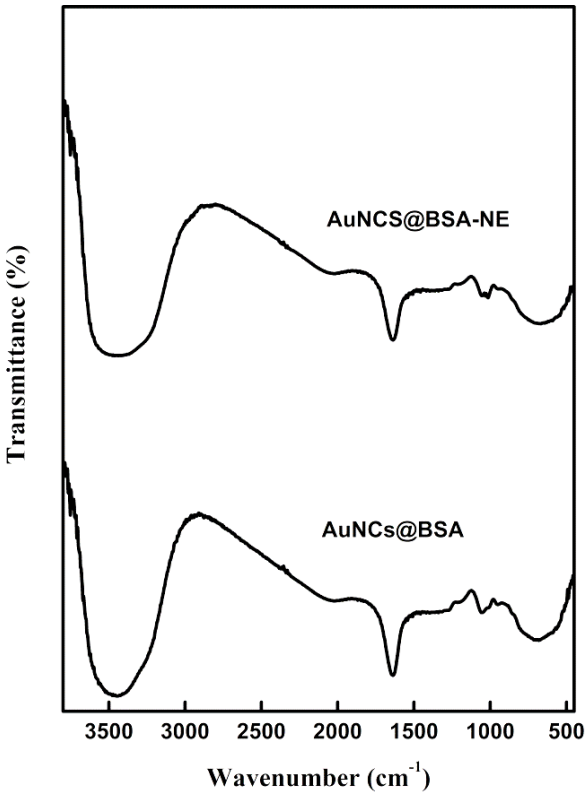

Figure 8.9: FTIR spectra of AuNCs before and after the addition of NE

8.3.8 Selectivity

In order to study the selectivity of the protein stabilized fluorescent probe towards NE, the emission intensity of AuNCs@BSA was measured in the presence of 4.76×10^{-7} M concentration of biologically important substances such as NE, epinephrine, creatinine, 3,4-dihyroxy phenylalanine, uric acid and ascorbic acid. As shown in Figure 8.10a only NE induced a dramatic increase in the fluorescence intensity of AuNCs, whereas no obvious fluorescence changes were observed in the presence of other species. This revealed the selectivity of the AuNC based fluorescent probe towards the determination of NE.

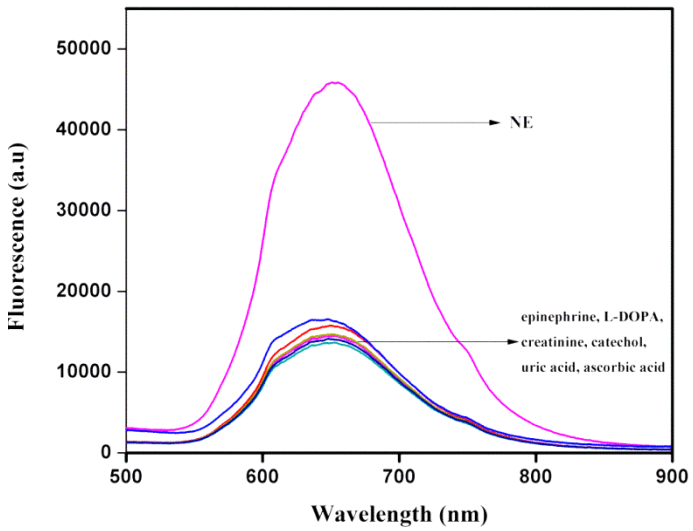

Figure 8.10a: Selectivity of the sensor: Fluorescence emission changes of AuNCs in the presence of other biologically important substances

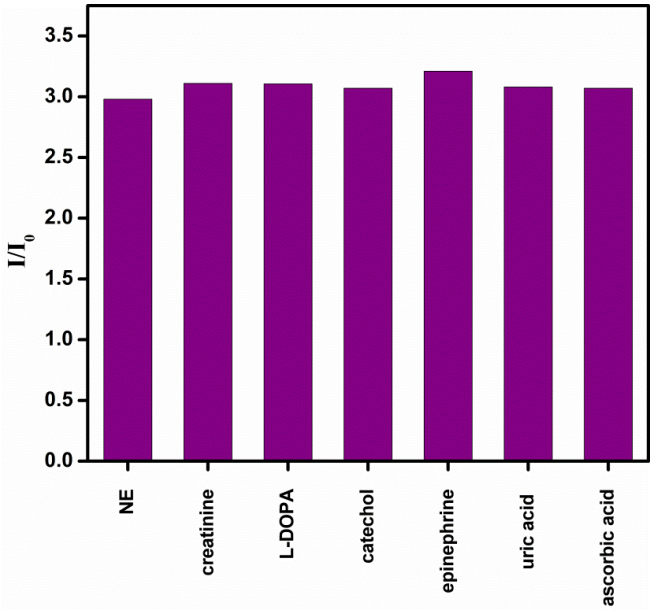

Figure 8.10b: Fluorescence behaviour of AuNCs in the presence of 4.76×10^{-7} M NE with the coexistence of other substances at 100 fold excess concentrations

Additionally, the fluorescence intensity of AuNCs was measured in the presence of NE (4.31×10^{-7} M) and various concentrations (1:1, 1:10 and 1:100) of the above mentioned foreign species. All the compounds tested except epinephrine did not interfere the determination of NE, and they can be tolerated up to 100 fold molar excess concentrations (Figure 8.10b). Epinephrine, when present at a concentration greater than 40 fold of NE, a signal change above 5% was observed and interfere the determination of NE severely (Table 8.2).

8.3.9 Application study

The practical application of the developed assay for the analysis of NE was tested by spiking the urine sample with a known amount of standard NE solutions and determining its recovery. The results were summarized in Table 8.3. Recoveries were obtained from 99% to 102%, which showed the reliability of the present method. A good agreement was observed between proposed method and HPLC method,[351] indicating that the present method can be used for the determination of NE in real samples. These results demonstrated that this novel sensing system has great potential for quantitative analysis of NE levels in urine samples.

8.4 Conclusions

A simple of fluorescent platform was developed for the sensing of NE based on the fluorescence enhancement of BSA templated AuNCs. Hydrogen bonding induced aggregation and the resulting restricted rotation of AuNCs was responsible for the observed fluorescence enhancement of nanoclusters in the presence of NE. Clear evidence for the aggregation of

AuNCs by the addition of NE was obtained from HRTEM analysis. The AuNCs based sensing system exhibited a very low limit of detection as low as 8.55×10^{-9} M. The developed turn on fluorescence sensor is simple, sensitive and was applied for the real sample analysis with satisfactory results.

Table 8.1: Comparison with other determination methods for NE

Method	Linear range (M)	LOD (M)	Reference
Spectrophotometry	1.18×10^{-4} to 5.91×10^{-6}	----------	355
Caplillary electrophoresis	1.00×10^{-4} to 1.00×10^{-6}	0.85×10^{-6}	356
Ion chromatography	0.295×10^{-4} to 5.91×10^{-8}	5.91×10^{-9}	358
HPLC-MS	2.36×10^{-5} to 5.91×10^{-6}	5.67×10^{-8}	359
Voltammetry	7.55×10^{-6} to 8.49×10^{-7}	5.91×10^{-8}	360
Fluorescence	4.76×10^{-7} to 4.98×10^{-8}	8.55×10^{-9}	Proposed method

Table 8.2: Effect of foreign species on the determination of NE (4.31×10^{-7} M)

Foreign Species	Concentration (M)	Signal change %
L-DOPA	4.31×10^{-5}	4.23
Catechol	4.31×10^{-5}	3.22
Ascorbic acid	4.31×10^{-5}	3.12
Uric acid	4.31×10^{-5}	3.45
Epinephrine	1.72×10^{-5}	4.53
Creatinine	4.31×10^{-5}	4.32

L-DOPA: 3,4-dihydroxyphenylalanine

Table 8.3: Determination of NE in urine sample

Added (M)	Proposed method			HPLC method		
	Found (M) *	RSD	Recovery %	Found (M) *	RSD	Recovery %
9.90×10^{-8}	9.91×10^{-8}	0.07	100.1	9.99×10^{-8}	0.04	100.9
2.44×10^{-7}	2.47×10^{-7}	0.09	101.2	2.38×10^{-7}	0.07	97.5
4.31×10^{-7}	4.29×10^{-7}	0.03	99.5	4.36×10^{-7}	0.11	101.2

*average of five replicate measurements

Chapter 9

SUMMARY AND FUTURE OUTLOOK

Contents

The objectives of the present work, summary of the work done are presented in this chapter. Future outlook is also discussed.

9.1 Objectives of the work

1) Preparation of chemically modified electrodes (CMEs) using nanomaterials and conducting polymers.

2) Characterization of CMEs using scanning electrochemical microscopy, electrochemical impedance spectroscopy and cyclic voltammetry (surface area calculations).

3) Development of electrochemical sensors for the quantification of food additives based on the above prepared CMEs.

4) Optimization of various experimental conditions for sensor fabrication.

5) Extraction of kinetic parameters of the electrode processes using voltammetric techniques.

6) Determination of analytical figures of merit of the fabricated voltammetric sensors.

7) Prediction of a plausible mechanism for the electro-oxidation of food additives.

8) Carry out the application studies in spiked food samples and validating the results with existing method.

9) Synthesis of nanostructured fluorescent probes such as gold nanoclusters (AuNCs) and CdS quantum dots.

10) Characterization of the synthesized fluorophores by transmission electron microscopy, UV-Vis absorption spectroscopy and fluorescence spectroscopy.

11) Determination of quantum yield of synthesized fluorophores.

12) Development of fluorescent sensors based on the above fluorophores for food additives and neurotransmitters.

13) Determination of analytical figures of merit of the developed fluorescent sensors.

14) Study of fluorescence enhancement mechanism based on the interaction between the fluorophore and analyte.

15) Carry out the application studies in spiked real samples and validating the results with existing method.

9.2 Summary of the work done

A total of seven sensors including four electrochemical sensors and three fluorescence sensors have been developed for food additives and neurotransmitters. The salient features of the sensors are compiled in Table 9.1.

Table 9.1: Details of the sensors developed

Sl. No	Type of sensor developed	Sensing probe	Linear range (M)	LOD (M)	Analyte
1	Electro chemical Sensor	MWCNT/GE	1.00×10^{-4} - 1.00×10^{-5}	6.30×10^{-7}	Propyl gallate
2		Poly (L-cys)/GCE	3.00×10^{-6} - 1.00×10^{-7}	3.61×10^{-9}	Allura red
3		AuNP/GCE	1.00×10^{-4} - 1.00×10^{-5}	7.06×10^{-7}	Sunset yellow
4		MWCNT/ AuNP/GCE	1.00×10^{-5} - 1.00×10^{-6}	4.03×10^{-8}	Sunset yellow
5	Fluorescence Sensor	AuNCs@BSA	4.31×10^{-6} - 4.98×10^{-7} 4.76×10^{-8} - 4.98×10^{-9}	8.99×10^{-10}	Butylated hydroxyanisole
6		TGA-CdS QDs	3.94×10^{-7} - 4.67×10^{-8}	2.55×10^{-9}	Dopamine
7		AuNCs@BSA	4.98×10^{-7} - 4.76×10^{-8}	8.55×10^{-9}	Norepinephrine

9.3 Future outlook

The demand for highly selective and sensitive sensing systems has increased greatly due to their emerging applications in clinical diagnostics, food quality control, environmental monitoring and drug delivery. Research

is progressing in these fields for the development of viable sensors. Even the commercialized sensors need to be improved in terms of sensitivity and stability over time.

Higher-order or orthogonal sensors and chemical sensing arrays are the recent trends in chemical sensors which have numerous future applications. Higher order indicates that more than one transduction principle is applied to the recognition layer. For example, an electrochemical sensor can be simultaneously interrogated optically thus producing orthogonal signatures of the analyte, which provides additional dimension for sensing. The increase in the order of the sensor is expected to improve the sensitivity and selectivity of the analysis. On the other hand, an array of different receptor layers with same transduction principle forms a sensor array of zero order.

A detailed understanding of the sensor – analyte interaction and investigation of the effect of physical variables such as humidity, temperature and pressure on the response of sensor will possibly lead to better performing chemical sensors for a wide variety of applications.

.....ꕥ.....

References

[1] K. Balasubramanian, M. Burghard, *Anal. Bioanal. Chem.*, **385**, 452 (2006).

[2] R.W. Cattrall, *Chemical Sensors*, *Oxford University Press Inc.*, New York, 2 (1997).

[3] J.A. Plambeck, *Electranalytical Chemistry: Basic Principles and Applications*, John Wiley and Sons Inc. New York, 66 (1982).

[4] K.Z. Brainina, E. Neyman, *Electroanalytical Stripping Methods*, J. Wiley and Sons, USA, 12 (1993).

[5] J. Wang, *Analytical Electrochemistry*, Wiley-VCH, USA, 107 (2000).

[6] J.L. Hardcastle, G.G. Murcot, R.G. Compton, *Electroanal.*, **12**, 559 (2000).

[7] J.C. Bokros, *Carbon*, **15**, 355 (1977).

[8] R.N. Adams, *Electrochemistry at Solid Electrodes*, Marcel Dekker, Inc., New York, 34 (1969).

[9] J.A. Plambeck, *Electranalytical Chemistry: Basic Principles and Applications*, John Wiley and Sons Inc. New York, 67 (1982).

[10] C. Zhong, M.D. Porter, *Anal. Chem*., **67**, 709A (1995).

[11] J.A. Plambeck, *Electranalytical Chemistry: Basic Principles and Applications*, John Wiley and Sons Inc. New York, 69 (1982).

[12] R.W. Murray, *Acc. Chem. Res*., **13**, 135 (1980).

[13] D.C. Tiwari, R. Jain and S. Sharma. *J. Sci. Ind. Res.*, **66**, 1011 (2007).

[14] K.D. Snell, A.G. Keenan, *Chem. Soc. Rev*., **8**, 259 (1979).

[15] J.M. Zen, A.S. Kumar, D.M. Tsai, *Electroanal.*, **15**, 1073 (2003).

[16] A.J. Downard, *Electroanal.*, **12**, 1085 (2000).

[17] R.A. Durst, A.J. Baumner, R.W. Murray, R.P. Buck, C.P. Andrieux, *Pure & Appl. Chem*., **69**, 1317 (1997).

[18] M. Elrouby, *J. Nano. Adv. Mat.*, **1**, 23 (2013).

[19] C.E. Banks, R.R. Moore, T.J. Davies, R.G. Compton, *Chem. Commun*., **6**, 1804 (2004).

[20] G.A. Rivas, M.D. Rubianes, M.C. Rodriguez, N.F. Ferreyra, G.L. Luque, M.L. Pedano, S.A. Miscoria, C. Parrado, *Talanta*, **74**, 291 (2007).

[21] C.E. Banks, R.G. Compton, *Analyst*, **131**, 15 (2006).

[22] R. Hirlekar, M. Yamagar, H. Garse, M. Viji, V. Kadam, *Asian J. Pharm. Clin. Res*., **2**, 17, (2009).

[23] P.J. Britto, K.S.V. Santhanam, V. Alonso, A. Rubio, P.M. Ajayan, *Adv. Mater*., **11**, 154, (1999).

[24] B.A. Bolto, R. McNeill, D.E. Weiss, *Aust. J. Chem*., **16**, 1090 (1963).

[25] C. Peng, S. Zhang, D. Jewell, G.Z. Chen, *Prog. Nat. Sci*., **18**, 777 (2008).

[26] C.M.A. Brett, G. Inzelt, V. Kertesz, *Anal. Chim. Acta,* **385,** 119 (1999).

[27] L. Xu, W. Chen, A. Mulchandani, Y. Yan, *Angew. Chem. Int. Ed.*, **44,** 6009 (2005).

[28] G.Y. Jin, Y.Z. Zhang, W.X. Cheng, *Sens. Actuat. B*, **107,** 528 (2005).

[29] A. Malinauskas, *Synth. Met.*, **107,** 75 (1999).

[30] D.T. McQuade, A.E. Pullen, T.M. Swager, *Chem. Rev*., **100,** 2537(2000).

[31] U. Lange, N.V. Roznyatovskaya, V.M. Mirsky, *Anal. Chim. Acta,* **614,** 1 (2008).

[32] S.K. Padigi, R.K.K. Reddy, S. Prasad. *Biosens. Bioelectron*., **22**, 829 (2007)

[33] M. Pandiaraj, T. Madasamy, P.N. Gollavilli, M. Balamurugan, S. Kotamraju, V.K. Rao, K. Bhargava, C. Karunakaran, *Bioelectrochemistry*, **91,** 1 (2013).

[34] J. Wang, *Analyst*, **130**, 421 (2005).

[35] R.Y. Zhang, H. Olin, *Int. J. Biomedical Nanoscience and Nanotechnology*, **2**, 112 *(*2011).

[36] J. Turkevich, P.C. Stevenson, J. Hillier, *Discuss. Faraday Soc*., **11**, 55 (1951).

[37] G. Frens, *Nature Phys. Sci*., **241**, 20 (1973).

[38] A.R. Raj, T. Okajima, T. Ohasaka, *J. Electrochem*., **543**, 127 (2003).

[39] R.M. Penner, C.R. Martin, *Anal. Chem*., **59**, 2625 (1987).

[40] H. Diehl, R.W.V. Haar, R.R. Sealock, *J. Am. Chem. Soc.*, **72**, 5312 (1950).

[41] J. Wang, *Analytical Electrochemistry*, Wiley-VCH, USA, 68 (2000).

[42] J. Osteryoung, J.J. Odea, *Electroanalytical Chemistry*, Marcel Dekker, New York, 209 (1986).

[43] A.J. Bard, L. R. Faulkner, *Electrochemical Methods: Fundamentals and Applications*, Wiley, 227 (2000).

[44] D. Vall, S. DuVall, M.C. Richard, *Anal. Chem.,* **71**, 4594 (1999).

[45] https://en.wikipedia.org/wiki/Cyclic_voltammetry

[46] T. Jose, *Square Wave Voltammetric Determination of Various Pharmaceuticals*, CUSAT, 6 (2015).

[47] G.N. Schrauzer, E. Deutsch, R.J. Windgassen, *J. Am. Chem. Soc.*, **90**, 2441 (1968).

[48] C.M.A. Brett, A.M.O. Brett, *Electroanalysis*, Oxford Science Publications, New York, 19 (1998).

[49] P. Delahay, *Double Layer and Electrode Kinetics*, Wiley-Interscience, New York, **137** (1965).

[50] D.D. Macdonald, *Electrochim. Acta*, **51**, 1376 (2006).

[51] http://www.gamry.com/application-notes/EIS/basics-of-electrochemical-impedance-spectroscopy/

[52] K. Peter; W.R. Heineman, *Laboratory Techniques in Electroanalytical Chemistry* Marcel Dekker, New York, 60 (1996).

[53] A.J. Bard, L.R. Faulkner, *Electrochemical Methods: Fundamentals and Applications*, Wiley, 12 (2000).

[54] G.C. Zoski, *Handbook of Electrochemistry*. Elsevier Science, 2 (2007).

[55] Z. Rasheed, A.E. Vikraman, D. Thomas, J.S. Jagan, K. Girish Kumar, *Food Anal. Methods*, **8**, 213 (2014).

[56] S. Chandran, L.A. Lonappan, D. Thomas, T. Jos, K. Girish Kumar, *Food Anal. Methods*, **7**, 741 (2014).

[57] N. Moheimanian, J.B. Raoof, A. Safavi, R. Ojani, *J. iran chem. Soc*., **11**, 1217 (2014).

[58] M. Wu, W. Tang, J. Gu, Q. Wang, P. He, Y. Fang, *Am. J. Anal. Chem*., **4**, 1 (2013).

[59] A. Bathinapatla, S. Kanchi, P. Singh, M.I. Sabela, K. Bisetty, *Biosens. Bioelectron*., **67**, 200 (2015).

[60] R.P. Caramit, A.G.F. Andrade, J.B.G. Souza, T.A. Araujo, L.H. Viana, M.A.G. Trindade, V.S. Ferreira, *Fuel*, **105**, 306 (2013).

[61] A. Thomas, A.E. Vikraman, D. Thomas, K. Girish Kumar, *Food. Anal. Methods*, **8**, 2028 (2015).

[62] W. Zhang, T. Liu, X. Zheng, W. Huang, C. Wan, *Colloid Surface B*, **74**, 28 (2009).

[63] Y. Zhang, X. Zhang, X. Lu, J. Yang, K. Wu, *Food Chem*., **122**, 909 (2010).

[64] P. Wang, X. Hu, Q. Cheng, X. Zhao, X. Fu, K. Wu. *J. Agri. Food Chem.*, **58**, 12112 (2010).

[65] G. Ziyatdinova, A. Gainetdinova, M. Morozov, H. Budnikov, S. Grazhulene, A. Red'kin, *J. Solid State Electrochem.*, **16**, 127 (2012).

[66] M.L.S. Silva, M.B.Q. Garcia, J.L.F.C. Lima, E. Barrado, *Talanta*, **72**, 282 (2007).

[67] K. Zhang, P. Luo, J. Wu, W. Wang, B. Ye, *Anal. Methods*, **5**, 5044, (2013).

[68] M.A. Xinying, *Int. J. Electrochem. Sci.*, **9**, 3181 (2014).

[69] X. Zhengz, D. Zhou, D. Xiang, W. Huang, S. *Russ. J. Electrochem*., **45**, 1183 (2009).

[70] X. Ma, M. Chao, *Russ. J. Electrochem.*, **49**, 1057, (2013).

[71] B. Unnikrishnan, P.L. Ru, S. M. Chen, V. Mani, *Sens. Actuators B*, **117**, 887, (2013).

[72] D. Thomas, Z. Rasheed, J.S. Jagan, K. Girish Kumar, *J. Food Sci. Technol*., (2015-In press).

[73] L.I. Jing, *Chin. J. Chem*., **27**, 2373 (2009).

[74] J. Qu, Y. Dong, Y. Wang, H. Xing, *Sensing and Bio-Sensing Research*, **3**, 74 (2015).

[75] S.M. Ghoreishi, M. Behpour, M. Golestaneh, *Food Chem*., **132**, 637 (2012).

[76] D. Thomas, A.E. Vikraman, T. Jos, K. Girish Kumar, *LWT-Food Sci.Technol.* (2015-In press).

[77] Y. Zhang, Y. Wang, *Am. J. Anal. Chem.*, **2**, 194 (2011).

[78] K. Li, X. Zhu, Y. Liang, *Pharmacol. Pharm.*, **3**, 275 (2012).

[79] S. Shahrokhiana, S. Rastgar, *Proceedings of the 4th International Conference on Nanostructures (ICNS4)*, Kish Island, I.R. Iran, 919 *(*2012).

[80] K.P. Carter, A.M. Young, A.E. Parmer, *Chem. Rev*., **114**, 4564 (2014).

[81] J.R. Albani, *Principles and Applications of Fluorescence Spectroscopy***,** Blackwell publishing, UK, 88 (2007).

[82] H.N. Kim, M.H. Lee, H.J. Kim, J.S. Kim, J. Yoon, *Chem. Soc. Rev*., **37**, 1465 (2008).

[83] https://en.wikipedia.org/wiki/Stokes_shift

[84] G. George, *Photochemical and Photophysical Studies of a few Bischromophoric Systems*, CUSAT, 144 (2010)

[85] http://en.wikipedia.org/wiki/Fluorescence-lifetime_imaging_microscopy

[86] J.R. Lakowicz, *Princiles of Fluorescence Spectroscopy*, Springer, Maryland, USA, 8 (2006).

[87] G. Grynkiewicz, M. Poenie, R.Y. Tsien, *J. Biol. Chem*., **260**, 3440 (1985).

[88] C.J. Murphy, *Anal. Chem.*, **74,** 520A (2002).

[89] J.R. Lakowicz, *Princiles of Fluorescence Spectroscopy*, Springer, Maryland, USA, 277 (2006).

[90] Z.X. Zhou, Y. Du, S.J. Dong, *Biosens. Bioelectron,*. **28**, 33 (2011).

[91] M. Cui, Y. Zhao, Q. Song, *TrAC Trends Anal. Chem*., **57**, 73 (2014).

[92] Z. Luo, K. Zheng, J. Xie, *Chem. Commun*., **50**, 5143(2014).

[93] L. Zhang, E. Wang, *Nano Today*, **9**, 132 (2014).

[94] B. Unnikrishnan, C.C. Huang, *Interactions of Nanomaterials with Emerging Environmental Contaminants*; ACS Symposium Series, 1150, Washington, 23, (2013).

[95] C. Zhou, S. Yang, J. Liu, M. Yu, J. Zheng, *Exp. Biol. Med.* 238, 1199 (2013).

[96] X. Huang, M. A. El-Sayed, *J. Adv. Res.*, **1**, 13 (2010).

[97] J.F. Hicks, A.C. Templeton, S. Chen, K.M. Sheran, R. Jasti, R.W. Murray, *Anal. Chem.*, **71**, 3703 (1999).

[98] X. Qu, Y. Li, L. Li, Y. Wang, J. Liang, J. Liang, *J. Nanopart.* (2015-In press).

[99] R. Jin, *Nanoscale*, 2, 343 (2010).

[100] W.L.; Barnes, A. Dereux, T. W. Ebbesen, *Nature*, **424**,824 (2003).

[101] A.P. Alivisatos, *Science*, **271**, 933 (1996).

[102] P. Apell, R. Monreal, S. Lundqvist, *Phys. Scr.*, **38**, 174 (1988).

[103] J. Zheng, P.R. Nicovich, R.M. Dickson, *Annu. Rev. Phys. Chem.*, **58**, 409 (2007).

[104] J. Li, J.J. Zhu, K. Xu, *Trends Anal. Chem.*, **58**, 90 (2014).

[105] Z. Wu, R. Jin, *Nano Lett.*, **10**, 2568 (2010).

[106] L.Y. Chen, C.W. Wang, Z. Yan, H.T. Chang, *Anal. Chem.*, **87**, 216 (2015).

[107] X. Wen , P. Yu , Y.R. Toh , A.C. Hsu , Y.C. Lee , J. Tang , *J. Phys. Chem. C,* **116** , 19032 (2012).

[108] P. Yu, X. Wen, Y.R. Toh, X. Ma, J. Tang, *Part. Part. Syst. Charact.*, **32,** 142 (2015).

[109] R. Hardman, *Environ. Health Perspect.*, **114**, 165, (2006).

[110] J. Xie, Y. Zheng, J.Y. Ying, *J. Am. Chem. Soc.*, **131**, 888 (2009).

[111] Y.H. Lin, W.L. Tseng, *Anal. Chem.*, **82**, 9194 (2010).

[112] F. Wen, Y. Dong, L. Feng, S. Wang, S. Zhang, X. Zhang, *Anal. Chem.*, **83**, 1193 (2011).

[113] P.L. Xavier, K. Chaudhari, P.K. Verma, S.K. Pal, T. Pradeep, *Nanoscale*, **2**, 2769 (2010).

[114] A.L. West, M.H. Griep, D.P. Cole, S.P. Karna, *Anal. Chem*., **86**, 7377 (2014).

[115] Y. Kong, J. Chen, F. Gao, R. Brydson, B. Johnson, G; Heath, Y. Zhang, L. Wu, D. Zhou, *Nanoscale*, **5**, 1009 (2013).

[116] P. Walter, E. Welcomme, P. Hallegot, N.J. Zaluzec, C. Deeb, J. Castaing, P. Veyssiere, R. Breniaux, J.L. Leveque, G. Tsoucaris, *Nano Lett.,* **6**, 2215 (2006).

[117] L. Brus, *J. Chem. Phys*., **79**, 5566 (1983).

[118] I.L. Medintz, H.T. Uyeda, E.R. Goldman, H. Mattoussi, *Nat. Mater.,* **4**, 435 (2005).

[119] M.Jr. Bruchez, M. Moronne, P. Gin, S. Weiss, A.P. Alivisatos, *Science*, **281**, 2013 (1998).

[120] W.C.W. Chan, S. Nie, *Science*, **281**, 2016 (1998).

[121] A. Maiti, S. Bhattacharyya, *Int. J. Chem. & Chem. Eng.*, **3**, 37 (2013).

[122] A. L. Efros, M. Rosen, *Annu. Rev. Mater. Sci*., **30**, 475 (2000).

[123] A. Henglein, B. Bunsenges. *Phys. Chem.*, **88**, 301 (1982).

[124] L. Spanhel, M. Haase, H. Weller, A. Henglein, *J. Am. Chem. Soc.*, **109,** 5649 (1987).

[125] C.J. Murphy, J. L. Coffer, *Appl. Spectrosc*., **56**, 16A (2002).

[126] S.K. Haram, B.M. Quinn, A.J. Bard, *J. Am. Chem. Soc.,* **123**, 8860 (2001).

[127] E. Kucur, W. Bucking, R.T. Giernoth, *J. Phys. Chem. B,* **109**, 20355 (2005).

[128] M.P. Fujii, Y. Yamaguchi, Y. Takase, K. Ninomiya, S. Hayashi, *Appl. Phys. Lett.*, **87**, 211919 (2005).

[129] Z. Chen, S. Qian, X. Chen, W. Gao, Y. Lin, *Analyst*, **137**, 4356 (2012).

[130] B. Aswathy, G. Sony, *Microchem. J.*, **116**, 151 (2014).

[131] H.W. Li, Y. Yue, T.Y. Liu, D. Li, Y. Wu, *J. Phys. Chem. C*, **117**, 16159 (2013).

[132] X. Chen, G. A. Baker, *Analyst*, **138**, 7299 (2013).

[133] X. Cao , H. Li , L. Lian, N. Xu , D. Lou , Y. Wu, *Anal. Chim. Acta*, **871**, 43 (2015).

[134] B. Hemmateenejad, F. Shakerizadeh-shirazi, F. Samari, *Sens. Actuators, B*, **199**, 42 (2014).

[135] J.M. Liu, M.L. Cui, S.L. Jiang, X.X. Wang, L.P. Lin, L. Jiao, L.H. Zhang, Z.Y. Zheng, *Anal. Methods***, 5**, 3942 (2013).

[136] Z. Chen, S. Qian, J. Chen, J. Cai, S. Wu, Z. Cai, *Talanta*, **94** 240 (2012).

[137] C.L. Zheng, Z.X. Ji, J.Zhang, S.N. Ding, *Analyst*, **139**, 3476 (2014).

[138] X. Yang , S. Zhu , Y. Dou, Y. Zhuo, Y. Luo, Y. Feng, *Talanta*, **122**, 36 (2014).

[139] Y. Xu, X. Yang, S. Zhu, Y. Dou. *Colloid. Surf. A*, **450**, 115 (2014).

[140] D. Hu, Z. Sheng, P. Gong, P. Zhanga, L. Cai, *Analyst*, **135**, 1411 (2010).

[141] Y. Tao, Y. Lin, J. Ren, X. Qu, *Biosens. Bioelectron*, **42**, 41 (2013).

[142] D. Tian, Z. Qian, Y. Xia, C. Zhu, *Langmuir*, **28**, 3945 (2012).

[143] Y. He, X. Wang, J.J. Zhu, S.H. Zhong, G.W. Song, *Analyst*, **137**, 4005 (2012).

[144] M.L. Cui, J.M. Liu, X.X. Wang, L.P. Lin, L. Jiao, L.H. Zhang, Z.Y. Zheng, S.Q. Lin, *Analyst*, **137**, 5346 (2012).

[145] H. Wei, Z. Wang, L. Yang, S. Tian, C. Hou, Y. Lu, *Analyst*, **135**, 1406 (2010).

[146] H. Kawasaki, K. Yoshimura, K. Hamaguchi, R. Arakawa, *Anal. Sci*., **27**, 591 (2011).

[147] H. Liu, G. Yang, E.S. Abdel-Halim, J.J. Zhu, *Talanta*, **104**, 135 (2013).

[148] G.L. Wang, H.J. Jiao, X.Y. Zhu, Y.M. Dong, Z.J. Li, *Talanta*, **93**, 398 (2012).

[149] W. Tedsana, T. Tuntulani, W. Ngeontae, *Anal. Chim. Acta*, **783,** 65 (2013).

[150] J. Abolhasani, J. Hassanzadeh, E.S. Jalali, *Int. Nano. Lett*., **4**, 65 (2014).

[151] J. Abolhasani, J. Hassanzadeh, E. Ghorbani-Kalhor, Z. Saeedi, *J. Chem. Health Risks*, **5**, 145 (2015).

[152] M. Liu, L. Xu, W. Cheng, Y. Zeng, Z. Yan, *Spectrochim. Acta, Part A*, **70**, 1198 (2008).

[153] G.L. Wang, Y.M. Dong, H.X. Yang, Z.J. Li, *Talanta*, **83**, 943 (2011).

[154] T.I. Chanu, D.P.S. Negi, *Chem. Phys. Lett*., **491**, 75 (2010).

[155] C. Jiang, S. Xu, D. Yang, F. Zhang, W. Wang, *Luminescence*, **22**, 430 (2007).

[156] S.Q. Han, J.L. Liu, Z.G. Gan, J.G. Liang, S.M. Zhao, *J. Chin. Chem. Soc*., **55**, 1069 (2008).

[157] M. Miller, *The Journal of the Hyperactive Children's Support Group*, **43**, 16 (1992).

[158] T.E. Tuormaa, *J. Orthomole. Med*., **9**, 225 (1994).

[159] J.M. Smith, *J. Clin. Nutr*., **45**, 17 (1991).

[160] R.A. Mederos, C. Romeu, R. Filho, O.F. Filho, *Food Chem.*, **123**, 886 (2010).

[161] T. Galeano Diaz, A. Guiberteau Cabanillas, M.F. Alexandre Franco, F. Salinas, J.C. Vire, *Electroanal.*, **10**, 497 (1998).

[162] S. Michalkiewicz, M. Mechanik, J. Malyszko, *Electroanal*., **16**, 588 (2004).

[163] Y. Guan, Q. Chu, L. Fu, T. Wu, J. Ye, *Food Chem*., **94**, 157 (2006).

[164] S. Gunckel, P. Santander, G. Cordano, J. Ferreira, S. Munoz, L.J. Nunez-Vergara , J.A. Squella, *Chem. Biol. Interact*., **114**, 45 (1998).

[165] M.E. Leteier, E. Rodriguez, A. Walace, M. Lorca, Y. Morello, J. Aldunate, *Exp. Parasitol.,* **71**, 357 (1990).

[166] L. Boyd, E.G. Beveridge, *Microbes*, **120**, 73 (1981).

[167] Y. Nagakawa, S. Tayama, *Arch. Toxicol.,* **69**, 204 (1995).

[168] L.F. Capitan- Vaiivey, M.C. Valencia, E.A. Nicolas, *Anal. Chim. Acta.*, **503**, 179 (2004).

[169] M.A. Ruiz, E. Garcia-Moreno, C. Barbas, J.M. Pinagarron, *Electroanal.*, **11**, 470 (1999).

[170] B. Saad, Y.Y. Sing, M.A. Nawi, N. Hashim, A.S.M. Ali, M.I. Saleh, *Food Chem.*, **105**, 389 (2007).

[171] C. Perrin, L. Meyer, *Food Chem.*, **77**, 93 (2002).

[172] W. Joseph, *Electroanal.*, **17**, 7 (2005).

[173] Q. Zhao, Z.H. Gan, Q.K. Zhuang, *Electroanal.*, **14**, 1609 (2002).

[174] T.J. Davies, G.G. Wildgoose, R.G. Compton, *Chem Commun*., **7**, 829 (2005).

[175] K.T. Al-Jamal, A. Nunes, L. Methven, H. Ali-Boucetta, S. Li, F.M. Toma, M.A. Herrero, W.T. Al-Jamal, H.M.M. ten Eikelder, J. Foster, S. Mather, M. Prato, A. Bianco, K. Kostarelos, *Angew. Chem. Int. Ed.*, **51**, 6389 (2012).

[176] S. Liu, C. Cai , *J. Electroanal. Chem.*, **602,** 103 (2007).

[177] S. Issac, K. Girish Kumar, *Drug Test Anal.*, **1**, 350 (2009).

[178] S.C. Tsang, Y.K. Chen, P.J.E. Harris, M.L.H. Green, *Nature*, **372**, 159 (1994).

[179] R. Hirlekar, M. Yamagar, H. Garse, M. Vij, V. Kadam, *Asian J. Pharm. Clin. Res.*, **2**, 17 (2009).

[180] C. Hu, S. Hu, *J. Sens.*, **7**, 1 (2009)**.**

[181] K. Balasubramanian, M. Burghard, *Anal. Bioanal. Chem*., **385**, 452 (2006).

[182] Y. Ni, L. Wang, S. Kokot, *Anal. Chim. Acta*., **412**, 185 (2000).

[183] M. Valearcel, S. Cardenas, B. M. Simonet, *Anal. Chem.*, **79**, 4788 (2007).

[184] J.E.B Randles, *Trans Faraday Soc*., **44**, 322 (1948).

[185] H.O. Finklea, D.A. Snider, J. Fedyk, *Langmuir*, **9**, 3660 (1993).

[186] E. Laviron, *J. Electroanal. Chem*., **52**, 395 (1974).

[187] H. Yi, K. Wu, S. Hu, D. Cui, *Talanta*, **55**, 1205 (2001).

[188] J.A.V. Butler. *Trans. Faraday Soc*., **19**, 729 (1924).

[189] J.A.V. Butler. *Trans. Faraday Soc*., **19**, 734 (1924).

[190] T. Erdey-Gruz, M. Volmer. *Z. Physik. Chem. A*, **150**, 203 (1930).

[191] A.J. Bard, L.R. Faulkner, *Electrochemical Methods Fundamentals and Application*, Wiley, New York, 236 (2001).

[192] E. Laviron, *J. Electroanal. Chem*., **101**, 19 (1979).

[193] A.J. Bard, L.R. Faulkner, *Electrochemical Methods: Fundamentals and Applications*, Wiley, New York, 287 (2001).

[194] M. Mazloum-Ardakani, H. Rajabi, H. Bietollahi, *The journal of the Argentine Chemical Society*, **97**, 106 (2009).

[195] O. Hammerich, B. Svensmark, *Anodic Oxidation of Oxygen Containing Compounds: Organic Electrochemistry*, Marcel Dekker, New York, 615 (1990).

[196] T. Yoshida, K. Mori, T. Hatano, T. Okumura, I. Vehara, K. Komage, Y. Fugita and T. Okuda, *Chem. Pharm. Bull*., **37**, 1919 (1989).

[197] M.J. Van derv Merwe, K. Jenkins, E. Theron and B.J. Van der Walt, *Biochem. Pharmacol*., **45**, 303 (1993).

[198] K. Helrich, *Official Methods of Analysis of the Association of Official Analytical Chemists*, Virginea, 1140 (1990).

[199] M.M. Montaser, M.E. Alkafafy, *Life Sci. J*., **10**, 2 (2013).

[200] http://en.wikipedia.org/wiki/Food_coloring

[201] A. Kro'licka, A. Bobrowski, J. Zarebski, I. Tesarowicz, *Electroanal.*, 2**6**, 756 (2014).

[202] T. Gan, J. Sun, Q. Wu, Q. Jing, S. Yu, *Electroanal.*, **25**, 1505 (2013).

[203] S.P. Alves, D. Mares Brum, E.C. Branco de Andrade, A.D.P. Netto, *Food Chem*., **107**, 489 (2008).

[204] T. Gan, J. Sun, S. Cao, F. Gao, Y. Zhang, Y. Yang, *Electrochim. Acta*, **74**, 151 (2012).

[205] Y. Zhang, X. Zhang, X. Lu, J. Yang, K. Wu, *Food Chem*., **122**, 909 (2010).

[206] T. Zou, P. He, A. Yasen, Z. Li, *Food Chem*., **138**, 1742 (2013).

[207] H.Y. Huang, Y. C. Shih, *J. Chromatogr. A*, ***959***, 317 (2002).

[208] M.A. Prado, L.F.V. Boas, M.R. Bronze, H.T. Godoy, *J. Chromatogr. A*, **1136**, 321 (2006).

[209] H. Oka, Y. Ikaia, T. Ohno, N. Kawamura, J. Hayakawa, K. Harada, M. Suzuki, *J. Chromatogr. A*, **674**, 301 (1994).

[210] J.J.B. Nevado, C. Guiberteau-Cabanillas, A.M. Contento-Salcedo, R. Martin-Villamuelas, *Anal. Lett*., **32**, 1879 (1999).

[211] L.F. Captan-Vallvey, M.D. Fernandez, I. De Orbe, R. Avidad, *Talanta*, **47**, 861 (1998).

[212] N. Yoshioka, K. Ichihashi, *Talanta*, **74**, 1408 (2008).

[213] K. Zhang, P. Luo, J. Wu, W. Wang, B. Ye, *Anal. Methods*, **5**, 5044 (2013).

[214] D.C. Tiwari, R. Jain, S. Sharma, *J. Sci. Ind.Res.*, **66**, 1011 (2007).

[215] M.M. Ardakani, H. Rajabi , H. Beitollahi , B.B.F. Mirjalili, A. Akbari, N. Taghavinia , *Int. J. Electrochem. Sci*., **5**, 147 (2010).

[216] S. Cosnier, J. Fombon, P. Lab'be, D. Limosin, *Sens. Actuators B*, **59**, 134 (1999).

[217] J.G. Manjunatha, B.E. Kumara swami, M. Deraman, G.P. Mamatha, *Int. J. Pharm. Pharm. Sci.*, **5**, 355 (2013).

[218] A. Malinauskas, *Synth. Met.*, **107,** 75 (1999).

[219] M.Y. Tang, R. Yuan, Y.Q. Chai, *Chin. J. Chem*., **24**, 1575 (2006).

[220] L. Zhang, X. Lin, *Anal. Bioanal. Chem*., **382**, 1669 (2005).

[221] W. Ma, D.M. Sun, *Acta Phys. Chim. Sin.* **23,** 332 (2007).

[222] C. Jiang, T. Yang, K. Jiao, H. Gao, *Electrochim. Acta*, **53,** 2917 (2008).

[223] C. Wang, C. Li, F. Wang, C. Wang, *Microchim. Acta*, **155**, 365(2006).

[224] J. Wang, S. Zhang, Y. Zhang, *Anal. Biochem.*, **396**,304 (2010).

[225] L. Mirmoghtadaie, A. A. Ensafi, M. Kadivar, M. Shahedi, M. R. Ganjali, *Int. J. Electrochem. Soc*., **8**, 3755 (2013).

[226] K. Zhang, P. Luo, J. Wang, B. Ye, *Anal. Methods*, **5**, 5044 (2013).

[227] H. Bahramipur, F. Jalali, *Afr. J. Pharm. Pharmacol*., **6**, 1298 (2012).

[228] E. Laviron, L. Roullier, C. Degrand, *J. Electroanal. Chem.*, **112**, 11 (1980).

[229] S. Chanlon, L. Joly-Pottuz, M. Chatelut, O. Vittori, J.L. Cretier, *J. Food Comp. Anal.*, **18**, 503 (2005).

[230] Y. Castrillejo, R. Pardo, E. Barrado, P.S. Batanero, *Electroanal*., **2**, 553 (1990).

[231] A.E. Vikraman, D. Thomas, S.T. Cyriac, K. Girish Kumar, *J. Electrochem. Soc*., **161**, B305 (2014).

[232] M. Chao, X. Ma, *Int. J. Electrochem. Sci*., **7**, 6331 (2012).

[233] M.E.G. Lyons, G.P. Keeley, *Sensors*, **6**, 1791(2006).

[234] Z. Pan, C. Shi, H. Fan, N. Bao, C. Yu, Y. Liu, R. Lu, Q. Zhang, H. Gu, *Sens. Actuators B*, **174**, 421 (2012).

[235] Z. Mai, X. Zhao, X. Zou, *Talanta*, **81**, 167 (2010).

[236] P.T. Kissinger, W.R. Heineman, *Laboratory Techniquies in Electroanalytical Chemistry*, Marcel Dekker, New York, 29 (1984).

[237] A.J. Bard, L.R. Faulknar, *Electrochemical methods, Fundamentals and Applications*, John Wiley and Sons, New York, 94 (2001).

[238] E. Laviron, *J. Electroanal. Chem*., **100**, 263 (1979).

[239] Y. Zheng, L. Ye, L.Yan, Y. Gao, Int. *J. Electrochem. Soc.*, **9**, 238 (2014).

[240] K. Helrich, *Official Methods of Analysis of the Association of Official Analytical Chemists*, Virginea, 1115 (1990).

[241] M. Panizza, G.Cerisola, *Electrochim. Acta*, **48**, 3491 (2003).

[242] R.A. Medeiros, B.C. Lourencao, R.C. Rocha-Filho, O. Fatibello-Filho, *Talanta*, **97**, 291 (2012).

[243] L.F. Capitan-Vallvey, M.D. Fernandez, I. Orbe, J.L. Vilchez, R. Avidad, *Analyst*, **122**, 351 (1997).

[244] E. Dinc, E. Baydan, M. Kanbur, F. Onur, *Talanta*, **579**, 58 (2002).

[245] Q. Chen, S. Mou, X. Hou, J.M. Rivello, Z. Ni, *J. Chromatogr. A*, **827**, 73 (1998).

[246] M. Yamada, M. Nakamura, T. Yamada, T. Mautani, Y. Goda, *Chem. Pharm. Bull.*, **44**, 1642 **(**1996).

[247] H. Liu, T. Zhu, Y. Zhang, S. Qi, A. Huang, Y. Sun, *J. Chromatogr. A***, 718,** 448 (1995).

[248] T.M. Coelho, E.C. Vidotti, M.C. Rollemberg, A.N. Medina, M.L. Baesso, N. Cella, A.C. Bento, *Talanta*, **81,** 202 (2010).

[249] B.P. Ramanbhai, R.P. Mukeshbhai, A.P. Ambubhai, K.S. Arvindbhai, G. Ajaybhai, *Analyst*, **111**, 577 (1986).

[250] S. Shahrokhiana, S. Rastgara, *Electrochim. Acta*, **78**, 422 (2012).

[251] Y.R. Wang, P. Hu, Q.L. Liang, G.A. Luo, Y.M. Wang, *Chin. J. Anal. Chem.*, **36**, 1011 (2008).

[252] J.Z. Xu, J.J. Zhu, Q. Wu, Z. Hu, H.Y. Chen, *Electroanal*., **15**, 219 (2003).

[253] L.Q. Jiang, L. Gao, *Carbon*, **41** 2923 (2003).

[254] K. Li, X. Zhu, Y. Liang, *Pharmacol. Pharm.*, **3**, 275 (2012).

[255] P. Norouzi, P. Daneshgar, M.R. Ganjali, A. Moosavi-Movahedi, *J. Braz. Chem. Soc.*, **18**, 231 (2007).

[256] A.I. Gopalan, K.P. Lee, D. Ragupathy, *Biosens. Bioelectron.*, **24**, 2211 (2009).

[257] X. Dai, R.G. Compton, *Anal. Sci.*, **22**, 567 (2006).

[258] C. Hu, S. Hu, *J. Sens.*, **2009**, 187615 (2009)

[259] E.D. Moorhead, M.M. Stephens, *J. Electroanal. Chem.*, **282**, l (1990).

[260] P.F. Salazar, S.Kumar, B.A. Cola, *J. Electrochem. Soc.*, **159**, B483 (2012).

[261] X.J. Huang, H.S. Im, O. Yarimaga, J.H. Kim, D.H. Lee, H.S. Kim, Y.K. Choi, *J. Phys. Chem. B*, **110**, 21850 (2006).

[262] K. Heloizy, G. Freitas, O. Fatibello-Filho, *Talanta*, **81**, 1102 (2010).

[263] S.J. Richard Prabakar, S. Sriman Narayanan, *Anal. Bioanal. Chem*., **386**, 2107 (2006).

[264] D. Thomas, Z. Rasheed, J.S. Jagan, K. Girish Kumar, *J. Food Sci. Technol*., (2015, in press, DOI:10.1016/j.lwt.2015.04.020).

[265] Z. Rasheed, A. E. Vikraman, D. Thomas, J. S. Jagan, K. Girish Kumar, *Food Anal. Methods,* **8,** 213 (2014).

[266] http://www.inchem.org/documents/jecfa/jecmono/v042je23.htm. *WHO Food Additives Series:* World Health Organization, Geneva, 42 (1999).

[267] T. Okubo, Y. Yokoyama, K. Kano, I. Kano, *Biol. Pharm. Bull*., **27**, 295 (2004).

[268] Y. Guan, Q. Chu, L. Fu, J. Ye, *J. Chromatogr. A*, **1074**, 201 (2005).

[269] V.U. Prasad, T.E. Divakar, T. Hariprasad, C.S.P. Sastry, *Food Chem*., **25**, 159 (1987).

[270] Y. Guan, Q. Chu, L. Fu, T. Wu, J. Ye, *Food Chem*., **94**, 157 (2006).

[271] M. González, E. Ballesteros, M. Gallego, M. Valcárcel, *Anal. Chim. Acta*, **359**, 47 (1998).

[272] M.A. Ruiz, E. García-Moreno, C. Barbas, J.M. Pingarrón, *Electroanal*., **11**, 470 (1999).

[273] L. Shang, G.U. Nienhaus, *Biophys. Rev*., **4**, 313 (2012).

[274] S. Palmal, N.R. Jana, *WIREs Nanomed. Nanobiotechnol*., **6**, 102 (2014).

[275] D.M. Chevrier, A. Chatt, P. Zhang, *J. Nanophoton*., **6**, 64504, (2012).

[276] R. Jin, *Nanoscale*, **2**, 343 (2010).

[277] J.F. Parker, C.A. Fields-Zinna, R.W. Murray, *Acc. Chem. Res.*, **43**, 1289 (2010).

[278] X. Wu, X. He, K. Wang, C. Xie, B. Zhou, Z. Qing, *Nanoscale*, **2**, 2244 (2010).

[279] L. Shang, N. Azadfar, F. Stockmar, W. Send, V. Trouillet, M. Bruns, D. Gerthsen, G. U. Nienhaus, *Small*, **7**, 2614 (2011).

[280] Y. Yang, S. Chen, *Nano Lett*., **3,** 75 (2003).

[281] J. Zheng, R.M. Dickson, *J. Am. Chem. Soc*., **124**, 13982 (2002).

[282] H. Xu, K.S. Suslick, *Nano*, **4**, 3209 (2010).

[283] Y. Wang, J. Chen, J. Irudayaraj, *ACS Nano*, **5**, 9718 (2011).

[284] J. Xie, Y. Zheng, J.Y. Ying, *J. Am. Chem. Soc*., **131**, 888 (2009).

[285] H. Wei, Z. Wang, L. Yang, S. Tian, C. Hou, Y. Lu, *Analyst*, **135**, 1406 (2010).

[286] P. Murawala, S.M. Phadnis, R.R. Bhonde, B.L.V. Prasad, *Colloid Surfaces B*, **73**, 224 (2009).

[287] P.R. Selvakannan, A. Swami, D. Srisathiyanarayanan, P.S. Shirude, R. Pasricha, A.B. Mandale, M. Sastry, *Langmuir*, **20**, 7825 (2004).

[288] P.R. Selvakannan, S. Mandal, S. Phadtare, A. Gole, R. Pasricha, S. D. Adyanthaya, M. Sastry, *J. Colloid Interface Sci.*, **269**, 97 (2004).

[289] Y. Zhou, W. Chen, H. Itoh, K. Naka, Q. Ni, H. Yamane, Y. Chujo, *Chem. Commun*., **23**, 2518 (2001).

[290] J.L. Burt, C. Gutierrez-Wang, M. Miki-Yoshida, M. Jose-Yacaman, *Langmuir*, **20**, 11778 (2004).

[291] J. Xie, J.Y. Lee, D.I.C. Wang, Y.P. Ting, *ACS Nano*, **1**, 429 (2007).

[292] C.L. Liu, H.T. Wu, Y.H. Hsiao, C.W. Lai, C.W. Shih, Y.K. Peng, K.C. Tang, H.W. Chang, Y.C. Chien, J.K. Hsiao, J.T. Cheng, P.T. Chou, *Angew. Chem. Int. Ed*., **50**, 7056 (2011).

[293] M. Zhu, C.M. Aikens, F.J. Hollander, G.G. Schatz, R. Jin, *J. of Am. Chem. Soc*., **130**, 5883 (2008).

[294] Y. Negeshi, N.K. Chaki, Y. Shichibu, R.L. Whetten, T. Tsukuda, *J. of Am. Chem. Soc*., **129**, 11322 (2007).

[295] G.L. Wang, T. Huang, R.W. Murray, L. Menard, R.G. Nuzzo, *J. Am. Chem. Soc*., **127**, 812 (2005).

[296] J. Zheng, J.T. Petty, R.M. Dickson, *J. Am. Chem. Soc.*, **125**, 7780 (2003).

[297] H.H. Lin, Y.C. Chan, J.W. Chen, C.C. Chang, *J. Mater. Chem*., **21**, 3170 (2011).

[298] B. Aswathy, G. Sony, *Microchem. J.*, **116**, 151 (2014).

[299] C. Yu, J. Yan, Y. Tu, *Microchim. Acta*, **175**, 347 (2011).

[300] A. Retnakumari, S. Setua, D. MEnon, P. Ravindran, H. Muhammed, T. Pradeep, S. Nair, M. Koyakkutty, *Nanotechnology*, **21**, 55103 (2010).

[301] C.T. Yuan, W.C. Chou, J. Tang, C.A. Lin, W.H. Chang, J.L. Shen, D.S. Chuu, *Opt. Express*, **17**, 16111 (2009).

[302] P. Apell, R. Monreal, S. Lundqvist, *Phys. Scripta*, **38**, 174 (1988).

[303] Z. Wu, R. Jin, *Nano Lett.*, **10**, 2568 (2010).

[304] D. Xiang, G. Zeng, K. Zhai, L. Li, Z. He, *Analyst*, **136**, 2837 (2011).

[305] K. Helrich, *Official Methods of Analysis of the Association of Official Analytical Chemists*, Virginea, 1138 (1990).

[306] http://en.wikipedia.org/wiki/Neurotransmitter

[307] R.M., Wightman, L.J. May, A.C. Michael, *Anal. Chem*., **60**, 769A (1988).

[308] F. Xu, M. Gao, L. Wang, G. Shi, W. Zhang, L. Jin, J. Jin, *Talanta*, **55**, 329 (2001).

[309] H. Zho, Y.Z. Zhang, Z.B. Yuan, *Analyst*, **126**, 358 (2001).

[310] S.R. Ali, Y. Ma, R.R. Parajuli, Y. Balogun, W.Y.C. Lai, H. He, *Anal. Chem*., **79**, 2583 (2007).

[311] R.P. da Silva, A.W.O. Lima, S.H.P. Serrano, *Anal. Chim. Acta*., **612**, 89 (2008).

[312] R. Baron, M. Zayats, I. Willner, *Anal. Chem*., **77**, 1566 (2005).

[313] C. Ji, W. Li, X. Ren, A.F. El-Kattan, R. Kozak, S. Fountain, C. Lepsy, *Anal. Chem*., **80**, 9195 (2008).

[314] F.C. Cheng, Y. Shih, Y.J. Liang, L.L. Yang, C.S. Yang, *J. Chromatogr. B*, **682**, 195 (1996).

[315] J. Huang, Y.Y. Gao, F. Shi, G. Wang, S.M. Shah, X. Su, *Analyst*, **137**, 1481 (2012).

[316] L.K. Abdulrahman, A.M. Al-Abachi, M.H. Al-Qaissy, *Anal. Chim. Acta*, **538**, 331 (2005).

[317] H. Yao, Y.Y. Sun, X.H. Lin, J.H. Cheng, L.Y. Haung, *Luminescence*, **21**, 112 (2006).

[318] F. Shang, L. Zhou, K.A. Mahmoud, S. Hrapovic, Y. Liu, H.A. Moynihan, J.D. Glennon, J.H.T. Luong, *Anal. Chem*., **81**, 4089 (2009).

[319] Y. Mao, Y. Bao, D. Han, F. Li, L. Niu, *Biosens. Bioelectron*., **38**, 55 (2012).

[320] Z. Wang, J. Xia, L. Zhu, X. Chen, F. Zhang, S. Yao, Y. Li, Y. Xia, *Electroanal.*, **23**, 2463 (2011).

[321] D. Thomas, L. Lonappan, L. Rajith, S.T. Cyriac, K. Girish Kumar, *J. Fluoresc*., **23**, 473 (2013).

[322] M.R. Hoffmann, S.T. Martin, W. Choi, D.W. Bahnemann, *Chem. Rev*., **95**, 69 (1995).

[323] N. Ma, J. Yang, K.M. Stewart, S.O. Kelley, *Langmuir*, **23**, 12783 (2007).

[324] M. Bruchez Jr, M. Moronne, P. Gin, S. Weiss, A.P. Alivisatos, *Science*, **281**, 2013 (1998).

[325] A.S. Susha, F. Caruso, A.L. Rogach, G.B. Sukhorukov, A. Kornowski, H., Mo¨hwald, M. Giersig, A. Eychmu¨ller, H. Weller, *Colloid. Surface A*, **163**, 39 (2000).

[326] G.L. Wang, H.J. Jiao, X.Y. Zhu, Y.M. Dong, Z.J. Li, *Talanta*, **93**, 398 (2012).

[327] H. Weller, *Angew. Chem. Int. Ed. Engl*., **32**, 41 (1993).

[328] T.I. Chanu, D.P.S. Negi, *Chem. Phys. Lett*., **491**, 75 (2010).

[329] Y.S. Xia, C.Q. Zhu, *Microchim. Acta*, **164**, 29 (2009).

[330] J.O. Winter, N. Gomez, S. Gatzert, C.E. Schmidt, B.A. Korget, *Colloid. Surface A*, **254**, 147 (2005).

[331] Y.C. Cao, J.H. Wang, *J. Am. Chem. Soc*., **126**, 14336 (2004).

[332] A.E. Saunders, I. Popov, U. Banin, *J. Phys. Chem. B*, **110**, 25421 (2006).

[333] W.W. Yu, L. Qu, W. Guo, X. Peng, *Chem. Mater*., **15**, 2854 (2003).

[334] M. Koneswaran, R. Narayanaswamy, *Sens. Actuators B*, **139**, 91 (2009).

[335] T. Gacoin, K. Lahlil, P. Larregaray, J.P. Boilot, *J. Phy. Chem. B*, **105**, 10228 (2001).

[336] Y.F. Chen, R.Z. Zeev, *Anal. Chem*., **74**, 5132 (2002).

[337] J.L. Chen, C.Q. Zhu, *Anal. Chim. Acta*., **546**, 147 (2005).

[338] Y.Tao, Y., Lin, J. Ren, X. Qu, *Biosens. Bioelectron*., **42**, 41 (2013).

[339] M. Shamsipur, M. Shanehaasz, K. Khajeh, N. Mollania, S.H. Kazemi, *Analyst, **137**,* 5553 (2012).

[340] U. Baruah, N. Gogoi, A. Konwar, M.J. Deka, D. Chowdhury, G. Majumdar, *J. Nanopart.*, **2014**, 178518 (2014).

[341] A. Yildirim, M. Bayindir, *Anal. Chem*., **86**, 5508 (2014).

[342] H.Z. Zheng, L. Liu, Z.J. Zhang, Y. M. Huang, D.B. Zhou, *Spectrochim. Acta A*, **71**, 1795 (2009).

[343] D.E. Moore, K. Patel, *Langmuir*, **17**, 2541 (2001).

[344] M. Hosseini, H. Khabbaz, A.S. Dezfoli, M.R. Ganjali, M. Dadmehr, *Spectrochim. Acta A*, **136**, 1962 (2015).

[345] G.L. Wang, Y.M. Dong, H.X. Yang, Z.J. Li, *Talanta*, **83**, 943 (2011).

[346] T. Dannhauser, M. ÓNeil, K. Johansson, D. Whitten, G. McLendon, *J. Phys. Chem*., **90**, 6074 (1986).

[347] W. Bae, R. Abdullah, R.K. Mehra, *Chemosphere*, **37**, 363 (1998).

[348] B. Aswathy, G. Sony, *Microchem. J*., **116**, 151 (2014).

[349] Y. Zhao, S. Zhao, J. Haung, F. Ye, *Talanta*, **85**, 2650 (2011)

[350] T.J. Panholzer, J. Beyer, K. Lichtwald, *Clin. Chem.*, **45**, 262 (1999).

[351] R.N. Goyal, Md. Abdul Aziz, M. Oyama, S. Chatterjee, A. R. Singh Rana, *Sens. Actuators B*, **153**, 232 (2011).

[352] D. Voet, J.G. Voet, *Biochemistry*, Wiley, New York, 76 (1995).

[353] S.W. Cole, Y.D. Korin, J.L. Fahey, J.A. Zack, *J. Immunol.*, **161**, 610 (1998).

[354] X. Ma, M. Chen, X. Li, A. Purushothaman, F. Li, *Int. J. Electrochem. Sci.*, **7**, 991 (2012).

[355] M. Zhu, X.M. Huang, J. Li, H.X. Shen, *Anal. Chim. Acta*, **357**, 261 (1997).

[356] S. Wei, G. Song, J.M. Lin, *J. Chromatogr. A*, **1098**, 166 (2005).

[357] N. Shafi, *J. Chem. Soc. Pak.*, **17**, 103 (1995).

[358] C.L. Guan, J. Quyang, Q.L. Li, B.H. Liu, W.R.G. Baeyens, *Talanta*, **50**, 1197 (2000).

[359] V. Carrera, E. Sabater, E. Vilanova, M.A. Sogorb, *J. Chromatogr. B*, **847**, 88 (2007).

[360] Z. Wang, *Int. J. Electrochem. Sci*., **8**, 5448 (2013).

[361] Y. Sun, J. Fei, J. Hou, Q. Zhang, Y. Liu, B. Hu, *Microchim. Acta*, **165**, 373 (2009).

[362] M. Ates, J. Castillo, A.S. Sarac, *Microchim. Acta*, **160**, 247 (2008).

[363] E.C. Chan, P.Y. Wee, P.Y. Ho, P.C. Ho, *J. Chromatogr. B*, **749**, 179 (2000).

[364] C. Sabbioni, M.A. Saracino, R. Mandrioli, S. Pinzauti, S. Furlanetto, G. Gerra, M.A. Raggi, *J. Chromatogr. A*, **1032**, 65 (2004).

[365] K.L. Ai, B. H. Zhang, L.H. Lu, *Angew. Chem. Int. Ed*., **48**, 304 (2009).

[366] S.W. Chen, R.S. Ingram, M.J. Hostetler, J.J. Pietron, R.W. Murray, T.G. Schaaff, J.T. Khoury, M.M. Alvarez, R.L. Whetten, *Science*, **280**, 2098 (1998).

[367] J.P. Wilcoxon, J.E. Martin, F. Parsapour, B. Wiedenman, D.F. Kelley, *J. Chem. Phys.*, ***108***, 9137 (1998).

[368] G. Schmid, *Chem. Rev*., **92**, 1709 (1992).

[369] M. Cui, Y. Zhao, Q. Song, *TrAC. Trend. Anal. Chem.*, **57**, 73 (2014).

[370] C. Zhou, M. Long, Y. Qin, X. Sun, J. Zheng, *Angew. Chem. Int. Ed.*, **123**, 3226 (2011).

[371] I. D´ıez, R.H.A. Ras, *Nanoscale*, **3**, 1963 (2011).

[372] H. Xu, K.S. Suslick, *Adv. Mater.*, **22**, 1078 (2010).

[373] C. Zhou, S. Yang, J. Liu, M. Yu, J. Zheng, *Exp. Biol. Med.*, **238**, 1199 (2013).

[374] G. Wang, T. Huang, R.W. Murray, L. Menard, R.G. Nuzzo, *J. Am. Chem. Soc*., **127**, 812 (2005).

[375] Z. Wu, R. Jin, *Nano Lett.*, **10**, 2568 (2010).

[376] H. Wei, Z. Wang, L. Yang, S. Tian, C. Hou, Y. Lu, *Analyst*, **135**, 1406 (2010).

[377] H. Kawasaki, K. Hamaguchi, I. Osaka, R. Arakawa, *Adv. Funct. Mater*. **21**, 3508 (2011).

[378] C.L. Liu, H.T. Wu, Y.H. Hsiao, C.W. Lai, C.W. Shih, Y.K. Peng, K.C. Tang, H.W. Chang, Y.C. Chien, J. K. Hsiao, J.T. Cheng, P.T. Chou, *Angew. Chem. Int. Ed*., **50**, 7056 (2011).

[379] H. Chi, B. H. Liu, G.J. Guan., Z.P., Zhang, M. Y. Han, *Analyst*, **135**, 1070 (2010).

[380] Y.Z. Zhao, M.M. Cai, Y. Qian, L.H. Xie, W. Huang, *Process. Chem.*, **25**, 296 (2013).

[381] R.J. Bera, R. Raj, *Analyst*, **136**, 1644 (2011).

[382] J.D. Luo, Z.L. Xie, J.W.Y. Lam, L. Cheng, H. Chen, C. Qiu, H.S. Kwok, X. Zhan, Y. Liu, D. Zhu, B.Z. Tang, *Chem. Commun*., **18**, 1740 (2001).

[383] Z. Li, Y. Dong, B. Mi, Y. Tang, M. Haussler, H. Tong, Y. Dong, J.W.Y, Lam, Y. Ren, H.H.Y. Sung, K.S. Wong, P. Gao, I.D. Williams, H.S. Kwok, B.Z. Tang, *J. Phys. Chem. B*, **109**, 10061 (2005).

[384] Y.N. Hong, J.W.Y. Lama, B.Z. Tang, *Sens. Actuat. B*, **191**, 445 (2014).

[385] Z. Wu, R. Jin, *Nano Lett.*, **10**, 2568 (2010).

[386] N. Vasimalai, S.A. John, *Biosen. Bioelectron.* **42**, 267 (2013).

[387] D. Xiang, G. Zeng, K. Zhai, L.Li, Z. He, *Analyst*, **136**, 2837 (2011).

[388] Y. Hong, J.W.Y. Lam, Y. Lam, B.Z. Tang, *Chem. Commun*., **29**, 4332 (2009).

.....ꕥ.....

Publications

[1] **E.V. Anuja**, A.R. Jose, M. Jacob, K. Girish Kumar, Thioglycolic acid capped CdS quantum dots as a fluorescent probe for the nanomolar determination of dopamine, *Analytical Methods* (2015**,** In press, DOI: 10.1039/ C5AY01412C).

[2] **E.V. Anuja**, D. Thomas, S.T. Cyriac, K. Girish Kumar, Kinetic and thermodynamic approach in the development of a voltammetric sensor for sunset yellow, *Journal of the Electrochemical Society*, **161**, B305 (2014).

[3] **E.V. Anuja**, Z. Rasheeed, L. Lonappan, L. Rajith, K. Girish Kumar, MWCNT modified gold electrode sensor for the determination of propyl gallate in vegetable oils, *Food Analytical Methods*, 6, 775 (2013).

[4] D. Thomas, **E.V. Anuja**, T. Jose, K. Girish Kumar, Kinetic approach in the development of a gold nanoparticle based voltammetric sensor for sudan I, *LWT-Food Science and Technology* (2015, DOI: 10.1016/j.lwt.2015.04.020).

[5] A. Thomas, **E.V. Anuja**, D. Thomas, K. Girish Kumar, Voltammetric sensor for the Determination of TBHQ in coconut Oil, *Food Analytical Methods*, **8**, 2028 (2015,).

[6] T. Jos, L. Lonappan, Z. Rasheed, **E.V. Anuja**, K. Girish Kumar, Voltammetric determination of guaifenesin on a MWCNT modified Pt electrode, *Electrochemistry Letters*, **3**, B23 (2014).

[7] Z. Rasheed, **E.V. Anuja**, D. Thomas, J.S. Jagan, K. Girish Kumar**,** Carbon-nnotube-based sensor for the determination of butylated hydroxyl anisole in food samples. *Food Analytical Methods,* **8,** 213 (2014).

[8] T. Jos, L. Lonappan, **E.V. Anuja**, Z. Rasheed, K. Girish Kumar, Diffusion controlled process at an AuNP/Pt electrode surface for the voltammetric determination of TAM, *Journal of Pharmaceutical Research and Development*, **2**, 224 (2013).

[9] M. Sobhana, T. Divya, **E.V. Anuja**, K. Girish Kumar, Manganese (II) – selective potentiometric sensor based on calix[4]resorcinarene in PVC matrix, *Frontiers in Sensors*, **1**, 74 (2013).

Conference papers

[1] Voltammetric determination of sunset yellow using MWCNT/AuNP nanocomposite film modified glassy carbon electrode (New Frontiers in Chemical Research, Sacred Heart College, Thevara, December 2014).

[2] Development of gold nanoparticles modified glassy carbon electrode sensor for the voltammetric determination of sunset yellow (Current Trends in Chemistry,CUSAT, January 2014).

[3] Development of gold nanoparticle based voltammertic sensor for the determination of sunset yellow (23rd Swadeshi Science Congress, M.G. University, Kottayam, November 2013).

[4] Propyl gallate sensing through multi walled carbon nanotube (MWCNT) modified gold electrode (Recent Advances in Surface Sciences, Gandhigram Rural Institute- Deemed University, Dindigul, February 2013).

[5] Electrochemical oxidation of propyl gallate on a multi walled carbon nanotube (MWCNT) modified gold electrode sensor (22nd Swadeshi Science Congress, Central Plantation Crops Research Institute, Kasaragod, November 2012).

[6] Carbon nano tube modified gold sensor in food analysis- determination of propyl gallate (24th Kerala Science Congress, Rubber Board, Kottayam, January 2012).